

https://dspace.org/

Catalytic properties of gold-zeolites and related materials

Magadu, Takalani

2008-03-11T07:10:02Z
http://hdl.handle.net/10539/4638

Downloaded from a DSpace repository. https://dspace.org/

CATALYTIC PROPERTIES OF GOLD-ZEOLITES AND RELATED MATERIALS

Takalani Magadzu

A thesis submitted to the Faculty of Science, University of the Witwatersrand, Johannesburg, in fulfilment of the requirements for the degree of Doctor of Philosophy.

Johannesburg, 2007

DECLARATION

I declare that this thesis was carried out exclusively by me under the supervision of Professor Mike S. Scurrell. It is being submitted for the degree of Doctor of Philosophy at the University of the Witwatersrand, Johannesburg. It has not been submitted before for any degree or examination at any other University.

_____

(Signature of candidature)

_____ day of _____ 2007

ABSTRACT

Zeolite catalysts were prepared by carrying out an ion-exchange process of transition metals and impregnation to incipient-wetness method of metal catalyst using a chlorine free gold precursor, $KAu(CN)_2$. The instability of Au/Y (3.74wt%Au) resulted in low CO oxidation activity (~ 18 % conversion at 450 ^{0}C), suggesting that the reduced gold metal atoms are bound to the zeolite by a weak interaction. This is subject to migration within the passages of the zeolite during use. The presence of proton stabilized most of Au clusters (electron deficient species) within the HY zeolite, resulting in small amounts of gold species migrating to the outer surface. Interestingly the CO oxidation activity of Au/HY is half that of Au/Y, which clearly indicate that the presence of metallic gold plays a significant role during CO oxidation.

The loading of Au/M-Y (M = Ni^{2+}, Fe^{3+}, Co^{2+} or Cr^{3+}) were varied from 1.67-7.48wt%Au and from 1.76-5.45wt%M. Modification of this Y structure with transition metals has been found to be beneficial for both activity and stability of smaller gold clusters, by strengthening the interaction between gold and zeolite exchange sites and by large magnitude in maintaining the dispersion of gold. This suggests that the unreduced chromium ions function as a chemical anchors for reduced Au metal and that the reduced atoms of gold may form small clusters with the anchoring metal. TPR profile has confirmed that the introduction of 1.67wt%Au on Fe-Y (1.88wt%Fe) increased the stability of Fe ions as stabilizer

metal. However, as the gold loading of Au/Fe-Y catalyst increases the TPR profile shows that the stability of Fe ions decreases and hence the activity of catalysts. An increase in transition metal content, above 1.88wt%Fe was found to lower the CO oxidation activity. A TPR profile has confirmed that as the reduction potential became more negative, the activity of supported Au increases following the sequence: Ni^{2+}, 0.23 << Fe^{3+}, -0.41 < Cr^{3+}, -0.56. The estimated particle sizes of gold by X-ray diffraction were found to be ~ 12 nm for Ni^{2+}, ~ 7 nm for Fe^{3+}, and ~ 5 nm for Cr^{3+} stabilized metal.

Samples of Au/HY (3.77wt%Au) have been prepared by an ion-exchange method using Au(III) ethylenediamine complex-ions, $[Au(en)_2]^{3+}$. Following a pre-treatment in an O_2 atmosphere, the catalyst showed the existence of an induction period before reaching a steady state activity; suggesting the need for activating gold prior to catalyzing CO oxidation reaction. As-prepared catalyst contained 85% of gold in the Au^{3+} valence state as confirmed by Mössbauer spectroscopy. The catalyst was treated with various reducing agents (such as $NaBH_4$); to yield stable and active smaller gold clusters (< 2 nm) inside the HY cavities, as revealed by X-ray Photoelectron Spectroscopy (XPS), X-ray Diffraction (XRD) and Uv-Vis Spectrophotometer. DRIFTS revealed that electron-deficient particles ($Au^{\sigma+}$-CO species) of gold clusters, inside the HY framework and in contact with protons are active species for CO oxidation. CO activity and formation of smaller gold clusters depends on the nature and molar ratio of reducing agents, and the source of gold. The induction period observed for unreduced Au catalyst is a slow step in the activation of gold active sites. Treatment of Au/Y (3.46wt%Au) with

sodium borohydride enhanced the activation of gold active species and hence improves the catalytic activity. The $NaBH_4$ treated Au/Y (3.73wt%Au) catalyst has shown, for the first time, activity of approximately 28% CO conversion. The catalyst showed almost the same activity and induction period as that of the untreated Au/HY (3.77wt%Au) catalyst, which leaves much to be investigated about the behaviour of Au on Y zeolite upon treatment with a proper reducing agent. The protons have been found to stabilize the smaller Au nanoparticles within the zeolite cavities.

The modification of zeolite-Y was carried out by treatment with different alkali metal nitrates such as $LiNO_3$, $NaNO_3$ and KNO_3 before introducing gold from different sources, (i.e. gold ethylenediamine complex ion, $Au(en)_2Cl_3$; chloroauric acid, $HAuCl_4$; or potassium dicyano aurate, $KAu(CN)_2$ complex). The CO oxidation activity of the catalysts was found to depend on the nature of the gold source and on the type of alkali metal nitrate used. The order of activity was as follows: $HAuCl_4 >> KAu(CN)_2 > Au(en)_2Cl_3$. It was found that the activity of catalysts prepared by deposition of Au from an aqueous solution of chloroauric acid on Na-modified zeolites-Y, increased as a result of an increase in the amount of Au deposited as confirmed X-ray fluorescence spectroscopy (XRF). The K-modified zeolite-Y had a smaller amount of Au deposited (i.e. Au/KY, 0.454wt%Au; Au/NaY, 0.772wt%Au and Au/LiY, 0.212wt%Au) and hence the CO oxidation activity was lower than that of Na-modified zeolites-Y. Thus, the order of the catalytic activity is as follows: Na > K > Li. The XRD studies have revealed that metallic gold particles sizes do not depend on the nature of alkali

metal nitrates used to modify the zeolite-Y surface and the zeolite-Y crystallinity has been maintained.

Monometallic Au/NaY (0.772wt%Au, treated with $NaNO_3$) was found to be active in ethylene hydrogenation with ~5% conversion. Treatment of catalysts with $NaBH_4$ was found to lower the catalytic activity of the catalysts, contrary to activities observed on CO oxidation and these concluded that cationic gold are responsible for the observed activity. The activity was found to depend on the source of Au used, and the order is as follows; $HAuCl_4$ >> $KAu(CN)_2$ > $Au(en)Cl_3$. Bimetallic catalysts of Au/M-Y (where Au represent gold from $KAu(CN)_2$, and M = Ni^{2+}, Fe^{3+}, or Cr^{3+}) were found to be more active compared to monometallic catalysts due to promotional effect of transition metal. The order of activity of the bimetallic system at 260 ^{0}C was as follows; Ni^{2+} >> Fe^{3+} > Cr^{3+}, and at 150 ^{0}C, was Ni^{2+} >> Cr^{3+} > Fe^{3+}, contradicting the order of activity observed on CO oxidation. Formation of carbonaceous deposits on the surface of the catalyst at temperature higher than 260 ^{0}C has been confirmed.

Cu modified Au/TiO_2 (anatase, 200m^2/g) has been prepared by incipient-wetness method by either introducing the modifier, before or after Au loading. Such catalysts were found to give high and stable activity for the water-gas shift (WGS) reaction, when compared to unmodified Au/TiO_2 catalysts. It has been suggested that an increase in activity on modified Au/TiO_2, is mainly due to the existence of a synergetic interaction between Cu and Au, since the activity of both Cu/TiO_2 and Au/TiO_2 is lower than that of bimetallic system. The presence of nitrates on

Cu^{c}-Au/TiO_2 (^{c} Cu precursor is $Cu(NO_3)_2$*2.5H_2O) has been found to be detrimental to the activity of Au on TiO_2; due to the poisoning of Au active sites and enhancement of Au agglomeration by NO_2^- formed during the reaction. An increase in Cu loading lowers the activity of Au. A XANES spectrum has confirmed that gold exists as either Au^+/Au^0 during WGS reaction and Cu exists as copper ions (Cu^+/Cu^{2+}) before and during WGS reaction. Formation of bimetallic particles was not detected by EXAFS data analysis. The observed effects are interpreted as a mutual influence of gold and copper ions and reduced species of gold and copper due to their competing for ion exchange sites. Cu has no promotional effect on low temperature CO oxidation and on preferential CO oxidation in excess of hydrogen.

Dedicated to my father: Musumuvhi Andries Magadzu

ACKNOWLEDGEMENTS

I would like to express my sincere gratitude to the following people for their invaluable support and assistance and without whom this thesis would not have been possible:

My supervisor, **Professor Mike S. Scurrell**, for his many hours of patient wisdom which made this work possible and his everlasting advice, assistance, enthusiasm and encouragement which made working with him a pleasure and an unforgettable experience in my life.

All of my colleagues in the lab: Lucky Sikhwivhilu, Charity Mbileni, Mpfunzeni wa Raphulu, Steven Ndou, Keneiloe Khoabane, John Moma, Walter Ngobeni, Kaushik Mallick, Sara Mohlala, Thabang Ntho, Linda Linganiso and the rest of the CATOMCER group for providing a great working environment.

Barry Fairbrother, Basil Chassoulas, David Moloto, Elias Baloyi and Steve van der Schyff, for their technical support.

With great gratitude, I would like to thank my Creator, with whom nothing is impossible. Indeed, he is the Alpha and Omega, the beginning and the end to everything we plan to accomplish.

In addition, I wish to thank National Research Foundation (NRF), Department of Labour Scarce Skills Scholarship (DoL), Daad In-Country Scholarship, Mellon Postgraduate Scholarship, Postgraduate Merit Award, Wits Organometallic/Catalysis Group and the University of Witwatersrand for financial support, both on a personal level and for the project.

PUBLICATIONS AND PRESENTATIONS

Publications

1. D. Boyd, S. Golunski, G. H. R. Hearne, T. Magadzu, K. Mallick, M. C. Raphulu, A. Venugopal, and M. S. Scurrell, Applied Catalysis A: General 292 (2005) 76-81.

2. T. Magadzu and M. S. Scurrell, Stability of gold particles in Y and HY-type zeolites: Influence of Co-exchanged metal cations; Applied Catalysis A: General, to be submitted.

Poster presentation

Second International Congress on Operando Spectroscopy, Fundamental and Technical Aspects of Spectroscopy of Catalysts under Working Conditions, April 2006; Toledo, Spain: *DRIFTS spectroscopy characterization of $NaBH_4$ reduced Au/HY and in-situ EXAFS/XANES analysis of gold-copper ion mixture in TiO2 (anatase), for Water-Gas Shift reaction.* T. Magadzu, J. H. Jang, J. D. Henao, M. C. Kung, H. H. Kung and M. S. Scurrell

Catalysis Society of South Africa (CATSA), at Riverside, Durban, South Africa; November 2003: *Catalytic Properties of Gold-Zeolites.* T. Magadzu and M. S. Scurrell.

Oral Presentations

Low-temperature, Water-Gas Shift reactions over Au supported on TiO_2, in the presence of modifier; presented at the **Gold Workshop Conference** held in Pennsylvania, Philadelphia; May 2005: T. Magadzu and M. S. Scurrell.

Catalytic Properties of Gold-Zeolites; presented at the **Gold Workshop Conference** held at Riverside, Johannesburg, South Africa; June 2003: T. Magadzu and M. S. Scurrell.

Catalytic Properties of Gold-Zeolites for CO oxidation and Ethylene hydrogenation; presented at the **Gold Workshop Conference** held in Paris, France, July 2004, T. Magadzu and M. S. Scurrell.

TABLE OF CONTENTS

DECLARATION II
ABSTRACT III
ACKNOWLEDGEMENTS IX
PUBLICATIONS AND PRESENTATIONS XI
TABLE OF CONTENTS XIII
LIST OF FIGURES XXVI
LIST OF TABLES XXXVI
LIST OF ABBREVIATIONS XXXVIII

CHAPTER 1 ..... **1**

INTRODUCTION 1
1.1 HISTORICAL BACKGROUND *1*
1.1.1 Gold supported on metal oxide 1
1.1.2 Gold supported on zeolites 2
1.2 THESIS STRUCTURE *3*
1.3 REFERENCES *7*

CHAPTER 2 ..... **9**

LITERATURE SURVEY 9
2.1 CATALYSIS ON ZEOLITES *9*
2.1.1 Introduction 9
2.1.2 Cations in zeolites 10
2.1.3 Hydroxyl groups in zeolites 11
2.1.4 The stability of the zeolite skeleton 12
2.1.5 Zeolite modification 13
2.1.6 Zeolites containing nickel, and iron ions as catalysts 14
2.1.6.1 Oxidation of carbon monoxide 14

2.1.7 Properties of nickel, iron, and chromium in zeolites 15
2.1.7.1 Nickel 15
2.1.7.1.1 Formation and location of Ni^{2+} in Y-zeolites 15
2.1.7.1.2 Reducibility of nickel ions in Y-zeolites 15
2.1.7.2 Iron 16
2.1.7.2.1 Formation and location of Fe^{3+} and Fe^{2+} in Y zeolites 16
2.1.7.2.2 Reducibility of iron ions in Y-zeolites 17
2.1.7.3 Chromium 17
2.1.7.3.1 Formation and location of Cr^{3+} and Cr^{2+} in Y zeolites 17
2.1.7.3.2 Reducibility of chromium ions in Y zeolites 18
2.2 CATALYSIS AT SURFACES 18
2.2.1 Introduction 18
2.2.2 Studies of surface reactions on zeolites 19
2.2.2.1 State of transition elements in zeolites 22
2.2.2.2 Factors affecting the redox ability and migration of transition metals to the external surface 24
2.2.2.3 Electronic state of highly dispersed metal particles and their interaction with the zeolite framework. 26
2.2.3 Adsorption of alkenes on zeolites 28
2.2.3.1 Introduction 28
2.2.3.2 Cations and olefins interactions 28
2.2.4 Temperature programmed desorption (TPD) 29
2.2.4.1 Introduction 29
2.2.4.2 Characterization of acidic properties of zeolites 29
2.3 SUPPORTED METAL CATALYSTS 32
2.3.1 Introduction 32
2.3.2 Supported monometallic catalysts 32
2.3.3 Supported bimetallic catalysts 34
2.3.4 Catalysts preparation methods 35
2.3.4.1 Incipient wetness or pore volume impregnation method 35
2.3.4.2 Ion exchange and preparation of gold/zeolite catalysts 37
2.3.4.3 Co-precipitation 38

2.3.4.4 Deposition-precipitation 38
2.4 SURFACE CHARACTERIZATION OF SUPPORTED METAL CATALYSTS 40
2.4.1 Determination of the metal particle size 40
2.4.1.1 Transmission electron microscopy 41
2.4.1.2 Scanning electron microscopy 41
2.4.1.3 Small-angle X-ray scattering analysis 42
2.4.2 Determination of nature and state of supported metal catalysts 44
2.4.2.1 Temperature-programmed reduction (TPR) 44
2.4.2.2 ^{197} Au Mössbauer spectroscopy 44
2.4.2.3 X-ray absorption spectroscopy (XAS) 45
2.4.2.3.1 X-ray absorption near edge structure (XANES) 46
2.4.2.3.2 Extended X-ray absorption fine structure (EXAFS) 48
2.5 CATALYSIS BY GOLD-BASED CATALYSTS: CO OXIDATION REACTION 51
2.5.1 Introduction 51
2.5.2 Preparation of gold nanoparticles 51
2.5.3 Nature of active gold species, for CO oxidation 55
2.6 GOLD CATALYSIS ON ALKALI-MODIFIED ZEOLITES FOR CO OXIDATION 56
2.6.1 Catalysis on alkali-modified zeolites 56
2.7 ETHYLENE HYDROGENATION REACTIONS 60
2.7.1 Introduction 60
2.7.2 Carbon and coke formation on supported metal catalysts 64
2.7.3 Supported-gold catalysts for ethylene hydrogenation 67
2.8 SUPPORTED METAL CATALYSTS FOR THE WATER-GAS SHIFT REACTION 69
2.9 PREFERENTIAL OXIDATION OF CO (PROX) IN THE PRESENCE OF EXCESS HYDROGEN 70
2.10 REFERENCES 72

CHAPTER 3 ..... **82**

EXPERIMENTAL 82

3.1 INTRODUCTION *82*

3.2 REAGENTS AND CHEMICALS *83*

3.3 PREPARATION OF MODIFIED ZEOLITES AND GOLD PRECURSOR *84*

3.3.1 Preparation of the acidic zeolites: HY 84

3.3.2 Preparation of alkali-modified zeolites-Y 84

3.3.3 Preparation of the organogold complex: $Au(en)_2Cl_3$ [7] 85

3.4 PREPARATION OF BOTH MONO- AND BI-METALLIC CATALYSTS *86*

3.4.1 Preparation of Au/M-Y (M = Ni^{2+}, Fe^{3+}, Co^{2+}, and Cr^{3+}): source of gold, $KAu(CN)_2$. 86

3.4.2 Preparation of Au/Y (3.49wt.%Au) and Au/HY (3.77wt.%Au): source of gold, $Au(en)_2Cl_3$ 90

3.4.2.1 In-situ reduction of Au on HY 90

3.4.2.1.1 In-situ reduction of Au in the absence of protecting agents 90

3.4.2.1.2 In-situ reduction of Au in the presence of polyethylene glycol (PEG), as the protecting agents on HY. 91

3.4.2.2 In-situ reduction of Au on Y (3.02wt.%Au) 91

3.4.3 Preparation of Au/Y (3.67wt.%Au): source of gold, $KAu(CN)_2$ 93

3.4.4 Preparation of Au on alkali-modified zeolite-Y 94

3.4.4.1 Catalysts preparation using ion-exchange methods 95

3.4.4.1.1 Gold source, $Au(en)_2Cl_3$ 95

3.4.4.1.2 Gold source, $HAuCl_4$ 95

3.4.4.2 Catalysts preparation using impregnation 96

3.4.4.2.1 Gold source, $KAu(CN)_2$ 96

3.4.5 Preparation of Au supported on TiO_2 modified with Cu 98

3.4.5.1 Preparation of Au-Cu/TiO_2 catalyst (2.84wt.%Au:0.32wt.%Cu) 98

3.4.5.1.1 Incipient-wetness impregnation of Cu onto TiO_2 (anatase, 200 m^2/g) 98

3.4.5.1.2 Deposition-precipitation of Au onto calcined Cu/TiO_2 (0.32wt.%Cu) 98
3.4.5.2 Preparation of $Cu-Au/TiO_2$ (0.44wt.%Cu:3.95wt.%Au) 99
3.4.5.2.1 Deposition-precipitation of Au onto TiO_2 (anatase, $200m^2/g$) 99
3.4.5.2.2 Incipient-wetness impregnation of Cu onto Au/TiO_2 100
3.4.5.2.2.1 $Cu(NO_3)_2*2.5H_2O$ as source of Cu 100
3.4.5.2.2.2 $Cu(OOCCH_3)_2*H_2O$ as the source of Cu..... 100
3.5 CATALYSTS CHARACTERIZATION..... *103*
3.5.1 Temperature programmed reduction and oxidation (TPR and TPO) 103
3.5.2 X-ray methods 104
3.5.2.1 Powder X-ray diffraction (XRD)..... 105
3.5.3 Inductively coupled plasma (ICP)..... 106
3.5.4 Ultraviolet-visible spectrophotometry (UV-Vis) 106
3.5.5 ^{197} Au Mössbauer spectroscopy..... 108
3.6 CATALYSTS ACTIVITY TESTS *109*
3.6.1 Catalysts testing of Au on Y in the presence of transition metal (M represent Ni^{2+}, Fe^{3+}, Co^{2+}, and Cr^{3+}) 109
3.6.2 Catalysts testing of $[Au(en)_2]^{3+}/HY$..... 109
3.6.3 Catalysts testing of Au supported on alkali-modified zeolite-Y 110
3.6.4 Catalysts testing of Au supported on Y-zeolite, for ethylene hydrogenation 111
3.6.5 Catalysts testing of Au supported on TiO_2 modified with Cu. 112
3.6.5.1 Catalysts testing for CO oxidation..... 112
3.6.5.2 Catalysts testing for selective CO oxidation in a H_2 rich stream 113
3.6.5.3 Catalysts testing for low temperature Water-gas shift reaction 113
3.6.5.4 In-situ XANES and EXAFS structural characterization of Au-Cu ions supported on TiO_2 (anatase) for the Water-gas shift reaction 114
3.7 REFERENCES *116*

CHAPTER 4 ..... **117**

STABILITY OF GOLD PARTICLES IN Y-TYPE ZEOLITES: INFLUENCE OF CO-EXCHANGED METAL CATIONS 117

4.1 INTRODUCTION *117*

4.2 EXPERIMENTAL *119*

4.2.1 Support and catalyst preparation 119

4.2.2 Temperature-programmed reduction (TPR) 119

4.2.3 X-ray powder diffraction (XRD) 119

4.3 RESULTS AND DISCUSSIONS *120*

4.3.1 TPR experiments 120

4.3.1.1 TPR profiles of Au/Y and in the presence of stabilizing metals Ni^{2+}, Fe^{3+} and Cr^{3+} 120

4.3.1.2 Effect of Au loading on the TPR profile of Au/Fe-Y 124

4.3.2 XRD results 127

4.3.2.1 Effect of gold loading 127

4.3.2.2 Effect of Ni^{2+}, Fe^{3+} and Cr^{3+} on stability of gold particles on Y zeolites. 128

4.3.3 Effect of acidity/proton on chemical state, gold particles size and hence CO oxidation activity. 131

4.3.4 Catalytic activities of gold on Y, promotional effect on Au by exchanged Ni^{2+}, Fe^{3+}, and Cr^{3+} on Y 133

4.3.4.1 Effect of nickel on activity of Au/Y (3.35wt%Au:1.79wt%Ni) 134

4.3.4.2 Effect of iron on activity of Au/Y (3.29wt%Au:1.88wt%Fe) . 136

4.3.4.3 Catalytic activities of Au/Cr-Y (3.26wt%Au:1.76wt%Cr) 137

4.3.4.4 Comparison of catalytic activities of Au/M-Y (M = Ni^{2+}, Fe^{3+}, Co^{2+}, and Cr^{3+}) 139

4.3.4.5 Effect of gold loading on CO oxidation activity of Au/Fe-Y (1.88wt%Fe) 143

4.3.4.6 Effect of increasing the Fe content on stability and activity of Au catalyst (containing 3.67wt%Au) 144

4.4 CONCLUSIONS *146*
4.5 REFERENCES *150*

CHAPTER 5 ..... **152**

REDUCTIVE PRE-TREATMENT OF AU/HY AND AU/Y, FOR CO OXIDATION 152
5.1 INTRODUCTION *152*
5.2 EXPERIMENTAL *154*
5.2.1 Support and catalyst preparation 154
5.2.2 UV-Vis spectrophotometry 155
5.2.3 X-ray powder diffraction (XRD) 155
5.2.4 X-ray photoelectron spectroscopy (XPS) 155
5.2.5 Diffuse Reflectance Infrared Fourier Transform spectroscopy 156
5.2.6 ^{197} Au Mössbauer spectroscopy 156
5.3 RESULTS AND DISCUSSIONS *157*
5.3.1 Ultraviolet-visible spectrophotometry (UV-VIS) 157
5.3.2 Inductively coupled plasma (ICP) analysis 158
5.3.3 Temperature-programmed reduction (TPR) and oxidation (TPO). 159
5.3.3.1 TPR and TPO of untreated Au/HY (3.77wt%Au) 159
5.3.3.2 TPR profile trisodium citrate treated Au/HY (3.66wt%Au) ... 161
5.3.3.3 TPR profile of $NaBH_4$ treated Au/HY (3.73wt%Au) 163
5.3.4 X-ray powder diffraction (XRD) 164
5.3.4.1 Effects of temperature on the mobility of Au^0 to the outer surface of zeolite crystal. 164
5.3.4.2 Effects of reducing agents on Au particles size formation on zeolite-HY 165
5.3.5 ^{197} Au Mössbauer spectroscopy 167
5.3.5.1 $[Au(en)_2]^{3+}$/Y (3.02wt%Au, Y same as NaY-zeolite) 168
5.3.5.2 $[Au(CN)_2]^-$/Y (~2wt%Au, Y same as NaY-zeolite) 169
5.3.6 X-ray photoelectron spectroscopy (XPS) 170
5.3.6.1 Untreated Au/HY (3.77wt%Au) 170
5.3.6.2 Au/HY (3.73wt%Au) treated with $NaBH_4$ (mole ratio = 1:1) 171

5.3.6.3 Au/HY (3.75wt%Au) treated with $NaBH_4$ (mole ratio = 1:4) 171
5.3.7 Diffuse Reflectance Infrared Fourier Transform spectroscopy (DRIFTS) 173
5.3.7.1 DRIFTS studies of as-prepared Au/HY (3.73wt%Au), treated with $NaBH_4$ (mole ratio = 1:1). 173
5.3.8 Catalytic activity of Au/Y system 177
5.3.8.1 Activity of ascorbic acid-treated Au/Y system. 177
5.3.8.2 Activity of $NaBH_4$ treated Au/Y system 178
5.3.9 Catalytic activity of the Au/HY system 179
5.3.9.1 Activity of ascorbic acid-treated Au/HY system 180
5.3.9.1.1 Activity of ascorbic acid-treated Au/HY system, in the absence of protecting agents. 180
5.3.9.1.2 Activity of ascorbic acid-treated Au/HY system, in the presence of protecting agents. 182
5.3.9.2 Activity of sodium borohydride-treated Au/HY system 184
5.3.9.2.1 The effects of washing the Au/HY (3.73wt%Au) catalyst after reduction 184
5.3.9.2.2 The effects of washing the Au/HY catalyst before reduction 185
5.3.9.2.3 The effects of $NaBH_4$ mole ratio, on the activity of Au/HY 187
5.3.9.2.4 Activity of $NaBH_4$-treated Au/HY system, effect of reduction temperature 189
5.3.9.3 Activity of trisodium citrate treated Au/HY catalyst 190
5.3.9.4 Effect of reductive pre-treatment of Au prior to ion-exchange on HY, on CO oxidation activity 191
5.3.10 Comparative studies of the reductive pre-treatment of Au supported catalysts prepared from $KAu(CN)_2$, $Au(en)_2Cl_3$ and $HAuCl_4$. 192
5.4 CONCLUSIONS *195*
5.5 REFERENCES *197*

CHAPTER 6 ..... **200**

THE EFFECT OF ALKALI METAL ADDITION ON THE SURFACE'S PROPERTIES OF Y-ZEOLITE AND ACTIVITY OF SUPPORTED GOLD 200

6.1 INTRODUCTION *200*

6.2 EXPERIMENTAL *201*

6.2.1 Support and catalyst preparation 201

6.2.2 Catalyst testing 202

6.2.3 Characterization techniques 202

6.3 RESULTS AND DISCUSSION *202*

6.3.1 X-ray powder diffraction (XRD) 202

6.3.1.1 Gold source, $Au(en)_2Cl_3$ 202

6.3.1.2 Gold source, $KAu(CN)_2$ 204

6.3.1.3 Gold source, $HAuCl_4$ 205

6.3.2 Activity of gold on alkali-modified zeolite-Y 206

6.3.2.1 Effect of Li, Na, and K on activity of gold supported on zeolite-Y (Gold source, $Au(en)_2Cl_3$) 206

6.3.2.2 Effect of Li, Na, and K on activity of gold supported on zeolite-Y (Gold source, $KAu(CN)_2$) 207

6.3.2.3 Effect of Li, Na, and K on activity of gold on supported zeolite-Y (Gold source, $HAuCl_4$) 209

6.3.3 Effect of different sources of gold on the unmodified zeolite-Y ... 211

6.3.4 Effect of different gold sources on the Li-modified zeolite-Y 212

6.3.5 Effect of different gold sources on Na-modified zeolite-Y 213

6.3.6 Effect of different gold sources on K-modified zeolite-Y 215

6.4 CONCLUSIONS *217*

6.5 REFERENCES *219*

CHAPTER 7 ..... **220**

CATALYTIC ACTIVITY OF ZEOLITE SUPPORTED GOLD FOR ETHYLENE HYDROGENATION 220

7.1 INTRODUCTION *220*

7.2 EXPERIMENTAL *221*

7.2.1 Catalyst preparation 221

7.2.2 Catalyst pre-treatments 221

7.2.3 Temperature-programmed reduction (TPR) 221

7.2.4 Catalytic activity 222

7.3 RESULTS AND DISCUSSIONS *223*

7.3.1 Reducibility of catalysts 223

7.3.1.1 Reducibility of gold and transition metals on Au-M/Y (M represent Ni^{2+}, Fe^{3+}, and Cr^{3+}) 223

7.3.1.2 Reducibility of gold from different sources supported on HY and Y 224

7.3.1.2.1 TPR profiles of Au/Y (3.67wt% Au) 224

7.3.1.2.2 TPR profile $NaBH_4$ treated Au/HY (3.73wt%Au) 224

7.3.2 Effects of flow rate on the activity of Au-Fe/Y (3.29wt%Au:1.88wt%Fe) 225

7.3.3 Activities of ethylene hydrogenation over gold/zeolites systems .. 226

7.3.3.1 Effect of temperature on the catalytic activity of Au-Fe/Y (1.67wt%Au:1.88wt%Fe) 226

7.3.4 Effect of Au loading on the activity of Au-Fe/Y (1.88wt%Fe, containing 1.67, 3.29, 5.45, and 7.48wt%Au, $KAu(CN)_2$ as source of gold) 228

7.3.5 Effect of Ni^{2+}, Fe^{3+}, and Cr^{3+} on the activity of Au/Y 229

7.3.5.1 Catalytic activity of Au-M/Y (M represent Ni^{2+}, Fe^{3+}, and Cr^{3+}) at 260 ^{0}C 229

7.3.6 Effect of preparation by using different source of Au supported on Y 232

7.3.7 The effect of $NaNO_3$ on the activity of Au/NaY (0.772wt.%Au, treated with $NaNO_3$, $HAuCl_4$ as the source of gold) 234
7.3.8 Treatment effect of $NaBH_4$ on the activity of Au/Y (3.46wt%Au) and Au/HY (3.73wt%Au) 236
7.3.8.1 $KAu(CN)_2$ as source of gold 236
7.3.8.2 $Au(en)_2Cl_3$ as source of gold 237
7.3.9 The activity of Au-Ni/Y (3.35wt.%Au:1.79wt.%Ni) catalyst submitted to different pre-treatment and running conditions 239
7.3.10 Regeneration of Au-Ni/Y (3.35wt.%Au:1.79wt.%Ni) catalyst under O_2 atmosphere 241
7.3.11 Comparison between ethylene hydrogenation and CO oxidation reactions 243
7.3.11.1 Activity of Au/HY (independent of the source of gold) 243
7.3.11.2 Activity of Au-M/Y (M represent Ni^{2+}, Fe^{3+}, and Cr^{3+}, $KAu(CN)_2$ as source of gold). 243
7.3.11.3 Effect of preparation by using different source of gold 244
7.4 CONCLUSIONS *246*
7.5 REFERENCES *248*

CHAPTER 8 ..... **250**

LOW-TEMPERATURE, WATER-GAS SHIFT REACTIONS OVER AU SUPPORTED ON TiO_2, IN THE PRESENCE OF MODIFIER: EXAFS/XANES ANALYSIS OF GOLD-COPPER ION MIXTURE IN TiO_2 (ANATASE) 250
8.1 INTRODUCTION *250*
8.2 EXPERIMENTAL *251*
8.2.1 Catalyst preparation 251
8.2.2 Characterization techniques 252
8.2.3 Catalyst testing 252
8.2.3.1 In-situ catalyst testing 252
8.2.3.2 Ex-situ catalyst testing 253
8.3 RESULTS AND DISCUSSION *253*

8.3.1 Catalyst characterization 253
8.3.1.1 X-ray fluorescence (XRF) and temperature-programmed reduction (TPR) 253
8.3.1.2 X-ray absorption near-edge structure (XANES) 254
8.3.1.3 Extended X-ray absorption fine structure (EXAFS) 258
8.3.2 Ex-situ catalytic activities 261
8.3.2.1 Quantification of the amount of H_2 produced, during the WGS reaction 261
8.3.3 Effect of modifier on the activity and stability of Au on TiO_2 (anatase). 264
8.3.3.1 Au-Cu^c/TiO_2 (2.84wt%Au:0.32wt%Cu) 264
8.3.3.2 Calcined-[Au-Cu^c/TiO_2 (2.84wt%Au:0.32wt%Cu)] and calcined-Au/TiO_2 (3.95wt%Au) 266
8.3.3.3 Cu^c-Au/TiO_2 (0.44wt%Cu:3.95wt%Au) 268
8.3.3.3.1 Effects of nitrates on as-prepared Cu^c-Au/TiO_2 (0.44wt%Cu:3.95wt%Au) 268
8.3.3.3.2 Effects of nitrates on as-prepared Cu-[calcined-Au/TiO_2 (0.44wt%Cu:3.95wt%Au)] 269
8.3.3.3.3 Effect of pretreatment on Cu-[calcined-Au/TiO_2 (0.44wt%Cu:3.95wt%Au)] at 350 ^{0}C. 270
8.3.3.3.4 Effect of Cu introduced by ion-exchange/deposition-precipitation method on a calcined-Au/TiO_2 (4.09wt%Au) 271
8.3.3.4 Catalysts prepared from Cu containing acetate, i.e. $Cu(OOCCH_3)_2*H_2O$ 273
8.3.3.4.1 Activity of calcined-[Cu^d-Au/TiO_2 (0.44wt%Cu:3.74wt%Au)] 273
8.3.3.4.2 Catalyst regeneration of calcined-[Cu^d-Au/TiO_2 (0.44wt%Cu:3.74wt%Au)] 274
8.3.3.5 Effect of Cu loading on the stability and activity of Au on TiO_2 (anatase, 200m^2/g) 276
8.3.4 Comparison of CO oxidation activity for Au-Cu^c/TiO_2 (2.84wt%Au:0.32wt%Cu) and Au/TiO_2 (3.95wt%Au) at -77 ^{0}C. 277

8.3.5 Preferential oxidation of CO in the presence of excess hydrogen stream over Au-Cu^c/TiO_2 (2.84wt%Au:0.32wt%Cu) and Au/TiO_2 (3.95wt.%Au) at 18 ^{0}C and 100 ^{0}C. 278

8.4 CONCLUSIONS *281*

8.5 REFERENCES *284*

CHAPTER 9 ..... **286**

GENERAL CONCLUSION 286

LIST OF FIGURES

CHAPTER 1 1

CHAPTER 2 9

Figure 2.1: Structure of the faujasite zeolite (left) and the zeolite supercage (right). Positions of cations are identified as types I, II, and III [10b]. 17

Figure 2.2: X-ray photoelectron spectroscopy of Ni $2p_{3/2}$ spectra on Y-zeolite as a function of pre-treatement conditions: (1) 500 ^{0}C, air + He; (2) 400 ^{0}C, H_2 + 400 ^{0}C, O_2; (3) 450 ^{0}C, H_2 + 500 ^{0}C, air [17]. 23

Figure 2.3: TPD spectra of NH_3 from H-ZSM-5 catalyst [11]. 1: Fresh catalyst, 2: deactivated catalyst, 3: partially reactivated catalyst. 30

Figure 2.4: Illustration of the stages in the preparation of supported metal catalysts: the pores of the support are initially impregnated with either a dilute or a concentrated solution of the metal salt [33]. 36

Figure 2.5: Schematic view of E4 X-ray beamline at Hamburg Synchrotron Radiation Laboratory (HASYLAB) at DESY in Hamburg [61]. 46

Figure 2.6: Normalized Cr K-edge profiles, displaced vertically, for the calcium chromate samples and Cr_2O_3, CaCrO4, and Cr metal. Energy scale is relative to the Cr K-edge in metal (5989.0 eV). The spectra were measured at EXAFS 2 beamline in HASYLAB at DESY in Hamburg [61]. 48

Figure 2.7: Schematics of the EXAFS process illustrating the origin of EXAFS oscillations due to the interference of an outgoing and backscattered photoelectron wave [61]. 50

Figure 2.8: Effects of particle size on the activity of titania-supported Au for the oxidation of CO [66] 53

Figure 2.9: CO conversion vs. time on stream at 40 ^{0}C over (a) Au/Y, (b) Au/Y(NP), and (c) [Au/Y(NP)]pH, which contained 0.0006 g of gold [92]. 58

Figure 2.10: Electron micrograph of 14% Ni/Al_2O_3 having undergone extensive carbon deposition during CO disproportionation at 400 ^{0}C, PCO = 4.55 kPa (magnification of 200,000; courtesy: BYU Catalysis Laboratory) [106]. 65

CHAPTER 3 82

Figure 3.1: The optical absorption spectra of [Au(en)$_2$]Cl_3 solution in 100 ml distilled water. 107

Figure 3.2: The optical absorption spectra of the filtrate (approximately 100 ml) after ion-exchange process. 108

Figure 3.3: Schematic diagram of CO oxidation flow chart: (a) Integrator, (b) Gas chromatograph equipped with thermal conductivity detector, (c) Tube reactor equipped with thermocouple, (d) Absorbance materials (activated carbon and NaOH pellets), (e) Gas cylinders. 111

Figure 3.4: An apparatus showing the in-situ cell containing a 13 mm diameter pressed sample disc taken before the start of water-gas shift reaction at Argonne Photon Source (APS), USA 115

CHAPTER 4 117

Figure 4.1: TPR profiles of Au/Y (3.67wt%Au), in the absence of transition metals, Conditions: 200 mg sample, 5%H_2/argon atmosphere (42ml/min) at 50C/min. 121

Figure 4.2: TPR profiles of Au/Ni-Y (3.35wt% Au:1.79wt%Ni), showing the effect of Ni^{2+} on the reduction of gold. Conditions: 200mg sample, 5%H_2/argon atmosphere (42ml/min) at 5^{0}C/min. TPR profile of this sample was recorded at

Northwestern University. Approximately 200 mg of sample was loaded on a U-tube reactor, fitted with molecular sieve to trap moisture..... 122

Figure 4.3: TPR profiles of stabilizing metals (Ni^{2+}, Fe^{3+}, and Cr^{3+}) on Au/Y. Conditions: 100 mg sample, 5%H_2/nitrogen atmosphere (30 ml/min) at 7 ^{0}C/min. The TPR profile of this sample was recorded at the Witwatersrand University. 123

Figure 4.4: TPR profiles of Au/Fe-Y (1.88wt%Fe), showing the effect of gold loading. Conditions: 100 mg sample, 5%H_2/nitrogen atmosphere (30 ml/min) at 7 ^{0}C/min. 126

Figure 4.5: Effect of gold loading on the sintering of gold particles..... 128

Figure 4.6: XRD profile of Au/Y showing the effect of transition metals on the stability of gold particles. 129

Figure 4.7: XRD profile of spent and unspent Au/Y (0.277wt%Au) and Au/HY (0.264wt%Au) respectively, showing the effect of acidity or proton on the particle size of gold. 132

Figure 4.8: Effect of acidity/proton on catalytic activity of Au supported on HY at 450 ^{0}C..... 133

Figure 4.9: Effect of Ni^{2+} ions on the activity of supported Au on Y as a function of temperature..... 135

Figure 4.10: Effect of Fe^{3+} ions on the activity of supported Au on Y (3.67wt%Au) as a function of temperature (3.29wt%Au:1.88wt%Fe). 137

Figure 4.11: Effect of Cr^{3+} ions on the activity of supported Au on Y (3.67wt%Au) as a function of temperature. 138

Figure 4.12: Effect of reduction potentials of transition metals of Ni^{2+}, Co^{2+}, Fe^{3+}, and Cr^{3+}, on the % CO conversion at 200 ^{0}C. 140

Figure 4.13: Effect of Ni^{2+}, Fe^{3+}, and Cr^{3+}, on Au supported on M-Y (M = Ni^{2+}, Fe^{3+}, and Cr^{3+}) system, as a function of temperature..... 141

Figure 4.14: Effect of Ni^{2+}, Fe^{3+}, and Cr^{3+}, on Au supported on M-Y (M = Ni^{2+}, Fe^{3+}, and Cr^{3+}) system, as a function of time on stream at 200 ^{0}C. 142

Figure 4.15: Time on stream CO oxidation activity for Au/Fe-Y, showing the effect of gold content at 200 ^{0}C. 143

Figure 4.16: Effect of Fe content on the activity of the catalyst, as a function of time on stream at 200 ^{0}C. 145

CHAPTER 5 152

Figure 5.1: Time on stream CO oxidation activity for the Au/HY (3.77wt%Au) at 450 ^{0}C. 153

Figure 5.2: TPO profile of 5%H_2/Ar reduced $[Au(en)_2]^{3+}$/HY (3.77wt%Au) sample. The sample was degassed at 150 ^{0}C for 30 minutes under N_2 and oxidized with 5% O_2/He. 160

Figure 5.3: TPR profile of untreated Au/HY (3.77wt%Au). 161

Figure 5.4: TPR profile of Au on HY (3.66wt%Au), treated with tri-sodium citrate. 162

Figure 5.5: TPR profile of Au on HY (3.73wt%Au), treated with $NaBH_4$. 164

Figure 5.6: XRD patterns of: (A) freshly prepared, $NaBH_4$ treated Au/HY (3.73wt%Au) and (B) spent, $NaBH_4$ treated Au/HY (3.73wt%Au) catalyst at 450 ^{0}C. 165

Figure 5.7: XRD patterns of Au/HY catalyst showing the effect of various reducing agents. 166

Figure 5.8: ^{197}Au Mössbauer spectra of $[Au(en)_2]^{3+}$/Y (3.02wt%Au, Y same as NaY-zeolite) at 6 K. Data are black solid circles, and solid lines through the black circles are the overall theoretical fits to the data. Shaded area is the fitted Au-metal (Au^0) component [8]. 168

Figure 5.9: ^{197}Au Mössbauer spectra of $[Au(CN)_2]^-$/Y (~2wt%Au, Y same as NaY-zeolite) at 6 K. Data are black solid circles, and solid lines through the black circles are the overall theoretical fits to the data. Shaded area is the fitted Au-metal (Au^0) component [8]..... 169

Figure 5.10: XPS spectra of untreated Au/HY (3.77wt%Au)..... 170

Figure 5.11: XPS spectra of Au/HY (3.73wt%Au) treated with $NaBH_4$ (mole ratio = 1:1)..... 171

Figure 5.12: XPS spectra of Au/HY (3.75wt%Au) treated with $NaBH_4$ (mole ratio = 1:4)..... 172

Figure 5.13: Drifts spectra of Au/HY (3.73wt%Au) treated with $NaBH_4$ (1:1) showing the changes on surface adsorbed CO as a function of temperature increase, from (1) 22, (2) 120, (3) 200, (4) 250, (5) 300, (6) 350, and (7) 400 ^{0}C respectively..... 175

Figure 5.14: CO oxidation activity of $NaBH_4$ treated Au/HY (3.73wt%Au) as a function of temperature increase, during an in-situ DRIFTS studies. 176

Figure 5.15: Plot of % CO conversion against time on stream showing the activity of $NaBH_4$ treated Au on Y zeolites..... 179

Figure 5.16: Comparison of CO oxidation activity of the ascorbic acid treated Au/HY with that of the untreated Au/HY (3.77wt%Au)..... 181

Figure 5.17: Comparison of the CO oxidation activity for the ascorbic acid-treated Au catalysts in the presence of protecting agents..... 183

Figure 5.18: Comparison of the CO oxidation activity for the $NaBH_4$ treated Au/HY (3.73wt%Au, molar ratio = 1:1) and the untreated Au/HY (3.77wt%Au) catalysts..... 185

Figure 5.19: Time on stream CO oxidation activity for the $NaBH_4$-treated Au/HY (3.77wt%Au) catalyst at 450 ^{0}C, showing the effect of washing before reduction. 186

Figure 5.20: Time on stream CO oxidation for the $NaBH_4$-treated Au catalysts, prepared at various Au/$NaBH_4$ mole ratios: (Au:$NaBH_4$ = 1:1), (Au:$NaBH_4$ = 1:3) and (Au:$NaBH_4$ = 1:4). 188

Figure 5.21: Comparison of the CO oxidation activity for the $NaBH_4$-treated Au catalysts in the presence of protecting agents..... 189

Figure 5.22: Comparison of the CO oxidation activity for the trisodium citrate treated Au/HY (3.66wt%Au, molar ratio = 1:1), untreated Au/HY (3.77wt%Au) and the effect of reduction temperature. 191

Figure 5.23: Comparison of the CO oxidation activity for the $NaBH_4$ treated Au/HY and Au/Y (Au:$NaBH_4$, molar ratio = 1:1, $KAu(CN)_2$ as source of gold). 193

CHAPTER 6 200

Figure 6.1: XRD profile of Au on Y and modified Y-zeolite (2wt%Au), showing the effect of different alkali metals on the size of metallic gold particles. 203

Figure 6.2: XRD profile of Au on Y and modified Y-zeolite (2wt%Au), showing the effect of different alkali metals on the size of metallic gold particles. 205

Figure 6.3: XRD profile of Au on Y and modified Y-zeolite, showing the effect of different alkali metals on the size of metallic gold particles. 206

Figure 6.4: Plot of % CO conversion against time on stream showing the effect of alkali-modified zeolites-Y on the catalytic activity of the gold catalyst..... 207

Figure 6.5: Plot of % CO conversion against time on stream showing the effect of alkali-modified zeolites-Y on the catalytic activity of the gold catalyst..... 208

Figure 6.6: Plot of % CO conversion against time on stream showing the effect of alkali-modified zeolites-Y on the catalytic activity of gold supported on Y-zeolite. 210

Figure 6.7: Comparison of different sources of Au for CO oxidation over gold supported on untreated zeolite-Y (2wt%Au)..... 212

Figure 6.8: Comparison of different source of Au for CO oxidation over gold supported on lithium-modified zeolite-Y (2wt%Au)..... 213

Figure 6.9: Comparison of different source of Au for CO oxidation over gold supported on sodium-modified zeolite-Y (2wt%Au). 214

Figure 6.10: Comparison of different source of Au for CO oxidation over gold supported on potassium-modified zeolite-Y (2wt%Au). 216

CHAPTER 7 220

Figure 7.1: Effect of temperature on the catalytic activity of Au/Fe-Y (1.67wt%Au:1.88wt%Fe) 226

Figure 7.2: Effect of Au loading on the ethylene hydrogenation of Au/Fe-Y at 260 ^{0}C. 229

Figure 7.3: Comparison of ethylene conversion of Au/M-Y (M represent Ni^{2+}, Fe^{3+}, and Cr^{3+}) system at 260 ^{0}C. 230

Figure 7.4: Comparison of ethylene conversion of Au/M-Y (M represent Ni^{2+}, Fe^{3+}, and Cr^{3+}) system at 150 ^{0}C. 232

Figure 7.5: Time on stream ethylene hydrogenation activity for the Au/Y catalysts at 260 ^{0}C, prepared using different source of gold. 233

Figure 7.6: Effect of sodium nitrate on the ethylene hydrogenation activity of Au/NaY (0.772wt%Au, treated with $NaNO_3$) at 260 ^{0}C..... 235

Figure 7.7: Comparison of the ethylene hydrogenation activity for the untreated Au/Y (3.67wt%Au) and Au/Y (3.46wt%Au) treated with $NaBH_4$ (Au:$NaBH_4$ = 1:1). 237

Figure 7.8: Comparison of the ethylene hydrogenation activity for the untreated Au/HY (3.77wt%Au) and Au/HY (3.73wt%Au) treated with $NaBH_4$ (Au:$NaBH_4$ = 1:1). 238

Figure 7.9: Ethylene hydrogenation over Au-Ni/Y (3.35wt%Au:1.79wt%Ni) showing the effect of pre-treatment and working conditions on C_2H_4 conversion. The catalyst pre-treatment and working conditions were performed at the indicated temperatures for each run. 240

Figure 7.10: The effect of oxygen on the regeneration of Au/Ni-Y (3.35wt%Au:1.79wt%Ni) catalyst. 242

CHAPTER 8 250

Figure 8.1: TPR profile of Au-Cu/TiO_2 showing the metal content and the temperature at which Au and Cu have been reduced. 254

Figure 8.2: Au K-edge XANES spectra of Au-Cu^c/TiO_2 (2.84wt%Au:0.32wt%Cu) taken before (1) and during (2) water-gas shift reaction. 255

Figure 8.3: Cu K-edge XANES spectra of as-prepared Au-Cu^c/TiO_2 (2.84wt%Au:0.32wt%Cu) and calcined Cu^d-Au/TiO_2 (3.74wt%Au:0.44wt%Cu) taken during water-gas shift reaction at 200 ^{0}C and after regeneration in O_2/He atmosphere at 300 ^{0}C 257

Figure 8.4: Au K-edge k^2 weighted Fourier Transform of Au/TiO_2 catalyst under: (A) helium @ 22 ^{0}C and (B) during water-gas shift reaction @ 200 ^{0}C. 259

Figure 8.5: Au K-edge k^2 weighted Fourier Transform of Au-Cu^c/TiO_2 (2.84wt%Au:0.32wt%Cu) catalyst under: (A) helium @ 22 ^{0}C and (B) during water-gas shift reaction @ 200 ^{0}C. 260

Figure 8.6: Cu K-edge k^2 weighted Fourier Transform of Au-Cu^c/TiO_2 (2.84wt%Au:0.32wt%Cu) catalyst under: (A) helium @ 22 ^{0}C and (B) during water-gas shift reaction @ 200 ^{0}C. 261

Figure 8.7: Water-gas shift of Au/TiO_2 (reference catalyst, 1.5wt%Au) and Au/TiO_2 (3.95wt%Au), during the quantification of percentage H_2 formed at 200 ^{0}C. 263

Figure 8.8: Calibration curve of H_2 concentration as a function of GC area 263

Figure 8.9: WGS on Au-Cu^c/TiO_2 (2.84wt%Au:0.32wt%Cu) and Au/TiO_2 (3.74wt%Au) at 200 ^{0}C, showing the effect of modifiers on activity and stability of Au. 265

Figure 8.10: Water-gas shift reaction of calcined Cu/TiO_2 (0.32wt%Cu) at 19 ^{0}C, 100 ^{0}C and 200 ^{0}C. The first three points of percentage CO conversions were taken at 19 ^{0}C, second three points at 100 ^{0}C and last three points at 200 ^{0}C..... 266

Figure 8.11: WGS reaction on calcined-[Au-Cu^c/TiO_2 (2.84wt%Au:0.32wt%Cu)] and calcined-Au/TiO_2 (3.95wt%Au) from 100 ^{0}C to 200 ^{0}C and back to 100 ^{0}C and lastly at 200 ^{0}C. 267

Figure 8.12: WGS of Cu^c-Au/TiO_2 (0.44wt%Cu:3.95wt%Au), Au-Cu^c/TiO_2 (2.84wt%Au:0.32wt%Cu) and Au/TiO_2 (3.95wt%Au) at 200 ^{0}C, showing the effect of modifier containing nitrates on activity of gold. 269

Figure 8.13: WGS of as-prepared Cu-[Calcined-Au/TiO_2 (0.44wt%Cu:3.95wt%Au)] and calcined-Au/TiO_2 (3.95wt%Au) at 200 ^{0}C, showing the effect of modifier containing nitrates on activity of gold. 270

Figure 8.14: WGS of Cu-[Calcined-Au/TiO_2 (0.44wt%Cu:3.95wt%Au)] at 200 ^{0}C, before and after treatment in N_2 for 1h at 350 ^{0}C. 271

Figure 8.15: WGS of Cu*-[Calcined-Au/TiO_2 (0.44wt%Cu:4.09wt%Au)] at 200 ^{0}C. * Cu was introduced by ion-exchange/deposition-precipitation method of $Cu(NO_3)_2$*$2.5H_2O$ (99.99% purity, Aldrich,) solution, of which the pH has been

adjusted to 5.0 at 70 ^{0}C for 1.5 h, prior to addition on suspended calcined-Au/TiO_2 (4.09wt%Au), on a doubly distilled water at 40 ^{0}C for 0.5 h. The mixture was kept at 60 ^{0}C for 12 h under constant and vigorous stirring. 272

Figure 8.16: Water-Gas shift activity of calcined-[Cu-Au/TiO_2 (0.44wt%Cu:3.74wt%Au)], calcined-Au/TiO_2 (3.74wt%Au), Cu^c-Au/TiO_2 (0.44wt%Cu:3.95wt%Au) and Au/TiO_2 (3.95wt%Au) at 200 ^{0}C, showing the positive role of Cu in the absence of nitrates. 274

Figure 8.17: Regeneration of Calcined-[Cu^d-Au/TiO_2 (0.44wt%Cu:3.74%wtAu)] in 2.5%O_2/He at 300 ^{0}C for 1 h. 275

Figure 8.18: Water-gas shift activity of calcined-[Cu^d-Au/TiO_2 (0.22wt%Cu:3.74wt%Au)], calcined-[Cu^d-Au/TiO_2 (0.44wt%Cu:3.74wt%Au)], and calcined-[Cu^d-Au/TiO_2 (0.88wt%Cu:3.74wt%Au)] at 200 ^{0}C, showing the effect of Cu loading on the catalytic activity of Au on TiO_2. 276

Figure 8.19: Time on stream CO oxidation of Au-Cu^c/TiO_2 (2.84wt%Au:0.32wt%Cu) and Au/TiO_2 (3.95wt%Au) at -77 ^{0}C..... 278

CHAPTER 9 286

LIST OF TABLES

CHAPTER 1 ..... **1**

CHAPTER 2 ..... **9**

Table 2.1: Comparison of some surface analysis methods *20*

Table 2.2: Chemical shifts of inner levels of transition elements, due to valence state changes of transition elements in zeolites [17]. *22*

CHAPTER 3 ..... **82**

Table 3.1: Metal loading of Au/Fe-Y sample *87*

Table 3.2: Metal loading of Au/Cr-Y sample *88*

Table 3.3: Metal loading of Au/Ni-Y sample *88*

Table 3.4: Metal loading of Au/Co-Y sample *89*

Table 3.5: Au content (wt%) and observed steady state activity for CO oxidation[a] *92*

Table 3.6: Au content (wt%) and observed steady state activity for CO oxidation[a] *94*

Table 3.7: Au content (wt%) and observed steady state activity for CO oxidation[a] *97*

Table 3.8: Au and Cu content (wt%) and observed steady state activity for WGSR[a] *101*

CHAPTER 4 ..... **117**

CHAPTER 5 ..... **152**

Table 5.1: Parameters of the sub-components in the overall fits of the two gold samples [8]. *167*

CHAPTER 6 ..... **200**

CHAPTER 7 ..... **220**

Table 7.1: Comparison of ethylene hydrogenation to CO oxidation reaction over gold supported catalysts, with or without promoters. *245*

CHAPTER 8 ..... **250**

Table 8.1: Effects of Cu on Au/TiO_2 for preferential oxidation CO in the presence of excess hydrogen *280*

CHAPTER 9 ..... **286**

LIST OF ABBREVIATIONS

AA	Ascorbic Acid
AES	Atomic Emission Spectroscopy
AFROX	African Oxygen LTD
Au	Gold
Al-O	Alumina and Oxygen bond
BE	Binding energy
Cl_2	Chloride
CN	Cyanide
CO	Carbon monoxide
Co	Cobalt
CO_2	Carbon Dioxide
Cr	Chromium
Cu	Copper
Drifts	Diffuse Reflectance Infrared Fourier Transform Spectroscopy
E_a	Activation energy
en	Ethylenediamine
ESR	Electron Spin Resonance
EXAFS	Extended X-Ray Absorption Fine Structure
Fe	Iron
FID	Flame Ionisation Detector
GC	Gas Chromatography
HOMO	Highest Occupied Molecular Orbital

HRTEM	High Resolution Transmission Electron Microscopy
HY	Proton containing Y-type zeolite
H_2	Hydrogen
h	Hour(s)
I_2	Iodine
ICP	Inductively Coupled Plasma
IR	Infra-red
ISS	Ion Scattering Spectroscopy
K	Potassium
KY	Type-Y zeolite containing K
L	Ligand
Li	Lithium
LiY	Type-Y zeolite containing Li
LUMO	Lowest Unoccupied Molecular Orbital
M	Transition Metals
MgO	Magnesium Oxide
Mn	Manganese
m.p.	Melting point
min.	Minute(s)
Na	Sodium
$NaBH_4$	Sodium Borohydride
Na_3-Citrate	Tri-Sodium Citrate
NaY	Type Y zeolite treated with $NaNO_3$

Ni	Nickel
NMR	Nuclear Magnetic Resonance
O_h	Octahedral
O_2	Oxygen
PEG	Polyethylene Glycol
Pt	Platinum
ppm	Parts per million
SFG	Sum Frequency Generation
SIMS	Secondary ion mass spectroscopy
S_{CO2}	Selectivity to carbon dioxide
Si/Al	Silica/alumina ratio
Si-O	Silica and Oxygen bond
T	Temperature
Type I, II, and III sites	Positions of cations within fajausite zeolite supercages
TCD	Thermal Conductivity Detector
TEM	Transmission Electron Microscopy
TiO_2	Titanium Dioxide
TPO	Temperature Programmed Oxidation
TPR	Temperature Programmed Reduction
T-O	Transition metals and Oxygen bond
UHP	Ultra High Purity
UV-Vis	Ultraviolet-Visible Spectroscopy
WGSR	Water-gas shift reaction

Wt.%	Percentage by weight
XANES	X-ray Absorption Near-Edge Structure
XAS	X-ray Absorption Spectroscopy
XPS	X-ray Photoelectron Spectroscopy
XRD	X-ray Diffraction
XRF	X-ray Fluorescence
% CO	Percent Carbon monoxide
% O_2	Percent Oxygen
Y	Y-zeolite (LZY52)

CHAPTER 1

INTRODUCTION

1.1 HISTORICAL BACKGROUND

During the last 20 years, there has been a rapid growth in interest in the topic of catalysis by gold [1-3]. Initially, most of this interest has been focused on the exciting discovery that supported gold catalysts, in particular Au/TiO_2 and Au/Fe_2O_3, could oxidize CO to CO_2 at and below ambient temperature [4-6]. Since 1998, there have been many reports on the preparation of highly dispersed gold and its catalytic applications [7-9].

1.1.1 Gold supported on metal oxide

Haruta *et al.*, improved the preparation of very small supported gold clusters and they report that gold is remarkably active for low temperature CO oxidation when it is well dispersed and deposited on various metal oxides or hydroxides of alkaline-earth metals [10, 11, 12]. This surprising activity is now being studied by other groups, because the low temperature CO oxidation is an attractive way of purifying air in houses and offices, of reducing CO in industrial and automobile emissions, and also finds applications in CO detection devices, etc. Haruta *et al.*,

have shown that gold is also active for the catalytic combustion of hydrocarbons, NO reduction, etc [11].

1.1.2 Gold supported on zeolites

Very few investigations have been reported on gold contained in zeolites, though Au/zeolite systems should be good model catalysts for CO oxidation. The first work concerning gold clusters supported on zeolites was reported by Boudart and Meitzner [13]. They found that the size of gold particles in Y faujasite was compatible with their location inside the zeolite lattice. However, the clusters were thermally unstable, and their size increased with thermal treatment. They concluded that this was due to the migration of the particles to the outside of the zeolite crystallites.

Ichikawa *et al*. [14-16] investigated gold supported on Y zeolites prepared by dispersing spontaneously a monolayer of $AuCl_3$ on zeolite powder. They found that a solid-vapour reaction at an ambient temperature is an efficient method for producing large amounts of active Au(I) ions and it was also noted that the introduction of coordinatively unsaturated Au(I) into Y zeolite enhanced the ability of the catalyst to adsorb CO. Kang *et al*. [17 - 19] prepared Au/Y and Au/Fe-Y catalysts by ion-exchange from a solution of $HAuCl_4$. On pure Au/Y, they obtained gold particles of 10 - 40 nm, in size while in the presence of iron, the mean diameter decreased to 5 - 8 nm. Their results suggested that the presence of iron retards the sintering of metallic gold during the preparation step.

Guillemot *et al*. [20] have prepared gold nanoparticles inside HY zeolite supercages using a new method involving the autoreduction of gold, $[Au(en)_2]^{3+}$ by its own ligand (i.e. bisethylenediamine). They found gold particles in the range of 2 - 3 nm, and 80% of these were reported to be below 2 nm and located inside the zeolite supercages, proven by TEM microtomy and ^{129}Xe NMR studies [20]. However, Guczi *et al*., found that gold particles in the presence of iron are larger than those measured in a Au/HY sample [21].

There is therefore contradictory data on the activity/structure relationship encountered for gold-zeolites, but overall very few accounts of the behaviour of such systems are available. It was noted that gold sources often contain gold in anionic form, e.g. $[Au(CN)_2]^-$, $[AuCl_4]^-$. Cationic complexes are less available, but $[Au(en)_2]^{3+}$ is known, as is $[Au(PPh_3)_2]^+$. In this thesis the comparison between anionic and cationic species of gold as precursors was taken into consideration.

1.2 THESIS STRUCTURE

In this thesis the catalytic activity of gold/zeolite systems (Au/HY, Au/Y and Au/M-Y, where Au represents gold from either $KAu(CN)_2$, $Au(en)_2Cl_3$ or $HAuCl_4$ and M = Ni^{2+}, Fe^{3+}, Co^{2+} and Cr^{3+}) have been investigated for the CO oxidation and the ethylene hydrogenation reaction. Cu promoted Au/TiO_2 systems have been investigated for water-gas shift, CO oxidation, and preferential oxidation of CO in excess H_2. To put the work in perspective a short review of the literature reports on supported gold catalysts is given (Chapter 2).

The literature survey was evaluated with respect to the following topics: (a) Catalysis on zeolites, (b) Catalysis at surfaces (studies of surface reactions on Zeolites), (c) CO oxidation reactions in general, (d) Ethylene hydrogenation reactions in general, (e) Gold catalyzed reactions in general, (f) Supported metal catalysts; (g) Surface characterization of supported gold catalysts; (h) Water-gas shift reactions; and the (i) Preferential oxidation of CO in excess H_2. The reviews on the above topics were undertaken with respect to the work done in this thesis.

The synthesis, preparation, characterization and catalytic activity of gold/zeolite systems (Au/HY, Au/Y, Au/LiY, Au/KY, Au/NaY and Au/M-Y, where Au represents gold from either $KAu(CN)_2$, $Au(en)_2Cl_3$ and $HAuCl_4$ and M = Ni^{2+}, Fe^{3+}, Co^{2+} and Cr^{3+}) and that of Cu promoted Au/TiO_2 systems, were undertaken. The results of this study will be presented in Chapter 3.

Gold nanoparticles were introduced on to NaY-zeolite supercages, using the incipient-wetness to impregnation method from potassium dicyanoaurate, $KAu(CN)_2$ and its catalytic activity for CO oxidation was undertaken. In this catalyst the source of gold used is chloride free, since chlorides poison the gold, necessitating a thorough washing as part of the synthesis procedure.

The addition of transition metals such as Ni^{2+}, Fe^{3+}, Co^{2+} and Cr^{3+}, as stabilizing metals before introducing gold onto Y was also taken into consideration (i.e., Au/M-Y and M/Au-Y respectively, where M = Ni^{2+}, Fe^{3+}, Co^{2+} and Cr^{3+}). Different concentrations of catalyst metal (i.e., Au) and stabilizing metal were

introduced and the behaviour of the catalysts was investigated for CO oxidation. The results of this study are presented in chapter 4.

Samples of Au/HY and Au/Y were prepared by ion-exchange in HY and Y using a trichlorobisethylenediamine gold complex, $Au(en)_2Cl_3$, and these were treated with various reducing agents (such as $NaBH_4$), to yield highly stable gold nanoparticles on HY-zeolite cages. The mole ratio of reducing agent (i.e., $NaBH_4$) was also studied with the hope of completely reducing gold to an active species (e.g. Au^+/Au^o), which might render an improved activity.

The role played by the source of gold have also been investigated, and in this case Au/HY and Au/Y catalysts where prepared from $HAuCl_4$ and $KAu(CN)_2$ and then reduced with either ascorbic acid or sodium borohydride, with the hope of reducing Au and hence improving the catalytic activity. CO oxidation was undertaken as the test reaction. The results of this study are presented in Chapter 5.

The modification of zeolite-Y by treatment with different alkali metal nitrates such as $LiNO_3$, $NaNO_3$ and KNO_3 before introducing gold (intended gold loading = 2wt%Au) from different sources, (i.e., $Au(en)_2Cl_3$, $HAuCl_4$ and $KAu(CN)_2$), in order to further our understanding of the role played by alkali metals and CO oxidation was undertaken as the test reaction. The results of this study are presented in Chapter 6.

In chapter 4, 5, and 6 several studies on CO oxidation were undertaken on gold/zeolite system that comprised [(Au/HY, Au/NaY treated with $NaNO_3$); and Au/M-Y (M represents Ni^{2+}, Fe^{3+}, or Cr^{3+})] and it was found that gold/zeolite systems are active catalysts for CO oxidation, with an activity depending on the source of gold, pre-treatment conditions and the support used. Herein we report on the catalytic behaviour of the same catalyst used for CO oxidation in ethylene hydrogenation, and our attempts to try to access whether ionic species (Au^{3+} or Au^{+}) or Au^{o} on zeolites are responsible for the ethylene hydrogenation reaction, as is speculated for CO oxidation. The results of this study are presented in Chapter 7.

Finally, Au/TiO_2 and Cu promoted Au on TiO_2 catalysts have been investigated for Low-Temperature Water-Gas Shift reaction, CO oxidation, and the preferential oxidation of CO in excess H_2. The state and role of both Au and Cu supported metals have been elucidated using in-situ XANES/EXAFS spectroscopy. Promotional effects of Cu have only been observed for the Water-Gas Shift reaction. The results of this study are presented in Chapter 8.

In this thesis; figures, schemes, and tables are integrated within the text, followed by a detailed listing of the references at the end of each chapter.

1.3 REFERENCES

[1] G.J. Hutchings, Gold Bull. **29** (1996) 123.

[2] G.C. Bond, D.T. Thompson, Catal. Rev. Sci. Eng. **41** (1999) 319.

[3] G.C. Bond, D.T. Thompson, Gold Bull. **33** (2000) 41.

[4] M. Haruta, T. Kobayashi, H. Samo, N. Yamada, Chem. Lett. (1987) 405.

[5] M. Haruta, N. Yamada, T. Kobayashi, S. Ijima, J. Catal. **115** (1989) 301.

[6] M. Haruta, S. Tsubota, T. Kobayashi, H. Kageyama, M.J. Genet, B. Delmon, J. Catal. **144** (1993) 175.

[7] I. Eskendinov, N.J. Coville and V. D. Sokolovskii, Catal. Lett., **35** (1995) 83.

[8] R.D. Waters, J.J. Weimer and J. E. Smith, Catal. Lett., **30** (1995) 181.

[9] M. Haruta, A. Ueda, S. Tsubota and R. M. Torres Sanchez, Catal. Today, **29** (1996) 443.

[10] M. Haruta, T. Kobayashi, S. Iijima and F. Delannay, Chem. Lett., **3** (1988) 206.

[11] M. Haruta, T. Kobayashi, S. Tsubota, H. Kageyama, M. J. Genet and B. Delmon, J. Catal., **144** (1993) 175.

[12] S. Tsubota, D. A. H. Cunningham, Y. Bando and M. Haruta, in Preparation of Catalysis VI, ed. G. Poncelet, Elsevier Science, Amsterdam, (1997) 227.

[13] M. Boudart and G. Meitzner, in EXAFS and Near Edge Structure III, ed. K. O. Hodgson, B.Hedman and J.E. Penner-Halm, Springer, Berlin, (1984) 217.

[14] S. Qui, R. Ohnishi, M. Ichikawa, J. Chem. Soc., Chem. Commun. (1992) 1425.

[15] T.M. Salama, T. Shido, H. Minagawa, M. Ichikawa, J. Catal. **152** (1995) 322.

[16] T.M. Salama, R. Ohnishi, T. Shido, M. Ichikawa, J. Catal. **162** (1996) 169.

[17] Y-M. Kang, B-Z. Wan, Appl. Catal. A: General **128** (1995) 53.

[18] Y-M. Kang, B-Z. Wan, Catal. Today **26** (1995) 59.

[19] Y-M. Kang, B-Z. Wan, Catal. Today **35** (1997) 379.

[20] D. Guillemot, V. Y. Borovkov, V. B. Kazansky, M. Polisset-Thfoin, J. Fraissard, J. Chem. Soc., Faraday Trans. **93** (1997) 3587.

[21] D. Horvath, M. Polisset-Thfoin, J. Fraissard, L. Guczi, Solid State Ionics, **141** (2001) 153.

CHAPTER 2

LITERATURE SURVEY

2.1 CATALYSIS ON ZEOLITES

2.1.1 Introduction

Aluminosilicates are amorphous, and much interest has been shown since the 1960's in crystalline aluminosilicates having the general formula $M_{\upsilon}(AlO_2)_x(SiO_2)_y.zH_2O$. These are known as zeolites, where M is a monopositive cation (e.g sodium or ammonium), υ equals to x; for divalent cations, υ equals $^{x}/_{2}$ (e.g. Ni^{2+}, or Co^{2+}) and so on [1]. Mordenite and faujasite are some of the classes of zeolite, and here are of great interest as catalysts. The basic unit of faujasite is the regular cubo-octahedron or sodalite unit consisting of 24 tetrahedral of either SiO_4^{4-} or AlO_4^{5-}.

The A-zeolite (y/x = 1) and X (y/x = 1.5) or Y-zeolite (y/x = 1.5 – 3) are the two general structures known, differing on how their sodalite units are joined together. Most of the literature review in this thesis will be focused on the Y-zeolites (joined together through hexagonal faces), since the experimental studies in this thesis were undertaken on this form of zeolite.

Zeolites have a very high internal surface area in the form of pores of fixed geometry and the effective pore diameter is determined by the kind of cation that balances the negative charge on the structure. Catalytic activity depends heavily on the nature of cation, which also affects the acidity of the hydroxyl groups.

2.1.2 Cations in zeolite

The ability of the zeolite skeleton to donate electron density to a cation coordinated at the cation position of the zeolite is important for the oxidation or reduction of the transition metal cation. The zeolite skeleton acts as a “buffer”, compensating the changes resulting from acceptance or donations of electron by the cations by greater or smaller donation of electron density [2, 3]. As mentioned above the lowest unoccupied molecular orbital (LUMO) is localized on cations located at the cation positions of the zeolite. Thus, the cations represent electron acceptor sites in the zeolite during interaction of the molecules with the zeolite.

It follows from the LUMO energies for zeolite clusters with various cations that the zeolite with alkali metal cation (the LUMO consists primarily of the s-AO of the cation) exhibits a lower ability to accept electrons (lower Lewis acidity) than cations of alkaline earth metals (Mg and Ca), and especially Al cations, which are assumed to be important Lewis sites on the zeolite [4-6]. The ability of the zeolite with a transition metal cation to accept or donate electron density depends markedly on the oxidation state of the cation.

For example, following the highest occupied molecular orbital (HOMO) and LUMO energies of zeolite clusters with Cu(I) or Cu(II) cations, that while the Cu(I) cation in the zeolite exhibits a tendency to donate electron density (i.e. to be oxidized), the Cu(II) cation rather exhibits a tendency to accept electron density (i.e. to be reduced) [2]. It was also reported that the Cr(II), Cr(III) and Ni(I) cations exhibit a tendency to donate electron density (i.e. to be oxidized), while the Cr(IV), Cr(VI), Fe(III) and Co(III) cations tend to accept electron density (i.e. to be reduced).

2.1.3 Hydroxyl groups in zeolite

Polyvalent cations localized in zeolites can split an H_2O molecule to form a cationic and a skeletal OH group [4-6]. For the application of zeolites in catalytic processes, it is necessary to know the properties of these cationic OH groups from the point of view of their participation in catalytic reactions. At the same time, the cationic OH group represent a fourth, additional ligand on the cation localized in the zeolite.

The skeletal OH groups of the zeolite are very important active sites participating in the great majority of catalytic processes occurring on zeolites [4, 6]. They constitute Bronsted acids sites, whose properties (acidity) are influenced by a number of factors, such as Si/Al ratio, various cations localized at the zeolite cation positions or by partial dehydroxylation of the zeolite. It is also important to

know which types of O atoms participate in the formation of OH groups, primarily because of their availability for the interacting molecules.

2.1.4 The stability of the zeolite skeleton

Catalytic reactions that occur in zeolite pores increase the active surface area of the zeolite catalyst considerably, and the reacting molecules are subject to the effect of the electrostatic field of the zeolite skeleton. The dimensions of the zeolite channels may be such as to cause steric hindrance of the formation of the product molecules in the catalytic reaction. It is apparent, therefore, that utilization of a zeolite in a certain catalytic process demands that the skeleton should exhibit both the necessary structural and physicochemical characteristics and sufficient structural stability to be capable of withstanding the rigorous hydrothermal conditions of catalytic processes and regeneration cycles.

It has been reported that the isomorphous substitution of Al(III) for Si(IV) results in a decrease in the bonding energy of the cluster by about 1600 kJ/mol, and the actual value depends on the initial Si/Al ratio, which leads to destabilization of the zeolite skeleton [7]. Calculations indicate that the skeletal Si-O bonds are generally much stronger than the Al-O bonds and are independent of the Si/Al ratio or the type of cation or proton. This confirms the well-known fact that the stability of the zeolite skeleton increases with increasing Si/Al ratio.

Transfer of electron density from the skeleton to the cations leads to a weakening of the T-O bonds of those O atoms that participate in the coordination of the cation. A higher electron accepting ability of the cation, results in an increase in the degree of weakening of the T-O bond. Protonation of the skeletal O atoms (formation of OH groups) always leads to weakening of the already weak Al-O bonds and thereby destabilizes the zeolite skeleton [7]. This explains the general lower structural stability of the H-forms of zeolites as compared with those of the cationic forms.

2.1.5 Zeolite modification

The H-forms of zeolites can be modified by thermal treatment (above 400 ^{o}C), leading to partial or complete dehydroxylation with the formation of tricoordinated Al and Si and these leads to the formation of Lewis sites in the zeolite (scheme 2.1) [4, 6].

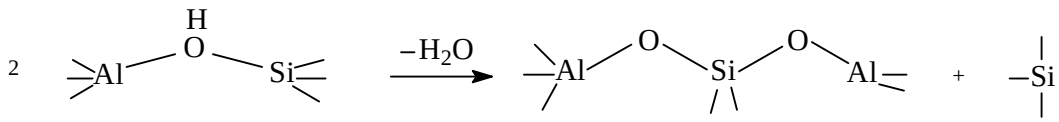

Scheme 2.1: Dehydroxylation of H-forms of zeolite

2.1.6 Zeolite containing nickel, and iron ions as catalysts

2.1.6.1 Oxidation of carbon monoxide

Roginski et al., have investigated the oxidation of carbon monoxide on Y zeolites containing transition metal ions and they found the sequence of activity of these zeolites to be: Ag ~ Co > Cu > Cr > Ni >Fe > Na > Mn [7]. In a similar study on X and Y zeolites, Kubo et al., found a high oxygen adsorption on iron-containing zeolite, while that on cobalt zeolites is low, and on those containing nickel it is near zero [8]. It was reported that the reaction is first order with respect to oxygen and the authors assume that the oxidation proceeds via the Rideal-Eley mechanism as presented in scheme 2.2.

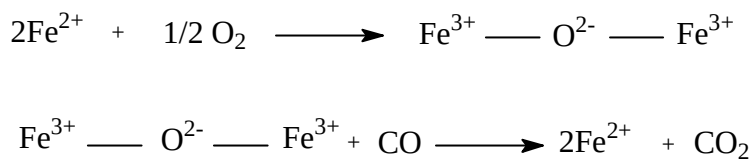

Scheme 2.2: Rideal-Eley mechanism, of CO oxidation on Fe^{n+} (n =1, 2) exchanged in zeolite Y.

Maximum activity in these reactions was found to be displayed by metal ions with intermediate redox potentials (e.g Fe^{2+}), while those of high redox potential (e.g. Co^{2+}, Mn^{2+}) are unable to adsorb oxygen efficiently.

2.1.7 Properties of nickel, iron, and chromium in zeolite

2.1.7.1 Nickel

2.1.7.1.1 Formation and location of Ni^{2+} in Y-zeolites

Ni^{2+} is usually introduced into the zeolite lattice using a dilute (0.005 M) solutions of nickel salts in order to eliminate side reactions during the ion-exchange process.

2.1.7.1.2 Reducibility of nickel ions in Y-zeolite

The reducibility of Ni^{2+} is strongly increased in the presence of atomic hydrogen [9]. Heavy metal ions introduced into a zeolite lattice by ion-exchange are surrounded by oxygen ions of the aluminosilicate lattice and, when no dehydration process was applied after the exchange, by water molecules. The reducibility of Ni^{2+} in faujasite (X and Y) is strongly influenced by the presence of a second cation in the lattice [9]. This was shown by Gullieux et al., for the case of Ni-Pt/X and Ni-Ce/X zeolites. At a reduction temperature of 523 K, the reduction degree of Ni^{2+} was distinctly higher in Pd- and Pt-containing X zeolites than that in the zeolite containing Ni alone and no alloy was observed at that temperature.

2.1.7.2 Iron

2.1.7.2.1 Formation and location of Fe^{3+} and Fe^{2+} in Y zeolites

Preparation of zeolites with Fe ions at the cationic sites poses some difficulties, because of the easy hydrolysis of Fe^{2+} and Fe^{3+} ions and the instability of the zeolite structure in acid media, such an example being zeolite-Y which is stable up to a pH of 4. The direct introduction of Fe^{3+} into Y zeolite cationic sites is attainable without structural collapse by maintaining a low concentration of Fe^{3+} ions (at higher Fe^{3+} loading, the formation of hydroxo-oxidic species increases and partial breakdown of the zeolite structure occurs) in the exchange solution (0.01 – 0.001 M), at room temperature and at short duration of the ion-exchange (evidenced by Mössbauer spectra and by the ESR signals) [7].

A major fraction of Fe^{2+} ions in dehydrated Y zeolites was confirmed by Mössbauer spectroscopy to be coordinated in high-spin O_h complexes with skeletal oxygen atoms within a hexagonal prism at the type I site. The IR spectra of CO adsorbed on Fe^{2+} ions in Y zeolite (IR band at 2195 cm^{-1}) were considered to be evidence of the presence of Fe^{2+} ions at accessible type II sites (figure 2.1) [10, 11]. However the exact position of cation in zeolite must be treated with care, since it is generally known that counter ions migrate easily throughout the zeolite structure, due to the character and concentration of adsorbates, the conditions of pre-treatment of zeolite, the presence of other cations, etc.

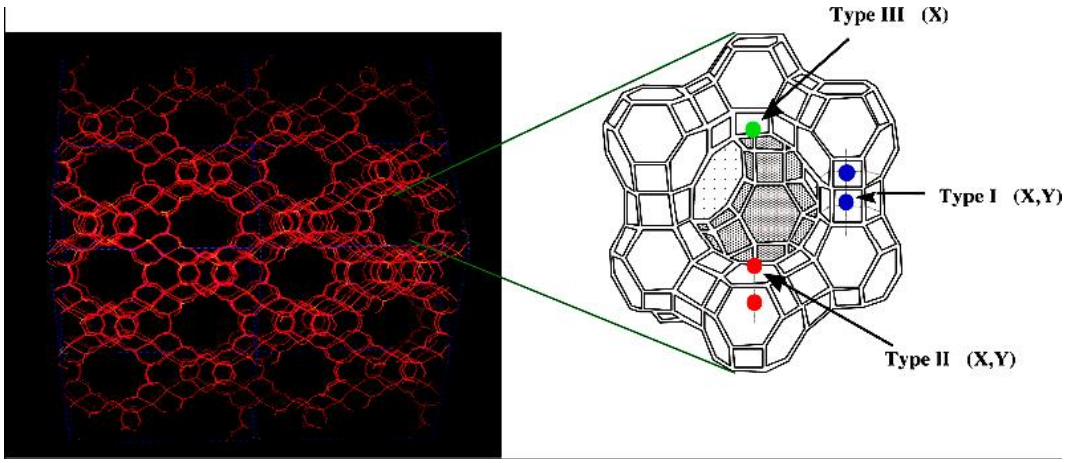

Figure 2.1: Structure of the faujasite zeolite (left) and the zeolite supercage (right). Positions of cations are identified as types I, II, and III [10b].

2.1.7.2.2 Reducibility of iron ions in Y-zeolites

Fe^{3+} is easily reduced to Fe^{2+} in zeolites, regardless of the cationic or hydroxo-oxidic form, but there is contrary to the fact that the second step, i.e. reduction to the metal, does not occur when dihydrogen or CO is used at temperatures up to 1000 K [12a, 12b].

2.1.7.3 Chromium

2.1.7.3.1 Formation and location of Cr^{3+} and Cr^{2+} in Y zeolites

The introduction of Cr^{3+} and Cr^{2+} ions into the cationic sites of Y zeolites is not difficult, compared with the introduction of Fe ions, because of the lower tendency for hydrolysis of Cr to occur when exchanged at pH 4 [7]. The Y zeolite structure is stable up to 50% Cr ion-exchange. It was found that the Cr^{3+} (as well

as Cr^{2+} after zeolite reduction) in Y zeolites is located predominantly at the type I site, the type II sites being occupied by Na^{+} alone (figure 2.1). However, a study of CO adsorption on Cr, H-Y zeolites has revealed the presence of Cr ions in the large cavities, too [7].

2.1.7.3.2 Reducibility of chromium ions in Y zeolites

Cr^{3+} ions are reduced to Cr^{2+} in the bulk of the zeolite, as well as in its surface layers, in a hydrogen or carbon monoxide atmosphere and is complete at a temperature of 770 K [13, 14].

2.2 CATALYSIS AT SURFACES

2.2.1 Introduction

Over the past decades heterogeneous catalysis has been empowered with qualitatively new concepts on the nature and structure of catalytically active centres in several reactions. This is possible due to the extensive use of new physical methods which can provide information on the atomic and electronic structures, and the chemical compositions of the surface and near-surface layers (0.5-3 nm) of solids [15a, 15b]. Progress has been made in developing methods which give information on the sizes and structures of small surface clusters in a subcrystalline state. These are EXAFS, RED, emission electron spectroscopy (XPS, AES, UPS), secondary ion mass spectrometry (SIMS) and high resolution

electron microscopy (HRTEM). With these techniques it has been possible to differentiate the states of components in the surface layers of catalysts and the nature of their bonds with reacting molecules.

2.2.2 Studies of surface reactions on zeolites

Among the methods used for analysis of the surface of multi-component polycrystalline catalysts, the most advanced is X-ray photoelectron spectroscopy [15a, 15b, 16], which has some important advantages, such as surface sensitivity (2-3 nm), the capability of giving direct information on the valence states, the effective charges, the bond ionicities and the band energy structures of solid catalysts. XPS is applicable for studies of almost all elements of the Periodic Table and allows quantitative analysis of surface and adsorption layers. Some characteristics of XPS and other surface analysis methods are presented in Table 2.1 [17].

Table 2.1: Comparison of some surface analysis methods

Method	Basic information	Element	Analysis Depth	Spatial resolution	Dielectric analysis
XPS*	Valence state, Surface comp.	All elements except H, He	1-3 nm	1-2 mm	Easy to perform, small extent destruction
AES*	Adsorbate phase, Surface composition	All elements except, H, He, Li	0.5-3 nm	50-500 nm	Possible with charge compensation
SIMS*	Adsorbate phase	All elements	0.3-2 nm	0.1 μm	Sample sputtering
ISS*	Surface composition	All elements	1-20 monolayer	100 μm	Ion-stimulated effects

* XPS = X-ray photoelectron spectroscopy, AES = Atomic emission spectroscopy, SIMS = Secondary ion mass spectroscopy, ISS = Ion scattering spectroscopy.

Earlier studies on zeolite catalysts by XPS made possible the establishment of the nature of the cation-zeolite framework bond, the demonstration of regularities as function of the valence state of transition elements (Cr, Fe, Ni, Co, Pd, Pt, Ag, Cu)

and their migration to the external surface, the revelation of a correlation between the XPS data and those obtained from zeolite catalytic studies in reactions of oxygen isotopic exchange, and others [17].

Minachev et al., have studied a wide range of problems relating to the formation and action of zeolite catalysts using XPS and other surface analysis techniques and these include:

- The surface compositions of zeolites of different structures, including highly siliceous zeolites of the pentasil family,
- The state of framework components and cation-zeolite framework bonds,
- The states of metals and ligands in complexes synthesized in a zeolite matrix,
- The reducibility of transition metal ions in mono- and bimetallic faujasite forms,
- The interaction of highly dispersed metal particles with the zeolite framework,
- Adsorbed forms of reactants.

Catalyst systems based on zeolites are highly modified, with both the zeolite framework (removal of Al) and the centres bound to cations (ion-exchange, complexation or the surface adsorption of transition metal complexes (TMC)) being modified. These completely change the distribution of active centres throughout the crystal.

2.2.2.1 State of transition elements in zeolites

It has been reported that transition metal cations may be distributed non-uniformly throughout a zeolite, unlike alkaline and alkaline earth elements. Further, zeolite heat treatment leads to a uniform cation distribution and these was also observed for samples containing two different transition cations [17]. Transition elements (Cr, Fe, Co, Ni, and Cu) located as isolated ions, as well as non-transition metal cations favour ionic bonds with the zeolite framework. This type of interaction is also characteristics of complex cations of Pd, Ru and Rh [18, 19].

Minachev et al. [17] have undertaken the X-ray photoelectron spectroscopy of the nickel in Y-zeolite, as a function of pre-treatment conditions (figure 2.2). In all cases the spectra of the Ni $2p_{3/2}$ level for nickel in Y zeolite, has shown that the formal degree of nickel oxidation is quite common (+2). However, the effective charge and spin density on the Ni were different, and in the case of dehydrated samples (500 ^{0}C, air), Ni occurs as individual Ni^{2+} cations interacting with O^{2-} of the zeolite framework. With redox treatment the dispersity of the resulting NiO was found to be high, due to its interaction with zeolite acidic centres. The effective charge on the Ni is increased which resulted in a positive shift (increase in binding energy) in the Ni $2p_{3/2}$ spectra.

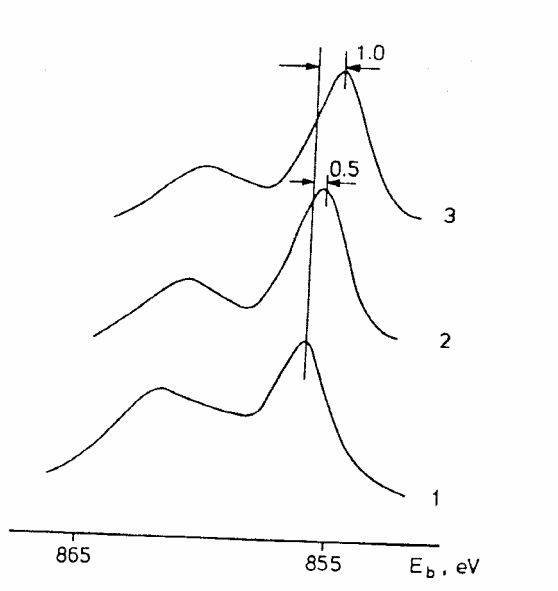

Figure 2.2: X-ray photoelectron spectroscopy of Ni $2p_{3/2}$ spectra on Y-zeolite as a function of pre-treatement conditions: (1) 500 ^{0}C, air + He; (2) 400 ^{0}C, H_2 + 400 ^{0}C, O_2; (3) 450 ^{0}C, H_2 + 500 ^{0}C, air [17].

2.2.2.2 Factors affecting the redox ability and migration of transition metals to the external surface

The state and distribution of the metals in the structure may vary strongly with the treatment of the sample. This is essential for complex ions in particular: ligands undergoing decomposition and removal may interact directly with the metal, affecting its state.

The chemical shifts observed following changes in the states of transition elements in zeolites are shown in table 2.2 and these in many cases is sufficient for the degree of reduction to be estimated quantitatively [17]. It was noted that many metals (Ni, Cu, Ru, Rh, Re) may have an intermediate state (M^{1+}), which can be stabilized by the zeolite framework field and the stability of these states is also affected by the second metal or by available ligands. The XPS of Ni $2p_{3/2}$ observed on the interaction of Ni-containing zeolite with CO, has shown the transition from Ni^{2+} to Ni^{+} and the presence of the second metal was found to affect the temperature range of Ni^{+} stability, with Cr promoting the formation of Ni^{+} at 250 ^{0}C.

Table 2.2: Chemical shifts of inner levels of transition elements, due to valence state changes of transition elements in zeolites [17].

Elements	Transition[(a)]	Level	E_b (eV)
Cr	$Cr^{3+} \rightarrow Cr^{5+}, Cr^{6+}$	$2p_{3/2}$	2.9
	$Cr^{3+} \rightarrow Cr^{2+}$	$2p_{3/2}$	0.9
Fe	$Fe^{3+} \rightarrow Fe^{2+}$	$2p_{3/2}$	1.2 – 1.3
Co	$Co^{3+} \rightarrow Co^{0}$	$2p_{3/2}$	4.0 – 4.2
Ni	$Ni^{2+} \rightarrow Ni^{0}$	$2p_{3/2}$	4.0 – 4.2
	$Ni^{3+} \rightarrow Ni^{+}$	$2p_{3/2}$	2.5
Ru[(b)]	$Ru^{3+} \rightarrow Ru^{0}$	$3d_{5/2}$	3.8
	$Ru^{3+} \rightarrow Ru^{0}$	$3d_{5/2}$	3.0
	$Ru^{3+} \rightarrow Ru^{2+}$	$3d_{5/2}$	1.8
Rh[(b)]	$Rh^{3+} \rightarrow Rh^{0}$	$3d_{5/2}$	2.6 – 3.0
	$Rh^{+} \rightarrow Rh^{0}$	$3d_{5/2}$	0.8[(c)]
Pd[(b)]	$Pd^{2+} \rightarrow Pd^{0}$	$3d_{5/2}$	3.7
	$Pd^{2+} \rightarrow Rh^{0}$	$3d_{5/2}$	4.0
	$Pd^{+} \rightarrow Rh^{0}$	$3d_{5/2}$	1.3
	$Pd^{+} \rightarrow Pd^{0}$	$3d_{5/2}$	1.9
Pt	$Pt^{2+} \rightarrow Pt^{0}$	$4d_{5/2}$	1.6
Cu	$Cu^{2+} \rightarrow Cu^{0}$ (Cu^{+})	$2p_{5/2}$	2.0
	$Cu^{+} \rightarrow Cu^{0}$	Cu LMM	2.0[(d)]

[(a)] $Mn^{+} \rightarrow$ M transitions correspond to reduction of isolated ions to metals with the formation of metal phase. [(b)] In the starting zeolite samples, Ru, Rh, Pd and Pt are

present in the form of complex ammonia ions. [(c)] Rh+ line position was obtained by computer deconvulation of the Rh 3d spectrum. [(d)] Shift of Cu LMM Auger line.

The interaction of transition metals introduced together into zeolite structure is responsible, in the first place for the reducibility and diffusion of metals to the external surface. Co facilitates Ni^{2+} reduction to Ni^{0} in faujasites, whereas Cu was found to retard it [17] and in bimetallic forms, the migration of Ni^{0} to the external surface is reduced.

Chemical shifts of inner levels of selected transition elements due to valance state changes of transition elements in zeolites was found to be as follows: Cr^{3+} to Cr^{5+}, Cr^{6+}, Eb = 2.9 (where Eb represent binding energy), or to Cr^{2+}, Eb = 0.9; Fe^{3+} to Fe^{2+}, Eb = 1.2; Co^{2+} to Co^{0}, Eb = 4.0; Ni^{2+} to Ni^{0} 4.0 or to Ni^{1+}, Eb = 2.5; Cu^{2+} to Cu^{0} (Cu^{1+}), Eb = 2.0. These changes are known to correspond to reduction of isolated ions to metals with the formation of metal phase [17].

2.2.2.3 Electronic state of highly dispersed metal particles and their interaction with the zeolite framework.

An XPS spectrum revealing Pd, Rh, Ru and Pt core levels was found to suggest that for metal particles localized in a highly dispersed state inside zeolite cavities, the clusters exhibited a positive shift and line broadening [17]. The very same effects were observed for highly dispersed particles (< 2-2.5 nm) of the metals on

other supports (i.e. Al_2O_3, C, MgO, SiO_2, etc.) with the chemical shift depending on the support and the particle size. The changes were thought to be due to:

- The specific electronic structure of small particles,
- The transfer of electron density from the metal to the accepting support region,
- A decrease in the extra-atomic relaxation energy (ER).

The sum of the shifts in the photoelectron and Auger-electron spectra will be, $\Delta E_b + \Delta E_k = 2\ \Delta ER$ [20]. The estimation of ΔER was found to show that this value is dependent mainly on the particle size, and for a cluster of about 1.0 – 1.5 nm it does not exceed 0.4 - 0.5 eV [20]. Hence, the shifts for Pd, Rh, Ru and Pt, may be partially due to the effective positive charges appearing on the metal clusters and the electron deficiency of small particles in zeolites is also indicated by IR and X-ray absorption spectroscopy [21].

It was suggested that the positive charge on the clusters may arise due to electron density transfer to the accepting regions of the framework. The authors also suggest that the electron deficiency of metal particles may differ considerably from the metal band structure [15a, 22].

2.2.3 Adsorption of alkenes on zeolites

2.2.3.1 Introduction

The most significant aspect of the studies of adsorbed alkenes is their interactions with the zeolitic cations, and interaction with the Brønsted and Lewis acid sites of the zeolite. There are of essential interest, because the acidic nature of the zeolite catalysts predetermines the possibility of interaction of the double bond with the Brønsted and Lewis sites on the catalyst surface.

2.2.3.2 Cations and olefins interactions

The IR spectra of ethylene complexes on Cu(I)-Y and Ag(I)-Y, FAU zeolites at room temperature was recorded by Huang et al. in 1980 [23]. The interaction of the ethylene molecule with calcium, zinc or copper (II) ions was much weaker. The complexes Cu(I)-C_2H_4 are presumed to be situated near the six-membered rings in the supercage, and in the case of silver the cations at all the S_{II} sites interact with ethylene.

2.2.4 Temperature programmed desorption (TPD)

2.2.4.1 Introduction

Temperature Programmed Desorption (TPD) is a useful technique for studying the bonding between a gas and a solid. TPD is mainly used for high surface area catalysts, generally oxides or supported metals samples, which are capable of evolving a gas. The concentration of this gas in the flowing carrier gas (He, N_2) is monitored to yield the desorption spectrum. The technique is important in characterizing the acidic properties, surface reactions of sorbed organic compounds and diffusion phenomena.

2.2.4.2 Characterization of acidic properties of zeolites

The first use of TPD in the study of a zeolite was reported by Cattanach et al., in 1968 [24]. Topsøe et al., have studied desorption of ammonia from H-ZSM-5 catalyst and they observed three TPD peaks as can be seen in figure 2.3 [25]. The TPD peaks indicate three states of adsorbed NH_3: weakly chemisorbed (α), chemisorbed (β) and strongly chemisorbed (γ). The good quality of the spectra permit, (by integration) reliable determination of the amounts of ammonia adsorbed in particular states. The activation energy of the γ state of desorption was confirmed by the maximum heat of adsorption found by microcalorimetry. The large γ peak width indicates a broad acidity spectrum of active sites and this

amount was found to confirm the literature suggestion that active sites are located at the channel intersections.

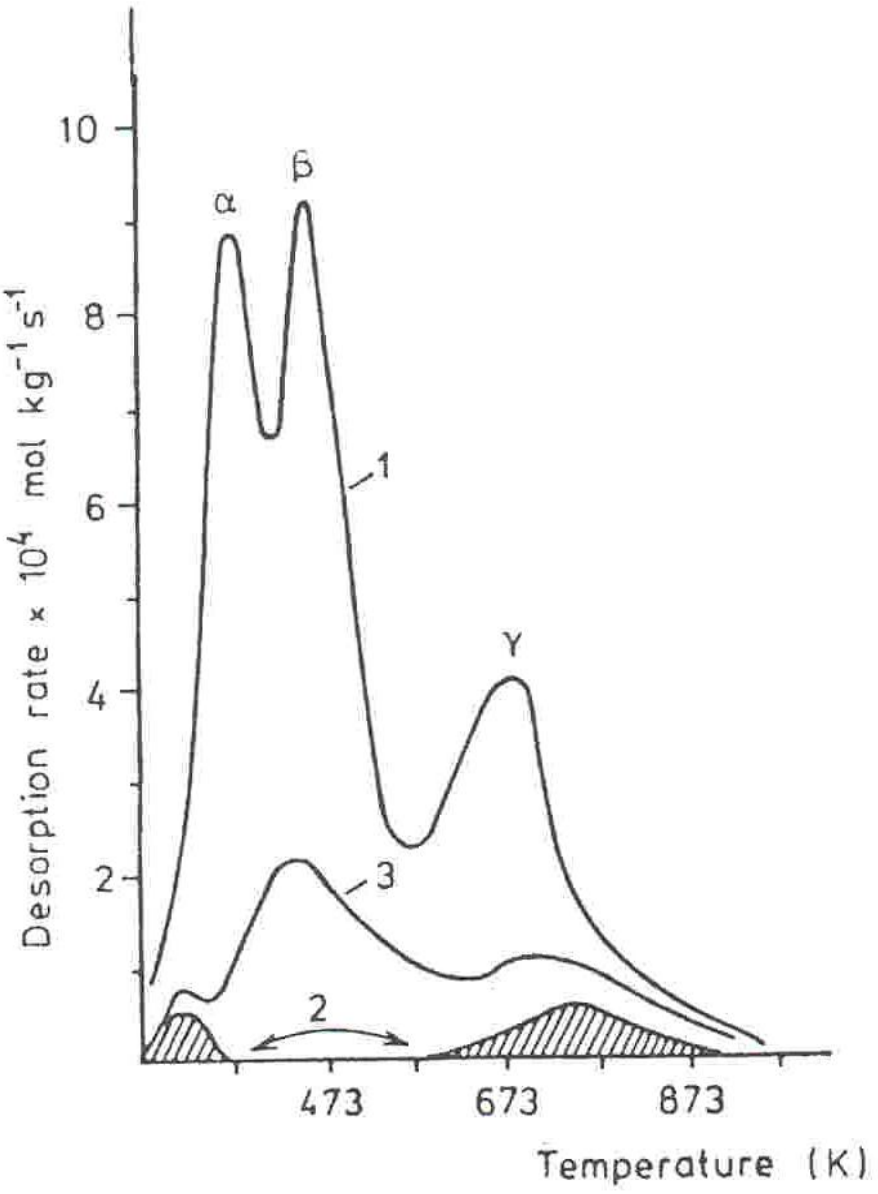

Figure 2.3: TPD spectra of NH_3 from H-ZSM-5 catalyst [11]. 1: Fresh catalyst, 2: deactivated catalyst, 3: partially reactivated catalyst.

Other authors, have previously studied the TPD characteristics of oxygen, carbon monoxide and carbon dioxide adsorbed on different support media, in order to

compare the catalytic oxidation of CO [26] steady-state catalytic decomposition, [27] catalytic reduction of NO by CH_4, [28] selective oxidation of propylene, [29] and the rate of CO_2 desorption [30].

Recent studies have shown that TPD studies are relatively important in the elucidation of the different adsorption sites, the particle size of well dispersed metals. These are the main determinant factors during CO oxidation, ethylene hydrogenation and other solid-gas phase reactions. For example Freund et al. [31] have recently reported on the adsorption of CO on gold particles deposited on well–ordered alumina and iron oxide films and they found that smaller particles adsorb CO more strongly. They also found that the interaction of CO with gold model catalysts on various supports is remarkably similar and they concluded that the support effects seen in CO oxidation on real catalytic systems must arise from the interaction with oxygen rather than of CO with the catalysts.

2.3 SUPPORTED METAL CATALYSTS

2.3.1 Introduction

By loading a reagent onto a carrier the site of reaction becomes clearly defined by the reduced dimensionality of the surface of the support. Such a compartmentalization necessarily implies a local accumulation of the immobilized agent. In addition to this purely geometrical argument, the chemical constitution of a given support material may also contribute to improve the overall reaction rate. Many of the commonly used inorganic support materials have polar properties or are polyelectrolytes. Any charged or polarizable substrates in solution will accumulate near the surface due to dipole-dipole and/or electrostatic interactions. This may increase the effective concentration of the dissolved reaction partner near the interface by several orders of magnitude and thus may result in a substantial acceleration of the reaction [32].

2.3.2 Supported monometallic catalysts

It has been noted that for metal particles to catalyze a certain reaction, such particle should be well dispersed to maximise their surface area. This is particularly important for noble metals such as Pt, Pd, Rh, Au, etc., which are expensive but of high catalytic activity for several reactions.

High activation of the metal often stems from an exceptional degree of dispersion. However, particles with an average diameter of only a few nanometers show a strong tendency towards aggregation, recrystallization, and sintering. All these phenomena are detrimental to activity. Adsorption of the clusters on an inert support may be a simple but efficient device to stabilize the cluster or, at least, to retard such undesirable morphological changes. The support as the name entails is available to support the finely divided particles in order to achieve a reasonable dispersion.

Advantages of thus supported metal particles include [33]:

- The catalyst is easily and safely handled.
- It may be used in a variety of reactors, and if used in a liquid medium may be recovered by filtration.
- Because the particles are well separated from each other they tend not to grow in size when heated to high temperature in a reduced atmosphere.
- The support provides a means of bringing the promoters into close contact with the metal.

The ideal support material should be a cheap, easily accessible fine powder which resists mechanical stress (grinding etc.) to some extent. This is why Al_2O_3, TiO_2, SiO_2, graphite, zeolites, charcoal etc. are widely used. The preparation of small particles in the laboratory is not an easy task due to the involvement of many experimental parameters and a lack of the mode of interaction of the gold precursor with an inorganic oxide.

It has been demonstrated that, the iso-electric point (IEP) of the support is a key factor in the preparation of supported catalysts. With the most commonly used gold precursor, $HAuCl_4$, the interaction with the support proceeds by an anionic adsorption process. As a result, oxides with IEP ≈ 7 such as TiO_2 (IEP = 6), CeO_2 (IEP = 6.75) [12], ZrO_2 (IEP = 6.7) [13], Fe_2O_3 (IEP = 6.5 – 6.9) [34] produce highly active catalysts while an acidic support such as SiO_2 (IEP = 1-2) or a basic support such as MgO (IEP = 12) will be inactive [35, 36]. The amphoteric character of Al_2O_3 (IEP = 8 – 9) renders it more interesting; it is reported as being either very active, or as expressing a certain degree of activity or even being inactive under certain conditions when used as a support for gold, during CO oxidation at room temperature, [37, 38, 39]. This suggests that the gold catalyst preparation on the Al_2O_3 support is not yet fully understood.

2.3.3 Supported bimetallic catalysts

Second metal components can be added to metal catalysts to systematically modify the size and in some instances, the electronic structure of catalytic surface sites [40]. Such components can also alter the reducibility of a metal catalyst and its deactivation behaviour. Aside from their industrial applications, bulk bimetallic catalysts or alloys play a major role in fundamental research, where one can study the effect of the second metal undisturbed by contributions from a support. In ideal bimetallic or multi-metallic systems, it is possible to theoretically predict the thermodynamic equilibrium composition of the surface as a function of

the bulk composition and temperature. In general, the metal with the lower energy of sublimation tends to segregate on the surface.

2.3.4 Catalysts preparation methods

Despite the widespread use of catalysts in industry, the preparation of catalysts is more often an "art" than a "science". Catalysts with the same chemical and physical properties may often differ in behaviour, indicating that these properties are not necessarily the only properties that determine its activity. The whole history of catalysis reveals that preparation plays an important role in catalyst behaviour [41].

There are many different methods used in preparing supported metal catalysts reported in the literature during the past 20 years or so, but a few of those predominate [42]:

2.3.4.1 Incipient wetness or pore volume impregnation method

When a sufficient solution is added into a pore volume (typically 1 cm^3/g) of the support to give the required metal content without exceeding the pore volume then impregnation to incipient wetness has been achieved. The concentration of the solution used and the rate of drying play an important role in the catalyst size produced as illustrated in figure 2.4. Thus high metal loadings tend to give larger particles than low loadings and the uniform distribution of the metal throughout

the support is achieved by drying quickly. If drying is performed slowly, the salt will migrate towards the external surface of the support particle [43].

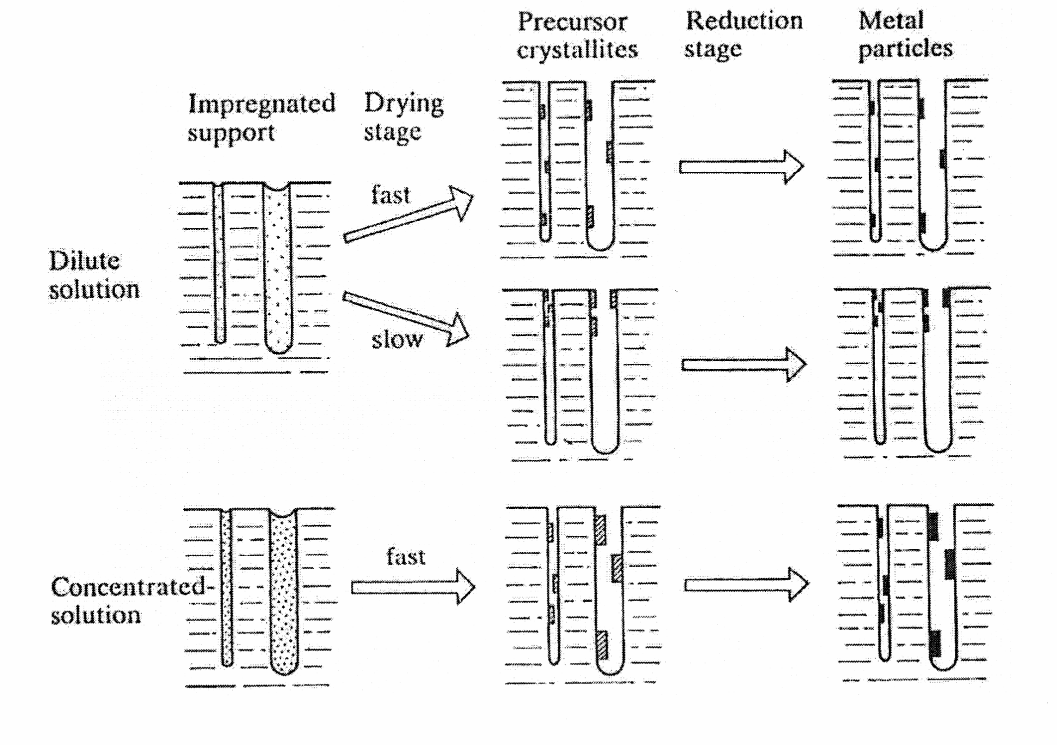

Figure 2.4: Illustration of the stages in the preparation of supported metal catalysts: the pores of the support are initially impregnated with either a dilute or a concentrated solution of the metal salt [33].

This is one of the widely used preparation method in catalysis. During impregnation, there is strong adsorption of ions on high surface area supports. Because of this, the adsorption equilibrium between support and solutions at various concentrations must be determined, before impregnation, to obtain the desired concentration of metal on the support [43]. Impregnated catalysts are more

economical because they require smaller amounts of the usually expensive active components than do precipitated and ion-exchanged catalysts.

2.3.4.2 Ion exchange and preparation of gold/zeolite catalysts

Ion-exchange of solid supports results in the binding of metal ions at the surface and within the pores. Transition metals usually form atomically dispersed species and these can be transformed to small metal particles by calcination and careful reduction [42]. Ion-exchange can also be used to remove catalytic poisons or to add promoters. For example, ammonium ions, sodium, etc. can also be loaded or modified by ion-exchange mechanisms. This procedure is especially effective with zeolites, which have ion-exchange properties.

Partial exchange of the sodium ions by ions of the precious metals (e.g. $[Au(en)_2]^{3+}$), followed by very careful reduction, can give extremely small metal particles containing less than ten atoms locked within the cavities of the zeolite structure. However, this method has not been often used due to limited number of cationic gold complexes available. The complexes available include that mentioned above as well as, $[Au(NH_3)_2]^+$, which was recently prepared, but has not yet been used for the preparation of catalysts as yet [44].

However, there is some controversy as to the procedure used to introduce gold from a diluted solution of chloroauric acid (80 ^oC for 16 h) into a NaY zeolite.

More difficult to understand is whether this procedure can be taken as ion exchange, or just as anionic adsorption onto a support [42].

2.3.4.3 Co-precipitation

This method involves the following steps:

- Preparation of chemical solutions with desired components,
- Complete mixing of the solutions, and formation of a precipitate,
- Removal of the precipitate by a suitable method, such as filtration or centrifugation, and
- Washing, drying, calcination and pre-treatment to activate the catalyst.

2.3.4.4 Deposition-precipitation

This method involves dissolving a suitable amount of chloroauric acid, $HAuCl_4$ in distilled water and adjustment of the pH of the solution by addition of a suitable base. The solution is allowed to hydrolyze for several hours prior to addition onto a suspended support. After several hours of stirring at a certain temperature the solution is filtered, washed and dried.

Although the method has been widely used [45] as it gives good dispersity of gold nanoparticles throughout the support, most of gold is lost during washing and filtration steps. Pitchon et al. [46], has recently, reported on a new preparation method for the formation of gold nanoparticles supported on alumina by the direct

anionic exchange (DAE) of the gold species with the hydroxyl groups of the support. They have suggested that this method differed from the commonly used method of deposition precipitation, because the method presents the advantage that no gold is lost during the filtration and washing steps (an expected loading of 2% Au was obtained).

2.4 SURFACE CHARACTERIZATION OF SUPPORTED METAL CATALYSTS

2.4.1 Determination of the metal particle size

It is known that the activity of metal dispersed catalysts is directly dependent on the size and the spatial dispersion of the metal particles in a matrix [47-49]. Therefore it is very important to characterise the particle size of this class of materials. When the metal is very finely dispersed and is present in small quantities, many techniques are limited in their ability to detect the active particles. In particular, if carbon is the support, transmission electron microscopy (TEM) is associated with serious difficulties in revealing particles smaller than say 4 nm. Chemisorption is problematic for the detection of gold.

Benedetti et al., have demonstrated that particle sizes could be quantitatively determined at a loading of 0.2 wt.% for a Au/C sample. They noted that, a large fraction of very finely dispersed particles that remained undetected using other methods could be easily detected by small angle X-ray scattering (SAXS) [50].

During the particle size determination, all catalytically active species are taken as metallic, even though it is known that a positive oxidation state may sometimes be involved. The estimation of particle size can be dertermined by the physical techniques listed below.

2.4.1.1 Transmission electron microscopy

Transmission Electron Microscopy (TEM) instruments which are widely used today operate in the range of 100 - 200 kV and are useful in providing a wide range of capabilities, from high resolution imaging to a variety of analytical techniques [51]. The technique of High Resolution Electron Microscopy (HREM) is performed with axial illumination using an objective aperture which allows several diffracted beams to be combined with the axial transmitted beam to form the image. Images obtained under such conditions can be directly related to the atomic structure of the material [51].

2.4.1.2 Scanning electron microscopy

Scanning Electron Microscopy (SEM) involves obtaining images by scanning a finely focused probe in a raster pattern on the specimen surface in synchrony with the raster scan on a cathode ray tube. The number of electrons emitted depends markedly on the angle of the specimen surface with respect to the electron beam and the detector. For example, as the electron probe approaches a vertical surface, a large fraction of the secondary electrons can escape and be collected. Hence, a vertical surface appears bright in an SEM image [51].

SEM gives high depth of field, contrasted images of specimen surfaces where particles appear shaded with a three-dimensional aspect. Its main drawback is the comparatively low resolution (5 – 10 nm), even with a small electron probe,

because of beam spreading in the specimen. Particles larger than 10 nm can be detected provided they are well isolated. However, SEM is mainly used to characterize particle sizes in the range 10^{-7} – 10^{-4} m (i.e. oxide phases, zeolite crystals, carbon grains, and unsupported metals), internal morphology and composition of sectioned catalyst pellets.

2.4.1.3 Small-angle X-ray scattering analysis

Small-Angle X-Ray Scattering Analysis (SAXS) has been very little used, although this technique allows not only the determination of the particle size distribution, but also measurement of the specific surface area of the metal as well as of the support [51]. The main drawbacks of the technique are that it requires special instrumentation.

However, SAXS is a sensitive technique and particle size distribution can be obtained for supported catalysts containing 0.5wt.% metal [51]. Furthermore, particles or clusters as small as 0.5 nm can be measured. Other advantages of this technique is as follows: A complete description of the catalyst texture, including particle size, pore size, and specific area, and can be used to calculate intrinsic catalytic activity. It can be used to interpret an activity pattern as a function of particle size, or to account for a particular mass transfer problem in the catalyst pores. The size of particles constituted by several crystallites, as well as the particle sizes of poorly crystalline or even amorphous solids, can also be

measured by SAXS. In contrast with electron microscopy, SAXS can be carried out in situ during catalyst treatment or catalytic reactions [51].

Benedetti et al. [52] have reported that anomalous small-angle X-ray scattering (ASAXS) and anomalous wide-angle X-ray scattering (AWAXS) have shown to be very promising techniques for studying metal catalysts supported on porous materials. They have been able to detect small nanoclusters, which remained undetected until the end of 20th century. The presence of a large fraction of very finely dispersed particles with sizes smaller than 2 nm was found to be a common situation for the kind of samples studied. In bimetallic catalysts (Au-Pd/C), ASAXS was found to be able to separate the contribution of the two metals [52].

In summary, various techniques of particle size measurement have advantages and drawbacks; ideally, a combination of two or more methods would be necessary to obtain an unambiguous evaluation of particle size [51]. There are few examples given in the literature, which compare the results given by several techniques mentioned above. However, in addition to intrinsic limitations discussed previously, there are practical limitations contingent on time, skill and the funds required to run a particular technique, let alone several techniques. Indeed, except for those involved in the development of characterization techniques, the question is what is the best routine technique capable of giving rapidly an accurate value of the mean particle size or dispersion?

2.4.2 Determination of nature and state of supported metal catalysts

2.4.2.1 Temperature-programmed reduction (TPR)

Temperature-Programmed Reduction (TPR) has gained increasing importance for the characterization of catalysts since its first application by Robertson et al. [53]. The TPR technique has been applied successfully to study the influence the support materials [54, 55], of pre-treatment procedures [56, 57], and of application of promoters [58, 59] on the reducibility of a catalyst.

For TPR measurements reported in the literature, the experimental conditions employed vary over a wide range. The reduction gas usually consists of a mixture of either hydrogen and nitrogen or hydrogen and argon. The reported hydrogen concentration range from 3 to 15%; the flow rates from 0.16 to 1 cm^3 (NTP)/s, and the sample volumes from 10 to 500 μmol. A comparison of the results reported in the literature often becomes very difficult due to the fact that the reduction profiles are sensitive to the experimental conditions used.

2.4.2.2 ^{197} Au Mössbauer spectroscopy

Mossbauer Spectroscopy is a nuclear resonance technique sensitive to the interaction of a metal with surrounding atomic electrons. In this regard it represents a local atomic-scale probe of the solid of interest because the electronic structure of the metal atom is determined by its valence state and may be

perturbed by the site symmetry (e.g. non-cubic environment) in which it resides. Therefore by measuring the interaction of a nucleus with the atomic electrons (nuclear hyperfine interactions) we may elucidate the chemical bonding, atomic valence and site symmetry of atoms in the host matrix, i.e. the chemical state of the metal within the compound [60].

It is of interest to know the chemical species of gold in a sample, i.e. whether metallic (Au) or ionic (Au^{+} or Au^{3+}). This is to confirm which species is active during catalysis. If this is elucidated and the chemistry/reactivity of gold in zeolites is better understood, it will aid in optimum catalyst design [60].

2.4.2.3 X-ray absorption spectroscopy (XAS)

With the availability of the synchrotron radiation sources, X-ray absorption spectroscopy techniques (XAS) has developed into a widely used tool for materials by identifying the local structure around atoms of a selected type in the sample.

High resolution X-ray absorption spectroscopy (XAS), that became available with the development of synchrotron radiation sources, has introduced powerful experimental methods for the investigation of atomic and molecular structures of materials. Synchrotron radiation high-flux monochromatic X-ray beams with the energy resolution $\Delta E/E$ of the order of 10^{-4} are easily obtainable, allowing measurements of high quality absorption spectra in a short time. In a typical

experimental set-up (Figure 2.5) ionisation chambers monitor the intensity of incident (I_o) and transmitted (I_1) monochromatic photon beam through the sample. With the well-known exponential attenuation of X-rays in a homogeneous medium, the absorption coefficient μ (E) at a given photon energy E can be obtained from the relation u = ln (I_1/I_o)/d, where d is the sample thickness. The energy dependence of the absorption coefficient is collected by a stepwise scan of the photon energy in the monochromatic beam with a Bragg monochromator.

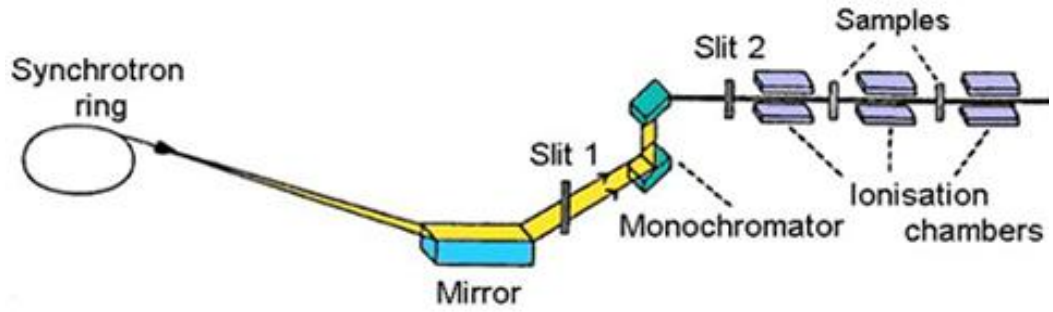

Figure 2.5: Schematic view of E4 X-ray beamline at Hamburg Synchrotron Radiation Laboratory (HASYLAB) at DESY in Hamburg [61].

2.4.2.3.1 X-ray absorption near edge structure (XANES)

In XANES (X-Ray Absorption Near Edge Structure) the valence state of the selected type of the atom in the sample and the local symmetry of its unoccupied orbitals can be deduced from the information hidden in the shape and energy shift of the X-ray absorption edge itself.

In XANES (X-ray Absorption Near Edge Structure) analysis, the shape of the absorption edge itself is examined in high resolution scan. In the energy region of the near absorption edge the slow photoelectron probes the empty electronic levels of the material. The resulting structure within about 30 eV of the threshold is rich in chemical and structural information. Although the theoretical picture is mostly too complex to allow a comprehensive analysis, some features of the spectral shape can reliably be used to determine the valence of the atom and the symmetry of its neighborhood.

The shape of the edge and the pre-edge resonances are characteristic for the local symmetry of the investigated atom sites and can be used as fingerprints in identification of its local structure (for example, Cr K-edge in figure 2.6) [61]. Tetrahedrally coordinated Cr materials, lacking an inversion centre, exhibits a single intense pre-edge peak which can be assigned to a dipole allowed transition of 1s electron to an unoccupied antibonding t_2* tetrahedral orbital. This typical pre-edge resonance is found in the $CaCrO_4$ sample, as well as in all three new calcium chromate samples, where Cr atoms are tetrahedrally coordinated by four oxygen atoms (figure 2.5). In the XANES spectra of Cr_2O_3 and Cr metal samples, where Cr is located at the crystal site with the centre of inversion, the pre-edge resonance does not appear. Cr_2O_3 builds a corundum structure with Cr atoms occupying octahedral sites in the lattice. Octahedral symmetry in XANES spectra is recognised by two small resonances in the pre-edge region assigned to transitions of 1s electron into antibonding orbitals with octahedral symmetry.

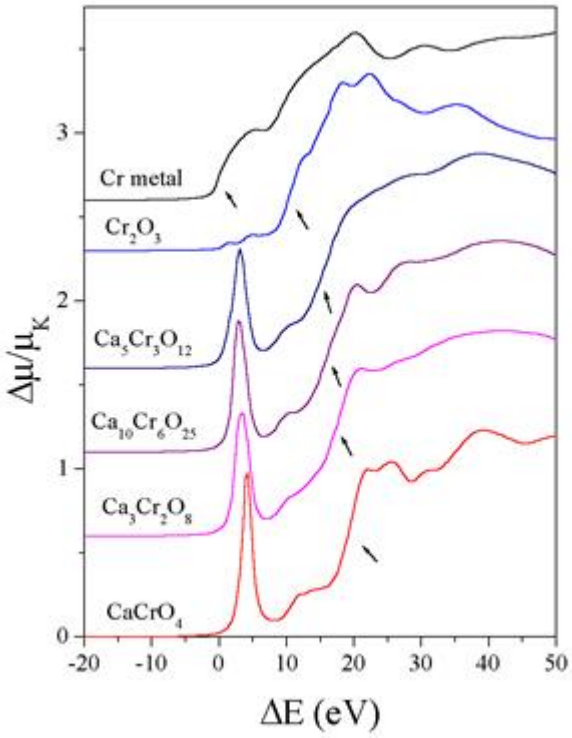

Figure 2.6: Normalized Cr K-edge profiles, displaced vertically, for the calcium chromate samples and Cr_2O_3, $CaCrO_4$, and Cr metal. Energy scale is relative to the Cr K-edge in metal (5989.0 eV). The spectra were measured at EXAFS 2 beamline in HASYLAB at DESY in Hamburg [61].

2.4.2.3.2 Extended X-ray absorption fine structure (EXAFS)

In EXAFS (Extended X-ray Absorption Fine Structure) the number and species of neighbour atoms, their distance from the selected atom and the thermal or structural disorder of their positions can be determined from the oscillatory part of the absorption coefficient above a major absorption edge. The analysis can be applied to crystalline, nanostructural or amorphous materials, liquids and molecular gases. EXAFS is often the only practical way to study the arrangement

of atoms in materials without long range order, where traditional diffraction techniques cannot be used.

EXAFS arises from the wavelike nature of the final photoelectron state of an atom. When an X-ray photon is absorbed an inner shell electron is preferentially ejected as a photoelectron with kinetic energy equal to the difference between the photon energy E and the inner-shell binding energy E_0. According to quantum theory this photoelectron can be visualized as an outgoing spherical wave centered at the excited atom (figure 2.7). The photoelectron wave vector is $k = 2\pi/\lambda$ given by:

$$k = \sqrt{\frac{2m}{h^2}(E - E_0)}$$

where, k - represent wave vector, m - represent mass of electron, h - represent planck's constant and E, E_o - represent photon energy and inner-shell binding energy.

This electron wave is scattered by neighbor atoms, and the new waves emanating from each scattering site are superposed to the initial outgoing wave. The interference of the initial and scattered waves at the absorbing atom affects the probability for photoeffect. With the increasing (X-ray) photon energy the wave vector of the photoelectron wave increases, leading to alternating constructive and destructive interference [61].

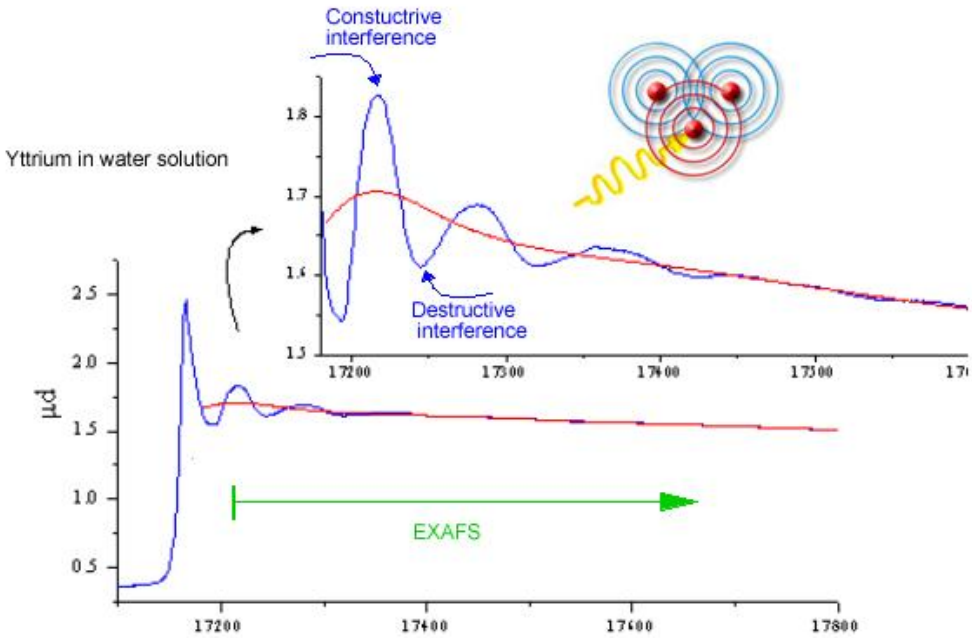

Figure 2.7: Schematics of the EXAFS process illustrating the origin of EXAFS oscillations due to the interference of an outgoing and backscattered photoelectron wave [61].

2.5 CATALYSIS BY GOLD-BASED CATALYSTS: CO OXIDATION REACTION

2.5.1 Introduction

Heterogeneous catalysis is based on reactions occurring on the active sites located at the surface of a catalyst. The reaction proceeds by a sequence of elementary steps including adsorption, surface diffusion, chemical rearrangements of the adsorbed reaction intermediates and products. For the development of new catalytic systems it is extremely important to investigate the changes of the surface electronic, chemical and structural properties during a particular process. A limit to many of the analytical techniques employed in heterogeneous catalysis is represented by the high vacuum environment required to obtain information rather than the real catalytic working conditions such as atmospheric or even high pressure environments [62].

2.5.2 Preparation of gold nanoparticles

For a long time, only very limited attention was paid to realizing catalysis by gold because its electronic structure, namely the completely filled d band

($[Xe]4f^{14}d^{10}6s^{1}$), is usually associated with very low catalytic activity [63]. However, it has recently been reported that metallic gold, highly dispersed on metal oxides, can present a remarkable activity towards low-temperature CO oxidation. Among the systems investigated, Au/Fe_2O_3 has been found to be one of the most active. However, a comparison of the literature data shows that the catalytic activity is strongly affected by the catalyst preparation method and the catalyst pre-treatment conditions used [64].

In the last few years, there has been growing interest in "nanosized" structures in the range 1 to about 20 nanometres in many different fields of research. There are many different methods of preparing gold particles in this nanometer size range and the major problem is the creation of small metallic units that are stable under reaction conditions. Gold particles are often deposited on a support, which can be a metal or a neutral porous material. Thus can be achieved by using gold complexes, but are stabilized by ligands [63]. Removal of the ligands can yield active metal/alloy particles having uniform sizes and discrete metal compositions. Generally, under catalytic reaction conditions, e.g. high temperature and pressure, the surface-bound metal clusters do not maintain their original cluster structures and readily collapse to give larger metal particles.

Most catalysts consist of nanometer-sized particles dispersed on a high-surface-area support. Advances in characterization methods have led to a molecular-level

understanding of the relationships between nanoparticle properties and catalytic performance. Together with novel approaches to nanoparticle synthesis, this knowledge is contributing to the design and development of new catalysts [65].

Goodman et al., have shown that the activity of the Au particles is very sensitive to their size and that only particles in the range of 2 to 3 nm are active for CO oxidation (figure 2.8) [66]. This effect has been ascribed to oxidation of the Au atoms that are in contact with the support, and nicely illustrates the importance of tuning the electronic properties of the metal particles to achieve high catalytic activity.

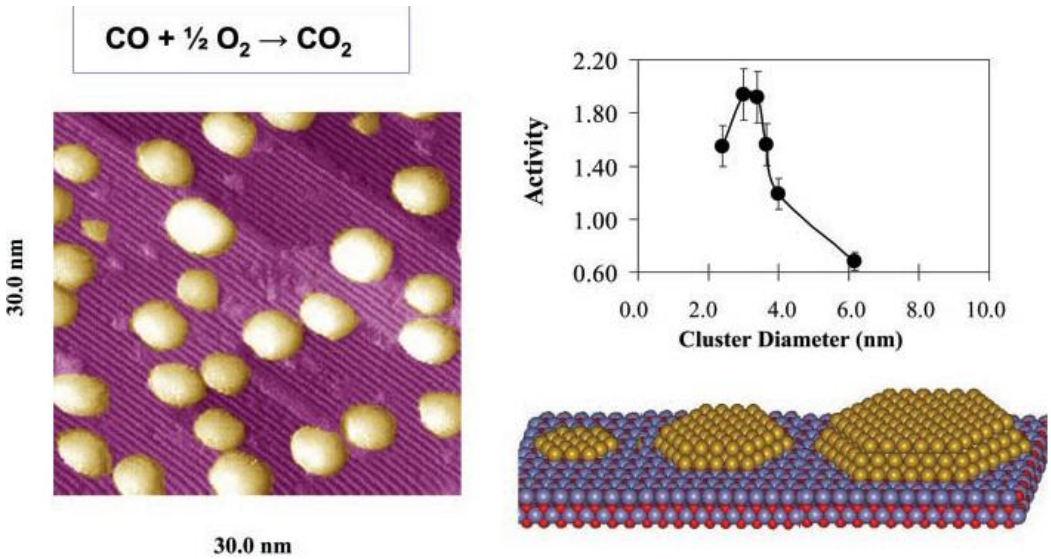

Figure 2.8: Effects of particle size on the activity of titania-supported Au for the oxidation of CO [66]

An important issue in surface chemistry and catalysis is how surface structures and features with nanometer dimensions affect reactivity in heterogeneous

systems [67-69]. Considerable effort has been focused on the development of synthetic techniques to generate nanophasic noble metallic materials and tailor their properties. In order to prevent the undesired agglomeration, these processes are often performed in the presence of ligands, polymers or various surfactants. However, the stability of metal colloids depends on the characteristics of the special protecting agents, which are usually stripped off from the metal surface in vacuum and/or with heating, resulting in agglomeration. Therefore, one alternative method for generating stabilized metal nanoparticles is to synthesise them on a neutral solid support, which helps to define particle size and serve to immobilize the resulting particles.

Considerable attention has been focused on metal nanoparticles because of their optical [70], catalytic [71] and electronic properties [71]. Gold nanoparticles are known to have a strong plasmon resonance absorption in the visible region due to the collective oscillation of free electrons in the conduction band [70]. Metal nanoparticles are being used for optical sensors [72], bioconjugation [73, 74] and SERS enhancement [73]. As more is understood about the properties and the mechanism of formation of these nanoparticles, a better control of their size, shape and applications can be achieved. Most methods of colloidal synthesis use thermal reduction of metal ion salts. Some electrochemical methods have been developed [75]. Recently, photochemical reduction methods have been developed to produce metal nanoparticles [76, 77]. Various different approaches are used in photochemical reduction such as use of a photosensitizer [76] use of dendrimers as stabilizers, or placement of metal salts in polymer films [77, 78]. Light has also

been used to modify the shape of nanoparticles [79-81]. Because both the precursor salt ($AuCl_4^-$) [82, 83, 84] and the final product (gold nanoparticles) [70], are colored, the progress of the reaction forming gold nanoparticles can be followed optically [85].

2.5.3 Nature of active gold species, for CO oxidation

Haruta et al. [86, 87] have suggested that the active species in Au catalyst is made of small metallic gold particles. More recently some authors have proposed that unreduced gold species, stabilised by an interaction with the support, are more active than Au^0 [64]. Minico et al., argued that exposure of the catalysts to a CO/O_2 mixture leads to the formation of Au^+ and Au^0 species and the Au^+ species is more active towards the CO oxidation than Au^0. However, Au^+ is not stable and tends to be irreversibly reduced to Au^0 during the reaction, accounting for the irreversible deactivation usually observed [64].

On the basis of experimental results, mainly of kinetic, TPD and FTIR measurements, Boccuzzi et al., [88] proposed a four step mechanism for CO oxidation over supported gold:

- adsorption of CO on metallic gold surface sites
- oxygen adsorption, probably on metal oxide site at the perimeter around gold particles
- formation of carbonate-like species chemisorbed on the perimeter sites
- decomposition of the carbonate-like species leading to CO_2 formation

2.6. GOLD CATALYSIS ON ALKALI-MODIFIED ZEOLITES FOR CO OXIDATION

2.6.1 Catalysis on alkali-modified zeolites

In the early 1990s, zeolites were used as base catalysts in their ion-exchanged and impregnated forms. Ion-exchanged zeolites possess only base sites of low strength, which limits their applicability in organic synthesis. They can, however, be handled in air, since these base sites are resistant to poisoning by water or carbon dioxide [89]. As reported by Campbell et al., impregnation with various alkali salts can be carried out in order to create stronger basic sites in the cavities of zeolites.

In other studies Campbell et al. created stronger base sites in the cavities of zeolites, by impregnating them with various alkali salts; they found that the materials were sensitive towards contact with air or water, which limits their utilization in catalysis [89]. In a different approach, Hathaway et al., formed intra-zeolitic alkali oxide clusters by impregnation methods [90]. The basic sites of the oxides were shown to be stronger than those of the zeolitic framework.

Ono et al. [91], found a new way of modifying zeolites to obtain basic materials. Alkali-exchanged zeolite-Y was immersed in a solution of metallic Na, Yb or Eu in liquid ammonia, and the solvent was removed by evacuation. From their results, it was concluded that the base sites were created on the impregnated

zeolite. The catalytic activity of Yb or Eu supported on the alkali-exchanged zeolite–Y was found to be strongly depended on the type of alkali cation present, and the order being: K > Rb > Cs > Na > Li.

Recent studies by Wan et al., suggests that prior to gold loading, the support should be treated with 1M $NaNO_3$ and the equilibrium pH obtained after two days [92]. They found that the catalysts were more active than expected and their analysis suggests that there is increase in sodium content after surface modification of the zeolite. They noted that for the Y-type zeolite, the amount of aluminum decreases with an increase of sodium after the surface modification. Thus was suggested to be due to the leaching of the aluminum in Y-type zeolite. Some of the protons on the ion exchange sites in Y-type zeolite were also exchanged by sodium ions in the 1M $NaNO_3$ solution.

The XRD results showed that all the structures of the Y-type catalysts were maintained after surface modification. Thus, it was suggested that the modification of a Y-type zeolite only caused a change of the surface properties and there was no significant collapse of the zeolite structure. Interestingly, the authors report that the gold loading in Au/Y is higher than that in Au/Y(NP), where NP represent normal preparation methods. The pH values of the filtrates after the preparation of gold in Au/Y and Au/Y(NP) are similar. This indicates that the gold species in the solutions for the preparation of these two catalysts were similar. They suggested that the different surface property of Y and Y(NP) caused different gold loadings in Au/Y and Au/Y(NP). Therefore, different

physical or catalytic properties of these two should arise from the effect of the surfaces formed during gold loading process [92]. Figure 2.9, shows the experimental results of CO conversions over as-prepared Au/Y(NP), Au/Y and $[Au/Y(NP)]_{pH}$ catalysts (each contained 0.0006 g of Au) at 40 ^{0}C.

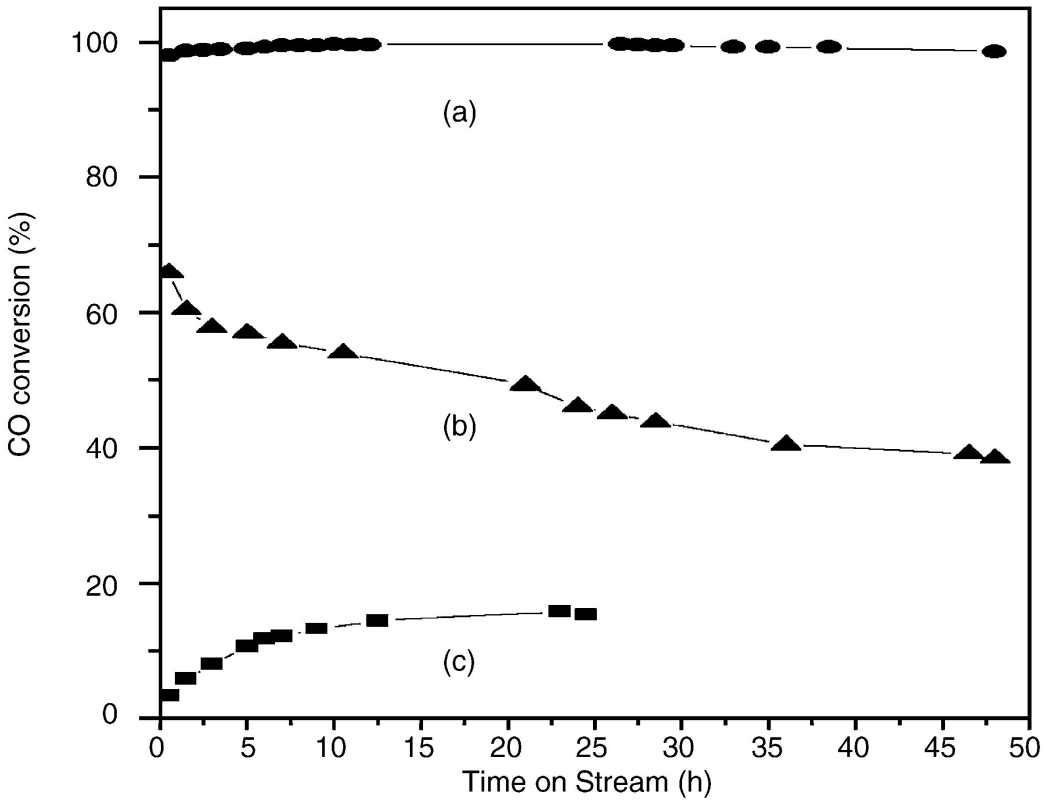

Figure 2.9: CO conversion vs. time on stream at 40 ^{0}C over (a) Au/Y, (b) Au/Y(NP), and (c) $[Au/Y(NP)]_{pH}$, which contained 0.0006 g of gold [92].

The authors reported the highest conversions for Au/Y, as shown in Figure 2.9a, from surface modified Y-zeolite. The catalyst maintained a CO conversion close to 99% for at least 48 h. However, Au/Y(NP), shown in Figure 2.9b, had an initial

conversion of 66%. Its catalytic activity decayed rapidly during the first five hours, to a CO conversion of 38% after 48 h. $[Au/Y(NP)]_{pH}$ (Figure 2.9c) showed the lowest CO conversion among these three catalysts. It had very low initial activity and then reached a conversion of 15% after 24 h [92a, 92b].

It has been suggested that the high-surface alkali metals serves as a base and as an electron transfer agent [85].

2.7 ETHYLENE HYDROGENATION REACTIONS

2.7.1 Introduction

Relatively little attention has been given to the development of Au-based hydrogenation catalysts and, in particular, the subject of the promotion of Au catalysts has been almost ignored. Until recently, there have been relatively few studies of Au as a hydrogenation catalyst. Some studies concerning CO and CO_2 hydrogenation [93-95] and alkadiene hydrogenation have been reported [96].

The first major system chosen for investigation involved the hydrogenation reaction of the smallest olefin (ethylene) and this system was chosen for its simplicity as only one product, ethane can be formed [97]. The first studies of ethylene hydrogenation were undertaken in 1934 by Horiciti et al., and they proposed that ethylene was hydrogenated stepwise from an adsorbed ethylene intermediate through ethyl group to ethane [98]. The hydrogenation of unsaturated hydrocarbons occurs efficiently on noble-metal catalyst such as the platinum group metals. The mechanism they proposed proceeds as follows:

- Hydrogen dissociation on the metal surface
- Alkene adsorption on the metal surface
- Subsequent hydrogen addition to alkene
- Adsorption of the alkene

It was concluded that the alkene hydrogenation is structure insensitive based upon experiments on single metal crystals [98].

The reactivity of alkenes adsorbed on metal surfaces is a determining factor in the overall conversion of hydrocarbons to alkanes on transition metal catalysts, and this in turn is the key for the design of many processes in the chemical industry [99]. It is therefore desirable to understand the chemistry of those adsorbed alkenes at a molecular level. Ethylene adsorbed on Pt (111) surfaces has been considered to be representative of a whole range of alkene-metal interactions and has consequently been given a great deal of attention in recent years.

The chemistry of ethylene on a metal surface is quite complex because there are at least two forms of adsorbed ethylene, namely, π-bonded species observed either at low temperatures or co-adsorbed systems and a di-σ bonded species that appears at higher temperatures [97, 98].

Shen et al., [97] investigated in situ ethylene hydrogenation near ambient pressure and temperature using sum frequency generation (SFG) spectroscopy. They found that ethylene primarily hydrogenates through a π-bonded intermediate rather than the more strongly adsorbed di-σ bonded ethylene species as shown in scheme 2.3. The π-bonded intermediate occupies only a few percent of surface sites during reaction and is in fast equilibrium with gas phase ethylene. Without gas phase ethylene, its presence on the surface is negligible at room temperature. This species hydrogenates through an ethyl intermediate to ethane with an identical

rate in the presence or absence of ethylidyne. By contrast, di-σ bonded ethylene competes directly for sites with ethylidyne and its presence or absence had no observable effect on the reaction rate.

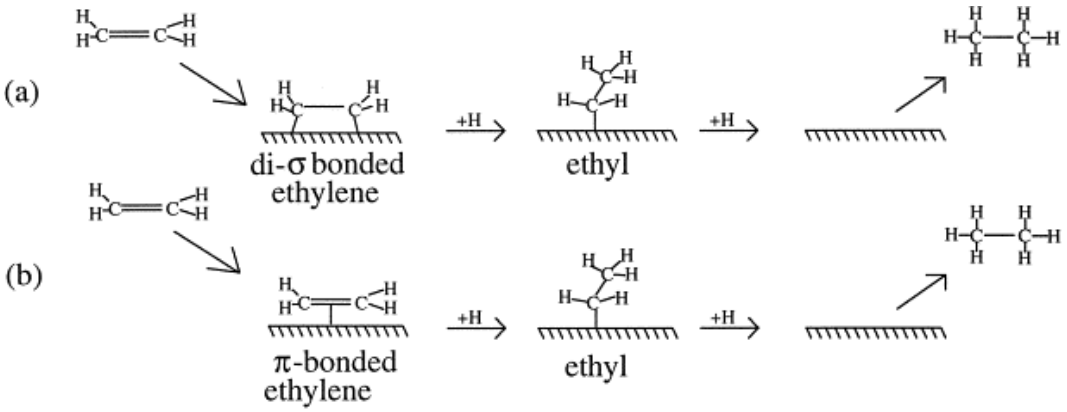

Scheme 2.3: Reaction pathways proposed for ethylene hydrogenation [97].

On other note, heating adsorbed ethylene on Pt(lll) leads to simultaneous activation of several processes, namely, molecular desorption, decomposition to ethylidyne, and hydrogenation to ethane. The selectivity in the conversion of adsorbed ethylene towards these different reactions appears to depend at least partly on the nature of the initial adsorption. It was illustrated by recent isothermal kinetic measurements with collimated beams of mixed hydrogen and ethylene that the production of ethane is closely correlated with the presence of weakly adsorbed ethylene, possibly a π-bonded state. The presence of hydrogen on the surface increased the amount of this weakly adsorbed ethylene which is essential for ethylene hydrogenation [97,99, 100].

Additional complications were found to arise from the build up of carbonaceous deposits on the surface of the catalyst under reaction conditions. This

carbonaceous layer is deposited on the surface by thermal decomposition of unsaturated hydrocarbon products via hydride elimination from an alkyl group and other intermediates. In the case of olefins, the end products are alkylidyne species formed from dehydrogenation of alkylidyne intermediates. At surface temperatures above -37 ^{o}C thus formation competes with both ethylene hydrogenation and ethylene desorption. It was reported that these deposits modify the properties of the exposed catalytic metal, by opening up new channels for mild reactions but still allowing for the occurrence of the more demanding reactions involved in hydrocarbon reforming and oxidation processes [101].

Zaera et al [100], has reported that the presence of alkylidyne on the surface of the metal does not influence the hydrogenation reaction in any other way than by blocking surface sites.

Ethylene hydrogenation was monitored over a Pd/Al_2O_3 supported catalyst in situ by using transmission infrared spectroscopy, by varying the ratio of ethylene to hydrogen. It was observed that hydrogenation occurred over surfaces both with and without an ethylidyne over-layer (scheme 2.4) [97].

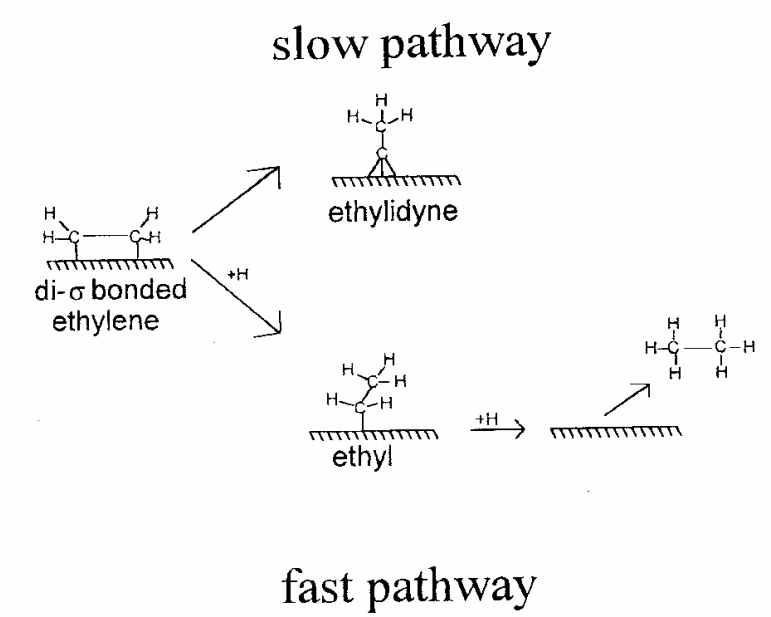

Scheme 2.4: The schematic representation of the reaction channels for di-σ-bonded ethylene on Pt(111) during ethylene hydrogenation at 22 ^{0}C [97].

2.7.2 Carbon and coke formation on supported metal catalysts

Catalyst deactivation, the loss of catalytic activity or selectivity over time, is a problem of great and continuing concern in the practice of industrial catalytic processes. Catalyst deactivation is inevitable for many processes; some of its intermediate, drastic consequences may be avoided, postponed, or even reversed [102 - 104]. Prevention of catalyst degradation poses substantial challenges in the design and operation of large scale catalytic processes.

The three most common causes of catalyst decay are fouling, poisoning or thermal degradation. Fouling involves the deposition of a material on a catalyst surface to block active sites. Coke deposition is the most common process, but the

deposition of rust and scale from elsewhere in the system is not uncommon (figure 2.10) [105]. Poisoning involves strong chemical interaction of a component of the feed or products with active sites on the catalyst surface.

During the transformation of organic compounds over solid catalysts, there is always formation and retention of heavy side-products, either in the pores or on the outer surface or in both positions of the catalyst. The formation of these non-desorbed products, generally called coke, is the most frequent cause of catalyst deactivation in industrial processes. Unfortunately, regeneration is often difficult owing to various secondary effects that occur under the severe conditions of coke removal: high temperature, presence of water, etc [106].

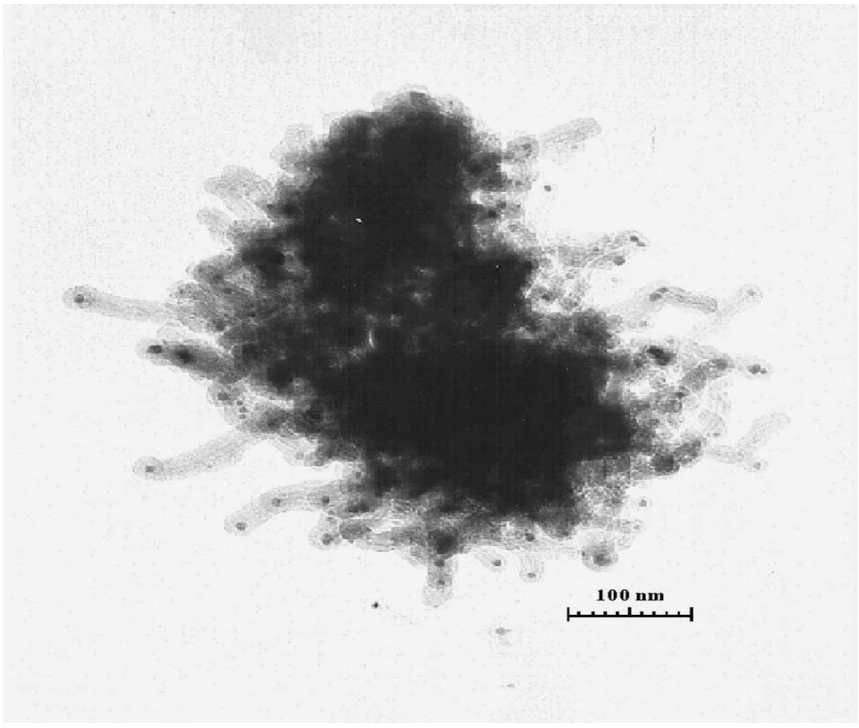

Figure 2.10: Electron micrograph of 14% Ni/Al_2O_3 having undergone extensive carbon deposition during CO disproportionation at 400 ^0C, P_{CO} = 4.55 kPa (magnification of 200,000; courtesy: BYU Catalysis Laboratory) [106].

The deactivation of supported metals by carbon or coke may occur chemically due to chemisorption, carbide formation, physical blocking of the surface sites, metal crystallite encapsulation, plugging of pores, and destruction of catalyst pellets by carbon filaments. Blocking of catalytic sites by chemisorbed hydrocarbons, surface carbides or relatively reactive films is generally reversible in hydrogen, steam, CO_2 or oxygen. Reaction temperature affects significantly the composition of "coke". The modes of "coke" formation are successively observed at low temperatures (below 200 ^{o}C) and at high temperatures (above 350 ^{o}C). At intermediate temperatures, "coke" formation occurs through both the high temperature and the low temperature modes.

All carbonaceous deposits may be removed by gasification, as described by the generalized reactions;

$C + O_2 = CO_2$

$C + 2H_2 = CH_4$

$C + H_2O = CO + H_2$

$C + CO_2 = 2CO$

Some degree of control can be achieved by heat exchange, as can be the case in catalytic cracking units. Alternatively, the use of different chemical reactions may be advantageous [106]. Thus, for example, the reaction to produce carbon monoxide (reaction 4) is much less exothermic than that to produce carbon dioxide (reaction 1). As a result, it may be advantageous to remove heat in two stages with the release of CO and CO_2 controlled by the supply of oxygen.

Yide et al., [103] reported that some carbonaceous deposits are active carbon species that help the formation of ethylene and benzene, while other carbonaceous deposits are inert and will cause the deactivation of the catalyst by covering the active metal species and/or the Brönsted acid sites.

Catalysis involves interfaces, and heterogeneous catalysts are prepared with high surface areas, a condition that is thermodynamically unstable. If a suitable condition arises such as high temperature in the absence or presence of a suitable chemical environment, catalysts will rearrange to form the more favourable lower surface area agglomerates, a process known as sintering [102-104].

2.7.3 Supported-gold catalysts for ethylene hydrogenation

Zeolites can act as dual-function catalysts after incorporating of a finely divided metal into the zeolite cavities [107]. Zeolite supported mono/bimetallic catalyst complexes are important industrial catalysts, for example, when used in the alkene polymerization reactions [108]. Mononuclear gold complexes are used frequently in organometallic chemistry and have been identified as catalysts for alkene hydrogenation, asymmetric aldol reactions, C-C bond formation etc. Supported gold catalysts have recently been found to be selective and surprisingly active for CO oxidation [109]. Their unique properties have been variously attributed to the smallness of the gold clusters and to the presence of clusters adjacent to cationic gold species at the support surface [110].

It has been reported that gold supported on oxides, namely SiO_2, Al_2O_3, and TiO_2 were found to be active for alkene hydrogenation and it was suggested that small gold clusters were the main catalytically active species [111]. It was further reported that the addition of gold to the oxides makes the oxides even less active for ethylene hydrogenation. The catalytic sites remain to be identified [112].

Gates et al., [113] reported that gold supported on magnesium oxide can also show activity for ethylene hydrogenation. They have reported on the preparation of a supported gold complex, $[Au(CH_3)_2\{OMg\}_2]$ and shows that it is a precursor of a mononuclear gold complex that catalyzes ethylene hydrogenation. Its steady state activity for ethylene hydrogenation was found to be less than 5%, corresponding to a reaction rate of 10^{-3} molecules of ethane converted $(Au\ atom)^{-1}s^{-1}$.

They have reported that EXAFS data did not indicate any Au-Au and Au-C contribution, suggesting that the mononuclear Au^{3+} complexes (oxidation state confirmed by XANES) is a catalytically active species for ethylene hydrogenation, and that the CH_3 ligands were removed before or during catalysis. As the Au-Au contribution increases they have noted that the activity decreases and that there was lack of activity on samples containing zerovalent Au [113]. They also reported that gold supported on magnesium oxide showed activity for CO oxidation and that the gold in the oxidation state (+1) appeared to play an important role on the catalytic reaction.

2.8 SUPPORTED METAL CATALYSTS FOR THE WATER-GAS SHIFT REACTION

The heterogeneously catalyzed water-gas-shift (WGS) reaction ($CO + H_2O \rightarrow CO_2 + H_2$) is a key step in fuel processing to generate H_2. Such heterogeneous catalysts should combine both high activity and structural stability in air and in cyclic operation; these are stringent requirements not met by the current commercially available low-temperature WGS catalysts. A new class of WGS catalysts based on cerium oxide (ceria) has been investigated extensively in recent years [114-119]. To provide low-temperature WGS activity, Pt-group metals (PM), Au, or Cu are suitably added in amounts that vary from 1 to 10 weight percent (wt%). A critical problem with Pt-ceria catalysts is their prohibitive economics [116] due to the cost of Pt, even if their issues of deactivation with time-on-stream are resolved. Similarly attractive would be ceria containing base metals or oxides. Flytzani-Stephanopoulos et al. [117-119] have reported recently that an excellent shift catalyst results from supporting Au or Cu on nanocrystalline ceria. This type of catalyst, if properly developed, would of course be much more economical, i.e., practical for large-scale fuel cell application. The PM-ceria catalysts have received considerable attention because of their use in the automobile catalytic converter [120, 121]. It is widely accepted that the oxygen in ceria plays an important role in the reaction pathway [114, 117, 122]. However, identification of the active sites for low-temperature CO oxidation, the WGS reaction, and other oxidation reactions on PM-ceria catalysts remains an issue of contention.

2.9 PREFERENTIAL OXIDATION OF CO (PROX) IN THE PRESENCE OF EXCESS HYDROGEN

In recent years, proton exchange membrane (PEM) H_2 fuel cells have been used for power generation in a variety of applications, and use of these devices is expected to grow as the energy sector moves toward hydrogen as an energy carrier. However, an important concern for the usage of PEM fuel cells is their sensitivity to low levels (ppm) of CO. In this respect, various studies have been conducted to explore CO-free fuel processing alternatives [123, 124]. A promising method to remove trace amounts of CO from H_2 supplied to the anode is by preferential oxidation of CO (PROX) in the presence of excess H_2 [123, 125]. An effective PROX catalyst should have high activity for CO oxidation as well as low activity for hydrogen oxidation, typically at low temperatures. For example, a good PROX catalyst should be able to selectively oxidize 10,000 ppm of CO to concentrations of less than 5 ppm, without decreasing the H_2 content of the reformate gas. The PROX reaction has been studied extensively on supported platinum catalysts such as Pt/Al_2O_3, Pt/Azeolite, Pt/modernite [126, 127]. In recent years, catalytic gold nano particles have attracted attention for PROX applications. Work on supported nano-gold catalysts by Haruta and co-workers [128] has shown that gold which was considered to be inert for catalytic applications [129], is in fact a good catalyst for low-temperature CO oxidation.

Depending on the nature of the support (Al_2O_3, TiO_2, MnOx, CeO_2 or a-Fe_2O_3) [130–134] and gold particle size, CO and H_2 oxidation reactions are affected to

different extents [135]. It has been reported that at low-temperatures Au/a-Fe_2O_3 shows higher PROX selectivity than a commercial Pt/c-Al_2O_3 catalyst [136]. Therefore, gold-based catalysts which have a relatively low and stable price compared to platinum group metals could help reduce the cost of fuel cell technologies [137]. Recent studies have also shown that Cu mixed with ceria oxide is a promising PROX catalyst [138, 139]. Other catalytic systems have also been examined for PROX applications, including bimetallic catalysts such as PtSn and PtAu [140, 141], and supported Ru, Rh and Pd [142, 143] catalysts. The results from low temperature water-gas shift, and CO oxidation reaction, over Au and Cu based catalysts, has been decribed as compared to more traditional Pt catalysts.

2.10 REFERENCES

[1] G. C. Bond, Heterogeneous Catalysis: Principles and Applications, Second edition, Clarendon. Oxford, (1990) 1.

[2] S. Beran, Chem. Phys. Lett. **84** (1981) 111.

[3] S. Beran, P. Jiru, B. Wichterlova, J. Chem. Soc. Faraday Trans. 1 **79** (1983) 1585.

[4] H. W. Haynes, Jr., Catal. Rev. Sci. Eng. **17** (1981) 273.

[5] D. H. Olson, E. Demsey, J. Catal. **13** (1969) 221.

[6] J. A. Rabo, (Ed.): Zeolite Chemistry and Catalysis. ACS Monograph 171, Washington 1976.

[7] Kh. M. Minachev, Catalysis on Zeolites, Budapest, Moscow, 1988.

[8] T. Kubo, H. Tomonaga, T. Kunugi, Bull. Chem. Soc. Japan **46** (1980) 3549.

[9] Z. Maskos, J.H.C. Van Hoof, J. Catal. **66** (1980) 73.

[10] (a) C. L. Angell, P. C. Schaffer, J. Phys. Chem. **70** (1970) 1413. (b) J. Sivaguru, A. Natarajan, L. S. Kaanumalle, J. Shailaja, S. Uppili, A. Joy, and V. Ramamyrthy, Acc. Chem. Res. **36** (2003) 509.

[11] D. Ballivet-Tkatchenko, G. Coudusier, Inorg. Chem. **18** (1981) 558.

[12] (a) R. L. Garten, W.N. Delgass, M. Boudart, J. Catal. **18** (1970) 90, (b) Y.Y. Huang, J. R. Anderson, J. Catal. **40** (1975) 143.

[13] C. Naccache, Y. ben Taarit, J. Chem. Soc. Faraday Trans. I, **69** (1973) 1475.

[14] B. Wichterlová, Z. Tvarůžková, J. Nováková, J. Chem. Soc. Faraday Trans. I, **79** (1983) 1573.

[15] (a) Kh.M. Minachev, G. V. Antoshin, E.S. Shpiro, Photoelectron spectroscopy and its application in catalysis. Nauka, Moscow (1981), (b) E. A. Stern, D.E. Sayers, F.W. Litle, Phys. Rev. B11, (1975) 48.

[16] P. Ratnasamy, A.J. Leonard, Catal. Rev. **6** (1972) 293.

[17] Kh.M. Minachev, Catalysis on Zeolites, Budapest, Moscow, (1988).

[18] J. C. Vedrine, M. Dufaux, C. Naccache, B. Imelik, J. Chem. Soc. Faraday Trans.. I, **74** (1978) 440.

[19] M. Primet, J. C. Vedrine, C. Naccache, J. Mol. Catal. **4** (1978) 4.

[20] M. K. Bahl, S. C. Tsai, Y.W. Chung., Phys. Rev. B **21** N4, (1980) 1344.

[21] R. A. Dalla Betta, M. Boudart, P. Gallezot, R. S. Weber, J. Catal. **69** (1981) 514.

[22] R. C. Baetzold, M. G. Mason, J. F. Hamilton, J. Chem. Phys. **72** (1980) 366.

[23] Y. Huang, J. Catal. **61** 461 (1980).

[24] J. Cattanach, E. I. Wu, P. B. Veenuto, J. Catal. **11** (1968) 342.

[25] N. Topsøe, K. Pedersen, E.G. Derouane, J. Catal. **70**, (1981) 41.

[26] H. Wise, P.R. Wentrcek, J.L. Falconer, J. Catalysis **45** (1976) 248.

[27] H. Wise, J. L. Falconer, J. Catal. **43** (1976) 220.

[28] U. S. Ozkan, J. M. Watson, J. Catal. **210** (2002) 295.

[29] O. V. Krylov, L.Ya. Margolis, M.Yc. Kutirev, A.A. Firsova, A.V .Sklyarov, G.W. Keulks, L. D. Krenzke, J. Catal. **52** (1978) 418.

[30] E. Iglesia, and M. Xu, J. Phys. Chem. B **102** (1998) 961.

[31] Sh. K. Shaikhutdinov, R. Meyer, M. Naschitzki, M. Baumer, and H.–J. Freund, Catalysis letters **86** (4), (2003) 211**.**

[32] A. Fürstner, Active Metals: Preparation, Characterization, and Application, Weinheim, (1996) 381.

[33] G. C. Bond, Heterogenous Catalysis: Principles and Applications, Second edition, Clarendon. Oxford, (1990) 78.

[34] M. Haruta, N. Yamada, T. Kobayashi, S. Ijima, J. Catal. **115** (1989) 301.

[35] A. Wolf, F. Schüth, Appl. Catal. A., **226** (2002) 1.

[36] J. L. Magitfalvi, A. Fási, M. Hegeds, F. Lónyi, S. Gbölös, N. Bogdanchikova, Catal. Today, **72** (2002) 157.

[37] A. Ueda, M. Haruta, Gold Bull. **32** (1) (1999) 3.

[38] R. J .H. Grisel, B.E. Nieuwenhuys, J. Catal. **199** (2001) 48.

[39] S. J. Lee, A. Gavriilidis, J. Catal. **206** (2002) 305.

[40] I. E. Wachs, and L.E. Fitzpatrick, Characterization of catalytic materials, Boston; Butterworth-Heinemann, (1992) 1.

[41] J. M. Thomas, and W.M. Thomas, Principles and practice of heterogeneous catalysis, VCH, (1997).

[42] G. C. Bond and D. T. Thompson, Catal. Review-sci. eng., **41** (3 & 4), (1999) 319.

[43] J. Weitkamp, M. Hunger, and U. Rymsa, Microporous and Mesoporous Materials, **48** (2001) 225.

[44] D. M. P. Mingos, J. Chem. Soc. Dalton Trans., (1996) 561.

[45] S. Tsubota, M. Haruta, T. Kobayashi, A. Ueda, Y. Nakahara, in: G. Poncelet, et al. (Eds.), Preparation of Catalysts, vol. V, Elsevier, (1991) 695.

[46] S. Ivanova, C. Petit, and V. Pitchon, Appl. Cat. A: General **267** (2004) 191.

[47] J. L. Lemaitre, P. G. Menon, F. Delannay, in F. Delannay (Ed.), Characterization of Heterogeneous Catalysts, Marcel Dekker, New York, (1984) 299.

[48] A Benedetti, Small-Angle scattering of heterogeneous catalysts, J. Appl. Crstallogr. **30** (1997) 647.

[49] A. Borodziski, M. Bonarowska, Relation between crystallite size and dispersion on supported metal catalysts, Langmuir, **13** (1997) 5613.

[50] A. Benedetti, G. Goerigk, F. Pinna, P. Riello, ASAXS Investigation of Au/C catalyst, J. Catal. **171** (1997) 345.

[51] P. F. Kane and B. Graydon, Characterization of solids surfaces, New york: plenum press, (1974).

[52] A. Benedetti, L. Bertoldo, P. Canton, G. Goerigk, F. Pinna, P. Riello, S. Polizzi, Catal. Today **49** (1999) 485.

[53] S. D. Robertson, B. D. McNicol, J. H. De Bass and S. C. Kloet, J. Catal. **37** (1975) 424.

[54] S. J. Gentry, and P. T. Walsh, J. Chem. Soc. Faraday Trans. I **78** (1982) 1515.

[55] P. A. Jacobs, J. Linart, H. Nijs, and J. B. Uytterhoeven, J. Chem. Soc. Faraday Trans. I **73** (1977) 1745.

[56] N. Wagstaff, and R. Prins, J. Catal **59** (1979) 434.

[57] B. H. Isaacs, and E.E. Petersen, J. Catal. **77** (1982) 43.

[58] A. Lycourghiotis, C. Defosse, F. Delannay, J. Lemaitre, and B. Delmon, J. Chem. Soc. Faraday Trans. I **76** (1980) 1677.

[59] S. D. Gentry, N.W. Hurst, and A. Jones, J. Chem. Soc. Faraday Trans. I **77** (1981) 603.

[60] G. R. Hearne, T. Magadzu and M. S. Scurrell, Unpublished report on ^{197} Au Mössbauer Spectroscopy of Au-Zeolites Catalysts; May 2005.

[61] D. C. Koningsberger, R. Prins, X-ray Absorption, Principles, techniques of EXAFS, SEXAFS and XANES, John Wiley & Sons, New York, 1988; I. Arčon, B. Mirtič, A. Kodre, Determination of valence states of chromium in calcium chromates by using X-Ray Absorption Near-Edge Structure (XANES) Spectroscopy, J. Am. Ceram. Soc. **81** (1998) 222; J. Wong, F.W. Lytle, R. P. Messmer, D. H. Maylotte, K-edge Absorption Spectra of Selected Vanadium Compounds, Phys. Rev., B **30**, (1984) 5596.

[62] M. Venecia, Catal. Today, **77** (2003), 359.

[63] M. Christian, and P. Claus, Science Progress, **84**, (2001), 311.

[64] S. Minico, S. Scire, C. Crisafulli, A. M. Visco and S. Galvagno, Catalysis Letters, **47** (1997) 273.

[65] A. T. Bell, Science, **299** (2003) 1688.

[66] M. Valden, X. Lai, and D. W. Goodman, Science **281** (1998) 1647.

[68] U. Heiz, , A. Sanchez., S. Abbet, & W. -D. Schneider, J. Am. Chem. Soc. **121** (1999) 3214.

[69] V. P. Zhdanov and B. Kasemo, Surf. Sci., **405** (1998) 27.

[70] M. A. Acc El-Sayed, Chem. Res., **34** (2001) 257.

[71] P. V. Kamat, J. Phys. Chem. B, **106** (2002) 7729.

[72] S.K. Ghosh, S. Nath, S. Kundu, K. Esumi, T. J. Pal, Phys. Chem. B, **108** (2004) 13963.

[73] Y. C. Cao, R. C. Jin, J. M. Nam, C. S. Thaxton, C. A. Mirkin, J. Am. Chem. Soc., **125** (2003) 14676.

[74] S. J. Park, A. A. Lazarides, J. J. Storhoff, L. Pesce, C. A. Mirkin, J. Phys. Chem. B, **108** (2004) 12375.

[75] Y. Y. Yu, S. S. Chang, C. L. Lee, C. R. C. Wang, J. Phys. Chem. B, **101** (1997) 6661.

[76] N. Kometani, H. Doi, K. Asami, Y. Yonezawa, Phys. Chem. Chem. Phys., **4** (2002) 5142.

[77] A. S. Korchev, M. J. Bozack, B. L. Slaten, G. J. Mills, Am. Chem. Soc., **126** (2004) 10.

[78] T. Hirose, T. Omatsu, M. Sugiyama, S. Inasawa, S. Koda, Chem. Phys. Lett., **390** (2004) 166.

[79] R. C. Jin, Y. C. Cao, E. C. Hao, G. S. Metraux, G. C. Schatz, C. A. Mirkin, Nature, **425** (2003) 487.

[80] R. C. Jin, Y. W. Cao, C. A. Mirkin, K. L. Kelly, G. C. Schatz, J. G. Zheng, Science, **294** (2001), 1901.

[81] A. Callegari, D. Tonti, M. Chergui, Nano Lett., **3** (2003) 1565.

[82] L. Longenberger, G. Mills, J. Phys. Chem., **99** (1995) 475.

[83] K. Kurihara, J. Kizling, P. Stenius, J. H. Fendler, J. Am. Chem. Soc., **105** (1983) 2574.

[84] A. K. Gangopadhayay, A. J. Chakravorty, Chem. Phys., **35** (1961) 2206.

[85] S. Eustis, H-Y. Hsu, and M. A. El-Sayed, J. Phys. Chem. B, **109** (2005) 4811.

[86] M. Haruta, N. Yamada, T. Kobayashi and S. IiJima, J. Catal., **115** (1989), 301.

[87] M. Haruta, S. Tsubota, T. Kobayashi, H. Kageyama, M. J. Genet and B. Delmon, J. Catal., **144** (1993), 175.

[88] F. Boccuzzi, A. Chiorino, S. Tsubota, and M. Haruta, Catalysis Letters **29** (1994) 225.

[89] V. A. Bondzie, C. Parker, and C. T. Campbell, Catalysis Letters, **63** (1999) 143.

[90] P. E. Hathaway, and M. E. Davis, J. Catal., **116** (1989) 263.

[91] T. Baba, G. J. Kim, and Y. Ono, J. Chem. Soc. Faraday Trans., **88** (1992) 891.

[92] (a) J. N. Lin, J. H. Chen, C. Y. Hsiao, Y. M. Kang, and B. Z. Wan, Appl. Cat. B: Env., **36** (2002) 19. (b) Lin, Y. N. and Wan, B. Z., Appl. Catal. B: Env. **41** (2003) 83.

[93] H. Sakuri, M. Haruta, Appl. Catal. **127** (1995) 93.

[94] H. Sakuri, S. Tsubota, M. Haruta, Appl. Catal. **102** (1993) 125.

[95] M. Shibata, N. Kawata, T. Matsumoto, H.M. Kimura, Chem. Lett. (1985) 1605.

[96] D. A. Buchannan, G. Webb, J. Chem. Soc., Faraday Trans. **270** (1978) 134.

[97] (a) P. S. Cremer, X. Su, G. A. Somorjai and Y. Ron Shen, J. Mol. Cat. A: Chemical, **131** (1998), 225. (b) P. S. Cremer, X. Su, G. A. Somorjai and Y. Ron Shen, J. Am. Chem. Soc., **118** (1996), 2942.

[98] A. M. Doyle, S. K. Shaikkhutdinov, S. D. Jackson, Angew. Chem. Int. Ed, **42** (2003), 5240.

[99] T. V. W. Janssens, D. Stone, J. C. Hemminger F. Zaera, J. Catal., **177**, (1988) 284.

[100] H. Ofner and F. Zaera, J. Phys. Chem. B: **101**, (1997) 396.

[101] F. Zaera, Catal. Letters., **91** (2003) 1.

[102] H. Calvin, E. W. Bartholom, Applied Catalysis A: General, **212** (2001), 17.

[103] H. Liu, L. Su, H. Wang, W Shen, X. Bao and B. X. Yide, Appl. Catal. A: General, **236** (2002) 263.

[104] H. S. Cerqueira, P. Ayrault, J. Datka, P. Magnoux and M. Guisnet, Journal of Catalysis, **196** (2000) 149.

[105] D. L. Trimm, Applied catalysis A: General, **212** (2001) 153.

[106] M. Guisnet and P. Mgnoux, Applied Catalysis A: General, **212** (2001) 83.

[107] J. M. Thomas and W.J. Thomas, Principle and Practice of Heterogeneous Catalysis WeinHeim. New York, Basel, Cambridge, Tokyo, (1997).

[108] G. G. Hlatky, Chem. Rev., **100** (2000) 1347.

[109] M. Haruta, S. Tsubota, T. Kobayashi, H. Kageyama, M. J. Genet, B. Delmon, J. Catal. **144** (1993) 175.

[110] (a) H.-S. Oh, C. K. Costello, C. Cheung, H.H. Kung, M.C. Kung, Stud. Surf. Sci. Catal. **139** (2001) 375. (b) J. Guzman, B. C. Gates, J. Phys. Chem. B **106** (2002) 7659.

[111] P. A. Sermon, G.F. Bond, P. B. Wells, J. Chem. Soc. Faraday Trans. I **75** (1979) 385.

[112] S. Lin, M.A. Vannice, Catal. Lett. **10** (1991) 47.

[113] J. Guzman and B. C. Gates, Angew. Chem. Int. ed, **42** (2003) 690.

[114] T. Bunluesin, R. J. Gorte, G. W. Graham, *Appl. Catal. B* **15** (1998) 107.

[115] S. L. Swartz, M. M. Seabaugh, C. T. Holt, W. J. Dawson, *Fuel Cell Bull.* **30** (2001) 7.

[116]J. M. Zalc, V. Sokolovskii, D. G. Loffler, *J. Catal.* **206**, 169 (2002).

[117] Y. Li, Q. Fu, M. Flytzani-Stephanopoulos, *Appl. Catal. B* **27,** 179 (2000).

[118] Q. Fu, A. Weber, M. Flytzani-Stephanopoulos, *Catal. Lett.* **77**, 87 (2001).

[119] Q. Fu, S. Kudriavtseva, H. Saltsburg, M. Flytzani-Stephanopoulos, *Chem. Eng. J.* **93**, 41 (2003).

[120] H. S. Gandhi, A. G. Piken, M. Shelef, R. G. Delosh, *SAETech. Papers* **55,** (1976) 201.

[121] M. Shelef, G. W. Graham, R. W. McCabe, in *Catalysis by Ceria and Related Materials*, A. Trovarelli, Ed., Catalytic Science Series, vol. 2 (Imperial College Press, London, 2002) 343–376.

[122] A. Trovarelli, *Catal. Rev. Sci. Eng.* **38**, 439 (1996).

[123] T. V. Choudhary and D. W. Goodman, Catal. Today **77** (2002) 65.

[124] R. R. Davda and J. A. Dumesic, Angew. Chem. Int. Ed. **42** (2003) 4068.

[125] O. Korotkikh and R. Farrauto, Catal. Today **62** (2000) 249.

[126] H. Igarashi, H. Uchida, M. Suzuki, Y. Sasaki and M. Watanabe, Appl. Catal. A Gen. **159** (1997) 159.

[127] M. J. Kahlich, H. A. Gasteiger and R.J. Behm, J. Catal. **171** (1997) 93.

[128] M. Haruta, S. Tsubota, T. Kobayashi, H. Kageyama, M. J. Genet and B. Delmon, J. Catal. **144** (1993) 175.

[129] B. Hammer and J. K. Nørskov, Nature **376** (1995) 238.

[130] R. M. T. Sanchez, A. Ueda, K. Tanaka and M. Haruta, J. Catal. **168** (1997) 125.

[131] R.J.H. Griesel and B.E. Nieuwenhuys, J. Catal. **199** (2001) 48.

[132] M. J. Kahlich, H. A. Gasteiger and R. J. Behm, J. Catal. **182** (1999) 430.

[133] G. K. Bethke and H. H. Kung, Appl. Catal. A Gen. **194** (2000) 43.

[134] T. V. Choudhary, C. Sivadinarayana, C. Chusuei, A. K. Datye, J. P. Fackler Jr and D. W. Goodman, J. Catal. **207** (2002) 247.

[135] M. M. Schubert, V. Plzak, J. Garche and R. J. Behm, Catal. Lett. **76** (2001) 143.

[136] G. Avgouropoulos, T. Ioannides, C. Papadopoulou, J. Batista, S. Hocevar and H. K. Matralis, Catal. Today **75** (2002) 157.

[137] D. Cameron, R. Holliday and D. Thompson, J. Power Sources **118** (2003) 298.

[138] G. Avgouropoulos, T. Ioannides, H. K. Matralis, J. Batista and S. Hocevar, Catal. Lett. **73** (2001) 33.

[139] D. H. Kim and J. E. Chua, Catal. Lett. **86** (2003) 107.

[140] M. M. Schubert, M. J. Kahlich, G. Feldmeyer, M. Huttner, S. Hackenberg, H.A. Gasteiger and R. J. Behm, Phys. Chem. Chem. Phys. **3** (2001) 1123.

[141] J. Zhang, Y. Wang, B. Chen, C. Li, D. Wu and X. Wang, Energy Conv. Mgmt. **44** (2003) 1805.

[142] P. V. Snytnikov, V. A. Sobyanin, V. D. Belyaev, P. G. Tsyrulnikov, N. B. Shitova and D. A. Shlyapin, Appl. Catal. A Gen. **239** (2003) 149.

[143] H. Tanaka, S. Ito, S. Kameoka, K. Tomishige and K. Kunimori, Catal. Commun. **4** (2003) 1.

CHAPTER 3

EXPERIMENTAL

3.1 INTRODUCTION

The efficiency of chemical reactions involving metals as catalysts or reducing agents for various transformations largely depends on the active surface area, which is generally a direct function of the degree of metal dispersion. The activity of the metals is greatly improved when they are finely and homogeneously distributed on an appropriate support [1]. Due to the continuing interest in metal activation, a considerable variety of activating procedures has been developed.

These methods invariably consist of two main strategies, either aiming at the effective removal of the deactivating oxide layers from the metal surface by chemical or mechanical means, or at achieving a fine distribution of the metal in an appropriate solvent. Many activation procedures have been developed, such as simple grinding, dispersion to form colloids [2], formation of amalgams [3] and ultrasonic irradiation [4], fine dispersions on various supports [5], and reduction of metal salts in solution or on a solid support interface.

For the conclusive elucidation of the morphology of heterogeneous catalysts, which is a prerequisite for understanding the relationship between morphology and activity, a combination of various analytical methods is called for [6]. X-ray

diffraction and X-ray absorption are powerful tools that provide structural information on the atomic scale, spatially averaged over a total of, generally, not less than some 10^{18} unit cells [6]. However, due to the heterogeneity of catalysts a complete knowledge of the morphology of these materials can only be obtained by also using microscopic methods.

3.2 REAGENTS AND CHEMICALS

All chemicals were generally reagent grade and were used as received except where otherwise mentioned. The gold precursors used included chloroauric acid, $HAuCl_4$ and potassium dicyanoaurate, $KAu(CN)_2$ both purchased from Next-Chemica (Pty) Limited/Johnson Matthey, and trichlorobisethylenediamine gold(III), $Au(en)_2Cl_3$ which were prepared in our laboratory from chloroauric acid [7]. Zeolite powder, Y (LZY-52) was obtained from Union Carbide Corporation (Linde Division). $Fe(NO_3)_3.9H_2O$, $Cr(NO_3)_3.9H_2O$, $NiNO_4.6H_2O$, and $Co(NO_3)_2.6H_2O$ were purchased from the Sigma-Aldrich company. Ethylenediammine, $NH_2CH_2CH_2NH_2$, and ethyl alcohol, CH_3CH_2OH, were both from Merck-Schuchardt. Tri-sodium citrate was obtained from BDH Chemicals Ltd and sodium borohydride ($NaBH_4$) was from SAARChem (Pty) Ltd. Potassium nitrate, KNO_3; sodium nitrate, $NaNO_3$; lithium nitrate $LiNO_3$; sodium hydroxide, NaOH; potassium hydroxide, KOH; were all from Merck-Schuchardt. African Oxygen Limited (AFROX) supplied all the gases used. Ultra high purity H_2 (UHP, 99.999%) was used as carrier gas, and 10 % O_2/He and 10 % CO/He were both used as gas mixture for CO oxidation reactions. 5% H_2 in He and 5% O_2 in He

were both used for Temperature Programmed Reduction (TPR) and Oxidation (TPO) studies respectively.

3.3 PREPARATION OF MODIFIED ZEOLITES AND GOLD PRECURSOR

3.3.1 Preparation of the acidic zeolites: HY

Approximately 24.00 g of Y-zeolite (UOP LZY-52, Si/Al = 2.8) was refluxed three times in an aqueous solution of 1M NH_4Cl (120-ml) for 3 h, at 80 ^{0}C. The slurry was filtered and washed thoroughly with distilled water, to remove the NaCl formed. The solution was checked for any remaining chlorides with a conductivity meter until the conductivity of 350 μs, which is equivalent to chlorine free deionized water, was achieved. The slurry was dried at 120 ^{0}C in an oven. Then the resultant powder of NH_4Y zeolite was heated in a stream of inert gas, N_2, for 30 h with a low rate of temperature increase (12 K/h) up to 673 K and then held at this temperature for 10 h. In this way the acidic HY type zeolite was obtained [8].

3.3.2 Preparation of alkali-modified zeolites-Y

Prior to the gold loading process zeolite-Y, was introduced into different alkaline metal nitrate solutions (i.e. $LiNO_3$, $NaNO_3$, and KNO_3), each having a

concentration of 1 M. The solution pH was adjusted to 6 with a 1 M nitric acid solution at room temperature, instead of using sodium hydroxide, (as used by Wan et al.[9]) since the pH of suspended zeolite in distilled water was above 6 and then refluxed at 60 ^{0}C for 48 hours. After two days the pH was approximately 6. Slurries of zeolite powder were filtered and dried at room temperature, then sieved through a 150 μm sieve and the samples were designated as LiY, NaY, and KY, depending on the alkali metal introduced.

3.3.3 Preparation of the organogold complex: $Au(en)_2Cl_3$ [7]

Reaction equation: $HAuCl_4 + 2\ en \rightarrow [Au(en)_2]^{3+}Cl^- + HCl$ (in ethereal solution)

Approximately, 1 ml of 1.2-ethanediamine monohydrate was added to 5 ml of diethyl ether. The resulting cloudy solution was added drop-wise to a solution of 1.022 g of $HAuCl_4$ in 10 ml ether in a 100 ml beaker. A gummy yellow precipitate was formed in a cloudy solution and the latter was decanted off into another beaker. The yellow precipitate was then dissolved in 3 ml of water forming an orange solution. A white precipitate formed upon the addition (with frequent swirling) of 20 ml of ethyl alcohol. The precipitate was allowed to settle down and the yellowish solution was carefully decanted. The white precipitate was once again dissolved in 2.3 ml of water and re-precipitated with 15 ml of ethyl alcohol [7]. The complex was then left to dry at room temperature.

3.4 PREPARATION OF BOTH MONO- AND BI-METALLIC CATALYSTS

3.4.1 Preparation of Au/M-Y (M = Ni^{2+}, Fe^{3+}, Co^{2+} and Cr^{3+}): source of gold, $KAu(CN)_2$.

Zeolite catalysts were prepared by carrying out ion-exchange process of metal stabilizers or modifiers and impregnation to incipient-wetness method of metal catalyst as discussed below: $Fe(NO_3)_3.9H_2O$ in degassed deionized water was added slowly into a well stirred zeolite-Y type (UOP LZY-52; Y, Si/Al = 2.8)/deionized water suspension (1 g/100 ml), which was previously acidified to pH 4 by dilution with HNO_3. Both reagents were flushed with nitrogen gas during the entire duration of the ion exchange process. The zeolite was then filtered off, washed thoroughly with deionized water and dried at room temperature for two days, to form a yellowish powder of Fe-NaY. Gold, from $KAu(CN)_2$ was introduced by incipient-wetness method to form a bimetallic catalyst, Au/Fe-Y (3.29wt%Au:1.88wt%Fe). Slurry of metal stabilizer-exchanged Y containing gold was then dried in an oven for overnight at 120 ^{0}C and then sieved through a 150 μm sieve. The metal loading of Au/M-Y (where M is the metal stabilizer consisting of transition metal loading in the range of 1.76 – 5.45 wt%M) and gold loading in the range of 1.67 – 7.48 wt% Au was used (Table 3.1).

Au/Cr-Y (3.26wt%Au:1.76wt%Cr), Au/Ni-Y (3.35wt%Au:1.79wt%Ni), and Au/Co-Y (3.47wt%Au:1.84wt%Co) were also prepared following the same

procedure as above and their metal loadings are as shown in Table 3.2, Table 3.3 and Table 3.4 respectively. Sources of chromium, nickel and cobalt used are $Cr(NO_3)_3.9H_2O$, $NiSO_4.6H_2O$ or $Ni(NO_3)_2.6H_2O$ and $Co(NO_3)_2.6H_2O$ respectively.

Table 3.1: Metal loading of Au/Fe-Y sample

Sample No.	Fe (wt%)[b]	Au (wt%)[b]	Fe-Au (Mass ratio)[a]
1	1.88	7.48	3.98
2	1.88	5.45	2.90
3	1.88	3.29	1.75
4	1.88	1.67	0.89

[a] mass ratio = Au (wt%)/Fe (wt%). [b] Gold and transition metal content was determined by X-ray Fluorescence Spectroscopy (XRF) at the Northwestern University, USA and/or by fire assay and gravimetric finish method at the Performance Laboratories in Randfontein, South Africa.

Table 3.2: Metal loading of Au/Cr-Y sample

Sample No.	Cr (wt%)[b]	Au (wt%)[b]	Cr-Au (Mass ratio)[a]
1	1.76	3.26	1.85

[a] mass ratio = Au (wt%)/Cr (wt%). [b] Gold and transition metal content was determined by X-ray Fluorescence Spectroscopy (XRF) at the Northwestern University, USA and/or by fire assay and gravimetric finish method at the Performance Laboratories in Randfontein, South Africa.

Table 3.3: Metal loading of Au/Ni-Y sample

Sample No.	Ni (wt%)[b]	Au (wt%)[b]	Ni-Au (Mass ratio)[a]
1	1.79	3.35	1.87

[a] mass ratio = Au (wt%)/Ni (wt%). [b] Gold and transition metal content was determined by X-ray Fluorescence Spectroscopy (XRF) at the Northwestern University, USA and/or by fire assay and gravimetric finish method at the Performance Laboratories in Randfontein, South Africa.

Table 3.4: Metal loading of Au/Co-Y sample

Sample No.	Co (wt%)[b]	Au (wt%)[b]	Co-Au (Mass ratio)[a]
1	1.84	3.47	1.89

[a] mass ratio = Au (wt%)/Co (wt%). [b] Gold and transition metal content was determined by X-ray Fluorescence Spectroscopy (XRF) at the Northwestern University, USA and/or by fire assay and gravimetric finish method at the Performance Laboratories in Randfontein, South Africa.

Prior to any catalytic test, samples of about 200 mg were pretreated in a quartz reactor for 2 h at 400 ^{0}C under 10%O_2 / He atmosphere (flow rate: 14 ml/min).

3.4.2 Preparation of Au/Y (3.49wt%Au) and Au/HY (3.77wt%Au): source of gold, $Au(en)_2Cl_3$

3.4.2.1 In-situ reduction of Au on HY

3.4.2.1.1 In-situ reduction of Au in the absence of protecting agents

Gold was introduced by ion-exchange on HY-zeolite counter-ions using, $[Au(en)_2]^{3+}$ as the source of gold. Approximately 0.315 g of $Au(en)_2Cl_3$ was dissolved in 100 ml of water in a round bottom flask. To the solution, 3.529 g of the zeolite HY was added so as to introduce 0.406 mmol of gold per g of zeolite. The mixture was stirred under reflux for 24 hours at 60 ^oC, after which 0.406 mmol of $NaBH_4$ (molar ratio, Au:$NaBH_4$ = 1:1) was introduced drop-wise into it and stirring was maintained for the next 24 hours at room temperature. The catalyst was then filtered and washed to remove any chlorides (which are notorious for catalyst poisoning). It was then left to dry at room temperature after which it was filtered with a 150 μm sieve. Prepared Au/HY was called **untreated** if $NaBH_4$ was not used after preparation and **treated** if $NaBH_4$ was used to reduce Au, before or after washing.

Similar preparation procedure as above was followed, on Au/HY while varying the molar ratio of Au to that of $NaBH_4$. The Au/HY was undertaken by using molar ratio of Au:$NaBH_4$ of 1:3 and 1:4, under the same conditions as reported above.

The disappearance of $[Au(en)_2]^{3+}$ ions and the formation of Au nanoparticles was monitored by UV-Vis spectra recorded on a Shimadzu UV-2201 recording spectrophotometer. X-Ray powder diffraction (XRD) patterns of the products were determined on a D/MAX-RA rotating anode X-Ray diffractometer with high intensity Cu-Kα radiation (λ = 0.151478 nm) and a graphite monochrometer at a scanning rate of 0.02 s^{-1} ranging from 40 to 90°.

3.4.2.1.2 In-situ reduction of Au in the presence of polyethylene gycol (PEG), as the protecting agents on HY.

Herein the protecting agent, polyethylene glycol (PEG) was introduced with the hope of preventing the agglomeration of gold nanoparticles formed immediately after reduction of gold [10]. Equal molar ratios of gold to that of the reducing agent (sodium borohydride, $NaBH_4$, ascorbic acid and tri-sodium citrate) were used. A higher molar ratio of protecting agent to that of metal was also used, with the hope of producing smaller gold particles [11, 12]. In the case of ascorbic acid, the ascorbic acid-PEG solution was neutralised with a 1M K_2CO_3 solution before being introduced drop-wise to the solution of ion-exchanged Au/HY catalysts.

3.4.2.2 In-situ reduction of Au on Y (3.02wt%Au)

The very same procedure as above, (using $Au(en)_2Cl_3$ as the source of gold) was followed to prepare the reduced Au/NaY (3.02wt%Au), which were then compared with that of **untreated** Au/Y (3.49wt%Au). An equivalent molar ratio

of reducing agents (ascorbic acid and $NaBH_4$) to that of gold was used in this case and such catalyst was called **treated** Au/Y (3.02wt%Au).

The samples prepared are shown in Table 3.5, which also gives detailed information on the catalyst parameters and some catalytic data under CO oxidation conditions (see data).

Table 3.5: Au content (wt%) and observed steady state activity for CO oxidation[a]

Sample	Au[b, c]	Reducing agents	Activity (%)[d]
Au/HY	3.77	untreated	17 ± 0.8
Au/HY	3.73	Au:$NaBH_4$, 1:1	27 ± 1
Au/HY	3.76	Au:$NaBH_4$, 1:3	30 ± 1
Au/HY	3.75	Au:$NaBH_4$, 1:4	60 ± 1
Au/HY	3.66	Au: Na_3-Citrate, 1:1	9 ± 2
Au/HY	2.72	Au: Ascorbic acid, 1:1	6 ± 0.8
Au/Y	3.49	untreated	0
Au/Y	3.02	Au:$NaBH_4$, 1:1	25 ± 1

[a] Reaction conditions: 10% CO/He and 10%O_2/He, Total Flow rate = 42ml/min, W/F = 0.005g.min/ml, pressure 1 bar, CO oxidation reaction performed at 450 ^oC. Pre-treated in O_2 at 400 ^0C for 2 h. [b] Au precursor is $Au(en)_2Cl_3$. [c] Gold content was determined by X-ray Fluorescence Spectroscopy (XRF) at the Northwestern University, USA and/or by fire assay and gravimetric finish method at the Performance Laboratories in Randfontein, South Africa. [d] Steady state catalytic activity calculated as CO_{in} - CO_{out}/ CO_{in}*100.

3.4.3 Preparation of Au/Y (3.67wt%Au): source of gold, $KAu(CN)_2$

Gold was introduced by the incipient-wetness method on Y-zeolite counter-ions using potassium dicyano aurate, $KAu(CN)_2$ as the gold source. Approximately 0.117 g of $KAu(CN)_2$ was dissolved in an equivalent amount of water so as to completely absorb Au particles within the pores of the zeolite (incipient-wetness). Slurries was dried at 120 ^{0}C for 16 h and then the Au/Y powder was introduced into the solution of ascorbic acid, and also $NaBH_4$, with an equivalent molar ratio to that of gold (i.e., 0.406 mmol). The mixtures were stirred for 16 h at room temperature. The reduced slurry was dried at 120 ^{0}C overnight and sieved through 150 μm sieve. A reduced Au/Y (3.46wt%Au) was called **treated** if trisodium citrate, ascorbic acid or $NaBH_4$ were used and **untreated** if the reducing agents were not used.

The samples prepared are shown in Table 3.6, which also gives detailed information on the catalyst parameters and some catalytic data under CO oxidation conditions (see data).

Table 3.6: Au content (wt%) and observed steady state activity for CO oxidation[a]

Sample	Au[b, c]	Reducing agents	Activity (%)[d]
Au/Y	3.67	untreated	18 ± 1
Au/Y	3.46	Au:$NaBH_4$, 1:1	26 ± 1
Au/HY	3.65	Au:$NaBH_4$, 1:1	45 ± 3
Au/Y	1.45	$Au(en)_2Cl_3$: Ascorbic acid, 1:1	0

[a] Reaction conditions: 10% CO/He and 10%O_2/He, Total Flow rate = 42ml/min, W/F = 0.005g.min/ml, pressure 1 bar, CO oxidation reaction performed at 450 ^{0}C. Pre-treated in O_2 at 400 ^{o}C for 2 h. [b] Au precursor is $KAu(CN)_2$, unless otherwise stated. [c] Gold content was determined by X-ray Fluorescence Spectroscopy (XRF) at the Northwestern University, USA and/or by fire assay and gravimetric finish method at the Performance Laboratories in Randfontein, South Africa. [d] Steady state catalytic activity calculated as CO_{in} - CO_{out}/ CO_{in}*100.

3.4.4 Preparation of Au on alkali-modified zeolite-Y

Anionic adsorption of chloroauric acid, $HAuCl_4$, and ion-exchange of $Au(en)_2Cl_3$, and incipient-wetness loading of $KAu(CN)_2$ were used. For each source four different catalysts were prepared from different supports (i.e. LiY, modified with $LiNO_3$ solution, 1M; NaY, modified with $NaNO_3$ solution, 1M; and KY, modified with KNO_3 solution, 1M) including the untreated zeolite-Y.

3.4.4.1 Catalysts preparation using ion-exchange methods

3.4.4.1.1 Gold source, $Au(en)_2Cl_3$

Approximately 0.043 g $Au(en)_2Cl_3$ was dissolved in 50 ml of distilled water and the solution was stirred while adjusting the pH to 6 with KOH or NaOH, depending on the support used. About 0.957 g of zeolite type-Y (unmodified, Y-zeolite), LiY (modified with $LiNO_3$ solution, 1M), NaY (modified with $NaNO_3$ solution, 1M) and KY (modified with KNO_3 solution, 1M), was added to the solution of $Au(en)_2Cl_3$ at room temperature so as to introduce a 2wt.% Au loading. The pH was adjusted to 6.8 over 30 minutes and thereafter the temperature was raised to 70 ^{0}C and the mixture was allowed to reflux for 20 hours with stirring. Then the catalyst was filtered and washed to remove any chloride and dried at room temperature for 24 hours. The catalyst powder was then sieved through a 150 μm sieve, to obtain uniform particle size.

3.4.4.1.2 Gold source, $HAuCl_4$

A similar procedure to that described above was followed to prepare Au/Y, Au/LiY, Au/NaY and Au/KY with $HAuCl_4$ as gold source. However, approximately 0.040 g of $HAuCl_4$ and 0.960 g of zeolite-Y were mixed to obtain a loading of 2 wt%Au.

3.4.4.2 Catalysts preparation using impregnation

3.4.4.2.1 Gold source, $KAu(CN)_2$

Approximately 0.029 g of $KAu(CN)_2$ was dissolved in 1 ml of distilled water. While stirring the gold containing solution, approximately 0.971 g of zeolite type-Y, LiY, NaY and KY, was added to the solution, so as to introduce 2wt%Au. The slurry formed was exposed to heat treatment at 80 ^{0}C with stirring to evaporate the water. The catalyst was dried in an oven at 120 ^{0}C for 48 hours and thereafter sieved through a 150 μm sieve.

The samples prepared are shown in Table 3.7, which also gives detailed information on the catalyst parameters and some catalytic data under CO oxidation conditions (see data).

Table 3.7: Au content (wt%) and observed steady state activity for CO oxidation[a]

Sample	Au[b, c]	Alkali metals	Activity (%)[d]
Au/Y	0.277	untreated	6 ± 1
Au/LiY	0.212	$LiNO_3$	5 ± 1
Au/NaY	0.772	$NaNO_3$	60 ± 2
Au/KY	0.454	KNO_3	40 ± 3

[a] Reaction conditions: 10% CO/He and 10%O_2/He, Total Flow rate = 42ml/min, W/F = 0.005g.min/ml, pressure 1 bar, CO oxidation reaction performed at 150 ^{0}C. Pre-treated in O_2 at 200 ^{0}C for 2 h. [b] Au precursor is $HAuCl_4$. [c] Gold content was determined by X-ray Fluorescence Spectroscopy (XRF) at the Northwestern University, USA and/or by fire assay and gravimetric finish method at the Performance Laboratories in Randfontein, South Africa. [d] Steady state catalytic activity calculated as CO_{in} - CO_{out}/ CO_{in}*100.

3.4.5 Preparation of Au supported on TiO_2 modified with Cu

3.4.5.1 Preparation of Au-Cu/TiO_2 catalyst (2.84wt%Au:0.32wt%Cu)

3.4.5.1.1 Incipient-wetness impregnation of Cu onto TiO_2 (anatase, 200 m^2/g)

Cu was introduced, first by an incipient-wetness method. About 0.0095g $Cu(NO_3)_2$*$2.5H_2O$ (99.99% purity, Aldrich), per gram TiO_2 (anatase 200 m^2/g) was dissolved in 1.2 cm^3 of doubly distilled water (DDI), and the solution's pH was raised to 5.1, before adding the solution onto the support (so as to obtain the Cu loading of 0.32wt.%). The catalyst was dried and exposed to the heat of a light bulb for 3 to 4 hours. Part of the as-prepared Cu/TiO_2 catalysts was calcined in air at 350 ^oC for 4 h, and such catalyst would be referred to as CuO/TiO_2 (0.32wt%) or calcined Cu/TiO_2 (0.32wt%).

3.4.5.1.2 Deposition-precipitation of Au onto calcined Cu/TiO_2 (0.32wt%Cu)

Au was introduced by deposition-precipitation method onto the calcined Cu/TiO_2 (0.32wt.%) powder as described below: About 0.636 g of $HAuCl_4$ was dissolved in 20 ml DDI at room temperature and the solution was transferred to 180 ml of DDI already in the 500 ml beaker at 70 ^0C. The 100 ml beaker was washed with a further 20 ml to completely transfer all the gold salt. In order to minimize possible light-sensitive reactions of the Au precursor, the synthesis was carried out with minimal exposure to light. About 0.33 g NaOH (in 40 ml DDI) solution was

added dropwise, to the Au solution until a solution pH of 7.2 was reached. After the pH was adjusted to 7.2, the Au solution was allowed to hydrolyze for 1 h at 70 ^{0}C. After hydrolysis at 70 ^{0}C and pH ~ 7.2, the Au solution was added with vigorous stirring to 3.7 g of calcined Cu/TiO_2 (0.32wt%) suspended in 100 ml of doubly distilled H_2O at 40 ^{0}C. The pH after adding Au solution onto the support was found to have dropped to ca. 6.6 and the pH was readjusted to pH 7.0 by adding two drops of NaOH. The mixture was stirred for 2 h at 40 ^{0}C. The sample was then suction filtered, re-suspended in 300 ml of room temperature deionized water, and suction filtered. This procedure was repeated again with 300 ml of water at room temperature followed by 300 ml of warm water (50 ^{0}C). The catalyst was dried at room temperature (covered with aluminium foil, to minimize exposure to light) overnight. The Au and Cu content in the obtained sample was determined by X-ray Fluorescence (XRF) Spectroscopy. After preparation, part of the sample [~ 0.5g Au-Cu/TiO_2 (2.84wt%Au:0.32wt%Cu)] was calcined in a very shallow ceramic dish in air at 350 ^{0}C for 4 h and thus catalyst would be referred to as calcined-[Au-Cu/TiO_2 (2.84wt%Au:0.32wt%Cu)].

3.4.5.2 Preparation of Cu-Au/TiO_2 (0.44wt%Cu:3.95wt%Au)

3.4.5.2.1 Deposition-precipitation of Au onto TiO_2 (anatase, 200m^2/g)

Gold was introduced first, by the deposition-precipitation method following similar procedures used in 3.4.4.1.2, above. However, about 0.9605g $HAuCl_4$ was used, with 4.00g TiO_2 (anatase, 200 m^2/g) as a support. The Au content of as-

prepared catalyst was determined by XRF and was found to be 3.95wt%Au. The sample would be referred to as Au/TiO_2 (3.95wt%Au). Other samples of Au/TiO_2 containing different Au loading were prepared as shown in Table 3.4.

3.4.5.2.2 Incipient-wetness impregnation of Cu onto Au/TiO_2

3.4.5.2.2.1 $Cu(NO_3)_2*2.5H_2O$ as source of Cu

About 1 g of Au/TiO_2 (3.95wt%Au) was used to introduce Cu (~ 0.44wt%Cu loading) from $Cu(NO_3)_2*2.5H_2O$ (99.99% purity, Aldrich) by the incipient-wetness method, following a similar procedure to that used in 3.4.4.1.1, above. Following the steps used, the catalyst was called Cu-Au/TiO_2 (0.44wt%Cu:3.95wt%Au). After preparation, part of the catalyst [~ 0.5g Cu-Au/TiO_2 (0.44wt%Cu:3.95wt%Au)] was calcined in a very shallow ceramic dish in air at 350 ^{0}C for 4 h and such catalyst was called calcined-[Cu-Au/TiO_2 (0.44wt%Cu:3.95wt%Au)].

3.4.5.2.2.2 $Cu(OOCCH_3)_2*H_2O$ as the source of Cu

Approximately 0.5 – 1.0 g of Au/TiO_2 (3.74wt%Au) and Au/TiO_2 (4.09wt%Au) were used to introduce Cu (ranging from 0.22 – 0.88wt.%Cu loading) from $Cu(OOCCH_3)_2*H_2O$ (99.99% purity, Aldrich) by the incipient-wetness method, as in 3.4.4.1.1. The pH (~5.3) of the solution was not adjusted, since it was already in the precipitating region of copper hydroxide (pH ~ 5.3). Following the steps

used, the catalyst would be referred to as Cu-Au/TiO_2 (0.44wt%Cu:3.74wt%Au). After preparation, some of the samples [~ 0.5g Cu-Au/TiO_2 (0.44wt%Cu:3.74wt%Au)] were calcined in a very shallow ceramic dish in air at 350 ^{0}C for 4 h.

The samples prepared are shown in Table 3.8, which also gives detailed information on the catalyst parameters and some catalytic data under forward water-gas shift conditions (see data).

Table 3.8: Au and Cu content (wt%) and observed steady state activity for WGSR[a]

Sample	Au[f]	Cu[f]	Calcination	Activity (%)[e]
Au/TiO_2	3.95			64
Au/TiO_2	4.09			66
Au/TiO_2	3.74			67
Cal[b]-Au/TiO_2	3.95		350 ^{0}C for 4h	46
Cal[b]-Au/TiO_2	4.09		350 ^{0}C for 4h	40
Cal[b]-Au/TiO_2	3.74		350 ^{0}C for 4h	47
Au-Cu[c]/TiO_2	2.84	0.32		74
Cal[b]-[Au-Cu[c]/TiO_2]	2.84	0.32	350 ^{0}C for 4h	20
Cu[c]-Au/TiO_2	3.95	0.44		31
Cu[d]-Au/TiO_2	4.09	0.44		32
Cal[b]-[Cu[d]-Au/TiO_2]	4.09	0.44	350 ^{0}C for 4h	52
Cal[b]-[Cu[d]-Au/TiO_2]	3.74	0.88	350 ^{0}C for 4h	21
Cal[b]-[Cu[d]-Au/TiO_2]	3.74	0.44	350 ^{0}C for 4h	49
Cal[b]-[Cu[d]-Au/TiO_2]	3.74	0.22	350 ^{0}C for 4h	49

[a] Reaction conditions: 1% CO/He or 1%CO/N_2:3%H_2O, Total Flow rate = 50ml/min, W/F = 0.002g.min/ml, pressure 50 psi, Support: TiO_2 (anatase, 200 m^2/g, Water-Gas Shift reaction performed at 200 ^{0}C. [b] Calcined in air at 350 ^{0}C for 4h. [c] Cu precursor is $Cu(NO_3)_2$*2.5H_2O. [d] Cu precursor is $Cu(OOCCH_3)_2$*H_2O. [e] Steady state catalytic activity calculated as CO_{in} - CO_{out}/ CO_{in}*100, Typical relative error is 1 – 2 % of the quoted activity value (e.g. 66 ±

0.5 %), unless explicitly specified in the table. [f] Gold and copper metal content was determined by X-ray Fluorescence Spectroscopy (XRF) at the Northwestern University, USA and/or by fire assay and gravimetric finish method at the Performance Laboratories in Randfontein, South Africa.

3.5 CATALYST CHARACTERIZATION

3.5.1 Temperature programmed reduction and oxidation (TPR and TPO)

Temperature-programmed reduction (TPR) was carried out using 5%H_2/Ar as a reducing gas in a conventional TPR reactor. The reactor was made up of an 8 mm I.D. quartz U-tube with sample of either 200 mg or 100 mg mounted on loosely packed quartz wool. Samples were firstly degassed under N_2 to remove moisture and any other impurities by raising the temperature linearly from room temperature to 150 ^{0}C (heating rate is 10 ^{o}C/min). The sample was allowed to remain at this temperature for a further 30 minutes. A sample was allowed to cool down to room temperature under nitrogen atmosphere. In other cases the outlet of the reactor was connected to a glass column packed with molecular sieve 5A in order to remove the moisture produced from the reduction. The flow rate of the reducing gas was kept at 30 or 42 ml/min by a mass flow controller. The temperature of the reactor was raised from room temperature to either 500 or 800 ^{0}C at a rate of either 10 or 7 ^{0}C/min by a temperature-programmable controller. The sample temperature was monitored by a K-type thermocouple situated close to the catalyst bed. The rate of hydrogen consumption was measured by a thermal conductivity detector (TCD) and recorded by an on-line personal computer. The TPR peak areas were separated and integrated by this computer using special software.

3.5.2 X-Ray methods

X-ray diffraction (XRD), in particular X-ray powder diffraction, has been used extensively to identify and characterize intercalated graphites, metal-graphites and supported-metal combinations. Single crystal and, more recently, powder XRD methods can be used to find atomic positions within the crystal structures of new and as yet uncharacterized materials. In particular, powder XRD is useful for identification of crystalline phases, and estimates of metal crystallite sizes [13].

A more recent addition to the diverse armoury of X-ray based methods is X-ray absorption spectroscopy (XAS) [14]. In contrast to X-ray diffraction methods, which derive their utility from the properties of well-defined crystallites, X-ray absorption methods are atomic probes, capable of obtaining both electronic and structural information about a specific type of atom. The study of absorption edge fine structure can provide information about the symmetry of an atom's environment, its oxidation state, and an assessment of bond length, and bond angles.

3.5.2.1 Powder X-ray diffraction (XRD)

Powder X-ray diffraction has been used for the bulk characterization of the catalysts in order to follow changes in the particle sizes of Au on zeolites and to determine if the zeolite crystallinity was retained during the various stages of catalyst synthesis. Samples used were firstly passed through a 150 μm sieve and were then pressed into a thin layer on a silicon disk. A Phillips PW 1710 difractometer was used equipped with a monochromator and a Cu cathode ray tube. A generator was operated at a voltage of 40 kV and a current of 20 mA. An automatic divergence slit as receiving slit of ~ 0.1 and irradiation length of 12 mm was used for all the samples. Samples were run in a continuous scan mode from either 5 - 40^0 or in the range 35–90^0 (in 2θ scale), using a step size of 0.020 (in 2θ scale) with time per step of ~1.0 second. Particles sizes were estimated using the Scherrer equation [13].

$$d = \frac{0.9\,\lambda}{\beta \cos\theta}$$

where, λ is the wavelength of the X-ray source and β (radians) the full width at half maximum of the X-ray diffraction peak at the diffraction angle θ. The diameter of the Au particles was calculated using the line broadening of the diffraction band at $2\theta = 38.3^o$, and $2\theta = 44.3^o$.

3.5.3 Inductively coupled plasma (ICP)

This technique was used to determine the percentage $[Au(en)_2]^{3+}$- exchanged into the zeolite supercages. The concentration of Au in 100-ml distilled water before ion-exchange was 11870 ppm and after ion-exchange, analysis of the gold content in the filtrate were substantially reduced to 120 ppm, which is equivalent to 98.99 % ion-exchange.

3.5.4 Ultraviolet-visible spectrophotometry (UV-Vis)

The technique was used to confirm that no gold had been washed out after the ion exchange process. Optical absorption measurements were carried out on a Cary 5E UV-Vis NIr spectrometry. Firstly, the UV-Vis spectrum of the gold precursor $Au(en)_2Cl_3$ dissolved in 100 ml distilled water was undertaken, and a peak at 325 ± 1 nm was observed (Figure 3.1).

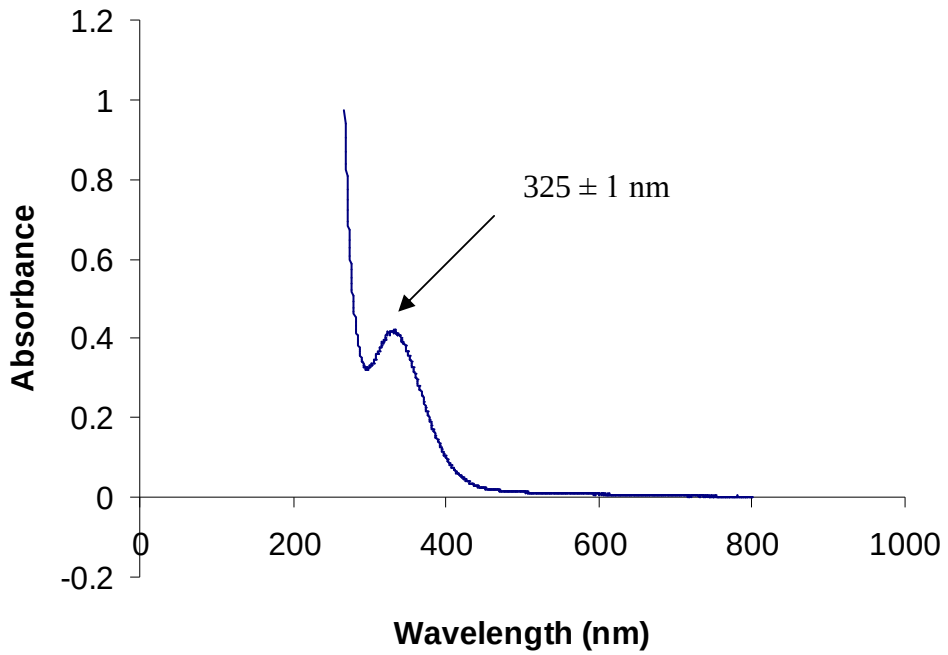

Figure 3.1: The optical absorption spectra of $[Au(en)_2]Cl_3$ solution in 100 ml distilled water.

After ion-exchange on HY-zeolite, the filtrate (approximately 100 ml) was analyzed for the presence of gold and the spectra suggest that only a very low gold content remains in the filtrate, since the absorbance peak at 325 ± 1 nm disappeared (figure 3.1). The broadened peak at 580 ± 2 nm (figure 3.2), which is ascribed to the surface plasmon resonance absorption of gold nanoparticles [10], inside the zeolite super-cages, was also observed. In the case of other reducing agents, the technique could not reveal any presence of gold within the filtrates.

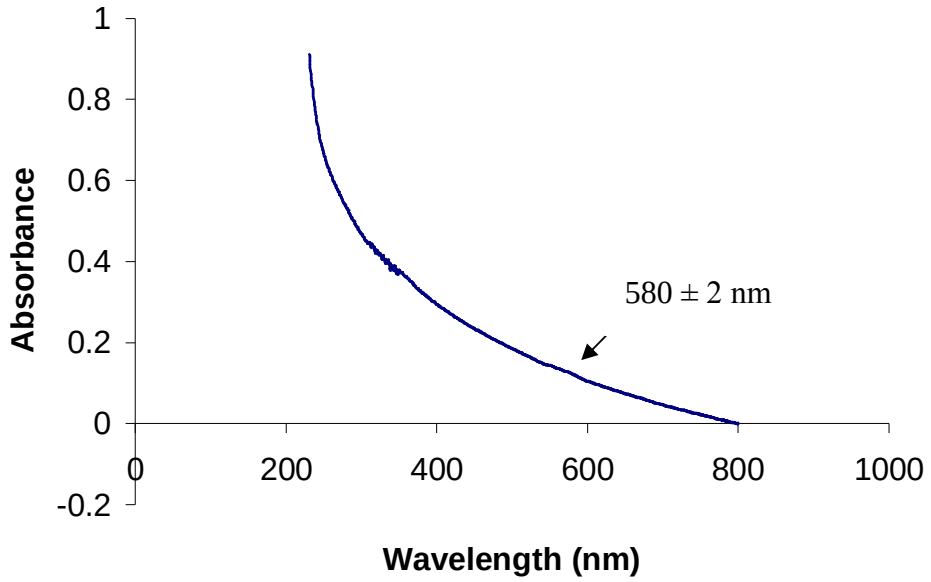

Figure 3.2: The optical absorption spectra of the filtrate (approximately 100 ml) after ion-exchange process.

3.5.5 ^{197}Au Mössbauer spectroscopy

Selected solids were also examined using Mössbauer effect spectroscopy, using ^{196}Pt sources, used some 6-10 h after neutron irradiation in an 18 MW reactor. The source and sample were maintained at *ca.* 6 K for the duration of the Mössbauer measurement. X-scale velocity calibration was obtained using the ^{57}Fe MS spectrum of a 25 μm Fe foil at room temperature. Each spectrum was analysed using the non-linear least squares fitting program NORMOS-90 (distributed by Wissenschaftliche Elektronik GmbH, Germany). A minimum number of Lorentzian components were used in the fitting procedure.

3.6 CATALYSTS ACTIVITY TESTS

3.6.1 Catalysts testing of Au on Y in the presence of transition metal

Approximately 200 mg of Au/Y (3.67wt%Au) and Au/M-Y (M represents Ni^{2+}, Fe^{3+}, Co^{2+} and Cr^{3+}) were pre-treated at 400 ^{0}C for 2 hours in a quartz reactor under an O_2 atmosphere (flow rate: 14 ml/min). Immediately after treatment, CO oxidation was measured as a function of time on stream at 200 ^{0}C, and as a function of temperature with a total flow rate of 42 ml/min of gas mixture. The reactor was linked to a gas chromatograph, equipped with a thermal conductivity detector. An integrator was used to determine CO consumption as a function of temperature increase or time on stream. In each measurement, the composition of the gas mixture used was 10% O_2/He and 10% CO/He.

3.6.2 Catalysts testing of $[Au(en)_2]^{3+}$/HY

Approximately 200 mg of the prepared $[Au(en)_2]^{3+}$/HY catalysts (untreated and those treated with different reducing agents) were pre-treated at 400 ^{0}C for 2 hours in a quartz reactor under an O_2 atmosphere (flow rate: 14 ml/min). Immediately after treatment, the temperature was raised to 450 ^{0}C, and CO oxidation was measured as a function of time on stream with a total flow rate of 42 ml/min of gas mixture. The reactor was linked to a gas chromatograph, equipped with thermal conductivity detector. An integrator was used to determine CO consumption as a function of temperature increase or time on stream. In each

measurement, the composition of the gas mixture was 10% O_2/He and 10% CO/He.

3.6.3 Catalysts testing of Au supported on alkali-modified zeolite-Y

Approximately 200 mg of Au/Y (no modification of zeolite were performed on these catalysts), Au/LiY (zeolite was modified by a solution of $LiNO_3$, 1M), Au/NaY (zeolite was modified by a solution of $NaNO_3$, 1M) and Au/KY (zeolite was modified by a solution of KNO_3, 1M) were pre-treated at 200 ^{0}C for the $HAuCl_4$ gold source and at 400 ^{0}C for $KAu(CN)_2$ and $Au(en)_2Cl_3$ as sources gold, for 2 hours in a quartz reactor under O_2 flow (flow rate: 14 ml/min.). After pre-treatment, CO oxidation was performed as a function of time on stream at 150 ^{0}C and 250 ^{0}C respectively (flow rate: 42 ml/min).

Figure 3.3 shows the schematic representation of the experimental set-up used for the CO oxidation reactions.

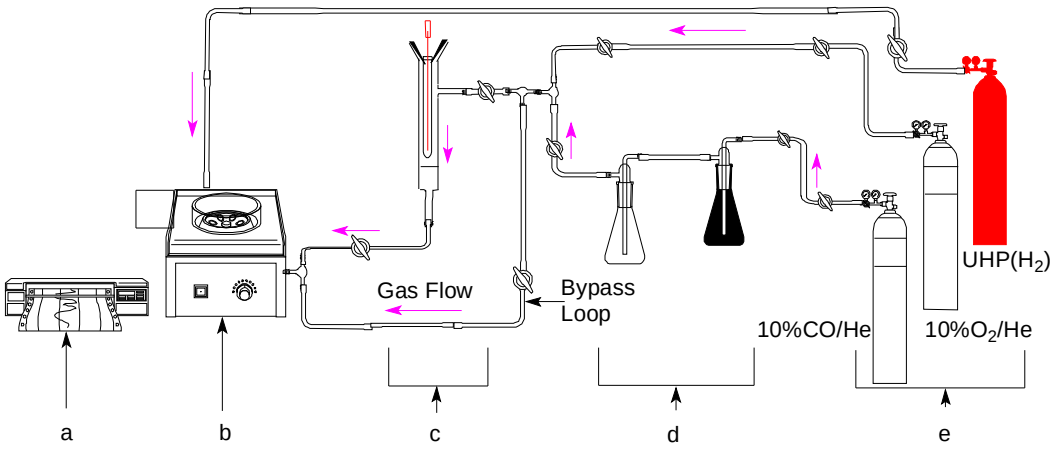

Figure 3.3: Schematic diagram of CO oxidation flow chart: (a) Integrator, (b) Gas chromatograph equipped with thermal conductivity detector, (c) Tube reactor equipped with thermocouple, (d) Absorbance materials (activated carbon and NaOH pellets), (e) Gas cylinders.

3.6.4 Catalyst testing of Au supported on Y-zeolite, for ethylene hydrogenation

Similar catalysts used above for CO oxidation were tested for ethylene hydrogenation as a function of time on stream at 260 ^{0}C and at different temperatures. Herein, prior to catalysts testing, all catalysts where pretreated at the respective conditions used under CO oxidation. i.e. 200mg of the catalysts: Au/Fe-Y (different gold loadings, 1.88wt%Fe), Au/NaY (0.772wt%Au, treated with $NaNO_3$), Au/HY (3.77wt%Au) were pre-treated at 260 ^{0}C and Au/M-Y (M represent Ni^{2+}, Fe^{3+} and Cr^{3+}) at 150 ^{0}C. Ethylene hydrogenation was undertaken

at 260 ^{0}C and at 150 ^{0}C in a quartz reactor under hydrogen and ethylene (flow rate: 160 ml/min H_2: 40 ml/min ethylene) linked to a gas chromatograph, equipped with FID (Flame Ionization detector). A data integrator monitored the ethylene consumption and ethane production as a function of time or temperature on stream.

3.6.5 Catalysts testing of Au supported on TiO_2 modified with Cu.

3.6.5.1 Catalysts testing for CO oxidation

Approximately 100 mg of the prepared Au-Cu/TiO_2 (2.84wt%Au:0.32wt%Cu) and Au/TiO_2 (different gold loading) catalysts were either used as-prepared, calcined or uncalcined, or pre-treated under 5%H_2/Ar (flow rate: 42 ml/min) at room temperature, 18 ^{0}C in a U-tube reactor fitted with a quartz wool. Immediately after treatment, the temperature was lowered to -77 ^{0}C under a helium atmosphere, where CO oxidation was measured as a function of time on stream with a total flow rate of 50 ml/min of gas mixture (2.5%volCO and 5%volO_2). The reactor was linked to an FTIR spectrophotometer, which was used to measure the concentration of gas phase CO as a function of time on stream. In some cases the reactor was linked to a gas chromatograph equipped with thermal conductivity detector and the results where manually integrated, to monitor CO consumption as a function of time on stream.

3.6.5.2 Catalysts testing for selective CO oxidation in a H_2 rich stream.

For selective CO oxidation, 5 – 20 mg of catalyst was mixed with 0.5 g of SiC and the mixture was placed in a U-tube reactor fitted with quartz wool. SiC was used because it is an excellent heat conductor and not reactive under these conditions. The feed was 1 % CO, 0.5 % O_2, 40 % H_2, and balance He. A trap filled with molecular sieve, was used to remove water in the feed. The feed flow rate was 200 - 250 ml/min and the reaction temperature was varied from room temperature to 100 ^{0}C, unless otherwise mentioned. The products were analyzed with a gas chromatograph using two columns: a molecular sieve 13X column for H_2, CO, and O_2, and a Haysep Q column for H_2O and CO_2. Selectivity of the reaction was calculated as:

$$S_{co} = \frac{0.5 \text{ x } [CO]_{in} - [CO]_{out}}{[O_2]_{in} - [O_2]_{out}} \text{ x } 100$$

where, $[CO]_{in}$, $[CO]_{out}$ represent incoming and outgoing concentration of carbon monoxide, S_{co} represent selectivity to CO and $[O_2]_{in}$, $[O_2]_{out}$ represent incoming and outgoing concentration of oxygen.

3.6.5.3 Catalysts testing for low temperature Water-gas shift reaction

Approximately 100 mg of catalysts were either used as-prepared, uncalcined or after calcinations for low temperature water-gas shift reaction in a U-tube reactor fitted with quartz wool. The temperature was raised to 200 ^{0}C (heating rate: 7 ^{0}C/min) under a reaction mixture of 1% CO/He or 1% CO/N_2 and 3% H_2O, with a

total flow rate of 50 ml/min, gas mixture. Reaction products were analyzed by gas chromatography (using two columns: a molecular sieve 13X column for H_2, CO, and O_2, and a Haysep Q column for H_2O and CO_2) equipped with thermal conductivity detector and results where manually integrated, to monitor CO consumption as well as H_2 production, as either a function of time on stream or temperature changes.

3.6.5.4 In-situ XANES and EXAFS structural characterization of Au-Cu ions supported on TiO_2 (anatase) for the Water-gas shift reaction

An in-situ cell equipped with a thermocouple which allows a free flow of moisturized carbon monoxide in helium has been used. Samples were studied in the form of 13 mm diameter pressed discs (figure 3.4). Au and Cu K-edge XANES and EXAFS spectra were recorded from room temperature to 200 ^{0}C in a fluorescence mode using a synchrotron radiation source which has been monochromatized by a Si(311) monochromator. Au and Cu K-edge EXAFS data were collected using the synchrotron source at the Argonne Photon Source, Chicago, USA. The WINXAS – version 3.1 program was used to analyze and fit the data.

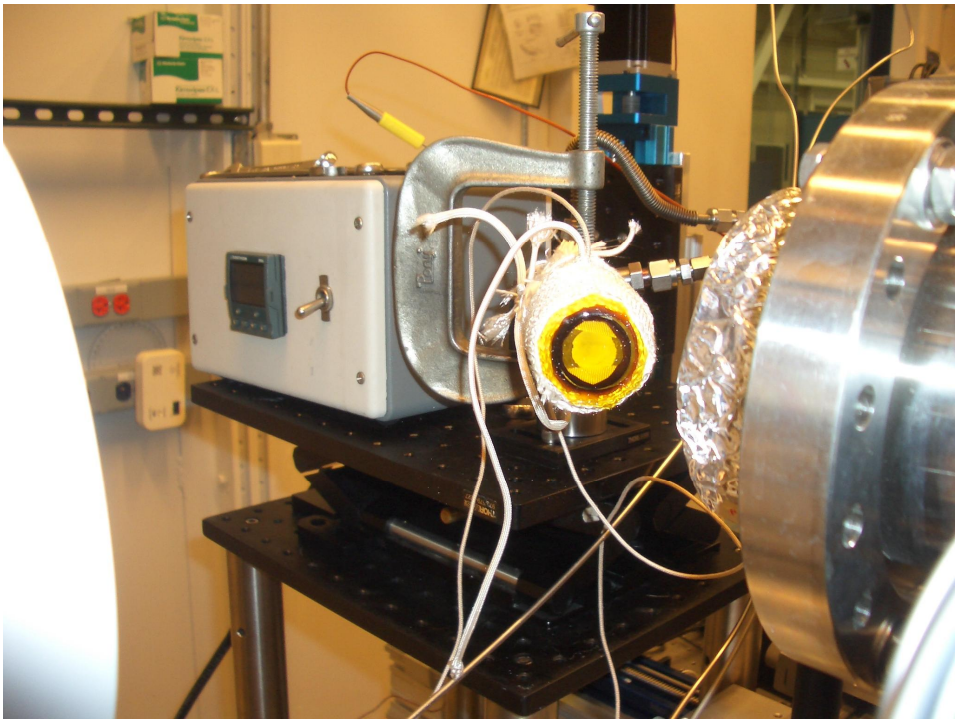

Figure 3.4: An apparatus showing the in-situ cell containing a 13 mm diameter pressed sample disc taken before the start of water-gas shift reaction at Argonne Photon Source (APS), USA.

3.7 REFERENCES

[1] A. Fürstner, Active Metals, VCH, Wenheim, 1996.

[2] A. Mendel, J. Organomet. Chem., **6** (1966) 97.

[3] C. S. Chao, C. H. Cheng, C. T. Chang, J. Org. Chem. **48** (1983) 4904.

[4] K. S. Suslick, S. J. Doktycs, J. Am. Chem. Soc. **111** (1989) 2342.

[5] R. Csuk, B. I. Glänzer, A. Fürstner, Adv. Organomet. Chem. **28** (1988) 85.

[6] J. W. Niemantsverdriet, Spectroscopy in Catalysis, VCH, Weinheim, 1993.

[7] B. P. Block and J. C. Bailar Jr., J. Am. Chem. Soc., **73** (1952) 4722.

[8] D. Guillemot, V. Yu. Borovkov, V. B. Kazansky, M. Polisset-Thfoin and J. Fraissard, J. Chem. Soc., Faraday Trans., **93** (1997) 3587.

[9] Lin J. N., Chen J. H., Hsiao C. Y., Kang Y. M. and Wan B. Z., *Appl. Cat. B: Env.*, **36** (2002) 19.

[10] Q. F. Zhou, J. C. Bao, and Z. Xu, J. Mater. Chem., **12** (2002) 384.

[11] H. Hirai, H. Wakabayashi and M. Komiyama, Chem. Lett., **19** (1983) 1047.

[12] P. A. Brugger, P. Cuendet and M. Gratzel, J. Am. Chem. Soc., **103** (1981) 2923.

[13] G. Ertl, H. Knözinger, J. Weitkamp, Handbook of Heterogeneous Catalysis, VCH, Weinheim (Germany), **2** (1997) 447.

[14] D. C. Koningsberger, R. Prins, X-ray absorption. Principles, Applications, Techniques of EXAFS, SEXAFS and XANES, Wiley, New York, 1988.

CHAPTER 4

Stability of gold particles in Y-type zeolites: Influence of co-exchanged metal cations

4.1 INTRODUCTION

Various supports such as TiO_2, Fe_2O_3 and MgO containing noble metal catalysts, such as platinum, and gold oxidize CO to carbon dioxide quite efficiently at low temperature. However, the rate of this oxidation is adversely affected by the presence of small amounts of soluble chlorine, which adsorb onto the active sites of the Au crystallites and block the carbon monoxide oxidation [1]. Research and development work in this field is directed towards understanding the factors affecting the reactivity of Au crystallites and dispersion of the metal particles, by using a chlorine free gold precursor. The aim is to produce a fine, uniform particle size distribution which is maintained during the catalytic reaction.

Major objectives of this work were (i) to determine how the surface changes from NaY to HY structure, affects the surface reactivity of metallic and bimetallic systems, (ii) to characterize the nucleation and growth of metals on zeolite surfaces and (iii) to understand the role of modifiers on the catalytic activity of gold on Y zeolites. The three main components of this effort are surface structure, surface chemistry, and surface electronic properties. Some of the factors which

have been noted to affect the size distribution and the stability of the metal particle are: the silicon-aluminium ratio (m/n) of the starting material, the degree of ion exchange, and the temperature and duration of the dehydration and reduction treatments. This work will also describe the techniques used and the results obtained in an investigation of gold, stabilized by nickel, iron and chromium in Y zeolite. The aim will be to elucidate the possible nucleation and growth mechanism of the metal particles.

Gold supported on Y zeolites was prepared by the incipient-wetness method from $KAu(CN)_2$. The catalyst was found to be active for CO oxidation at a temperature above 300 ^{0}C. The same source of gold was introduced on HY zeolite and it was noted that the activity of Au/HY (0.264wt%Au) at 450 ^{0}C is half that of Au/Y (0.277wt%Au). The activity of Au/Y (3.67wt%Au) for CO oxidation was followed by firstly modifying Y structure with different transition metals (introduced by ion-exchange methods). Modification of the Y structure with Ni^{2+}, Fe^{3+}, Co^{2+} and Cr^{3+} (~ 2wt% of transition metals) have been found to be beneficial for both activity and stability of smaller gold clusters. CO oxidation activity decreased upon further increase in Fe^{3+} content on the Y zeolite. An increase in gold loading on Fe-Y (1.88wt%Fe) was also found to result in a lower activity for CO oxidation at 200 ^{0}C.

4.2 EXPERIMENTAL

4.2.1 Support and catalyst preparation

All chemicals were generally reagent grade and used as received except where otherwise mentioned. Gold supported on zeolite-Y in the presence of transition metal have been prepared as described in Chapter 3. Prior to any catalysts testing for CO oxidation, samples were pre-treated at 400 ^{0}C for 2 h, under an oxygen atmosphere (flow rate = 14 ml/min). Further details are contained in Chapter 3 (i.e feed composition etc.)

4.2.2 Temperature-programmed reduction (TPR)

Temperature-programmed reduction (TPR) was carried out on freshly prepared uncalcined samples using either 5%H_2/Ar or 5%H_2/N_2 as a reducing gas in a conventional TPR reactor as described in Chapter 3.

4.2.3 X-ray powder diffraction (XRD)

A Phillips PW 1710 difractometer equipped with monochromator and Cu cathode ray tube was used. A 150 μm sieved powdered sample of either freshly prepared uncalcined or calcined catalysts were used as described in chapter 3.

4.3 RESULTS AND DISCUSSIONS

4.3.1 TPR experiments

4.3.1.1 TPR profiles of Au/Y and in the presence of stabilizing metals Ni^{2+}, Fe^{3+} and Cr^{3+}.

The sample of Au/Y (3.67wt%Au) catalyst, shown in figure 4.1, was prepared by incipient wetness from $KAu(CN)_2$ on Y zeolite. The TPR profile of this sample was recorded at Northwestern University. Approximately 222 mg of as-prepared sample was loaded on a U-tube reactor, fitted with molecular sieve to trap moisture. The TPR was recorded under a flow of $5\%H_2$/Ar atmosphere (42ml/min) at 5^0C/min from room temperature until the reduction has complete.

As shown in figure 4.1, the profile suggests that gold on Y zeolite has been reduced starting from 225 ^{0}C and the peak maxima was observed at 258 ^{0}C. These results give an idea on the temperature range at which gold supported on Y is reduced. However, the sample of Au/Y zeolite did not show the reduction of gold when approximately 100 mg sample were used. Thus was due to the pre-treatment of the sample at 400 ^{0}C in air for 2 h, before reduction. Gallezot et al. [2] have noted that the activation of Pt/Y at 600 ^{0}C resulted in most of the Pt^{2+} ions being atomically dispersed in the sodalite cages; on reducing at 300 ^{0}C the platinum was found not to chemisorb hydrogen.

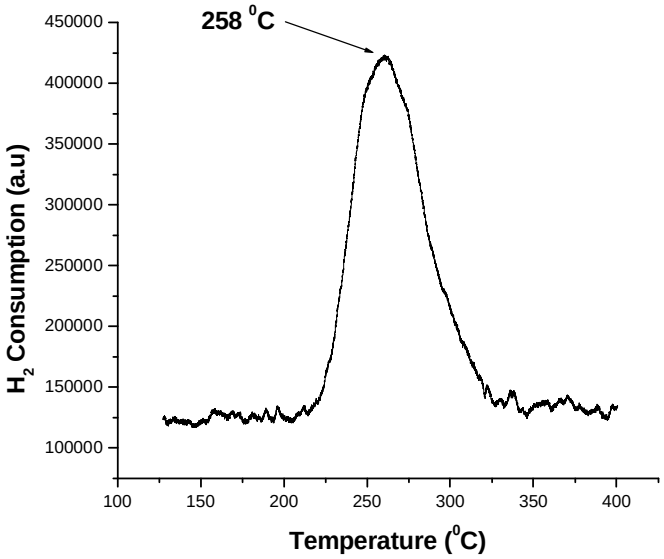

Figure 4.1: TPR profiles of Au/Y (3.67wt%Au), in the absence of transition metals, Conditions: 200 mg sample, 5%H_2/argon atmosphere (42ml/min) at 5^0C/min.

In the presence of a transition metal, the results suggest that the reducibility of either catalytic metal or Ni^{2+} has been enhanced (figure 4.2). Similar to this case, Sachtler et al. [3] have reported that the reducibility of Ni is significantly increased if Mn^{2+} or Cr^{3+} ions are exchanged in a zeolite prior to Ni ion exchange. Similar behaviour has been observed as shown figure 4.2, suggesting a simultaneous reduction of both metals and changes in the reducibility of the catalytic metal. This result suggests that Ni^{2+} lowers the stability of gold, as can be seen by the faster reduction. This suggests that the reduction of Au^+ to Au^0 might be the underlying factor for the behaviour of Au in the CO oxidation reaction. Suggestions by Minico et al. [4], that ionic gold might be the active species, which usually undergo irreversible reduction to metallic gold seems to be

the main reason for the low activity or deactivation of Au/Ni-Y (3.35wt%Au:1.79wt%Ni).

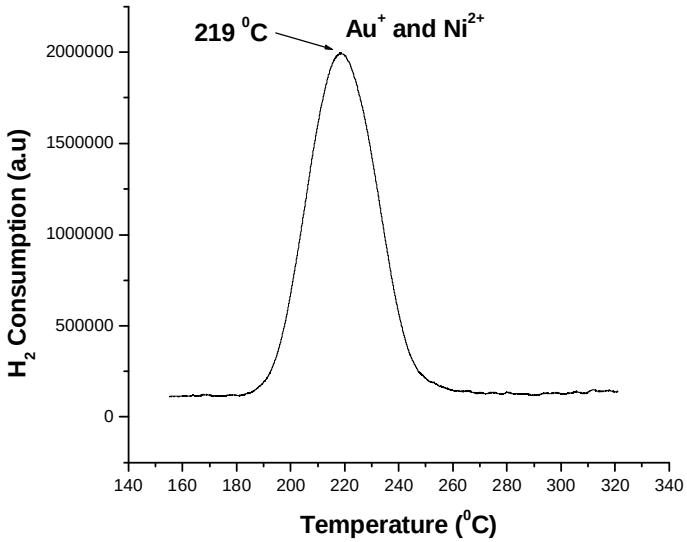

Figure 4.2: TPR profiles of Au/Ni-Y (3.35wt% Au:1.79wt%Ni), showing the effect of Ni^{2+} on the reduction of gold. Conditions: 200mg sample, 5%H_2/argon atmosphere (42ml/min) at 5^0C/min. TPR profile of this sample was recorded at Northwestern University. Approximately 200 mg of sample was loaded on a U-tube reactor, fitted with molecular sieve to trap moisture.

The TPR profile in figure 4.3 confirms that there is an overlap of gold and transition metal reduction peaks, similar to that discussed in figure 4.2. The difference in peak shape is due to the difference in thermal conductivity detector (TCD) sensitivity, between the two instruments used. The large amount of gold was reduced at lower temperature (peak maxima at 264 ^{0}C), in the presence of Ni^{2+} as compared to samples containing Fe^{3+} and Cr^{3+} (peak maxima at 270 ^{0}C

and 279 ^{0}C respectively). The reduction potential of the stabilizing metal plays a significant role on the stability of gold supported on zeolite. The lower reduction potential (- 0.23) of Ni^{2+} (peak maxima also at 264 ^{0}C), suggests that it will be easily reduced to its metallic state. Since smaller gold cluster are no longer stabilized by the ionic form of the transition metal. The probability that ionic gold/smaller gold cluster will be reduced to metallic gold particles, which eventually sinter or coalesce with time on stream, is enhanced. This leads to the observed low activity.

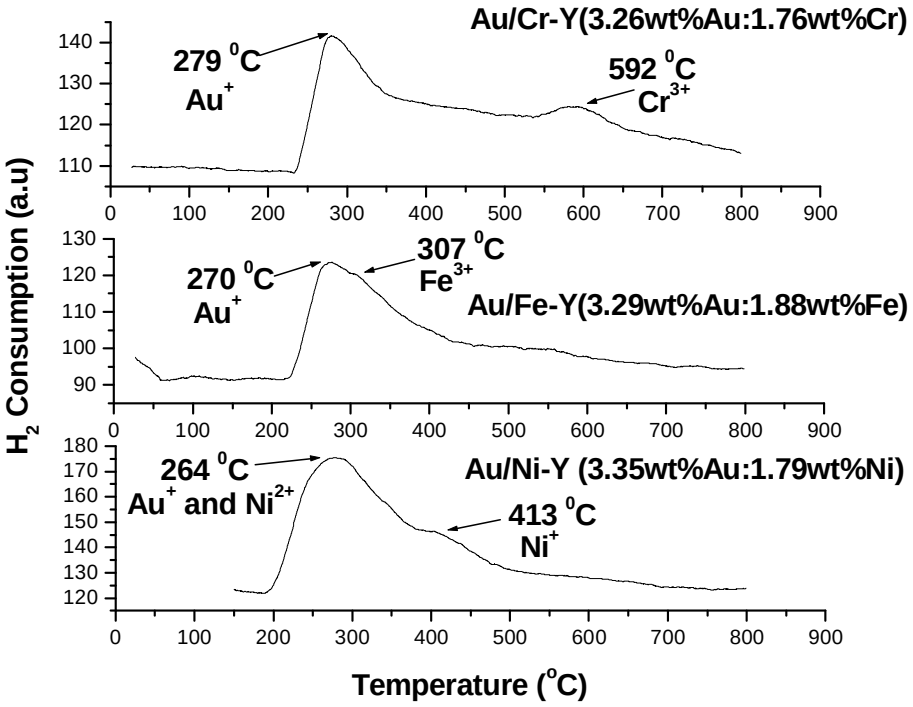

Figure 4.3: TPR profiles of stabilizing metals (Ni^{2+}, Fe^{3+}, and Cr^{3+}) on Au/Y. Conditions: 100 mg sample, 5%H_2/nitrogen atmosphere (30 ml/min) at 7 ^{0}C/min. The TPR profile of this sample was recorded at the Witwatersrand University.

However, in the presence of both Fe^{3+} and Cr^{3+} exchanged on zeolite-Y (peak maxima at 307 ^{0}C and 592 ^{0}C respectively, figure 4.3), ionic gold/smaller gold cluster stability seems to have been enhanced. Sachtler et al. [5] have noted that the presence of co-exchanged multivalent cations, e.g., Fe^{2+}, can effectively block the sodalite cages and hexagonal prisms, thus forcing Pt^{2+} ions to stay in a supercage. This eventually prevents the formation of large particles on the external surface of zeolites even at higher temperatures. Our samples containing these two transition metals were found to give higher activity for CO oxidation, suggesting that ionic gold/smaller gold clusters are the one responsible for the observed higher activity.

4.3.1.2 Effect of Au loading on the TPR profile of Au/Fe-Y

The introduction of 1.67wt%Au on Fe-Y (1.88wt%Fe) increased the stability of both Au and Fe ions as shown in figure 4.4. The reduction peak maxima of Fe-Y (Fe^{3+}) alone occured at 307 ^{0}C while that of Au/Fe-Y (1.67wt%Au:1.88wt%Fe) occurred at 344 ^{0}C. However, as the gold loading is increased the stability of both Au and Fe decreases as can be seen for Au/Fe-Y (3.29wt%Au:1.88wt%Fe). Here the Au reduction peak maxima occurs at 274 ^{0}C and Fe^{3+} reduction peak maxima occurs at 307 ^{0}C. As a result of the early reduction of Fe^{3+}, the activity of such catalysts containing gold loading, of above 3.29wt%Au, was found to be lower. The presence of a higher gold loading can be confirmed by an increase in the amount of H_2 consumed as the gold loading increases. This confirms the simultaneous reduction of both gold and iron to lower oxidation states. The

lowering of activity seems to occur after reaching a “saturation level” of gold loading, which is approximately in the range of 3.29wt%Au and above. CO oxidation decreased when the Au content was increased to 5.45wt% and 7.48wt%.

The instability of Fe ions, in the case where it is supposed to act as a stabilizer metal can also be understood on the basis that as the concentration of the catalytic metal increases, the surface area of the catalyst metal (Au) is reduced. The effect arises from the agglomeration of gold particles. This suggests that the particle size is playing a significant role in the catalytic activity and shows that it is necessary to make the particles as small as possible, i.e. to maximize the fraction of the atoms of gold that are on the surface. This also confirms that the percent conversion of CO correlate with the surface area of the active sites or phase, since at lower concentration of gold, the particle size is usually small.

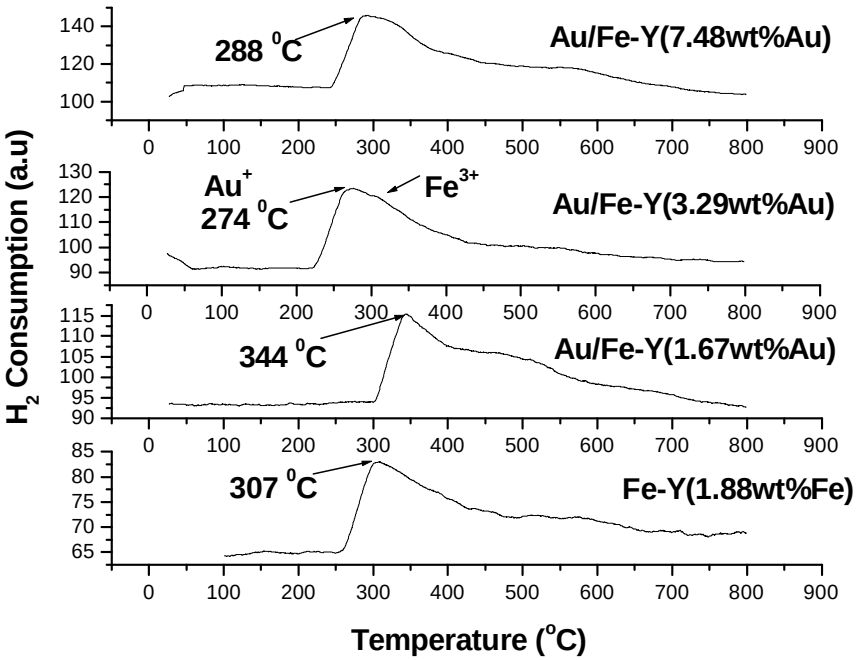

Figure 4.4: TPR profiles of Au/Fe-Y (1.88wt%Fe), showing the effect of gold loading. Conditions: 100 mg sample, 5%H_2/nitrogen atmosphere (30 ml/min) at 7 ^{0}C/min.

The XRD profile of Au/Fe-Y (7.48wt%Au:1.88wt%Fe), as discussed in the next section has shown an increase in the formation of metallic gold, as a result of an increase in gold content. This suggests that too high a gold loading might saturate the stabilizer metal and as such there seems to be an interaction between the smaller active sites of gold and the stabilizer metal (i.e. Fe in this case). When this interaction is lost due to the presence of the large particle size of gold formed, the stabilizer metal is then reduced at a lower temperature as observed. Some mutual interaction between the two metals on the surface of zeolite or possibly, any other support, is suggested.

4.3.2 XRD results

4.3.2.1 Effect of gold loading

The XRD profile in figure 4.5 shows the peak intensity of gold particles formed on spent Au/Fe-Y, after CO oxidation up to a maximum temperature of 500 ^{0}C. An increase in gold loading from 1.67wt%Au, 3.29wt%Au and 5.45wt%Au, shows that there is an increase in intensity of Au(111) peak due to large amount of metallic gold particles formed. It appears that the catalytic metal has migrated outside the zeolite pores. The formation of metallic gold has led to the observed lower activity of Au/Fe-Y (7.48wt%Au:1.88wt%Fe) and such a catalyst was found to show earlier reduction of the stabilizing metal, i.e. Fe^{3+} as shown in the TPR profile (figure 4.4). The presence of large gold particles on Au/Fe-Y catalysts as reported by Guczi et al. [6] might have been influenced by the molar ratio between the two metals.

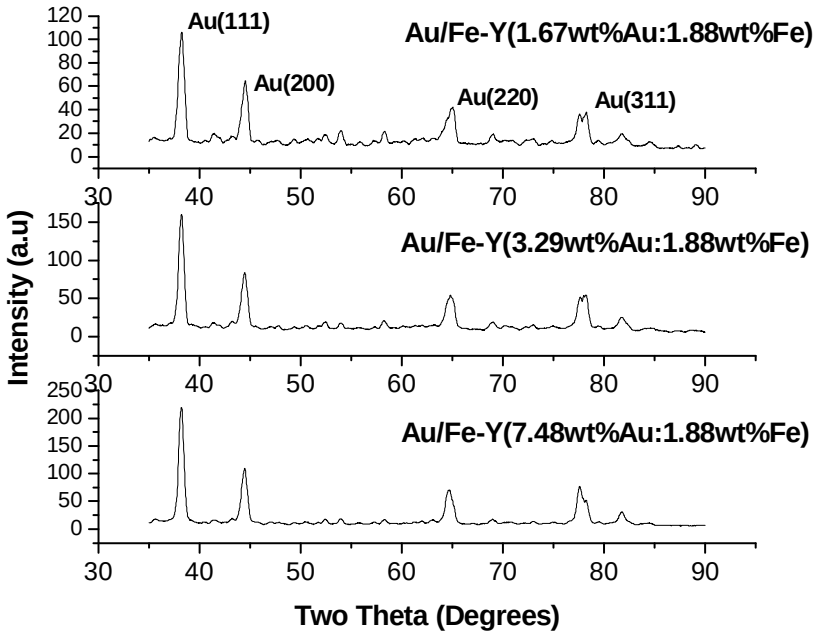

Figure 4.5: Effect of gold loading on the sintering of gold particles.

4.3.2.2 Effect of Ni^{2+}, Fe^{3+} and Cr^{3+} on stability of gold particles on Y zeolites.

The XRD profile of as-prepared Au/Y (3.67wt%Au) as shown in figure 4.6, shows that small metallic particles of gold are present before any catalysis is performed. This suggests that before any catalysis or exposure to pre-treatment conditions most of the gold particles are within the zeolites cages (roughly 1.3 nm in diameter and surface area of ~ 900 m^2/g [7]). These particles migrate to the outer surface of the zeolite immediately after they are exposed to high temperature as reported by Meitzner et al. [8] (see spent Au/Y (3.67wt%Au) in figure 4.6). The introduction of nickel (Ni^{2+}) on the Au-Y (3.35wt%Au) catalyst, had slight significant effect on the size of metallic gold being produced as a result of sintering (based on the intensity of Au(111) peak). The estimated size of Au

crystallites using the scherrer equation on the Au-Y (3.67wt%Au) catalyst was in the range of 15 – 20 nm, while in the presence of nickel, the mean diameter decreased to 10 - 13 nm. This clearly shows that the particles sizes observed are on the outer surface of the zeolite cages.

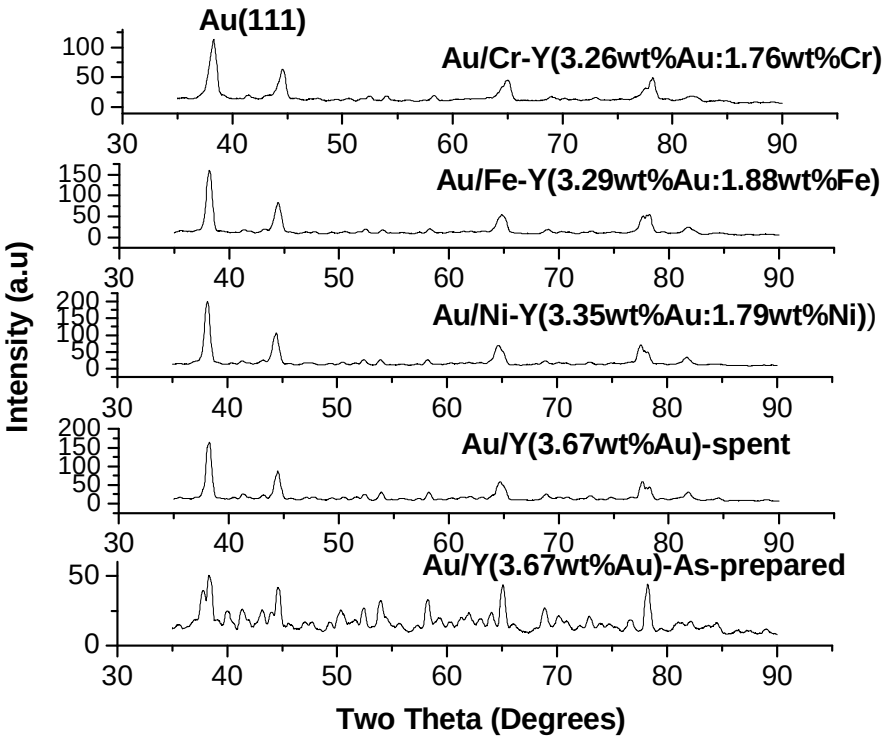

Figure 4.6: XRD profile of Au/Y showing the effect of transition metals on the stability of gold particles.

However, the introduction of iron (Fe^{3+}) and chromium (Cr^{3+}) do show that the amount and size of metallic gold produced is significantly reduced, depending on the potential strength of both iron (Fe^{3+}) and chromium (Cr^{3+}) as stabilizers. This is probably due to an increase in stability of gold particles, as a result of the stabilizing effect of Fe^{3+} and Cr^{3+}. The average particle size of gold can be

estimated, by considering the peak width and intensity of Au on Y (3.67wt%Au) on as-prepared sample. This suggests that much of the Au has been highly dispersed throughout the support and a small Au signal was detected by X-ray diffraction, which proves a very small size of Au particles using scherrer equation. The mean estimated size of Au crystallites using X-ray diffraction were ~ 7 nm for Fe^{3+}, and ~ 5 nm for Cr^{3+} stabilized metal. Wan et al. [9a] reported similar results suggesting that the presence of iron retards the sintering of metallic gold.

XRD shows a weak and broad Au (111) peak of Au/Cr-Y (3.26wt%Au:1.76wt%Cr) sample, which implies a significantly smaller Au particle size (~ 5 nm) and a lower number of large Au particles. The stability of smaller Au particles on Au/Cr-Y (3.26wt%Au:1.76wt%Cr) sample is due to high negative reduction potential of Cr^{3+}, as observed by the late reduction of chromium at 592 ^{0}C, on the TPR profile in figure 4.3. Sachtler et al. [10] and Wan et al. [9] have noted that exchanging Fe^{2+} ions into NaY dramatically decreases the size of Pt and Au particles, respectively, when exposed to high temperatures.

4.3.3 Effect of acidity/proton on chemical state, gold particles size and hence CO oxidation activity.

The XRD profile in figure 4.7 shows the unspent and spent Au/Y (0.277wt%Au) and Au/HY (0.264wt%Au) catalysts respectively. The spent catalysts were tested for CO oxidation at 450 ^{0}C and it was found that the activity of Au/HY (0.264wt%Au) is half that of Au/Y (0.277wt%Au), see figure 4.8. However, the intensity of the metallic gold produced as a result of sintering, was much higher for Au/Y (0.277wt%Au), suggesting that most of gold particles in Y-zeolite are not stable at higher temperature compared to HY zeolite which shows less formation of metallic gold.

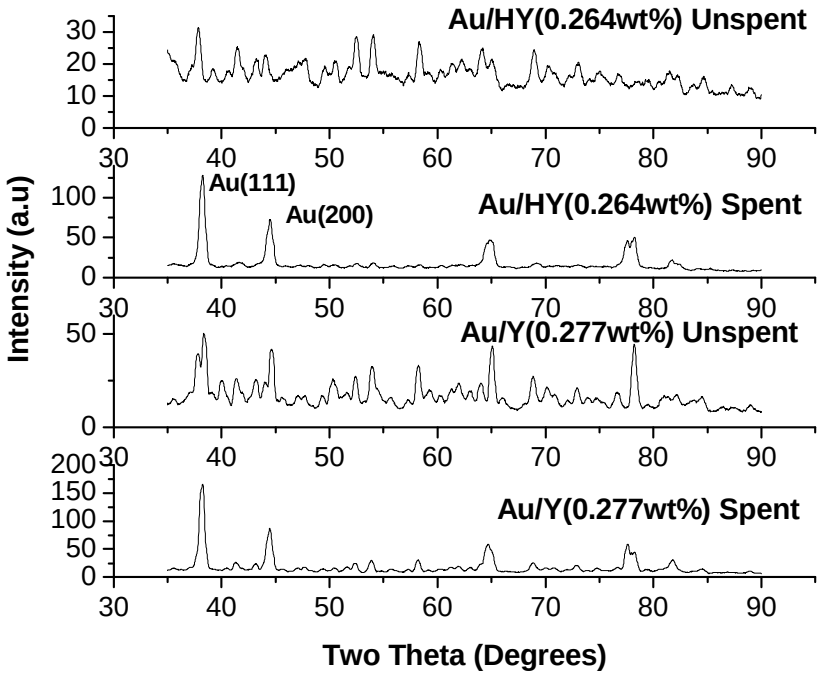

Figure 4.7: XRD profile of spent and unspent Au/Y (0.277wt%Au) and Au/HY (0.264wt%Au) respectively, showing the effect of acidity or proton on the particle size of gold.

The presence of proton on HY has stabilized most of Au clusters (electron-deficient species) within HY zeolite cages as reported by Guillemot et al. [9a]. Thus has resulted in small amount of gold species migrating to the outer surface of the zeolite, as compared to the similar clusters of gold within the Y-zeolite. These results clearly suggest that the presence of metallic gold plays a significant role in the CO oxidation reaction. The results suggest that adsorptive properties of zeolite encaged metal clusters [in Au/HY (0.264wt%Au)] can be 'altered' by other ions sharing the same cavities.

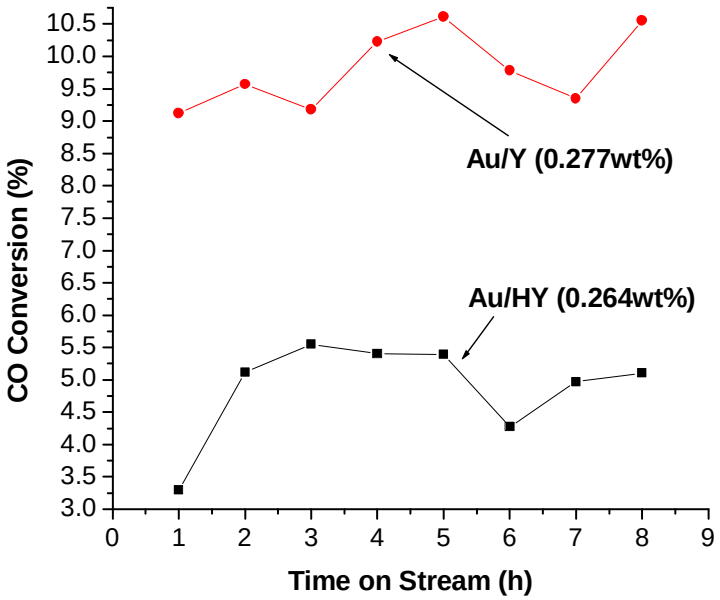

Figure 4.8: Effect of acidity/proton on catalytic activity of Au supported on HY at 450 ^{0}C.

4.3.4 Catalytic activities of gold on Y, promotional effect on Au by exchanged Ni^{2+}, Fe^{3+}, and Cr^{3+} on Y.

Catalysts formed from the dispersion of catalytic metals in zeolites supports have not been used as extensively as other catalysts for commercial purposes [2]. Most of the preferred supports for metals such as gold and palladium or bimetallic combinations thereof have been alumina (Al_2O_3), silica (SiO_2) and Titania (TiO_2). Dispersion of catalytic metal on alumina or Titania has been found to be much more stable in use than zeolite supported catalysts. Under elevated temperature conditions as commonly encountered in the use of such catalysts, metal particles tend to migrate in the zeolite support, coalesce, and aggregate into larger particles with consequent loss of catalytic activity [2, 5].

Herein, the results of dispersion of gold on Y zeolite from cyanide complexes are discussed. Catalysts were pre-treated in an oxygen atmosphere at 400 ^{0}C. An auto reduction reaction was also expected to sement highly dispersed metal particles entrapped in zeolite cavities. If metal ions on zeolite are reduced at high temperature, large metal particles may be formed, resulting in reduced catalytic activity. Even the highly dispersed metals obtained by low temperature reduction still tend to agglomerate to large metal aggregates during use. Such difficulties in obtaining and maintaining particle dispersion are indicative of a weak interaction (weak van der Waals forces, [11]) of the metal particles within the zeolite framework. The use of the ionic form of transition metals such as Ni^{2+}, Fe^{3+} and Cr^{3+} assists in strengthening the interaction between gold and zeolite exchange sites.

4.3.4.1 Effect of nickel on activity of Au/Y (3.35wt%Au:1.79wt%Ni)

Figure 4.9 shows the catalytic behaviour of Ni-Y (1.79wt%Ni) and that of Au/Y (3.67wt%Au) for CO oxidation. It was found that the activity of Ni-Y (1.79wt%Ni) is less than that of Au/Y (3.67wt%Au), as a function of temperature up to 500 ^{0}C. However, when gold was introduced (by incipient wetness method) on Ni-Y (1.79wt%Ni), an increase in activity was observed, which suggests that the presence of Ni has significant effect on Au supported on Y. Though the activity has improved, the steady state was reached above 400 ^{0}C without achieving 100% CO conversion. For comparison, Fe^{3+}, Cr^{3+} and other transition

metals were exchanged on Y zeolite in order to understand the role of transition metal on supported gold.

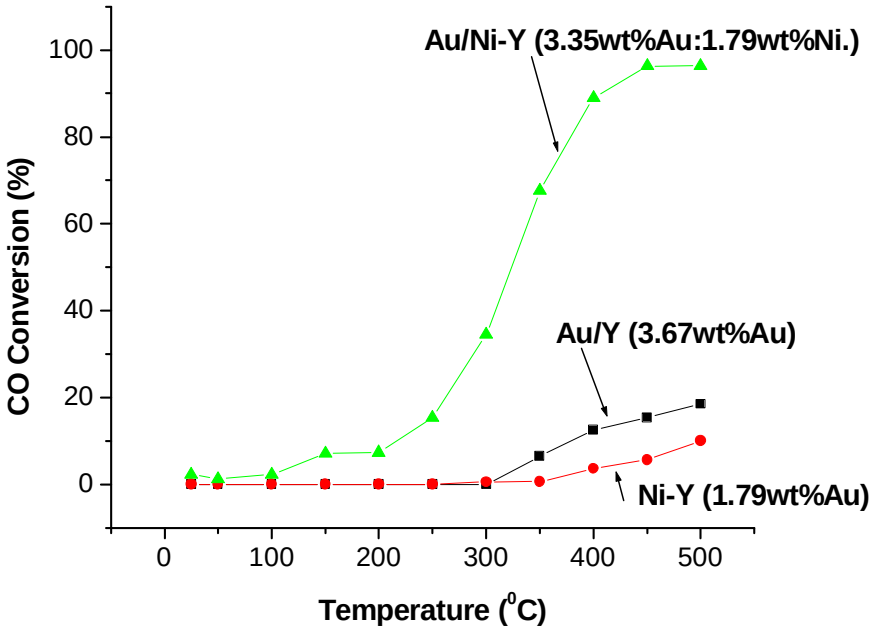

Figure 4.9: Effect of Ni^{2+} ions on the activity of supported Au on Y as a function of temperature.

The activity of Au/Y (3.67wt%Au) above suggests that the reduced gold metal atoms as shown in the TPR profile in figure 4.1 are bound to the zeolite by a weak interaction. This contrasts with the stronger metal support interactions on catalyst supports such as alumina [12]. Therefore, either during the reduction step or in subsequently use, the reduced gold is subject to migration within the passages of the zeolite. This result has been confirmed by the presence of large particles of gold as shown by the XRD spectra (figure 4.6). However, ion-exchange of Ni^{2+} ions within the zeolite, has been found to influence the extent of migration of gold in the zeolite and also can significantly improve the maintenance of the dispersion

of gold, and hence leads to improved catalytic activity. This suggests that the unreduced nickel ions function as chemical anchors for the reduced gold metal and that the reduced atoms of gold may form small clusters with the anchoring metal.

4.3.4.2 Effect of iron on activity of Au/Y (3.29wt%Au:1.88wt%Fe)

The effects of the metal stabilizers were further investigated by exchanging 1.88wt.% of Fe^{3+} on Y-zeolites. The result clearly suggests that an increase in reduction potential of the stabilizing metal readily reduced the induction period observed on nickel stabilized gold catalyst by two-fold, as can be seen in figure 4.10. Au/Fe-Y (3.29wt%Au:1.88wt%Fe), reached steady state activity with conversion of approximately 94% at around 400 ^{0}C. The lower activity observed on Au/Ni-Y (3.35wt%Au:1.79wt%Ni) might be due to its earlier reduction. Hoof et al. [13] reported that the reducibility of nickel in faujasite (X and Y) is strongly influenced by the presence of a second cation in the lattice.

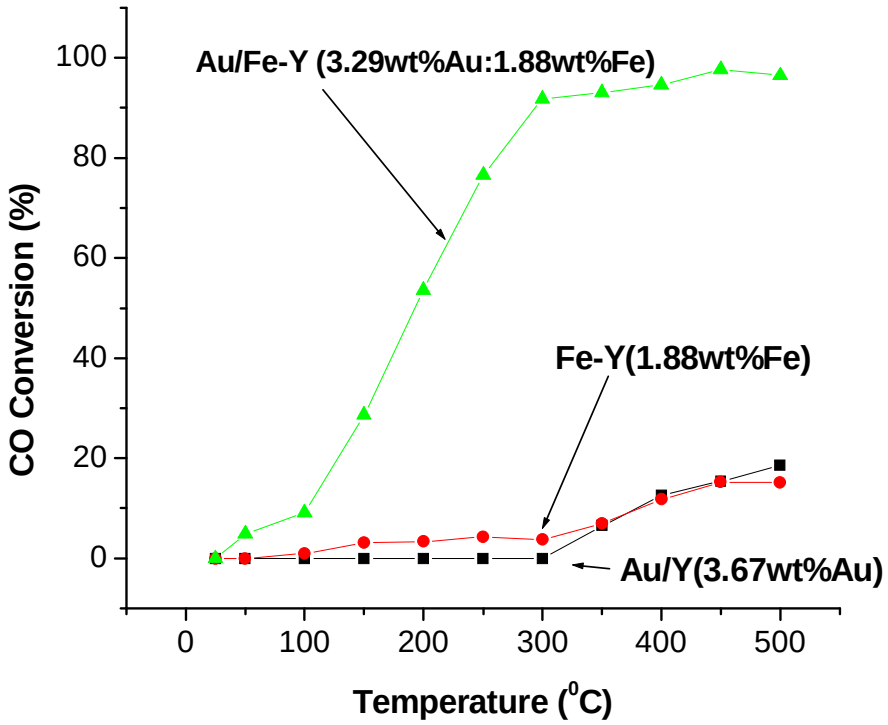

Figure 4.10: Effect of Fe^{3+} ions on the activity of supported Au on Y (3.67wt%Au) as a function of temperature (3.29wt%Au:1.88wt%Fe).

4.3.4.3 Catalytic activities of Au/Cr-Y (3.26wt%Au:1.76wt%Cr)

Au on Cr-Y (3.26wt%Au:1.76wt%Cr) showed that the induction period seems to resemble that of Fe^{3+}-exchanged metal ion on Y and the catalyst had the highest activity in comparison with nickel and iron as stabilizing metal. The conversion of approximately 98% was obtained at a temperature below 300 ^{0}C as can be seen in figure 4.11. The high activity of chromium exchanged metal ion on Y-zeolite as compared to Fe^{3+}-exchanged metal ion on Y-zeolite might be due to easier introduction into the cationic sites of Y-zeolite. Minachev et al. [14] reported that the introduction of Cr^{3+} and Cr^{2+} ions into the cationic sites of Y is not difficult,

compared to introduction of iron ions, because of the lower tendency for hydrolysis of chromium to occur when exchanged at pH 4. The high reduction temperature observed (see TPR profile, figure 4.3), similar to that reported by Taarit et al. [15, 16] had stabilized most of smaller gold clusters within the zeolite lattice.

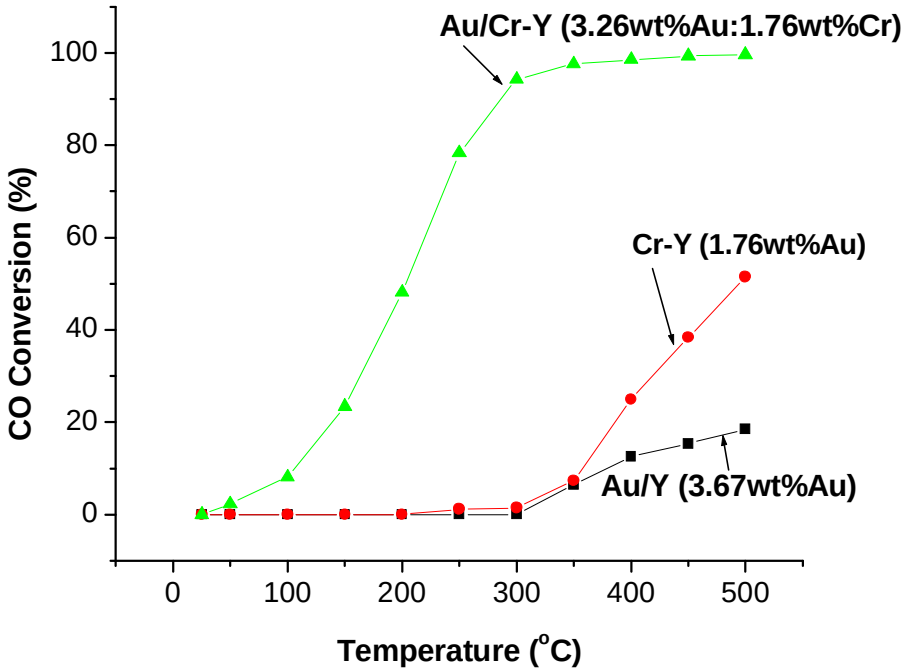

Figure 4.11: Effect of Cr^{3+} ions on the activity of supported Au on Y (3.67wt%Au) as a function of temperature.

4.3.4.4 Comparison of catalytic activities of Au/M-Y (M = Ni^{2+}, Fe^{3+}, Co^{2+} and Cr^{3+})

The catalytic activity of Au on zeolite-Y exchanged with Ni^{2+} has shown that the reduction potential of the stabilizing metal plays a crucial role on the stability or maintenance of gold dispersion throughout the zeolites cavities (figure 4.13 and figure 4.14). The activity of Au/Ni-Y (3.35wt%Au:1.79wt%Ni), suggests that almost 90% of the exchanged Ni^{2+} has been reduced to the zero-valent state, as confirmed the by TPR profiles with reduction peak maxima at 219 ^{0}C (see TPR profile in figure 4.2). As the reduction potential becomes more negative, the activity of gold supported on zeolites was found to increase following the sequence: Ni^{2+}, - 0.23 << Fe^{3+}, - 0.41 < Cr^{3+}, - 0.56.

This clearly suggests that an increase in gold activity by Fe^{3+}, and Cr^{3+} exchanged zeolite-Y has been achieved. At least 90% of gold has been reduced to zero-valent state while at least 90% of the stabilizing metals (Fe^{3+}, and Cr^{3+}) remains in the ionic state in these samples. Such dependence of gold catalysts on reduction potentials of transition metals was also noted on Co^{2+} exchanged on zeolite-Y, which has the reduction potential of - 0.28, as illustrated in figure 4.12.

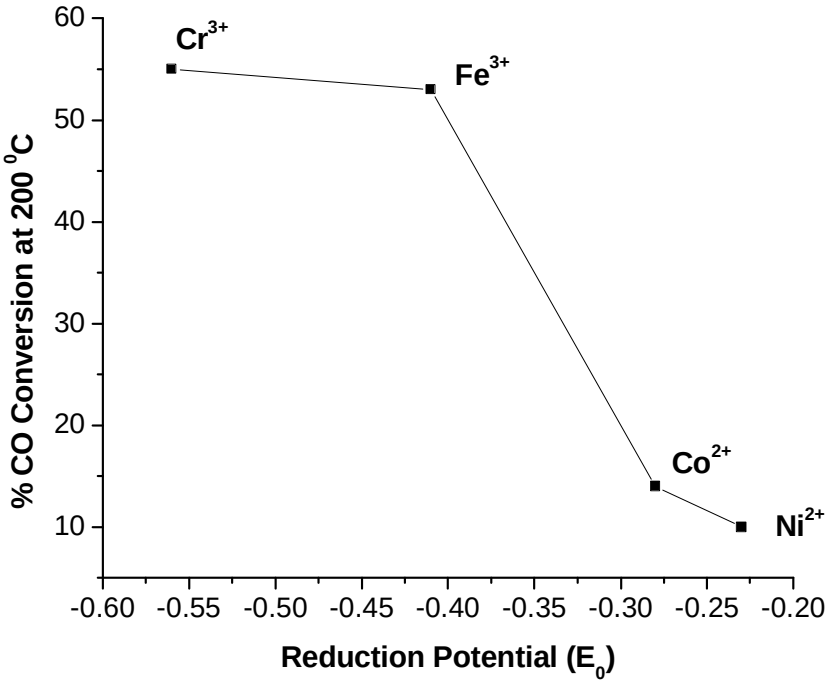

Figure 4.12: Effect of reduction potentials of transition metals of Ni^{2+} Co^{2+}, Fe^{3+}, and Cr^{3+}, on the % CO conversion at 200 ^{0}C.

The activity of Au/Co-Y (3.47wt%Au:1.84wt%Co) was found to be less or comparable to that of Au/Ni-Y (3.35wt%Au:1.79wt%Ni), and is related to the less negative reduction potential of cobalt ion.

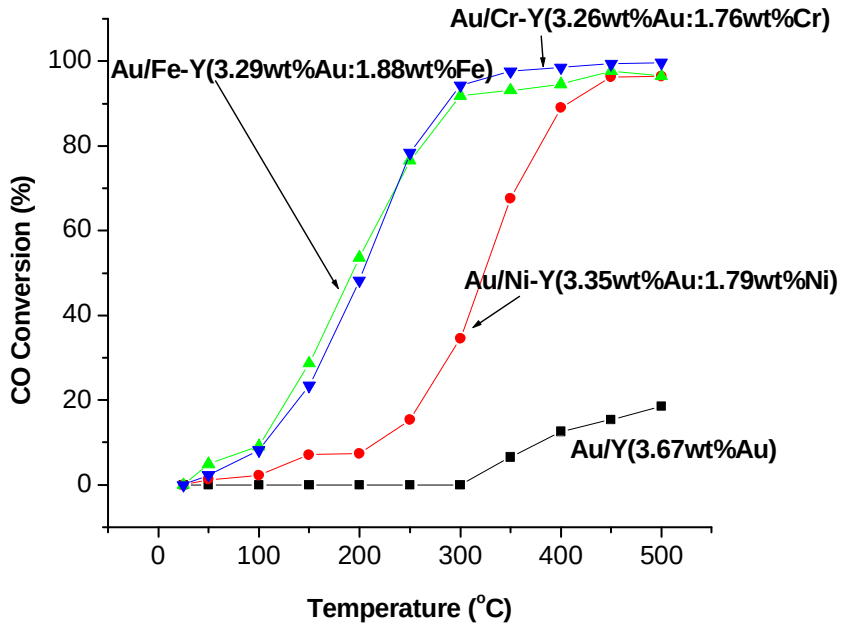

Figure 4.13: Effect of Ni^{2+}, Fe^{3+}, and Cr^{3+}, on Au supported on M-Y (M = Ni^{2+}, Fe^{3+}, and Cr^{3+}) system, as a function of temperature.

However, the catalytic activity of chromium and that of iron metal as stabilizers were found to be very close, which agrees with the closeness of their reduction potentials. Such closeness in activity has also been illustrated by time on stream related performance at 200 ^{0}C. As discussed above the activity of the catalyst increases with an increase in the reduction potential of the metal stabilizers. Figure 4.14 shows that the activity of Au on Fe^{3+}, - 0.41 and Cr^{3+}, - 0.56; containing zeolite is approximately the same, as observed when the same catalysts where studied as a function of temperature. The activity of Au-Y (3.67wt%Au) as a function of time on stream is zero at 200 ^{0}C and is therefore not shown in figure 4.14.

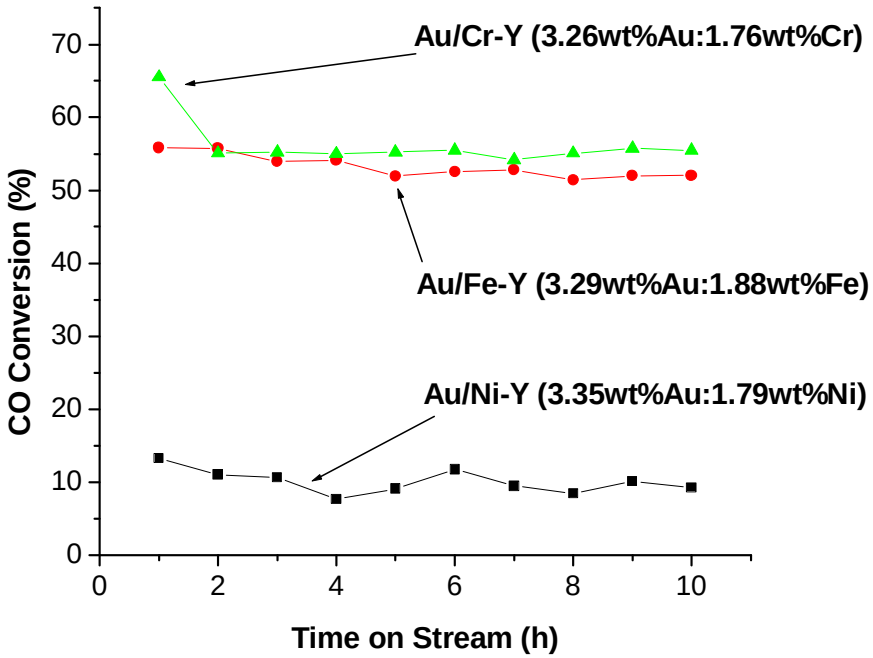

Figure 4.14: Effect of Ni^{2+}, Fe^{3+}, and Cr^{3+}, on Au supported on M-Y (M = Ni^{2+}, Fe^{3+}, and Cr^{3+}) system, as a function of time on stream at 200 ^{0}C.

The anchoring ions (Ni^{2+}, Fe^{3+}, and Cr^{3+}) and the catalytic metal both have incompletely filled d- or f-orbitals and the attractive interaction between gold atoms and the anchor ion is possible. Satchler et al. [5] have suggested that the energy of the lowest occupied orbital of one gold atom can be similar to that of the highest occupied orbital of the metal ion, which permit, good overlap of the corresponding orbital for providing an attractive interaction.

4.3.4.5 Effect of gold loading on CO oxidation activity of Au/Fe-Y (1.88wt%Fe).

Figure 4.15 shows the CO oxidation activity for the Au/Fe-Y (1.88wt%Fe, consisting of 1.67wt%, 3.29wt% and 5.45wt% Au) as a function of temperature. The Au/Fe-Y (1.67wt%Au) catalyst showed a lower activity with an average steady state activity of 23% CO conversion. However, the time on stream study of a 3.29 % gold content catalyst (Au/Fe-Y (3.29wt%Au)) showed an initial high activity of 54% CO conversion. A further increase in gold content to 5.45wt%Au lowered the activity to an initial activity of 45% CO conversion.

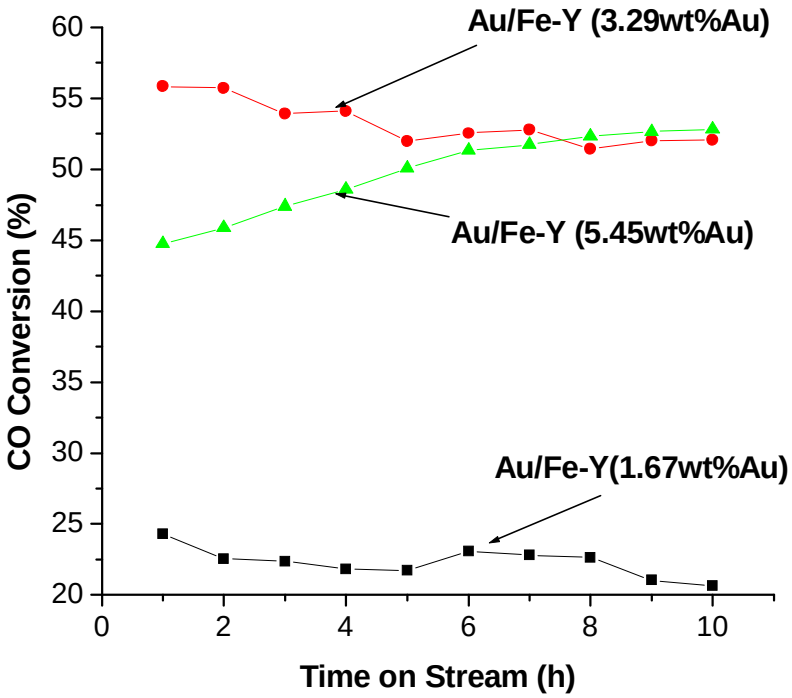

Figure 4.15: Time on stream CO oxidation activity for Au/Fe-Y, showing the effect of gold content at 200 ^{0}C.

This result suggests that a further increase in Au content lowers the CO conversion as a result of particle agglomeration, since the interaction of Au particles with the stabilizing metal is being lost. This suggests that the particle size plays a significant role on the catalytic activity and that it is necessary to make the particles as small as possible, i.e. to maximize the fraction of the atoms of the gold that are on the surface. It can be suggested that most of gold once introduced on the pores of Fe-Y zeolites, are immediately covered by ionic species in this case of iron. This probably occurs during pre-treatment which increases the dispersion of Au, which tends to be readily adsorbed on the surface of zeolite-Y. Higher CO oxidation activity of Au/Fe-Y (3.29wt%Au), suggests that a significant amount of smaller Au particles sizes and a lower number of large Au particles were formed, which then surrounded by stabilizer metal-Fe. Generally, a catalytically-effective amount of the catalyst metal employed together with an amount of the second metal ions provides effective dispersion stabilization.

4.3.4.6 Effect of increasing the Fe content on stability and activity of Au catalyst (containing 3.67wt%Au)

Figure 4.16 shows the time on stream CO oxidation activity for the Au/Fe-Y (1.88wt%Fe) at 200 ^{0}C. The catalyst showed an initial high activity of 55% CO conversion. However the time on stream study indicated that the Au catalyst was not stable and continuously deactivated with time. Over a period of 10 hours the CO conversion decreased from 55 to 51%, suggesting that the Au catalyst is relatively stable. However an increase in Fe^{3+} content on Au/Fe-Y (~ 4wt%Fe),

showed a lower activity of 37% CO conversion. A further increase in Fe^{3+} content to ~ 6wt%Fe lowered the activity to a steady state CO conversion of 27%. These results suggest that the amount of the stabilizing metal should be less than that of the metal catalyst. This clearly suggests that a sufficient concentration of the unreduced Fe ions should be present throughout the zeolite [14], such that gold atoms may be trapped at an early stage in their migration from the exchanged sites. Too much of the stabilizing metal might reduce the availability of exchange sites for the metal catalyst-Au (3.67wt%) and hence reduce the activity.

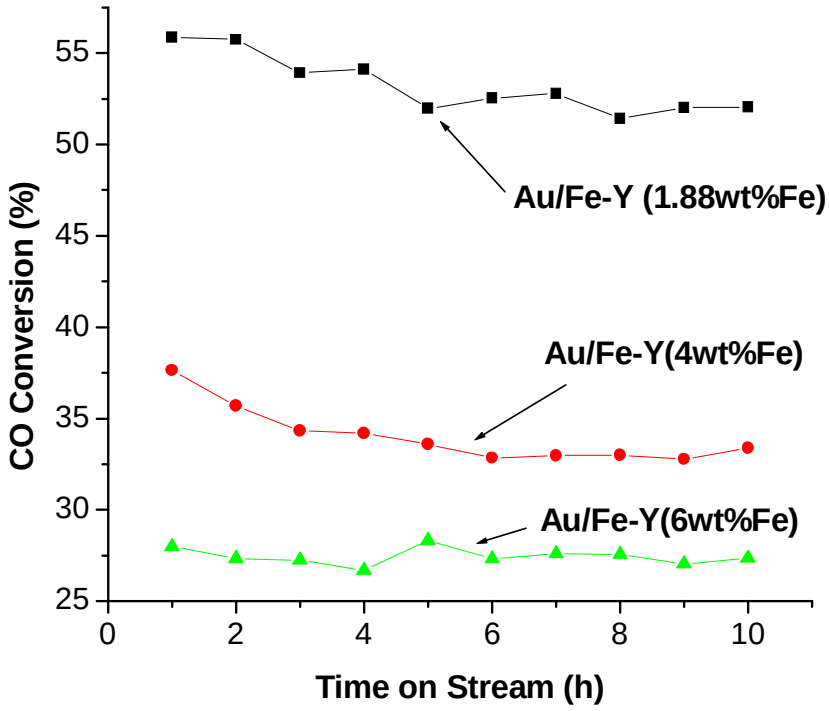

Figure 4.16: Effect of Fe content on the activity of the catalyst, as a function of time on stream at 200 ^{0}C.

4.4 CONCLUSIONS

Gold supported on Y and HY zeolite has been prepared by the incipient-wetness of $KAu(CN)_2$ salt solution onto the zeolites. It has been found that the activity of supported gold depends on the type of the support used. XRD profile has shown that when the gold is introduced onto the zeolite, such as on Au/Y and Au/HY initially a very high degree of dispersion is obtained. This suggests that individual ions are localized at the cation exchange sites of the zeolite, which are localized at the zeolite cavities and in the channels of the zeolite. When these Au ions are reduced to the zero valent state, the ionic bonding is neutralized, which results in weak interaction between the zeolite and the gold atoms. During the pre-treatment or reduction step, and also any subsequent use, the reduced gold is subject to migration within the passages of the zeolite.

TPR profiles, suggest that Au particles on Cr^{3+}-exchanged Y are more stable when compared to Fe^{3+}. Both of the above are highly stable when compared to Ni^{2+}. XRD profiles has shown smaller gold particles ~ 5 nm, for Cr^{3+}-exchanged Y systems, than that of Ni^{2+}-exchanged Y systems. This is related to the observed catalytic activity of Au/Cr-Y. At a higher reduction temperature, the migration of Au in the absence of an “anchor” is pronounced, resulting in Au particles as large as 20 nm presumably located at the external surface of the zeolite. However, in the presence of chromium, the migration of the Au is impeded because of the enhanced interaction with the zeolite. As a result Au particles remained smaller than 5 nm. It can be concluded that multivalent irreducible transition elements and

or metal ions, such as Fe^{3+} and Cr^{3+}, can increase the interaction of Au particles with the aluminosilicate framework surface and consequently increase their thermal stability. Transition metals which are electrostatically bound to the zeolite matrix interact chemically with the Au metal particles.

Gold supported on M-Y (M = Ni^{2+}, Fe^{3+}, Cr^{3+}) systems, have been prepared by incipient-wetness of $KAu(CN)_2$ on transition metal exchanged Y-zeolites. Both Fe^{3+} and Cr^{3+}-exchanged Y had much higher catalytic activity for CO oxidation than Ni^{2+}-exchanged Y and that of Y-zeolite without transition metal. As the reduction potential becomes more negative, the activity of gold supported on the zeolites was found to increase, following the sequence: Ni^{2+}, - 0.23 << Fe^{3+}, - 0.41 < Cr^{3+}, - 0.56.

An increase in gold activity on Fe^{3+}, and Cr^{3+} exchanged zeolite-Y has been achieved because at least 90% of the gold has been reduced to the zero-valent state while at least 90% of the stabilizing metals (Fe^{3+}, and Cr^{3+}) remains in the ionic state. This indicates that during the preparation of gold-zeolite system, the addition of a stabilizing metal in ionic form has a marked effect in improving the initial dispersion of the reduced gold catalyst and also in maintaining a highly-dispersed state of reduced gold particles during use. The atomic ratio of stabilizing metal ions to that of the gold metal plays a crucial role for maximizing the dispersion/stabilizing effects. On the other hand, the transition metals used, can also act as promoters of catalytic activity of gold supported on zeolite. The added chromium metal on Y zeolites seems to appear as the promoter of the gold

catalytic activity to a greater extent than can be accounted for by the improved dispersion of gold.

It has been noted that a further increase in Au content lowers the CO oxidation activity as a result of agglomeration of Au particles, since the interaction of Au particles with the stabilizing metal is being lost due to its unavailability. This suggests that the particle size is playing a significant role on the catalytic activity and this shows that it is necessary to make the Au particles as small as possible, i.e. to maximize the fraction of the atoms of gold that are on the surface.

It has been noted that as the Fe content is increased, the catalytic activity of these system decreases. This is thought to be due to the loss of interaction between Au and the support interface. This clearly suggests that a sufficient concentration of the unreduced Fe ions should be present throughout the zeolite, such that gold atoms may be trapped at an early stage in their migration from the exchanged sites. This suggests that too much stabilizing metal might reduce the availability of the exchange sites for the metal catalyst and hence the activity.

It has been noted that the presence of protons stabilizes most of the Au clusters (electron-deficient species) within the HY cages and thus results in a smaller amount of gold species migrating to the outer surface of the zeolite. The results further suggest that formation of metallic gold on Y result in higher CO oxidation activity and hence the necessity of metallic gold. The results suggest that

adsorptive properties of zeolite encaged metal clusters can be ‘altered’ by other ions sharing the same cavities.

4.5 REFERENCES

[1] (a) S. D. Lin, M. Bollinger, and M. A. Vannice, *Catal. Lett.* **17** (1993) 245.

(b) H.-S. Oh, J. H. Yang, C. K. Costello, Y. M. Wang, S. R. Bare, H. H. Kung, and M. C. Kung, Journal of Catalysis **210** (2002) 375.

[2] P. Gallezot, A. Alarcon-Diaz, J-A. Dalmon, A. J. Renouprez and B. Imelik, J. Catal., **39** (1975) 334.

[3] M. S. Tzou, H. J. Jiang, and W. M. H. Sachtler, React. Kinet. Catal. Lett. **35** (1987) 207.

[4] (a) K. Kishi and S. Ikeda, J. Phys. Chem, **78** (1974) 107.

(b) M. Ichikawa, R. Ohnishi and S.Qiu, J. Phys. Chem. **98** (1994) 2719.

(c) S. Galvagno, A. M. Visco, C. Crisafulli, S. Scire and S. Minico, Catalysis Letters, **47** (1997) 273.

(d) B-Z. Wan and Y-M. Kang, Catalysis Today, **26** (1995) 59.

(e) R. L. Augustine and S. K. Tanielyan, Applied Catalysis A: General, **85** (1992) 73.

(f) M.S Helge and P. Bera, Catalysis Letters, 79 (2002) 75.

(g) S. Hayashi, S. Deki and K. Sayo, J. Materials Chemistry, 9 (1999) 937.

[5] M. S. Tzou, B. K. Teo, and W. M. H. Sachtler, J. Catal., (1988) 220.

[6] D. Horvath, M. Polisset-Thfoin, J. Fraissard, L. Guczi, Solid State Ionics, **141** (2001) 153.

[7] Linde and Union Carbide, Linde Molecular Sieves, Zeolite data, USA, (1988).

[8] M. Boudart and G. Meitzner, in EXAFS and Near Edge Structure III, ed. K. O. Hodgson, B. Hedman and J. E. Penner-Halm, Springer, Berlin, (1984) 217.

[9] (a) D. Guillemot, V. Yu. Borovkov, V. B. Kazansky, M. Polisset-Thfoin and J. Fraissard, J. Chem. Soc., Faraday Trans., **93** (1997) 3587; (b) Lin J. N., Chen J. H., Hsiao C. Y., (c) Kang Y. M. and Wan B. Z., *Appl. Cat. B: Env.*, **36** (2002) 19.

[10] M. S. Tzou, H. J. Jiang, and W. M. H. Sachtler, Appl. Catal. Lett. **20** (1986) 231.

[11] P. A. Jacobs, Structure and Reactivity of Modified Zeolites, Elsvier, New York, Amsterdam, (1984) 313.

[12] C-K. Chang, Y-J. Chen, and C-t. Yeh, Appl. Catal. A: General **174** (1998) 13.

[13] Z. Maskos, J.H.C. Van Hoof, J. Catal. **66** (1980) 73.

[14] Kh. M. Minachev, Catalysis on Zeolites, Budapest, Moscow, 1988.

[15] C. Naccache, Y. ben Taarit, J. Chem. Soc. Faraday Trans. I, **69** (1973) 1475.

[16] B. Wichterlová, Z. Tvarůžková, J. Nováková, J. Chem. Soc. Faraday Trans. I, **79** (1983) 1573.

CHAPTER 5

Reductive pre-treatment of Au/HY and Au/Y, for CO oxidation.

5.1 INTRODUCTION

Nanoparticles of noble metals hold promise for use as advanced materials with novel electronic, optical and thermal properties as well as catalytic properties [1, 2]. In order to prevent the undesired agglomeration of nanoparticles, the preparations are often performed in the presence of ligands, polymers or various surfactants. However, the stability of metal colloid depends on the characteristics of the special protecting agents, which are usually stripped off from the metal surface in vacuum and/or after heating, resulting in agglomeration.

The activity of a freshly prepared Au/HY (3.77wt%Au) when exposed to a stream of gas mixture containing CO and O_2, was studied at 450 ^{0}C as a function of time on stream. It was found that an induction period was obtained, before the activity reaches its steady state as shown in figure 5.1 [3].

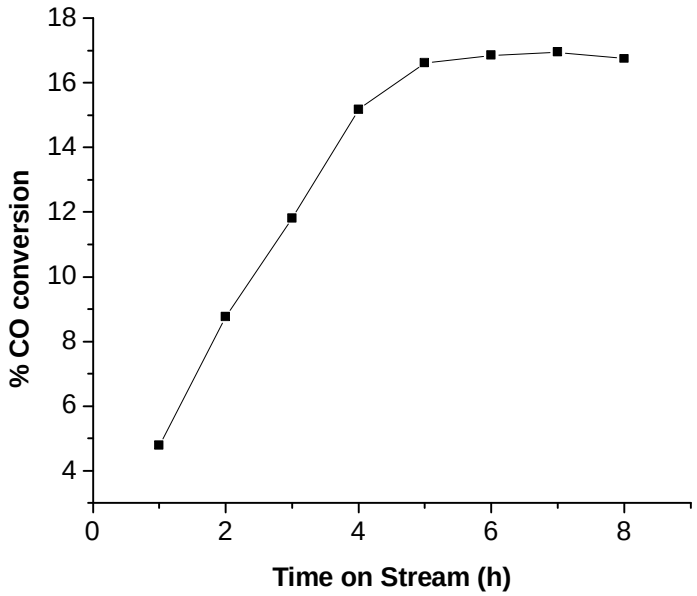

Figure 5.1: Time on stream CO oxidation activity for the Au/HY (3.77wt%Au) at 450 ^{0}C.

This work seeks to examine the proposal that the reduction of gold from Au^{3+} to lower oxidation states Au^{+}/Au^{0}, is the slow step in the activation of gold, which manifests itself in the observed induction period. The approach described below has been followed for this study. Two variables were explored: Treatment of Au on HY with various reducing agents, and the role of protecting agents on the induction period. In principle if the activation of gold from Au^{3+} to Au^{+}/Au^{0} could be responsible for the slow induction period. Then the induction period should be reduced (or eliminated) when Au is pre-reduced with an appropriate reducing agent.

In the studies it has been noted that when Au was incorporated into Y zeolites, the gold particles are thermally unstable during the pre-treatment conditions resulting

in low or no activity as reported by Meitzner et al. [3, 4]. With the hope of preparing thermally stable Au nanoparticles inside the Y zeolites super-cages, the Au/Y (3.49wt%Au) system was treated with different reducing agents, prior to CO oxidation reactions.

5.2. EXPERIMENTAL

5.2.1 Support and catalyst preparation

Gold supported on HY and Y were prepared from, $Au(en)_2Cl_3$ unless otherwise stated. Gold nanoparticles supported on HY and Y were obtained by an ion-exchange method which involves an exchange of complexed cations of gold $[Au(en)_2]^{3+}$, with counter-ions of the acidic zeolite, HY or Y. Subsequently reduction of the gold cations by ascorbic acid, trisodium citrate and sodium borohydride as described in Chapter 3 was performed. All the catalysts discussed in this Chapter were loaded with 4wt%Au.

The protecting agent polyethylene glycol (PEG) was also used in some preparations in order to prevent agglomeration of gold nanoparticles formed. Ascorbic acid and trisodium citrate were also used as reducing agents in the preparation of the reduced catalyst systems. In the case of ascorbic acid, the ascorbic acid-PEG solution was neutralised with a 1M K_2CO_3 solution before being introduced drop-wise to the solution of ion-exchanged Au/HY catalysts.

5.2.2 UV-Vis spectrophotometry

UV-Vis Spectrophotometry is a valuable tool in providing information on the nature of gold particles formed in the zeolite lattice. The disappearance of $[Au(en)_2]^{3+}$ ions and the formation of Au nanoparticles were monitored by UV-vis spectrometry using a Cary 5E UV-VisNir recording spectrophotometry.

5.2.3 X-Ray powder diffraction (XRD)

X-ray powder diffraction (XRD) patterns of the products were determined on a D/MAX-RA rotating anode X-ray diffractometer with high intensity Cu-Kα radiation (λ = 0.151478 nm) and a graphite monochrometer at a scanning rate of 0.02 s^{-1} ranging from 40 to 90 ^{0} theta. Temperature programmed reduction (TPR) was used to monitor the reduction of gold on the zeolites using a purpose built facility in our laboratory.

5.2.4 X-ray photoelectron spectroscopy (XPS)

X-ray photoelectron spectroscopy (XPS) was used for surface analysis and examination of the oxidation states of gold supported on HY and NaY zeolite. Analyses of the samples were undertaken at the National Metrology Laboratory of the CSIR, South Africa.

5.2.5 Diffuse Reflectance Infrared Fourier Transform spectroscopy (DRIFTS)

Diffuse reflectance IR spectra of the powdered sample of treated and untreated Au/HY (treated with sodium borohydride) were measured using a Bruker Opus NT spectrophotometry equipped with a diffuse reflectance unit. Spectra were transformed into Kubelka-Munk representations and corrected by background subtraction, as appropriate.

Since Au/zeolite samples were stored with no particular precautions, they were treated again before any gas adsorption study. For the IR study, samples were activated by heating to 400 ^{0}C (10 ^{0}C/min), under flowing N_2 for 30 min prior to CO adsorption. After cooling the sample to room temperature, CO was adsorbed on the sample at atmospheric pressure. The coverage of the metal surface with CO was gradually decreased by flushing the sample with N_2. On as-prepared Au/HY (3.77wt%Au) samples and samples reduced with $NaBH_4$ (equal mole ratio to that of gold), CO was adsorbed at different temperature from room temperature to 450 ^{0}C.

5.2.6 ^{197}Au Mössbauer spectroscopy

Selected solids were also examined using Mössbauer spectroscopy as described in chapter 3.

5.3 RESULTS AND DISCUSSIONS

5.3.1 Ultraviolet-visible spectrophotometry (UV-VIS)

Immediately after catalysts were treated with the related reducing agent, they were washed in order to remove chlorides and any organic protecting agents used during the preparation. After washing, filtrates were analysed for the presence of gold. The optical absorption spectra of an aqueous solution of $Au(en)_2Cl_3$ (100 ml) before ion-exchange on HY having the absorbance peak at 325 ± 1 nm was discussed in chapter 3, figure 3.1. Analysis of the filtrates (after ion-exchange on HY) of ascorbic acid treated Au/HY catalyst, suggested the presence of small amount of gold, since the absorbance peak at 325 ± 1 nm was observed. However, in the case of other reducing agents, (i.e. trisodium citrate and sodium borohydride) the technique could not reveal the presence of small amount of gold in the filtrates. This suggests that the trisodium citrate and sodium borohydride treated Au/HY resulted in negligible amounts of gold being washed off the zeolite.

Figure 3.2 in chapter 3 illustrated the optical absorption spectrum for the as-prepared solid sample solution of $[Au(en)_2]^{3+}$ on HY after 24 h ion-exchange. A broadened peak at 580 ± 2 nm, which is ascribed to the surface plasmon resonance absorption of gold nanoparticles [5] inside the zeolite cages, was observed in the gold-zeolite solution, while the peak at 325 ± 1 nm for $[Au(en)_2]^{3+}$ ions

disappeared. The optical absorption behaviour of the solid sample as well as that of the solution indicated the formation of Au nanoparticles.

5.3.2 Inductively coupled plasma (ICP) analysis

Inductively Coupled Plasma-(ICP) was used to determine the percentage of Au-exchanged onto the zeolite-HY cavities. It was noted that the initial concentration of an aqueous solution of $Au(en)_2Cl_3$ (in 100 ml distilled water) before being exchanged was 11870 ppm and after ion-exchange the concentration was dratically reduced to 120 ppm. This exchange process was found to be equivalent to 98.99% of Au exchanged on HY zeolite, and the intended 4wt%Au loading had been essentially achieved.

5.3.3 Temperature-programmed reduction (TPR) and oxidation (TPO)

TPR and TPO studies discussed below were undertaken both at the University of the Witwatersrand (UW) and at the Northwestern University, USA. The TPR profiles obtained at UW were not satisfactory, probably due to the sensitivity of the equipment used at the time. The TPR profiles obtained in the USA were very much more reliable (see below).

5.3.3.1 TPR and TPO of untreated Au/HY (3.77wt%Au)

Temperature programmed reduction (TPR) studies of treated and untreated Au/HY were undertaken to follow the reducibility of Au supported catalysts. TPR studies (after degassing at 150 ^{0}C in N_2) undertaken on treated Au/HY at UW gave poor results with negligible or no hydrogen consumption.

However, on exposure of the same Au catalyst to 5% O_2/He, the temperature programmed oxidation (TPO) profile showed oxygen consumption with a peak maxima at 223 ^{0}C (figure 5.2). The results suggested that gold in the lower oxidation state was present in the zeolites even though the exact oxidation state of the metal is not known, since oxygen uptake by the untreated Au/HY was observed at 223 ^{0}C.

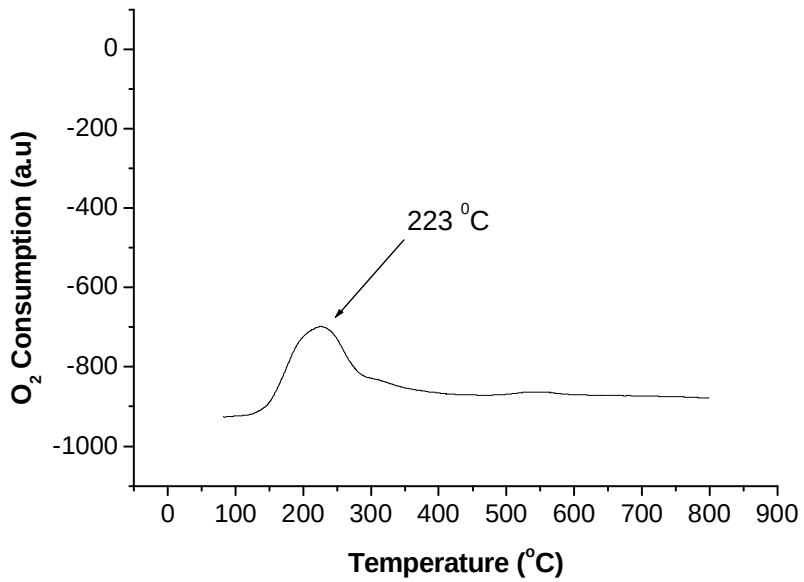

Figure 5.2: TPO profile of 5%H_2/Ar reduced $[Au(en)_2]^{3+}$/HY (3.77wt%Au) sample. The sample was degassed at 150 ^{0}C for 30 minutes under N_2 and oxidized with 5% O_2/He.

Temperature programmed reduction (TPR) of the same Au catalyst used in the temperature programmed oxidation (TPO) study above was immediately tested for H_2 consumption. Figure 5.3 shows the TPR results, which seems to show H_2 consumption with peak maxima at 309 ^{0}C and 453 ^{0}C.

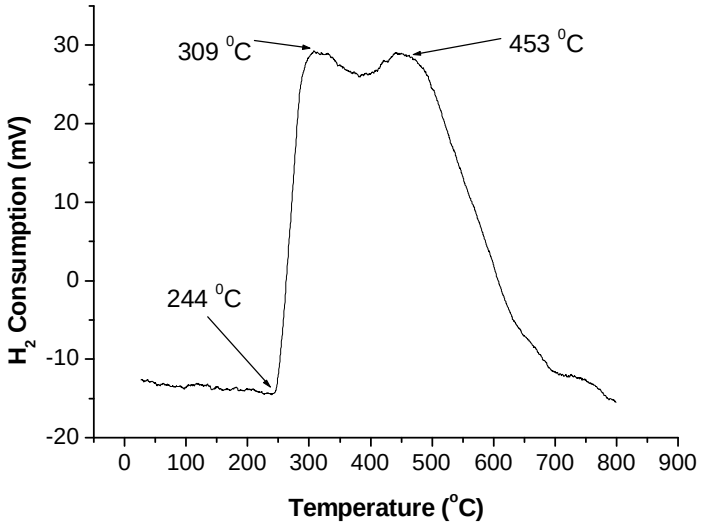

.

Figure 5.3: TPR profile of untreated Au/HY (3.77wt%Au).

However, when the same sample were exposed to H_2/Ar (flow rate = 42ml/min) atmosphere and recorded on the TPR experiments at Northwestern university, the reduction profiles were easily obtained, with clear and sharp peaks maximums and the results are discussed as follows.

5.3.3.2 TPR profile trisodium citrate treated Au/HY (3.66wt%Au)

TPR profile of a trisodium citrate treated catalyst (1:1 mole ratio) showed a reduction peak maxima at 130 ^{0}C, which indicates that Au was not washed off the zeolite (figure 5.4). Although the colour changes of the powder after reduction went from reddish to mauve, the TPR profile suggests that most of the gold species had remained in ionic form or in an unreduced state. This implies that, the nature of reducing agents plays an important role on the reduction of exchanged Au species, which is thought to be ionic species as suggested by the absence of

metallic particle signal in the XRD profile of the same catalyst. This shows that ionic species of Au were readily introduced by ion-exchange within the zeolite cages. The catalyst was found to be less active as compared to a catalyst reduced with $NaBH_4$ (1:1 mole ratio), which also showed a reduction peak maxima at 143 ^{0}C. This suggest that a certain amount of metallic Au (small Au particles were observed on XRD profile of $NaBH_4$ treated catalyst) is needed for this catalyst to be active for CO oxidation. $NaBH_4$ is a stronger reducing agent when compared with trisodium citrate.

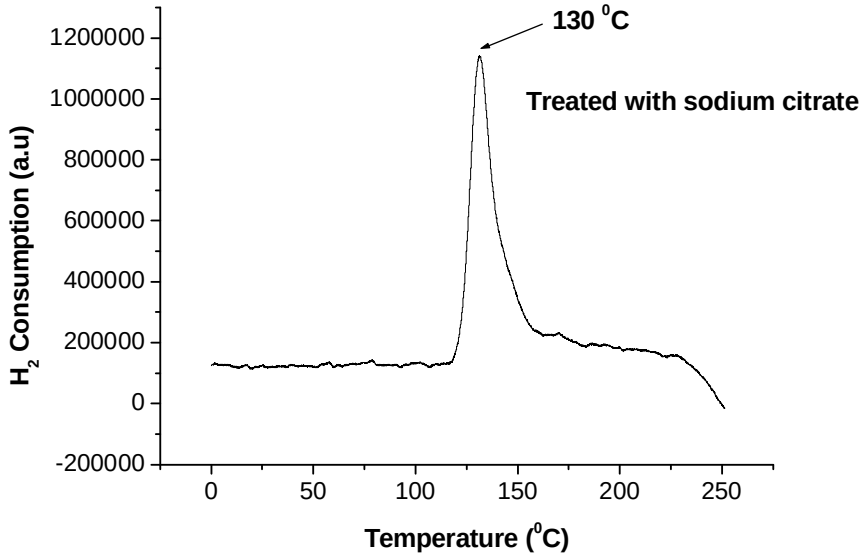

Figure 5.4: TPR profile of Au on HY (3.66wt%Au), treated with tri-sodium citrate.

5.3.3.3 TPR profile of $NaBH_4$ treated Au/HY (3.73wt%Au)

The $NaBH_4$ treated catalysts (1:1 mole ratio) has shown that reduction of Au is a crucial step in the activation of active Au species responsible for the activity of the catalysts. However, the TPR profile of this catalyst with peak maxima at 143 ^{0}C has shown that the reduction was not complete (figure 5.5). The XRD profile of this catalyst has shown the presence of smaller Au particles compared with the situation found for ascorbic acid treated catalysts, which showed the presence of large gold particles. X-ray spectroscopy (XPS), has shown the presence of a lower binding energy at 84.3 eV, (on both treated and untreated Au catalyst) which is associated with smaller metallic Au species of approximately < 2 nm on the surface of zeolites [7]. This was further confirmed by the TPR profile of $NaBH_4$ treated catalysts prepared using a higher molar ratio of sodium borohydride to that of gold (1:3 and 1:4 mole ratio). Both solids showed no reduction profile, suggesting that a complete reduction had already occurred. The activity of $NaBH_4$ treated Au/HY (3.73wt%Au) increased with increasing ratio of $NaBH_4$ to Au, which suggests that a higher amount of metallic species, is needed to actively catalyze CO oxidation with higher efficiency.

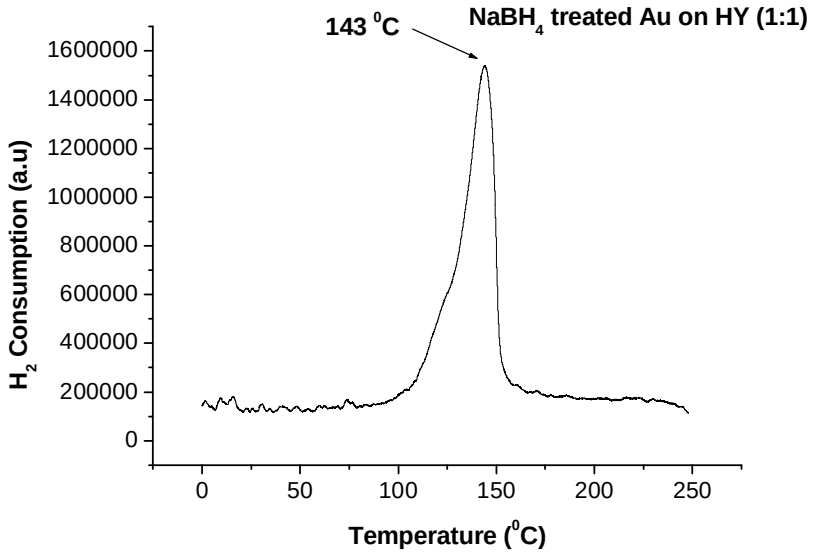

Figure 5.5: TPR profile of Au on HY (3.73wt%Au), treated with $NaBH_4$.

5.3.4 X-ray powder diffraction (XRD)

5.3.4.1 Effects of temperature on the mobility of Au^0 to the outer surface of a zeolite crystal.

Figure 5.6 shows a comparison of the diffraction patterns of both the spent and freshly prepared sodium borohydride treated Au/HY (3.73wt%Au) catalysts. The results show the intense Au(111) signal of the freshly prepared Au catalysts, suggesting that the most of gold particles are on the outer surface of the zeolites. On exposing the catalysts to CO oxidation at 450 ^{0}C, the spent Au catalysts shows the intensity of Au(111) peak increases, suggesting a further movement of Au^0 particles to the outer surface of the zeolites and/or with particles growth.

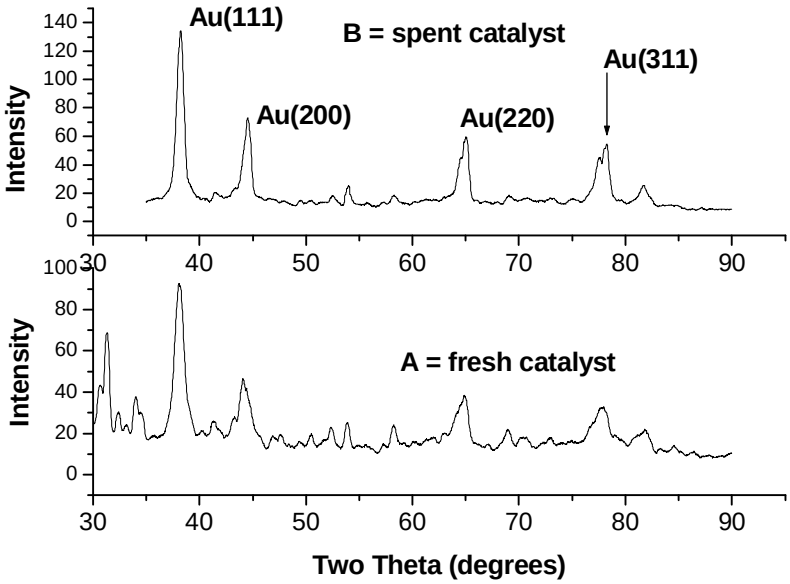

Figure 5.6: XRD patterns of: (A) freshly prepared, $NaBH_4$ treated Au/HY (3.73wt%Au) and (B) spent, $NaBH_4$ treated Au/HY (3.73wt%Au) catalyst at 450 ^0C.

5.3.4.2 Effects of reducing agents on Au particles size formation on zeolite-HY

Figure 5.7 shows the diffraction patterns of freshly prepared, untreated Au/HY (3.77wt%Au) and freshly prepared Au/HY treated with various reducing agents. The XRD pattern of untreated Au/HY (3.77wt.%Au) catalyst, similar to Na-HY zeolites has shown the absence of Au(111) peaks, suggesting that Au exists in ionic form within the untreated Au/HY (3.77wt%Au) catalyst. Trisodium citrate treated Au catalyst also show the absence of Au(111) peaks, suggesting that a smaller amount of Au particles were insufficiently crystallise and/or below detection limits.

The XRD profiles show a weak and broad Au(111) peak of sodium borohydride treated Au catalyst. This implies a significantly smaller Au particles size and a lower number of large Au particles. The stability of smaller Au particles on $NaBH_4$ treated Au/HY (3.73wt%Au) is due to high reducing ability of $NaBH_4$. This clearly suggests that the Au catalyst needs to be in a highly dispersed form to be active for CO oxidation. On the other hand, the XRD shows a strong and narrow Au(111) peak for the ascorbic acid treated Au catalyst, suggesting the presence of large Au particles. The lower activity of ascorbic acid treated Au catalyst for CO oxidation reaction may be attributed to larger particle size and/or the Au content (< 3wt%Au). The catalyst was found to have lower gold content, because most of the gold had been washed out during preparation.

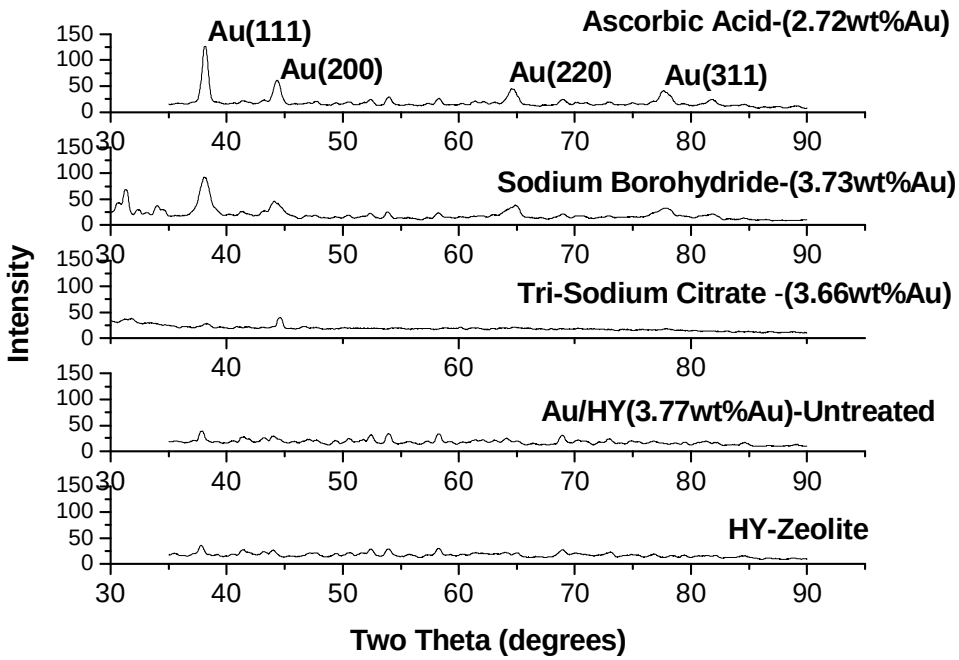

Figure 5.7: XRD patterns of Au/HY catalyst showing the effect of various reducing agents.

5.3.5 ^{197}Au Mössbauer spectroscopy

The results in table 5.1, shows the hyperfine interaction parameters of each of the sub-components in the overall fits of the samples measured. The parameters are linewidth Γ, isomer shift δ, quadruple splitting QS, and abundance obtained from the integrated area under the sub-component. The table shows the state of the gold species in percentage abundances of the two samples.

Table 5.1: Parameters of the sub-components in the overall fits of the two gold samples [8].

Sample	Γ (mm/s)	δ/Au[a]	QS (mm/s)	Abundances[b] (%)	Attribution
$[Au(en)_2]^{3+}$/	3.3	4.5	4.5	85	Au^{3+}
NaY	2.1[c]	0	0	15 ± 5	[c]Au^0
$[Au(CN)_2]^-$	2.2	4.4	11	83	Au^+
/NaY	2.1[c]	0	0	17 ± 5	[c]Au^0

[a] Isomer shift quoted with respect to Au metal at 6 K. [b] Typical relative error is 10 – 15 % of the quoted abundance value (e.g. 85 ± 9 %), unless explicitly specified in the table. [c] Fixed linewidth values of the parameters, because of strongly overlapping sub-spectra. The resonance at near-zero or negative velocities is broadened, thus suggesting the existence of this component. Fixed linewidth values are primarily based on the amount of gold in the sample [7]

5.3.5.1 $[Au(en)_2]^{3+}$/Y (3.02wt%Au, Y same as NaY-zeolite)

A minimum number of two components (i.e. singlet and doublet) have been used to fit the spectrum. These sub-components are attributed to Au^0 metal (~ 15 % abundance), and the rest of the gold is in the Au^{3+} valence state (see Table 5.1 and figure 5.8). The linewidth of this component is somewhat broad, viz, Γ = 3.3 mm/s, suggesting that the crystal chemistry is such that Au^{3+} exists in a distribution of atomic local environments. This is due to a combination of different (but similar) crystallographic sites for the Au^{3+}, poor crystallinity, nearest-neighbour consideration, etc [8].

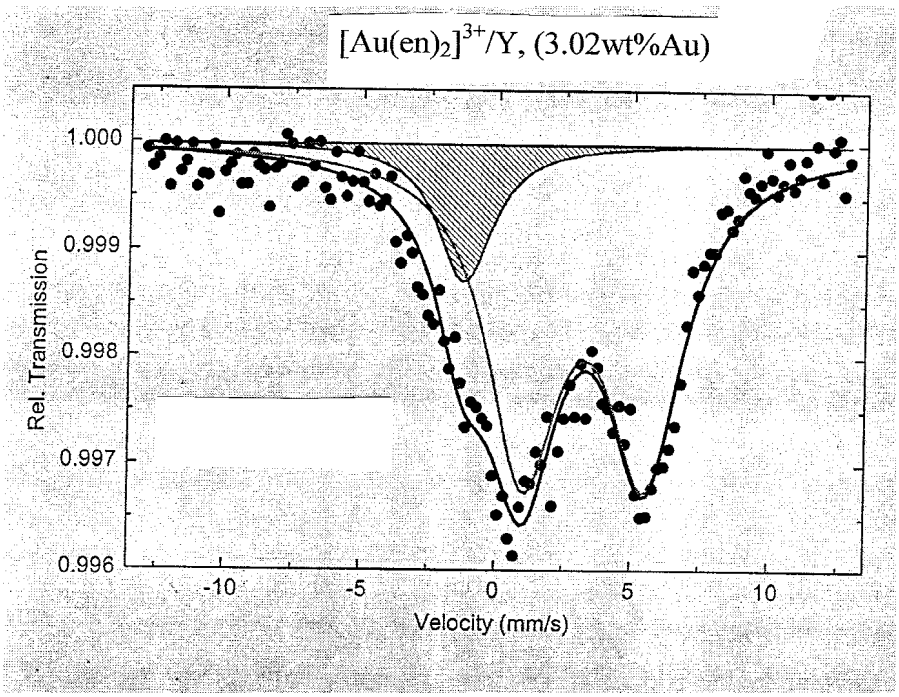

Figure 5.8: ^{197}Au Mössbauer spectra of $[Au(en)_2]^{3+}$/Y (3.02wt%Au, Y same as NaY-zeolite) at 6 K. Data are black solid circles, and solid lines through the black circles are the overall theoretical fits to the data. Shaded area is the fitted Au-metal (Au^0) component [8].

5.3.5.2 $[Au(CN)_2]^-$/Y (~2wt%Au, Y same as NaY-zeolite)

This sample has a sub-component that has typical Au^+ parameters. The abundance of this species is ~83 % and the remaining proportion of gold is metallic Au^0 (figure 5.9). Note that the linewidths of sub-components in this sample are narrower than in $[Au(en)_2]^{3+}$/Y. This suggests a more unique crystal chemical environment (crystallographic site) for the Au^+ species.

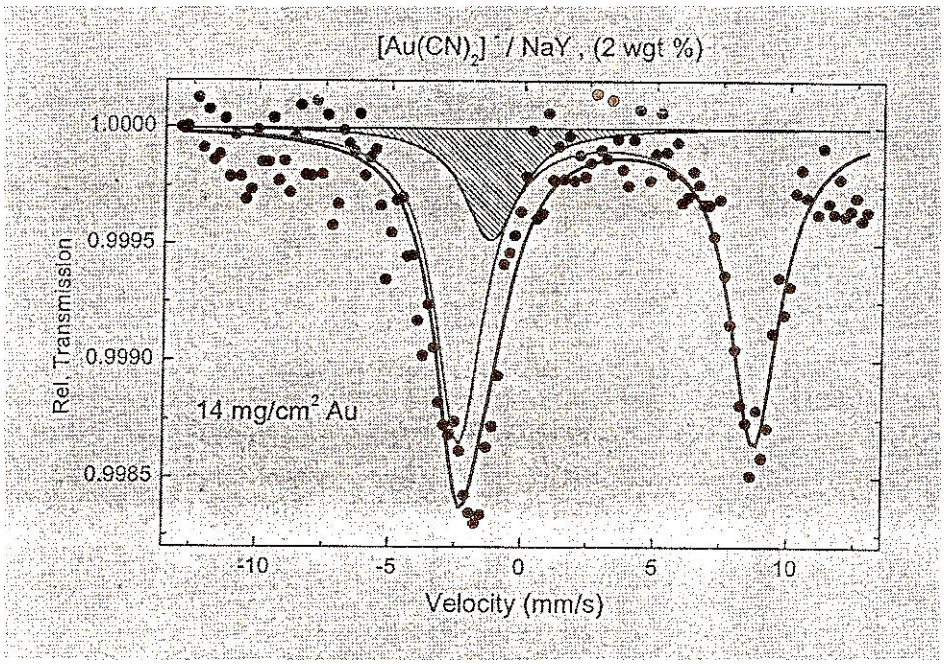

Figure 5.9: ^{197}Au Mössbauer spectra of $[Au(CN)_2]^-$/Y (~2wt%Au, Y same as NaY-zeolite) at 6 K. Data are black solid circles, and solid lines through the black circles are the overall theoretical fits to the data. Shaded area is the fitted Au-metal (Au^0) component [8].

The spectra in figure 5.8 and figure 5.9 do not have ideal high signal-to-noise ratios for a detailed analysis to be reliable. Note that the resonance absorption effect is very weak (< 0.4 %) due to, the low quantity of Au in the sample and the

possible entrapment of the Au in the cage-like structure of the zeolite. Cage-like structures like these in which entrapped atoms easily ‘’rattle’’ around (i.e. have large mean-square-displacement) are expected to give weak Mössbauer signals. However, the chemical valence of the Au species may be quite readily identified and also the abundances of the gold species in the sample may be obtained with reasonable accuracy [8].

5.3.6 X-ray photoelectron spectroscopy (XPS)

5.3.6.1 Untreated Au/HY (3.77wt%Au)

The XPS spectrum shown in figure 5.10, after deconvulation, suggests that only ionic species of gold are present on as-prepared Au/HY (3.77wt%Au). The binding energy of 87.0 eV, which is due to $[Au(en)_2]^{3+}3OH^-$, show that gold is easily exchanged within the zeolite cavities as Au^{3+} state. ^{197}Au Mössbauer spectroscopy has confirmed that within a freshly prepared, uncalcined Au/Y (3.02wt%Au), 85% of Au exists in the Au^{3+} state [8].

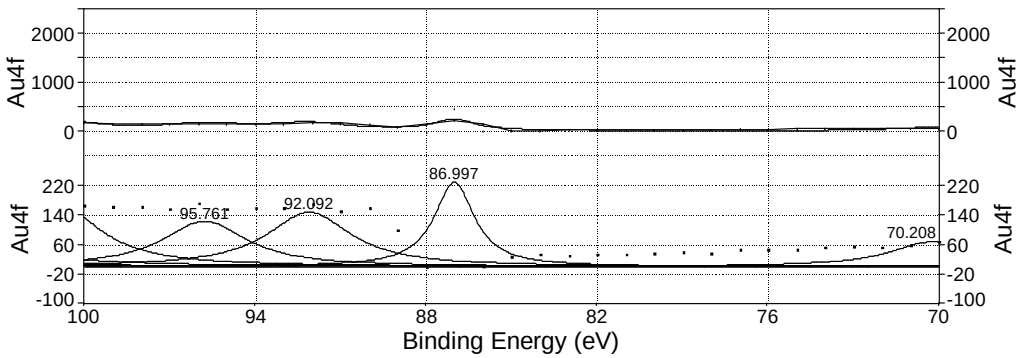

Figure 5.10: XPS spectra of untreated Au/HY (3.77wt%Au)

5.3.6.2 Au/HY (3.73wt%Au) treated with $NaBH_4$ (mole ratio = 1:1)

Immediately after Au/HY (3.73wt.%Au) was treated in-situ with $NaBH_4$ (mole ratio = 1:1), the XPS spectra suggested the formation of metallic gold with the binding energy at 84.1 eV as shown in figure 5.11 [9]. However, the reduction was not complete as the spectrum shows the presence of the higher binding energy peak at 87.9 eV, which has been ascribed to Au^{3+}. The TPR profile of the same sample has confirmed that the reduction of Au was not complete (see figure 5.5).

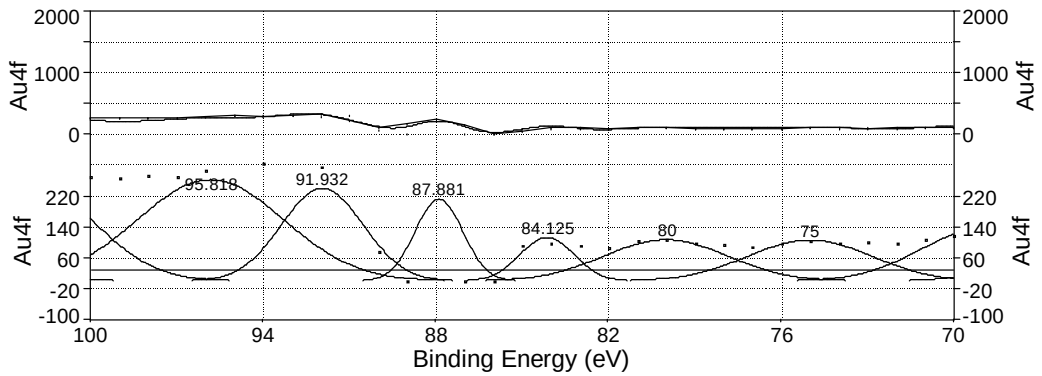

Figure 5.11: XPS spectra of Au/HY (3.73wt%Au) treated with $NaBH_4$ (mole ratio = 1:1).

5.3.6.3 Au/HY (3.75wt%Au) treated with $NaBH_4$ (mole ratio = 1:4)

Further treatment of Au/HY (3.75wt%Au) with $NaBH_4$ at a higher molar ratio of reducing agent to that of gold resulted in the formation of an additional metallic gold as shown in figure 5.12. Quantitative analysis of the area under the peak, suggests that as the molar ratio of reducing agent to Au is increased the formation of metallic gold is increased and consequently the consumption of Au^{3+}.

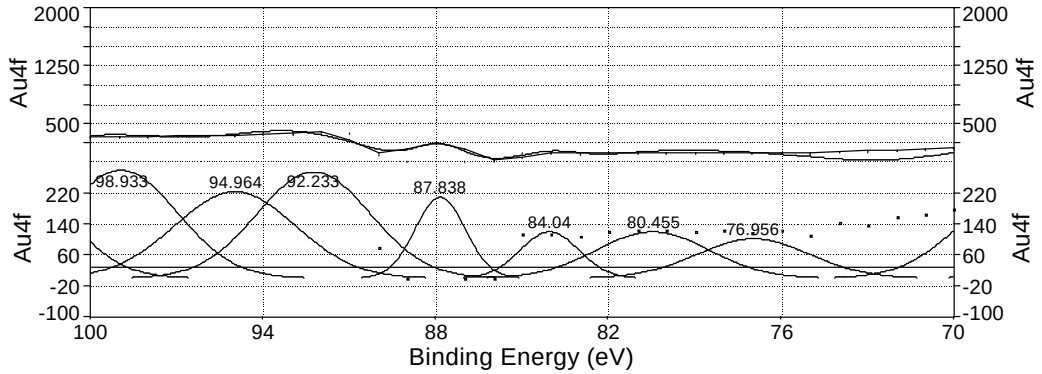

Figure 5.12: XPS spectra of Au/HY (3.75wt%Au) treated with $NaBH_4$ (mole ratio = 1:4).

In summary, XPS analysis has shown the existence of several gold species on both treated and untreated gold catalysts. The results show that the gold species present on the zeolite can be classified into metallic gold (Au^0) and ionic gold (Au^{3+}). The binding energy of metallic gold on Au/HY catalysts treated with both $NaBH_4$ and tri-sodium citrate is higher (i.e. 84.1 eV) than those of bulk gold (BE < 84 eV, were BE represent binding energy) [10]. This suggests the existence of small gold metal clusters in both $NaBH_4$ and tri-sodium citrate treated Au/HY catalysts. Wan *et al*. [6], and Rao *et al.* [11], have observed similar BE shifts of the Au 4f lines of the small gold clusters. Wan *et al*. [6], have mentioned that smaller gold clusters with a mean diameter < 2 nm show significantly larger binding energy than that of bulk gold metal. This suggests that the gold particles of our catalysts are smaller than 2nm. This results are consistent with that observed from the data obtained from the XRD profile of $NaBH_4$ treated Au/HY (3.73wt%Au).

5.3.7 Diffuse Reflectance Infrared Fourier Transform spectroscopy (DRIFTS)

5.3.7.1 DRIFTS studies of as-prepared Au/HY (3.73wt%Au), treated with $NaBH_4$ (mole ratio = 1:1).

Figure 5.13 shows DRIFTS spectra of CO adsorbed on $NaBH_4$ treated Au/HY (3.73wt%Au, molar ratio = 1:1), at various temperatures. The catalyst has been incompletely reduced, as suggested by the TPR profile (see figure 5.5). The adsorption of a CO molecule has been followed by monitoring changes on surface adsorbed CO from room temperature to 400 ^{0}C. The spectra showed a decrease in the two broad band with maxima at ca. 2170 and 2115 cm^{-1} as the temperature is increased from 22 to 400 ^{0}C. These bands may not be ascribed to gaseous CO, since the spectra were obtained in the diffuse reflectance mode, and as similar results had been observed by Fraissard *et al*., [12]. The 2115 cm^{-1} band, which is easily removed by outgasing, has been ascribed to CO linearly adsorbed on Au^0 [12]. Salama *et al*., [13] who investigated CO adsorption on the $AuCl_3$/NaY system have observed a similar band at ca. 2120 cm^{-1}.

The band at ca. 2170 cm^{-1} is at too high a wavenumber to be attributed to chemisorbed CO on metallic gold. One interpretation of this band is due to CO adsorbed on acidic OH groups [14]. This band has been detected within 1 min of CO adsorption at room temperature and it was easily removed by flushing with N_2. Fraissard et al., [12] have observed a similar band at 2169 cm^{-1} on reduced or

fully reduced Au/HY and suggested that the band corresponded to CO adsorbed on oxidized gold (probably Au^{+}). A similar band has been observed by Yates, [15], and Lee and Schwank, [16] for CO adsorbed on unreduced or incompletely reduced gold. They attributed this band to complexes of CO with Au^{n+} cations, but did not discriminate between the two possible oxidation states of gold, +1 and +3. They reported that these species could be easily removed by short evacuation of pre-adsorbed CO at room temperature.

In our Mössbauer spectroscopy work (figure 5.8), it has been found that 85% of gold species on as-prepared $[Au(en)_2]^{3+}$/NaY are in the Au^{3+} valence state. However, the adsorption of CO molecules within the zeolite cavities results in irreversible reduction of gold. Furthermore, the shoulder representing the band at ca. 2169 cm^{-1} observed by Fraissard et al. [12] is less intense than the band at ca. 2111 cm^{-1}. Our TPR studies (figure 5.5) of this reduced sample confirmed that the reduction was incomplete. We therefore suggest that the band at ca. 2170 cm^{-1}, which is more intense, corresponds to CO adsorbed on oxidized gold (i.e. either Au^{+} or Au^{3+}).

The results in figure 5.14 shows that the adsorption of CO on Au/HY (3.73wt%Au) depends on temperature, since from 22 ^{0}C to 200 ^{0}C the two broad band observed at maximum frequency of 2170 and 2115 cm^{-1} where the only available band. However, as the temperature is raised to 250 ^{0}C, a sharp band at ca. 2142 cm^{-1} was found to appear and this continued to increase in intensity as the temperature was increased. A similar band at ca. 2142 cm^{-1}, was observed by

Fraissard et al. [12], and they have noted that the band remained even after evacuation of pre-adsorbed CO at room temperature. They suggested that the band at 2142 cm^{-1} is due to electron-deficient particles ($Au^{\sigma+}$-CO species) of gold clusters, inside the HY framework and in contact with protons. This band was found to be the only band available above 300 ^{0}C, suggesting that CO is strongly adsorbed on these species of gold and more weakly adsorbed on CO adsorbed on large neutral particles (Au^0, 2114 cm^{-1}) and gold cations (2170 cm^{-1}).

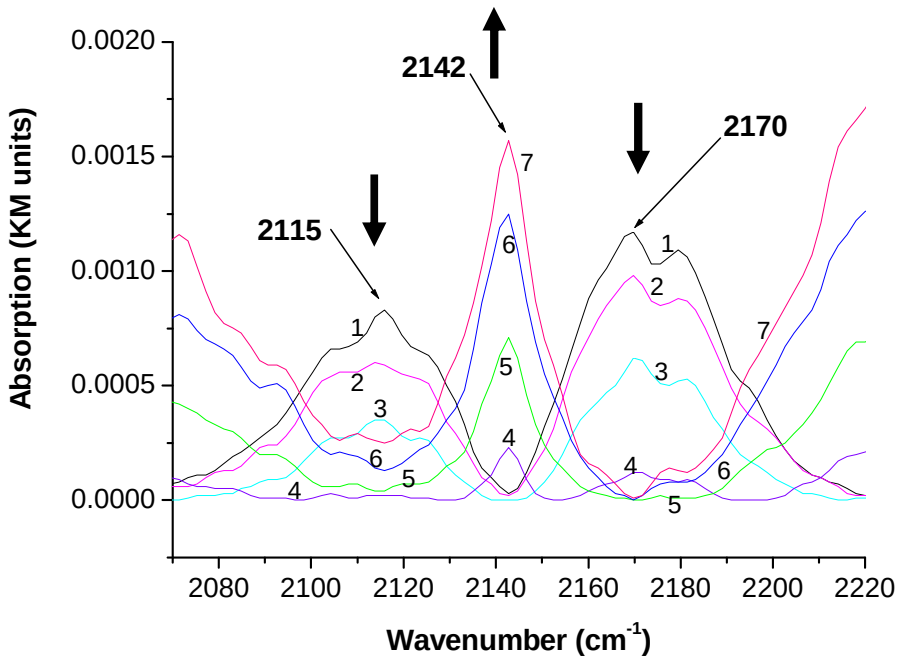

Figure 5.13: Drifts spectra of Au/HY (3.73wt%Au) treated with $NaBH_4$ (1:1) showing the changes on surface adsorbed CO as a function of temperature increase, from (1) 22, (2) 120, (3) 200, (4) 250, (5) 300, (6) 350, and (7) 400 ^{0}C respectively.

In this study the band at ca. 2142 cm^{-1} can further be associated with the oxidation of CO, since the activity was observed only at a temperature above 250 ^0C and increased with an increase in temperature (see figure 5.14). During the CO oxidation reaction at 450 ^0C, the intensity of the band at 2142 cm^{-1} remains the same for 8 hours. This clearly suggests that the electron-deficient species ($Au^{\sigma+}$-CO species) stabilised by protons are responsible for the observed CO conversion.

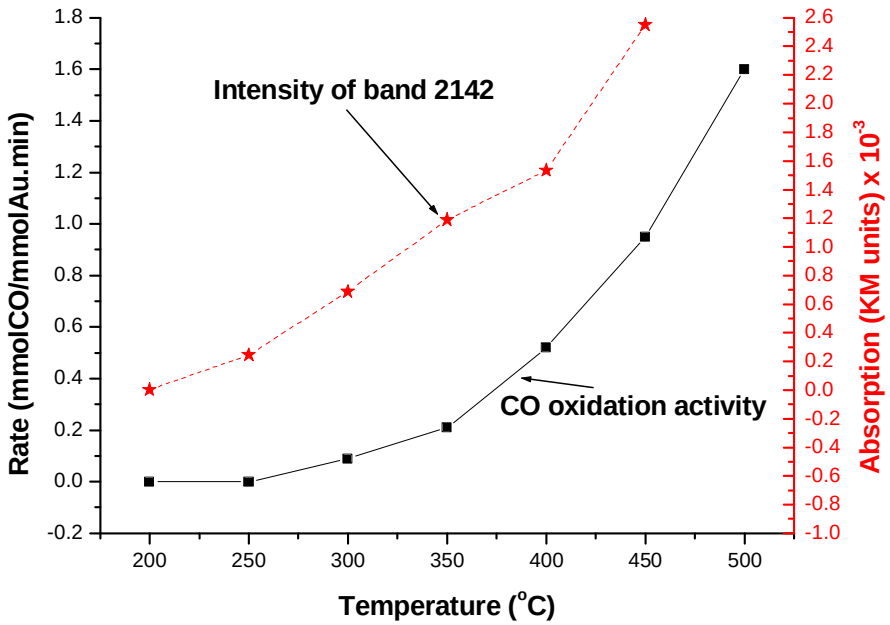

Figure 5.14: CO oxidation activity of $NaBH_4$ treated Au/HY (3.73wt%Au) as a function of temperature increase, during an in-situ DRIFTS studies.

5.3.8 Catalytic activity of Au/Y system

All catalysts samples were pre-treated at 400 ^{0}C for 2 hours under 10% O_2 in He (14 ml/min) after which the temperature was immediately raised to 450 ^{0}C. CO oxidation (mixture of 10%CO/He and 10%O_2/He, 42 ml/min) was then recorded as a function of time on stream or temperature.

5.3.8.1 Activity of ascorbic acid-treated Au/Y systems

Herein we report on the reductive pre-treatment of Au/Y (1.45wt%Au) using ascorbic acid as the reducing agent. The reduction step was undertaken to reduce Au^{3+} to lower oxidation states, such as Au^0, as claimed by Guczi *et al*. [17, 18, 19], Au^{n+} as claimed by Ichikawa *et al*. [20-26], or both Au^{n+} and Au^0 as claimed by Hutchings et al. [27-30]. These are variously thought to be the active species responsible for activity of the supported gold catalysts. It was noted that when gold is supported on Y, using $[Au(en)_2]^{3+}$/Y (1.45wt%Au), [3] and that of Boudart et al. [4], no/or less activity for CO oxidation was observed, due to thermal instability of gold within the zeolite lattice.

The ascorbic acid treated Au/Y (1.45wt%Au) sample (purple) was pre-treated at 400 ^{0}C in 10% O_2/He for 2 hours (after which it had turned a reddish-brown or mauve colour). Activity was monitored as a function of temperature, from 50 ^{0}C to 500 ^{0}C, and the ascorbic acid treated sample showed no activity for CO oxidation. Such behaviour has been attributed to the presence of a low gold

content in the sample. Most of the gold had been washed off the zeolite during filtration as detected by Ultraviolet-Visible spectroscopy. The XRD profile of the sample has shown the presence of much bigger particles which are thought to be on the outer surface of the Y zeolite and these suggests that the nature of the reducing agent plays a significant role in the formation of stable and active gold species.

5.3.8.2 Activity of $NaBH_4$ treated Au/Y system

When, Au/Y (3.46wt%Au) was treated with $NaBH_4$ and pre-treated under the same conditions, the catalyst was found to be active for CO oxidation (figure 5.15). The maximum activity displayed was more or less the same as that shown by Au supported on HY zeolites (treated under the same conditions with the same reducing agent, figure 5.18). However, the observed induction period was slightly longer (~7 h) for Au/Y (3.46wt%Au), compared to that of Au/HY (3.77wt%Au) which was approximately 2.5 h (see section 5.3.8.2.1, figure 5.18). These suggested that Au reduction in HY was fast; whilst in the case of the Y zeolites it took a longer time to reduce the same amount of gold to the lower oxidation state(s). These results also suggest that an important role is played by the proton in stabilizing the gold nanoparticles inside the cavities of the zeolite system.

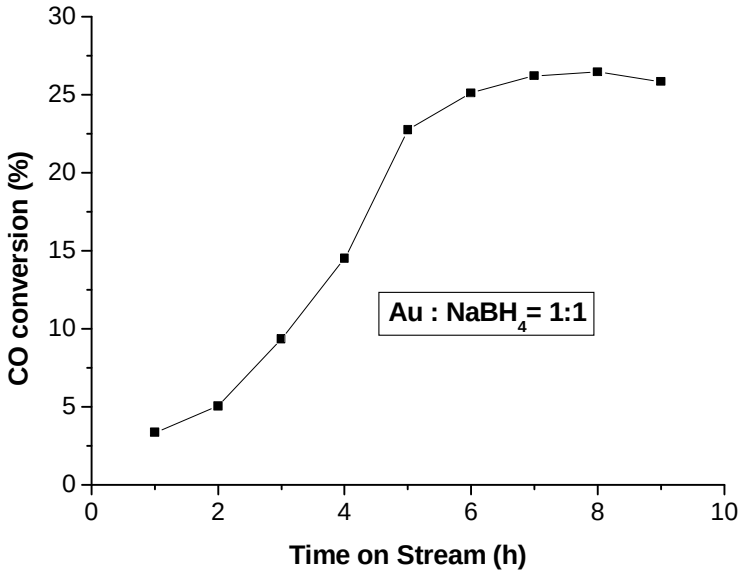

Figure 5.15: Plot of % CO conversion against time on stream showing the activity of $NaBH_4$ treated Au on Y zeolites

5.3.9 Catalytic activity of the Au/HY system

Smaller gold clusters are formed inside the supercages of the zeolite framework during thermal treatment due to the reduction of the gold cations by the contained ligands, (en = H_2N-CH_2-CH_2-NH_2). The use of acidic zeolites favours the dispersion of the metal and the thermal stability of the gold particles. This stability is explained by chemical anchoring of metal clusters by the Bronsted sites of the support [31].

When gold is supported on the acid modified HY zeolite, the gold particles exist in three different forms: electron-deficient particles ($Au_n^{\sigma+}$), neutral crystallites

and oxidized gold species (probably Au^{+}) [12]. The gold located inside the zeolite lattice seems to be electron-deficient, since 80% of the counter-ions are protons [12]. Results discussed in the next sections describe in detail the behaviour of Au supported on acidity modified Y-zeolite, treated with different reducing agents.

5.3.9.1 Activity of ascorbic acid-treated Au/HY system

5.3.9.1.1 Activity of ascorbic acid-treated Au/HY system, in the absence of protecting agents.

When ascorbic acid was added dropwise to a colourless solid sample solution of Au/HY (2.72wt%Au, molar ratio of ascorbic acid to that of Au = 1:1) the solution's colour changes to dark purple. The colour change was indicative of the reduction of the metal ion to lower oxidation states. Figure 5.16 shows the time on stream CO oxidation activity for the ascorbic acid-treated Au/HY catalyst at 450 ^{0}C. The catalyst showed lower CO activity with 6% steady-state CO conversion, compared with the untreated Au/HY catalyst, which had a steady-state CO conversion of 17%. The decrease in the activity of the ascorbic acid-treated Au/HY (2.72wt.%Au) catalyst has been caused by the loss of gold during the washing steps, as detected by UV-Vis spectroscopy (analysis of filtrates for the presence of gold). The XRD profile confirmed the presence of bigger gold particles, of which most were on the outer surface of zeolite-HY and in the metallic form.

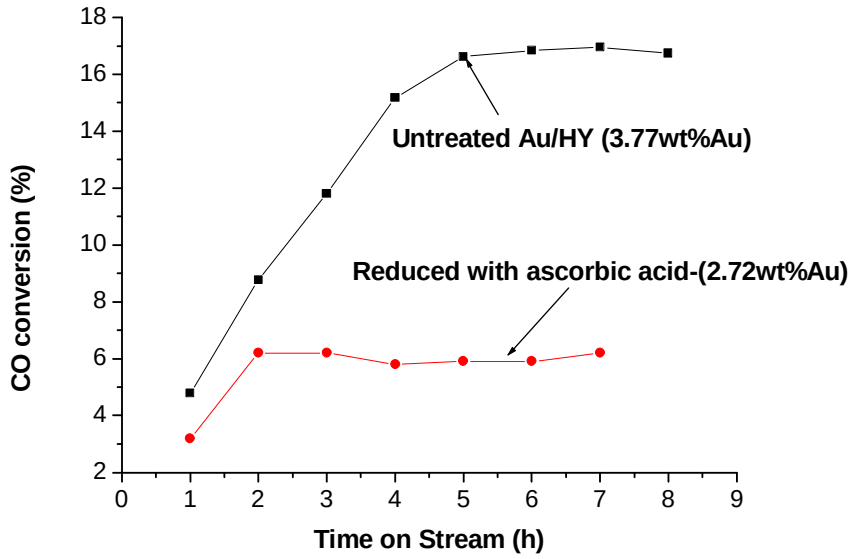

Figure 5.16: Comparison of CO oxidation activity of the ascorbic acid treated Au/HY with that of the untreated Au/HY (3.77wt%Au).

Interestingly, time on stream CO oxidation studies of the ascorbic acid-treated Au/HY catalyst recorded a shorter induction period (~2 h) as compared to that of the untreated Au catalyst (~6 h). These data show that the reducing agent did alter the induction period of the Au catalyst, even though the activity has decreased compared with that of the untreated Au/HY catalyst. The results suggest that the slow activation of gold from Au^{3+} to Au^{1+}/Au^{0} manifests itself as the pronounced induction period observed on the untreated Au catalyst.

5.3.9.1.2 Activity of ascorbic acid-treated Au/HY system, in the presence of protecting agents.

In an attempt to vary the size of gold particles, the studies were repeated by changing the molar ratio of gold to that of ascorbic acid and by introducing the protecting agent (polyethylene glycol, PEG) [32, 33]. Figure 5.17 shows the time on stream CO oxidation activity for the ascorbic acid-treated Au/HY (molar ratio = 1:1), protected Au catalyst (1:1:1) and protected Au catalyst (1:2:4) at 450 ^{0}C. The capped Au catalyst (1:1:1) showed a high initial activity with 9% CO conversion, compared with the ascorbic acid-treated Au/HY (molar ratio = 1:1, no capping agent) which had a steady-state CO conversion of 6%.

However the time on stream study indicated that the Au catalyst was not stable and continuously deactivated with time. Over a period of seven hours the CO conversion decreased from 9.0 to ~ 8.0%. Interestingly, time on stream CO oxidation studies of the capped Au catalyst (1:1:1) had no induction period as compared to that of the ascorbic acid-treated Au/HY sample (molar ratio = 1:1, no protecting agent). This clearly suggests that the protecting agent has altered the dispersion state of Au catalyst and hence the induction period. An increase in molar ratio of reducing agent and that of protecting agent does not show a significant change in activity to that of protected Au catalyst (1:1:1). However, a slight increase in induction period by three hours is observed (see, protected Au catalyst (1:2:4)).

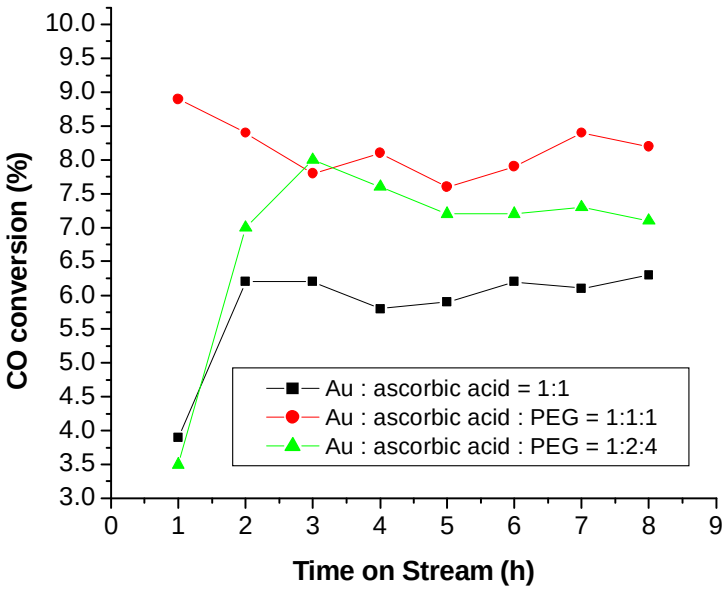

Figure 5.17: Comparison of the CO oxidation activity for the ascorbic acid-treated Au catalysts in the presence of protecting agents.

5.3.9.2 Activity of sodium borohydride-treated Au/HY system

5.3.9.2.1 The effects of washing the Au/HY (3.73wt%Au) catalyst after reduction

Figure 5.18 shows the time on stream CO oxidation activity for the $NaBH_4$-treated Au/HY (3.73wt%Au) catalyst at 450 ^{0}C. The catalyst showed a lower initial activity with 14% CO conversion. However the time on stream study indicated that the Au catalyst had an induction period of 2 h before reaching a steady-state CO conversion of ~27%. Interestingly, the induction period of the $NaBH_4$-treated Au catalyst was shortened by half to that of untreated Au/HY (3.77wt%Au) catalyst. The $NaBH_4$-treated Au catalyst also showed higher catalytic activity, which is as a result of a strong reducing ability of sodium borohydride. An XRD profile of the $NaBH_4$-treated Au catalyst has confirmed the presence of smaller gold particles on the surface of the HY zeolite and the ultraviolet-visible spectroscopy of the solid sample solution immediately after ion-exchange has confirmed the presence of gold nanoparticles (Au^+/Au^0 clusters). The results suggest that the Au particles on $NaBH_4$-treated Au catalyst are well dispersed on the support leading to an increase in CO conversion.

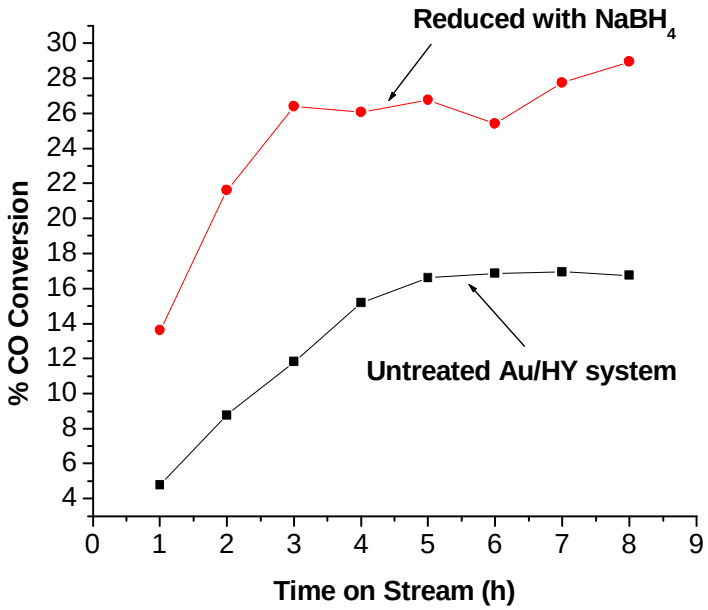

Figure 5.18: Comparison of the CO oxidation activity for the $NaBH_4$ treated Au/HY (3.73wt%Au, molar ratio = 1:1) and the untreated Au/HY (3.77wt%Au) catalysts.

5.3.9.2.2 The effects of washing the Au/HY catalyst before reduction

A powdered sample of freshly prepared Au/HY (3.77wt%Au) has been washed with distilled water, immediately after ion-exchange and then treated with $NaBH_4$ as described in chapter 3. Figure 5.19 shows the time on stream CO oxidation activity at 450 ^{0}C, for the washed Au/HY (3.77wt%Au) catalyst followed by reduction. The catalyst showed a high initial activity with ~ 44% CO conversion, which is thought to be a result from the presence of a smaller amount of chlorine ions (due to their tendency to act as a poison of catalytically active sites). However, the time on stream study indicated that the Au catalyst was not stable

and continuously deactivated with time. Over a period of eight hours the CO conversion decreased from 44 to 24%. The deactivation may be attributed to irreversible reduction of Au^{+} to zero-valent Au particles, Au^{0} which tend to sinter with time as reported by Minico et al. [22].

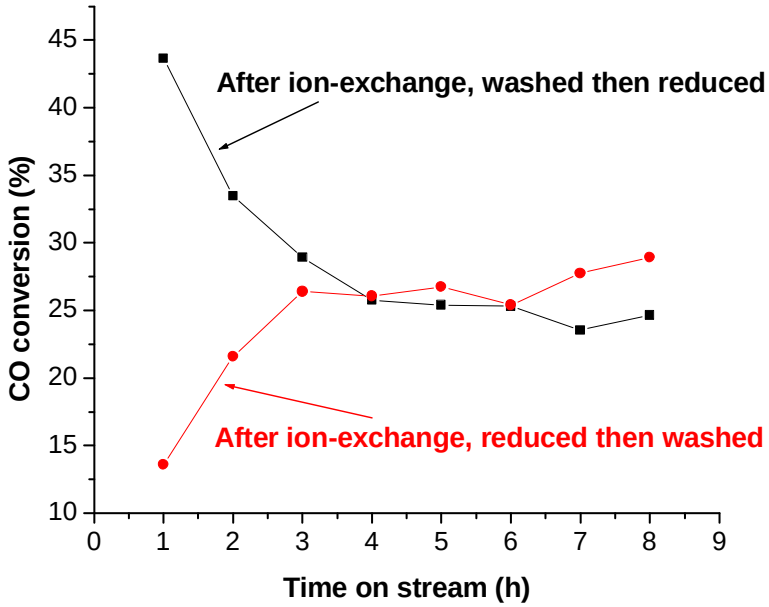

Figure 5.19: Time on stream CO oxidation activity for the $NaBH_4$-treated Au/HY (3.77wt%Au) catalyst at 450 ^{0}C, showing the effect of washing before reduction.

Interestingly, the Au catalyst that has been washed after ion-exchange, followed by reduction, showed no induction period and had a quite significantly higher activity. An increase in activity and complete removal of the induction period is an indication that the washing of Au/HY catalyst, prior to reduction was to basically remove chlorides. This suggests that in the absence of Cl^{-} ions, the reduced Au particles easily interact with the zeolite lattice and also the reduction of gold is enhanced.

5.3.9.2.3 The effect of $NaBH_4$ mole ratio, on the activity of Au/HY

Figure 5.20 shows the time on stream CO oxidation activity for the $NaBH_4$-treated Au/HY (3.73wt%Au, mole ratio = 1:1) catalyst at 450 ^{0}C. The catalyst showed an initial activity with 14% CO conversion. However the time on stream study indicated that the Au catalyst had an induction period of 2 h before reaching a steady-state CO conversion of ~27%. The presence of the induction period of two hours, suggests that not all Au particles has been completely reduced to the lower oxidation state. This result has been confirmed by the TPR profile of the $NaBH_4$-treated Au catalyst (mole ratio = 1:1) which shows the consumption of H_2 with peak maxima at 143 ^{0}C. Interestingly, an increase in molar concentration of $NaBH_4$ to that of Au, completely removed the induction period of the $NaBH_4$-treated Au catalyst (mole ratio = 1:3) and a high initial activity of 40% CO conversion was obtained. No reduction peak signal observed on the TPR profile of the $NaBH_4$-treated Au catalyst (mole ratio = 1:3), suggesting that all ionic Au has been reduced to zero-valent gold, Au^0. It is noteworthy, that a further increase in $NaBH_4$ molar concentration for the $NaBH_4$-treated Au catalyst (mole ratio = 1:4) gave an even higher CO activity with a steady-state conversion of 60%. Again the TPR profile did not show any uptake of H_2, confirming that a complete reduction of Au had taken place.

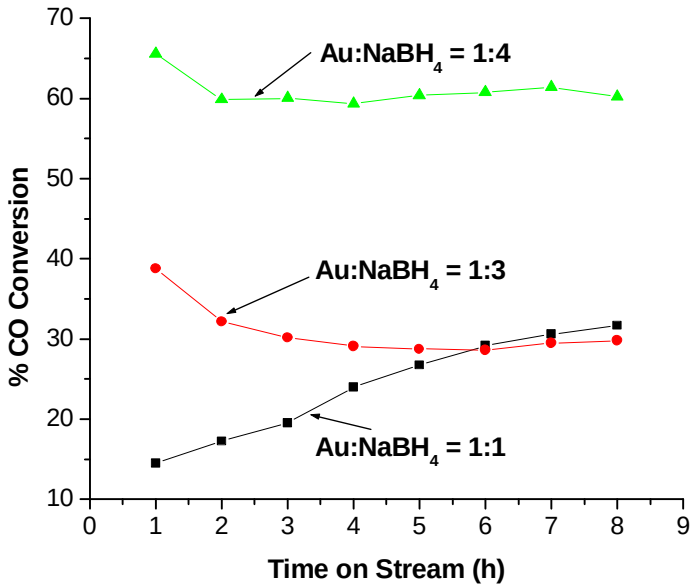

Figure 5.20: Time on stream CO oxidation for the $NaBH_4$-treated Au catalysts, prepared at various Au/$NaBH_4$ mole ratios: (Au:$NaBH_4$ = 1:1), (Au:$NaBH_4$ = 1:3) and (Au:$NaBH_4$ = 1:4).

Since the TPR profiles of both samples (mole ratios Au:$NaBH_4$ = 1:3; and Au:$NaBH_4$ = 1:4) confirmed a complete reduction of gold, an increase in CO activity of $NaBH_4$-treated Au catalyst (1:4) may be attributed to a high dispersion of Au nanoparticles formed on the surface of the zeolite lattice. Use of a mole ratio of (Au:$NaBH_4$ = 1:4) more readily forms neutral gold atoms than does (Au:$NaBH_4$ = 1:3) and this faster reduction leads to smaller nanoparticles for (Au:$NaBH_4$ = 1:4). This clearly suggests that the lower oxidation states, Au^{+}/Au^{0}, are the underlying factor responsible for an increase in activity and the Au catalyst needs to be in a highly dispersed form to be active for CO oxidation.

5.3.9.2.4 Activity of $NaBH_4$-treated Au/HY system; effect of reduction temperature.

Figure 5.21 shows the time on stream CO oxidation activity at 450 ^{0}C, for the $NaBH_4$-treated Au/HY (molar ratio = 1:1, reduced at room temperature), and $NaBH_4$-treated Au/HY (molar ratio = 1:1, reduced at 60 ^{0}C). The $NaBH_4$-treated Au/HY (molar ratio = 1:1, reduced at 60 ^{0}C) showed lower activity with an average of 6% CO conversion, compared with the $NaBH_4$-treated Au/HY (molar ratio = 1:1) which had a steady-state CO conversion of ~ 27%. The results suggest that an increase in reduction temperature is detrimental to the reductive pre-treatment of the Au catalyst with $NaBH_4$.

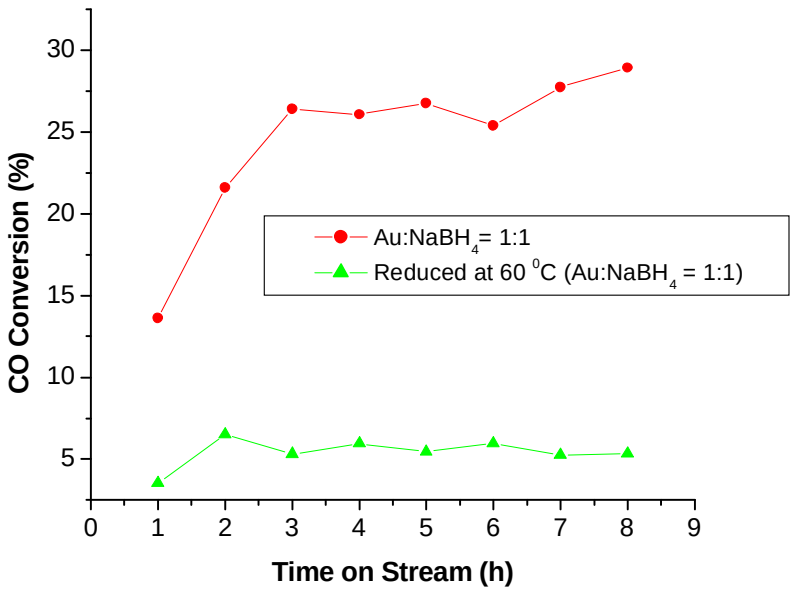

Figure 5.21: Comparison of the CO oxidation activity for the $NaBH_4$-treated Au catalysts in the presence of protecting agents.

5.3.9.3 Activity of trisodium citrate treated Au/HY catalyst

When a solution of tri-sodium citrate, was added drop-wise to a suspended solid sample solution of Au/HY (3.66wt%Au, mole ratio =1:1), the colour of the solid sample solution remain the same. Figure 5.22 shows the CO activity for the tri-sodium citrate treated Au/HY (molar ratio = 1:1, reduced at room temperature), trisodium citrate-treated Au/HY (molar ratio = 1:1, reduced at 60 ^{0}C) and untreated Au/HY catalyst. The trisodium citrate-treated Au/HY (molar ratio = 1:1, reduced at room temperature) showed activity with < 5% CO conversion. However, the trisodium citrate-treated Au/HY (molar ratio = 1:1, reduced at 60 ^{0}C) showed a slightly higher activity to that of Au/HY (molar ratio = 1:1, reduced at room temperature) with an initial steady state CO conversion of 9%. This suggests that the reduction of Au on HY zeolite by trisodium citrate needs to be activated by high temperature.

Interestingly, no induction period was observed on both trisodium citrate-treated Au catalysts, (at room temperature and 60 ^{0}C) as compared to the untreated Au/HY catalyst. Both trisodium citrate-treated Au/HY catalysts showed lower CO conversion as compared to the untreated Au/HY catalyst. Lower activity of Au catalyst treated with trisodium citrate is attributed to its poor ability to reduce gold. The TPR profile of the trisodium citrate treated Au catalyst showed the H_2 consumption signal with peak maxima at 130 ^{0}C, suggesting an incomplete reduction of Au.

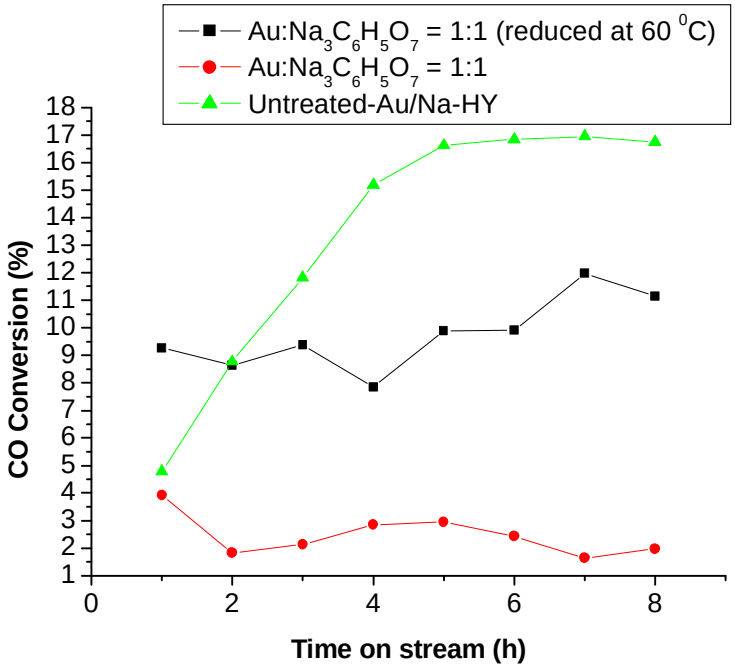

Figure 5.22: Comparison of the CO oxidation activity for the trisodium citrate treated Au/HY (3.66wt%Au, molar ratio = 1:1), untreated Au/HY (3.77wt%Au) and the effect of reduction temperature.

5.3.9.4 Effect of reductive pre-treatment of Au prior to ion-exchange on HY, on CO oxidation activity

When a solution of the gold complex, $Au(en)_2Cl_3$, was reduced with $NaBH_4$ before being ion-exchanged onto HY zeolite, purple colloids of gold were formed and after ion-exchange on HY, yellowish gold particles were seen on the zeolite surface. When the catalyst was tested for CO oxidation, no CO conversion was observed, due to the large particles of gold that formed on the outer surface of the zeolite and which were catalytically inactive. Goodman et al. [34] reported that the activity of the Au particles is sensitive to their size and that only particles in

the range of 2 to 3 nm are active for CO oxidation (see figure 2.8, chapter 2). This result suggests that the interaction between the support and the metal atoms is of importance in determining CO oxidation catalytic activity.

5.3.10 Comparative studies of the reductive pre-treatment of Au supported catalysts prepared from $KAu(CN)_2$, $Au(en)_2Cl_3$ and $HAuCl_4$.

Figure 5.23 shows the time on stream CO oxidation activity for the $NaBH_4$-treated Au/HY (3.65wt%Au, $KAu(CN)_2$ as source of gold; mole ratio = 1:1) catalyst at 450 ^{0}C. The catalyst showed a high initial activity with ~ 65% CO conversion and deactivated to lower CO conversion of ~42%. However, Au/HY performed from $Au(en)_2Cl_3$ as source of gold (3.73wt.%Au, mole ratio = 1:1, figure 5.18) catalyst showed a lower initial activity of 14% CO conversion and reached a steady-state CO conversion with ~27%, under the same conditions. Although the stability constant of $KAu(CN)_2$ is higher than that of $HAuCl_4$ (source of $Au(en)_2Cl_3$), the redox potential is quite different for Au^+/Au(E^0 = 1.68 V) and Au^{3+}/Au(E^0 = 1.50 V). The high activity of the Au catalyst prepared from $KAu(CN)_2$, is as a result of the absence of chlorine ions (due to their tendency to act as a poison of catalytically active sites) and that the mono-cation Au^+, more readily forms neutral gold atoms than does Au^{3+}. This faster reduction leads to smaller nanoparticles when $KAu(CN)_2$ is the source of Au. This clearly suggests that, the Au catalysts need to be in a highly dispersed form to be active for CO oxidation.

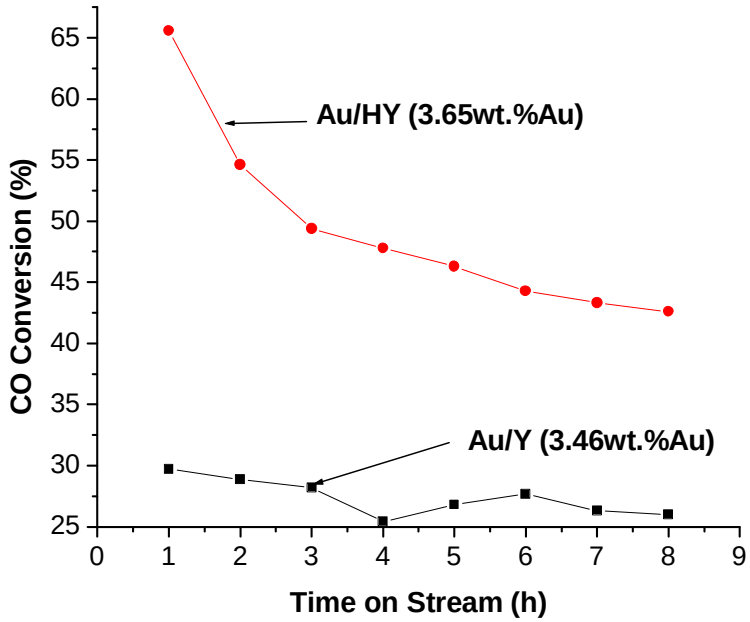

Figure 5.23: Comparison of the CO oxidation activity for the $NaBH_4$ treated Au/HY and Au/Y (Au:$NaBH_4$, molar ratio = 1:1, $KAu(CN)_2$ as source of gold).

On the other hand the presence of a proton on the $NaBH_4$-treated Au/HY (3.65wt%Au, $KAu(CN)_2$ as source of gold, mole ratio = 1:1, figure 5.23) plays an important role in the overall CO oxidation activity, compared to the case in which Au is supported on Y (absence of protons). Smaller gold clusters which are formed after reduction of Au have been found to be stabilized by protons within the zeolite cages [12].

Relatively all gold catalysts prepared in this study had poor CO oxidation activity. The cause is thought to be due to several factors related to the structure of zeolite as a support and metal incorporation within the exchange sites of zeolite cages. Gupta et al. [35] has reported the possible explanation for the synergistic catalytic

activity of Au/Fe_2O_3 for the CO oxidation reaction. They suggested the transfer of chemisorptions energy from the metal particle to the support. Thus lead to localized temperature surge at the metal /support interface, which may act as the sites of higher CO oxidation [35]. Based on the model catalyst studies by Goodman et al. [36], the following factors are important for high CO oxidation activity: (a) bilayered Au structure (appropriate Au morphology); (b) Intimate wetting of the support by the Au cluster (high dispersion); (c) strong bonding between the Au atoms at the interface with surface defects (reduced Ti sites); (d) electron-rich Au. They concluded that high CO oxidation activity exhibited by Au catalysts is related to the Au dispersion; highly dispersed Au catalysts are important for obtaining Au catalysts with high activity [36]. However, extensive model studies have shown that in addition to Au dispersion, [36, 37] other factors, such as (a) Au morphology and (b) Au-defect Ti sites interaction, are crucial for high CO oxidation activity [38]. Most of gold catalysts exchanged on zeolite in this work, were not well dispersed. The lack of interaction between the support and metal catalyst was observed. The presence of second metal such as chromium played a significant role in strengthening the interaction between the metal catalyst and zeolite lattice.

5.4 CONCLUSIONS

Ascorbic acid treated Au on Y, similar to an unreduced Au catalyst, was found to be inactive towards CO oxidation. However, when the Au catalyst was treated with $NaBH_4$, the catalyst became active and the activity increased slowly with almost the same induction period as that of the untreated Au/HY (3.77wt%Au) catalyst. Reduction of Au supported on Y with $NaBH_4$ led to well dispersed Au nanoparticles. This clearly suggests that the Au catalysts need to be in a highly dispersed form to be active for the CO oxidation reaction.

The induction period of Au supported on the HY zeolites is a function of how rapidly Au^{3+} can be reduced to the lower oxidation states. It was found that the choice of a reducing agent plays a significant role in the reduction of gold. The tri-sodium citrate treated catalyst was found to show lower activity and the reduction temperature was also found to have a slight effect on the catalytic activity of the catalyst.

The sodium borohydride treated catalyst, when tested for CO oxidation, had a much shorter induction period that the untreated catalyst (~ 4 h difference). This confirmed that the slow induction period observed in the untreated catalyst is due to the slow reduction of gold from Au^{3+} to the lower oxidation states. It also had a higher catalytic activity (~25%) than the untreated catalyst (~16%). Washing the catalyst prior to reduction was also found to increase the catalytic activity to ~ 43% with no induction period.

The protecting agent, PEG, did not play any significant role in the catalytic activity of the treated catalyst. The induction period seen for all the treated catalysts was found to decrease or disappear completely, depending on the strength of the reducing agent used. In this work, it has been established that the reactivity and concentration of reducing agents, the molar ratio of Au/$NaBH_4$ and the redox potential of Au cations have significant effects on the formation and growth of Au nanoparticles within or on the surface of zeolites.

5.5 REFERENCES

[1] L. N. Lewis, Chem. Rev., **93** (1993) 2693.

[2] Y. Volokitin, J. Sinzig, L. J. De Jong, G. Schmid, M. N. Vargaftik and I. I. Moiseev, Nature, **384** (1996) 621.

[3] T. Magadzu and M. S. Scurrell, Preparation, Characterization and Catalytic activity of gold, $Au(en)_2Cl_3$ supported on NaY and Na-HY, Unpublished results, (2002) 1.

[4] M. Boudart and G. Meitzner, in EXFAS and Near Edge Structure III, ed. K. O. Hodgson, B. Hedman and J. E. Penner-Halm, Springer, Berlin, (1984) 217.

[5] Q. F. Zhou, J. C. Bao, and Z. Xu, J. Mater. Chem., **12** (2002) 384.

[6] J. N. Lin, J. H. Chen, C. Y. Hsiao, Y. M. Kang and B. Z. Wan, *Appl. Cat. B: Env.*, **36** (2002) 19.

[7] T. Viegers, ^{197}Au Mossbauer Spectroscopy Hyperfine Interactions and Dynamical Behavior of Gold in Molecular Crystals and Small Particles, PhD Thesis, Nijmegen-Netherlands, 1976.

[8] T. Magadzu, G. R. Hearne, and M. S. Scurrell, Report on ^{197}Au Mössbauer Spectroscopy of Au-Zeolite Catalysts, unpublished work.

[9] T. Magadzu and M. S. Scurrell, Characterization of Gold-Zeolites samples by X-ray Photoelectron Spectroscopy, Unpublished results, (2004) 1.

[10] C. D. Wagner, W. M. Riggs, L. E. Davis, J. M. Moulder, G. E. Muilenberg, Handbook of X-ray Photoelectron Spectroscopy, Perikin-Elmer, Eden Prairie, 1979.

[11] C. N. R. Rao, V. Vijayakrishnan, H. N. Aiyer, G. U. Kulkarni, G. N. Subbanna, J. Phys. Chem. **97** (1993) 11157.

[12] D. Guillemot, V. Yu. Borovkov, V. B. Kazansky, M. Polisset-Thfoin and J. Fraissard, J. Chem. Soc., Faraday Trans., **93** (1997) 3587.

[13] T. M. Salama, R. Ohnishi and M. Ichikawa, J. Chem. Soc., Faraday Trans., 2 (1996) 301.

[14] A. Zecchina and C. Otero Arean, Chem. Soc. Rev., **25** (1996) 187.

[15] D. J. C. Yates, J. Colloid Interface Sci., **29** (1969) 194.

[16] J. Y. Lee and J. Schwank, J. Catal., **102** (1986) 207.

[17] A. Zwijnenburg, A. Goossens, M. W. J. Craje, A. M. Van der Kraan, M. Makke, J. A. Moulijn and L. J. De Jongh, Catalysis Today, **72** (2002) 95.

[18] M. A. Vanice and M. Bollinger, Appl. Catalysis B: Environmetal, **8** (1996) 417.

[19] L. Guczi, D. Horvath, Z. Paszti and G. Peto, Catalysis Today, **72** (2002) 101.

[20] K. Kishi and S. Ikeda, J. Phys. Chem, **78** (1974) 107.

[21] M. Ichikawa, R. Ohnishi and S.Qiu, J. Phys. Chem. **98** (1994) 2719.

[22] S. Galvagno, A. M. Visco, C. Crisafulli, S. Scire and S. Minico, Catalysis Letters, **47** (1997) 273.

[23] B.-Z. Wan and Y. –M. Kang, Catalysis Today, **26** (1995) 59.

[24] R. L. Augustine and S. K. Tanielyan, Applied Catalysis A: General, **85** (1992) 73.

[25] M. S Helge and P. Bera, Catalysis Letters, **79** (2002) 75.

[26] S. Hayashi, S. Deki and K. Sayo, J. Materials Chemistry, **9** (1999) 937.

[27] D. T. Thompson and G. C. Bond, Bulletin, **33** (2000) 41.

[28] N. Bogdanchikova, J. L. Margitfalvi, A. Fasi, M. Hegedus, F. Lonyi and S. Gobolos, Catalysis Today, **72** (2002) 157.

[29] G. J. Hutchings, N. A. Hodge, C. J. Kiely, R. Whyman, M. R. H. Siddiqui, Q. A. Pankhurst, F. E. Wagner, R. R. Rajaram and S. Golunski, Catalysis Today, **72** (2002) 133.

[30] S. Galvagno, C. Milone, A. Donato, G. Neri, F. Neri and A. M. Visco, Phys. Chem., **1** (1999) 2869.

[31] G. Riahi, D. Guillemot, M. Polisset-Thfoin, A. A. Khodadedi and J. Fraissard, Catalysis Today, **72** (2002) 115.

[32] A. S. Korchev, M. J. Bozack, B. L. Slaten, G. J. Mills, Am. Chem. Soc., **126** (2004) 10.

[33] T. Hirose, T. Omatsu, M. Sugiyama, S. Inasawa, S. Koda, Chem. Phys. Lett., **390** (2004) 166.

[34] M. Valden, X. Lai, and D. W. Goodman, Science **281** (1998) 1647.

[35] N. M. Gupta, and A. K. Tripathi, Gold Bulletin **34** (2001) 120.

[36] T.V. Choudhary, D.W. Goodman., Applied Catalysis A: General **291** (2005) 32.

[37] M. Valden, S. Pak, X. Lai, and D. W. Goodman, Catal. Lett., **56** (1998) 7.

[38] M. Valden, X. Lai, D.W. Goodman, Science **281** (1998) 1647.

CHAPTER 6

The effect of alkali metal addition on the surface's properties of Y-zeolite and activity of supported gold

6.1 INTRODUCTION

The preparation and partial characterization of alkali-modified Y-zeolites for use as base catalysts are presented in this chapter. From this work, it is shown that upon impregnation to incipient wetness of $KAu(CN)_2$, anionic exchange of $HAuCl_4$ and ion-exchange of $Au(en)_2Cl_3$ on alkali-modified Y-zeolite with identical loadings of gold, the activity of sodium modified Au catalyst [Au/NaY (0.277wt%Au, treated with $NaNO_3$)] is an order greater than that observed on unmodified Au/Y (0.277wt%Au).

The structural effects of sodium or other alkali metals on the chemical composition and the catalytic activity of a system based on supported gold have been discussed. The activity of the catalysts was found to depend on the nature of the gold source and on the type of alkali metal nitrate used. It was found that when chloroauric acid was used as a source of gold, on Na-modified/exchanged zeolite-Y, the catalyst activity increased tremendously (approximately 60% CO conversion). However, when K-modified/exchanged zeolite-Y was used for CO oxidation, the catalytic activity was found to be less than that of Na-

modified/exchanged zeolite-Y, a result which does not follow the periodic table trend as expected. It has been established that the addition of sodium to supported gold or to other transition metals produces an electron transfer to the metal. As a consequence of the increased electron density, the metal is available for the back-bonding to the 2p* orbitals of CO and diatomic adsorbed molecules, enhancing their dissociation capacity. Therefore, the effect of sodium promotion is to improve the activity of gold based catalysts.

This work aims at securing a better understanding of the role of alkali metals on Au supported on Y-zeolite and their catalytic behaviour for CO oxidation, once gold is introduced into the surface-modified zeolite-Y.

6.2 EXPERIMENTAL

6.2.1 Support and catalyst preparation

Modification of Y-zeolite was undertaken, using sodium nitrate, lithium nitrate and potassium nitrate solutions at 1 M concentration. During the modification of Y-zeolite the pH of the solution was lowered to 6, following the method used by Wan *et al*. [1], and the pH of the gold solution was also adjusted to pH 6.8. After adjusting the pH of the gold solution, the solution was added dropwise into a suspended alkali-modified zeolite-Y. Gold was loaded onto the modified and unmodified Y-zeolite by ion exchange of an $Au(en)_2Cl_3$ solution, anionic exchange of $HAuCl_4$ and by impregnation to incipient-wetness of $KAu(CN)_2$ as

described in chapter 3. The prepared modified zeolite samples are referred to as Au/NaY, Au/LiY and Au/KY, the name depended on the source of nitrate solution used. The unmodified zeolite sample is referred to as Au/Y (intended gold loading = 2wt%Au).

6.2.2 Catalyst testing

The catalysts were evaluated for oxidation of carbon monoxide using 10% O_2/He and 10% CO/He at 150 ^{0}C (catalysts prepared by anionic exchange of $HAuCl_4$), and at 250 ^{0}C (for catalysts prepared by ion exchange of $Au(en)_2Cl_3$ solution, and those prepared by impregnation to incipient-wetness using $KAu(CN)_2$).

6.2.3 Characterization Techniques

The results of the characterization by X-ray diffraction (XRD) are presented.

6.3 RESULTS AND DISCUSSION

6.3.1. X-ray powder diffraction (XRD)

6.3.1.1 Gold source, $Au(en)_2Cl_3$

The XRD results show metallic gold particles formed after exposing the catalyst at 250 ^{0}C (figure 6.1). The average gold crystallite size is in the range of 8-13 nm.

The estimated gold particle sizes of Au/Y and Au/LiY are 8 and 9 nm respectively and slightly larger for Au/NaY and Au/KY, with 11.4 nm and 13.2 nm respectively. This suggests that the modification of Y-zeolite did not improve the stability of smaller gold clusters on the zeolite, but rather it led to the formation of even much bigger particles. These results are in agreement with the activity studies performed of these catalysts, which show that all the alkali metals used had no influence on the catalytic activity of gold (i.e. no improvement was observed).

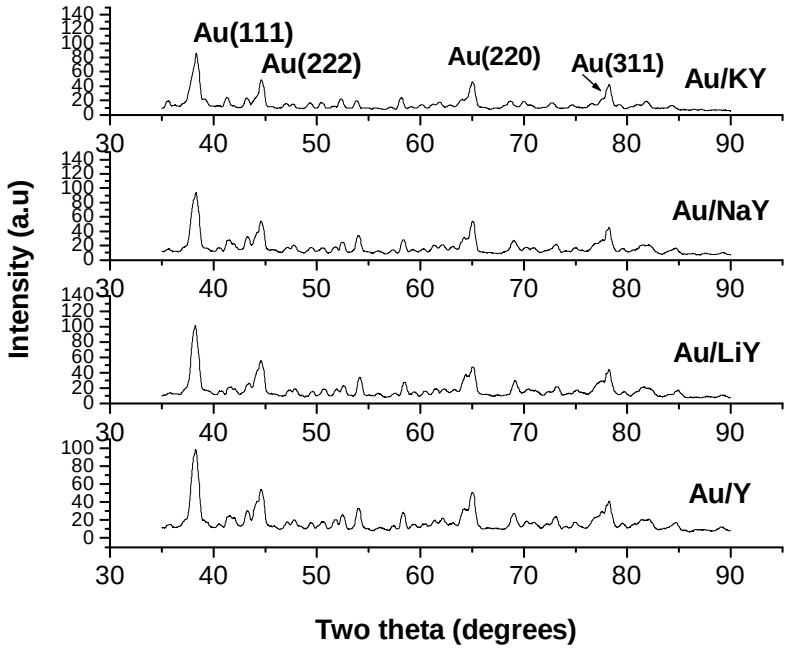

Figure 6.1: XRD profile of Au on Y and modified Y-zeolite (2wt%Au), showing the effect of different alkali metals on the size of metallic gold particles.

6.3.1.2 Gold source, $KAu(CN)_2$

The XRD results shown in figure 6.2, reveals that metallic gold particles formed after exposing the catalyst at 250 ^{0}C. Comparison of the unmodified Y-zeolite, to the catalysts modified with $NaNO_3$ or $LiNO_3$ in the presence of cyanide, indicates that these three catalysts have an average crystallite size of 13.2 nm. These results suggest that again the alkali metals did not show any influence on the stability of gold particles. No improvement on the catalytic activity was observed, which is in agreement with these results (figure 6.4). However, the XRD results of potassium-modified zeolite-Y shows the Au(111) signal to be less intense when compared to the other three samples. These results suggest that gold particles are more stable on this catalyst and the activity of this sample has improved relative to the other sample (figure 6.4). These suggest that the concentration of the modifier does play a significant role in promoting the activity of gold, which agrees well with our findings since the source of gold used contains a significant amount of potassium.

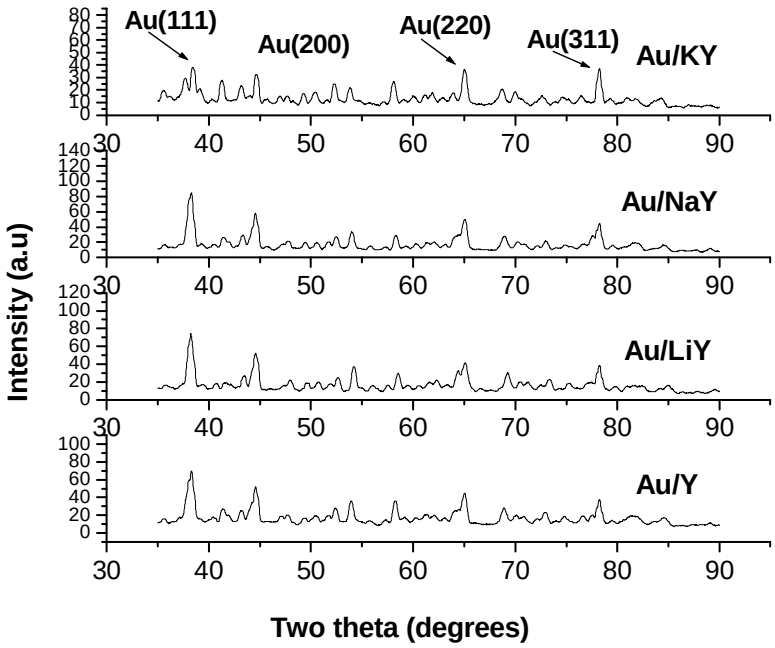

Figure 6.2: XRD profile of Au on Y and modified Y-zeolite (2wt%Au), showing the effect of different alkali metals on the size of metallic gold particles.

6.3.1.3 Gold source, $HAuCl_4$

The XRD results shown in figure 6.3, reveals the size of metallic gold particles formed after exposing the catalyst at 150 ^{0}C. The XRD peak signals at Au(111) shows the presence of metallic gold particles. However the peak width of the Au/NaY (0.772wt%Au) sample suggests the presence of smaller gold particle compared to Au/Y (0.277wt%Au) and Au/LiY (0.212wt%Au). These results are in agreement with the observed higher or improved activity on Au/NaY (0.772wt%Au) sample (figure 6.6) and related to that observed by Hutchings et al. [2]. Although the XRD peak signal, Au(111) of Au/KY (0.454wt%Au) is negligible, suggesting the presence of smaller gold clusters, surprisingly the

activity studies shows less activity when compared to that of Au/NaY (0.772wt%Au).

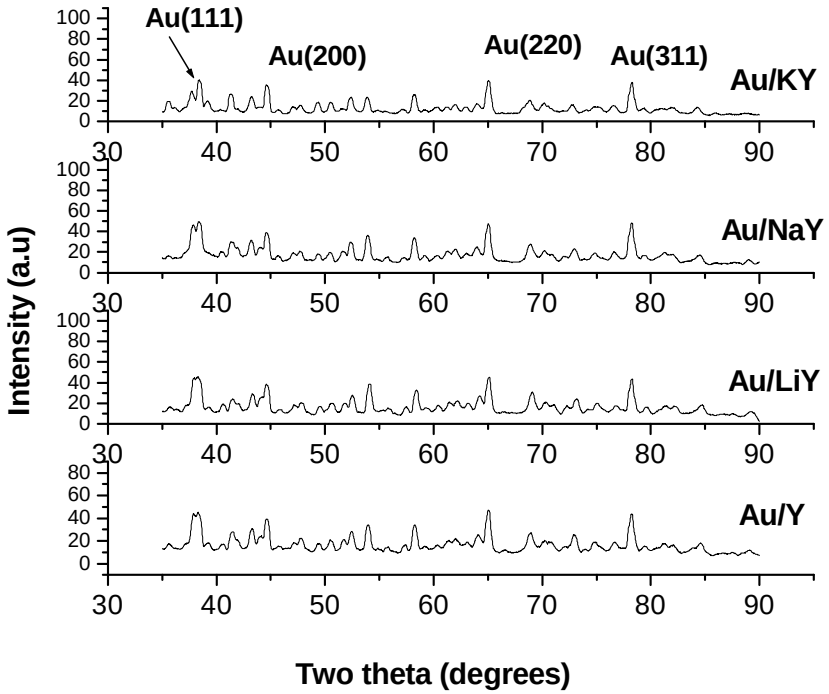

Figure 6.3: XRD profile of Au on Y and modified Y-zeolite, showing the effect of different alkali metals on the size of metallic gold particles.

6.3.2 Activity of gold on alkali-modified zeolite-Y

6.3.2.1 Effect of Li, Na, and K on activity of gold supported on zeolite-Y (Gold source, $Au(en)_2Cl_3$)

The catalysts were pre-treated at 400 ^{0}C for 2 h under 10% O_2/He atmosphere and then CO oxidation was undertaken at 250 ^{0}C as a function of time on stream. The results in figure 6.4 show an activity of less than 5% for both alkali-modified

zeolite-Y and unmodified Y-zeolite. These results suggest that alkali metals have no influence on the activity of gold obtained from $Au(en)_2Cl_3$, which is in agreement with the XRD results. The XRD results have shown that the instability of gold has either deteriorated or remain unchanged.

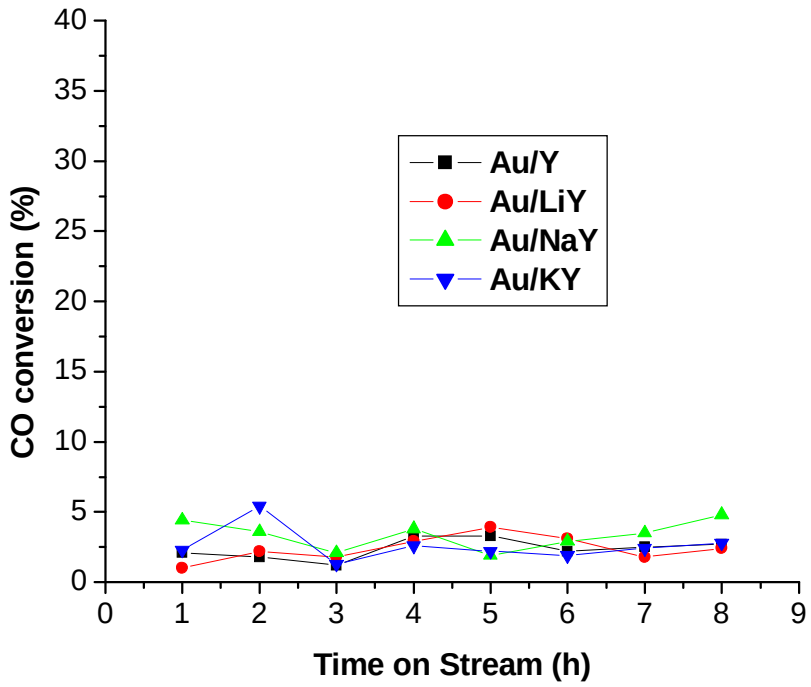

Figure 6.4: Plot of % CO conversion against time on stream showing the effect of alkali-modified zeolites-Y on the catalytic activity of the gold catalyst.

6.3.2.2 Effect of Li, Na, and K on activity of gold supported on zeolite-Y (Gold source, $KAu(CN)_2$)

The catalysts were pre-treated at 400 ^{0}C for 2 h under 10% O_2/He atmosphere and then CO oxidation was undertaken at 250 ^{0}C as a function of time on stream. The results in figure 6.5 show that the activity of Au/LiY (2wt%Au), and Au/NaY

(2wt%Au) has not improved and on average it has remained the same as that of unmodified Au/Y (2wt%Au) at roughly 5% conversion. However, the Au/KY (2wt%Au) catalyst has shown an improvement in the activity (15%), which agrees with the XRD results (figure 6.2).

The improved activity of the Au/KY (2wt%Au) catalyst seems to have been influenced by concentration of the alkali metal present. These might be so since the $KAu(CN)_2$ already contain potassium and further modification by KNO_3 has just increase the amount of potassium metal within the catalyst.

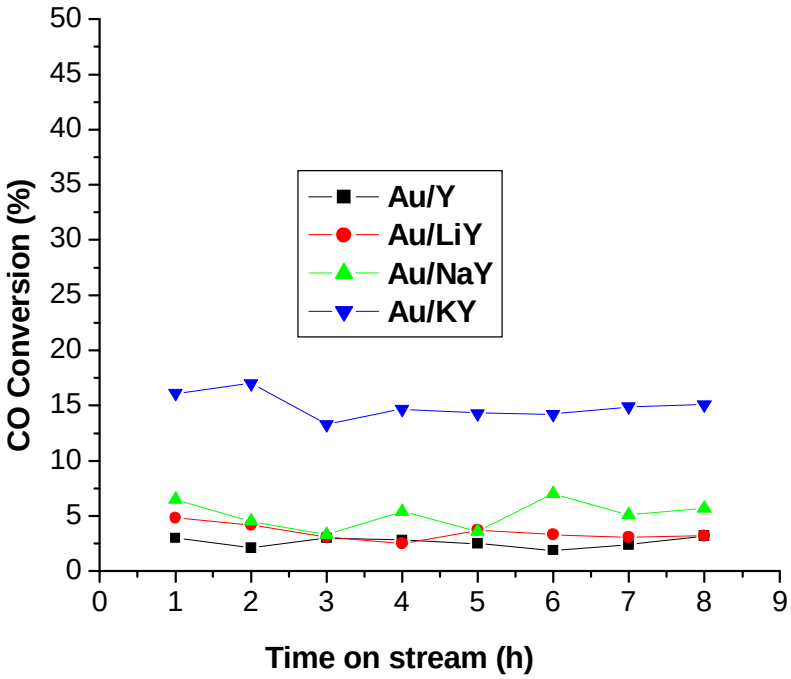

Figure 6.5: Plot of % CO conversion against time on stream showing the effect of alkali-modified zeolites-Y on the catalytic activity of the gold catalyst.

6.3.2.3 Effect of Li, Na, and K on activity of gold on supported zeolite-Y (Gold source, $HAuCl_4$)

The catalysts were pre-treated at 200 ^{0}C for 2 h under 10% O_2/He atmosphere and then CO oxidation was undertaken at 150 ^{0}C as a function of time on stream. The results in figure 6.6 show that the catalytic activity of Au/Y (0.277wt%Au) is less than 5% and it has remained the same on Au/LiY (0.212wt%Au) catalyst. However, the modification of Y-zeolite with sodium nitrate gave higher CO conversion (ca. 60%). Earlier studies by Wan et al. [1], have reported similar results on the promotion of CO oxidation activity by sodium nitrate treatment. They have suggested that the cause of such improvement in activity was due to the change in surface properties of Y-type zeolite, which has resulted in a higher gold loading being observed on sodium nitrate modified Y-zeolite. Our analysis of Au/NaY (0.772wt%Au, see Table 3.7 in chapter 3) with X-ray fluorescence spectroscopy (XRF) gave similar results, suggesting that modification of Y-zeolite with sodium nitrate allows the adsorption of more gold on zeolite cavities during the catalyst preparation.

Surprisingly, the potassium-modified zeolites-Y showed a lower CO conversion (ca. 40%) which suggests that the alkali metal or cation might not be the only promoter of gold activity. These results suggest that the anions, in this case, nitrates are also playing a significant role on the improved activity, which is related to the report by Hutchings et al. [2]. The effect of alkali-modified zeolite-Y doped with gold from chloroauric acid suggests that the order of activity is as

follows: Na > K >> Li. The results contradicted those reported by Ono et al. [3] on the activity of Yb supported on alkali-exchanged Y-zeolite. They reported that the activity dependent strongly on the type of alkali cation present and the order being: K > Rb > Cs > Na > Li.

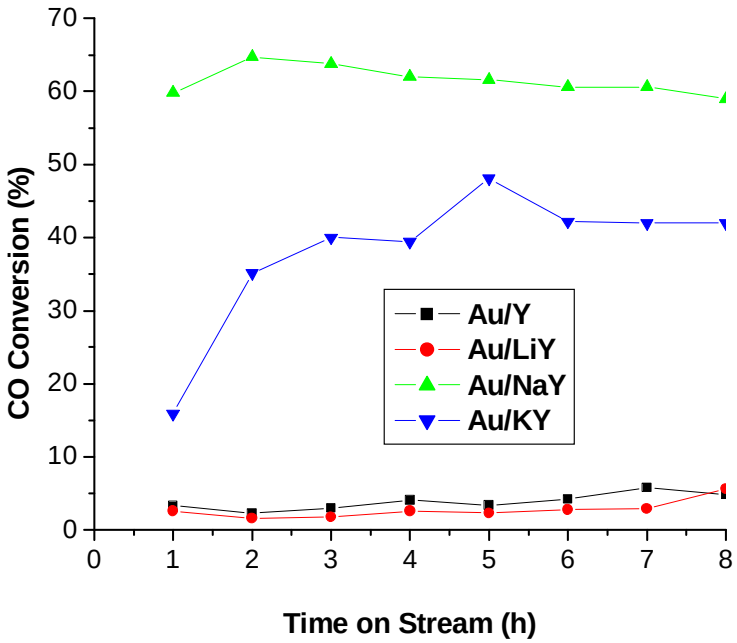

Figure 6.6: Plot of % CO conversion against time on stream showing the effect of alkali-modified zeolites-Y on the catalytic activity of gold supported on Y-zeolite.

Using X-ray photoelectron spectroscopy (XPS), Okamoto et al. [4] studied the effect of zeolite composition and the type of cation on the BE (binding energy) of the constituent elements for Y-zeolites ion-exchanged with a series of alkali cations. They noted that the BE of O_{1s} decreases as the Al content increases and they also found that as the electronegativity of the cation increases (i.e. $Cs^+ < K^+ < Na^+ < Li^+$), the O_{1s} BE increases. This trend though not completely seen in our results (the order of activity is as follows: Na > K >> Li), does suggest that lattice

oxygen might be participating or influencing the oxidation of CO and if that is the case the binding energy of lattice oxygen will influence the activity. These suggests that lithium modified Y-zeolite will posses lower CO conversion compared to any other alkali metal because of the stronger binding energy of lattice oxygen.

Huang et al. [5, 6] have studied pyrrole as the probe molecule adsorbed on basic sites of alkali cation-exchanged Y-zeolites by XPS, and information about the strength of the basic sites were obtained. In such studies they have measured the N_{1s} of BE of pyrrole adsorbed on alkali cation-exchanged Y-zeolites. The N_{1s} envelope was deconvulated into three peaks. One of the peaks was assigned to pyrrole adsorbed on the framework oxygen adjacent to the alkali cations other than the sodium cation. The BE of the peak was found to vary with the exchanged cation in such a way that the N_{1s} BE deceases as the basic strength of the zeolite increases as Li < Na < K < Rb < Cs. These suggest that electrons are localized significantly on $M^{+}(AlO_2)^{-}$ units.

6.3.3 Effect of different sources of gold on the unmodified zeolite-Y

Results in figures 6.7 show the time on stream CO conversion at 250 ^{0}C of gold prepared by incipient wetness of an aqueous solution of $KAu(CN)_2$ and by ion-exchange of aqueous solution of $Au(en)_2Cl_3$. The activity of gold prepared by anionic exchange of aqueous solution of $HAuCl_4$ were recorded at 150 ^{0}C. The results show that the activity of gold on unmodified Y-zeolite is less than 5% CO

conversion, with activity of Au from $HAuCl_4$ having a slightly higher CO conversion.

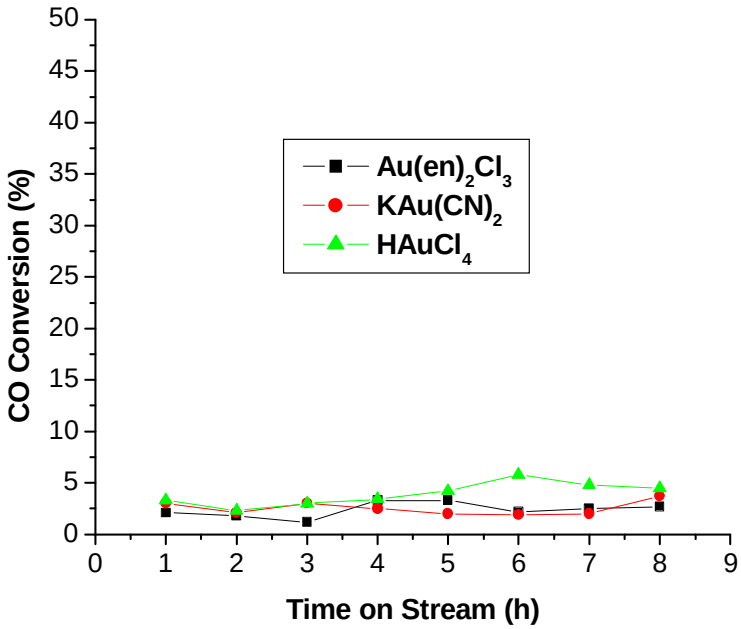

Figure 6.7: Comparison of different sources of Au for CO oxidation over gold supported on untreated zeolite-Y (2wt%Au).

6.3.4 Effect of different gold sources on the Li-modified zeolite-Y

The results in figure 6.8 show the activity of three Au catalysts supported on $LiNO_3$ treated zeolite-Y. It can be seen that when the zeolite is modified with lithium nitrate there is no distinct effect of Au source on the CO oxidation activity of the three Au catalysts. This suggests that the treatment of zeolite-Y with lithium nitrate does not influence the activity of the Au catalysts, on any source of gold. This clearly suggests that, similar to the CO oxidation reaction of the

unmodified Au catalysts, the treatment of zeolite-Y with $LiNO_3$ gave similar activity.

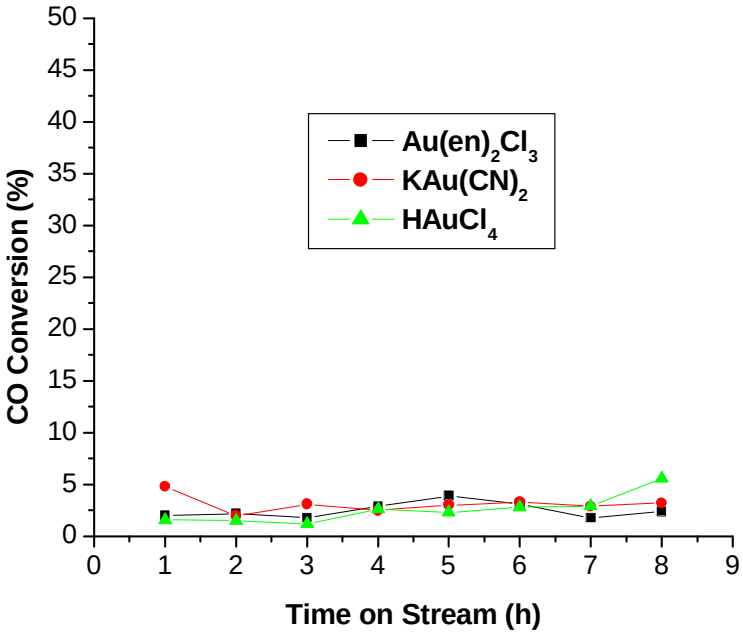

Figure 6.8: Comparison of different source of Au for CO oxidation over gold supported on lithium-modified zeolite-Y (2wt%Au).

6.3.5 Effect of different gold sources on Na-modified zeolite-Y

Results in figure 6.9 show the activity of three Au catalysts supported on $NaNO_3$ treated zeolite-Y. The Au catalysts prepared by incipient wetness to impregnation and ion-exchange of zeolite with an aqueous potassium dicyanoaurate and trichlorobis-ethylenediammine gold solutions respectively, have shown poor dispersion from our XRD results. An average Au particle size of 10.4 nm was observed in this case. XRD results of Au catalysts prepared by anionic exchange of zeolite with an aqueous solution of chloroauric solution showed high

dispersion; with an average Au particle size of less than 5.2 nm observed. The CO oxidation activity of the well dispersed Au catalysts from $HAuCl_4$ solution is of an order of magnitude higher than that of poorly dispersed Au catalysts. While an average of 58% CO conversion was observed for the well dispersed Au catalysts at 150 ^{0}C, the CO conversion was less than 10% for the poorly dispersed Au catalysts at 250 ^{0}C. This suggests that dispersion and CO oxidation activity of Au catalysts depend on the nature of the gold source used.

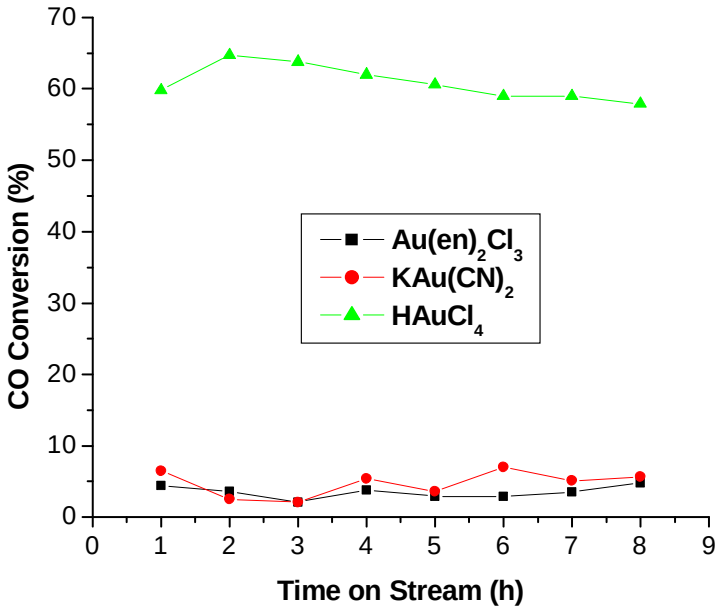

Figure 6.9: Comparison of different source of Au for CO oxidation over gold supported on sodium-modified zeolite-Y (2wt%Au).

6.3.6 Effect of different gold sources on K-modified zeolite-Y

Results in figure 6.10 show the time on stream CO oxidation activity of three Au catalysts supported on KNO_3 treated zeolite-Y. Au catalyst prepared by anionic exchange of zeolite with an aqueous solution of chloroauric solution showed a high steady state activity with an average of 40% CO conversion. Interestingly time on stream CO oxidation of Au catalyst prepared by incipient-wetness to impregnation of zeolite with an aqueous potassium dicyanoaurate showed an activity less than that of Au catalysts prepared from $HAuCl_4$, though it was expected for Au catalyst prepared by incipient-wetness to impregnation of potassium dicyanoaurate to show higher CO activity due to the presence of large amount of potassium. The Au catalyst prepared by ion-exchange of zeolite with aqueous solution of $Au(en)_2Cl_3$ showed an activity with less than 5% CO conversion. However, similar to the above observations on Au catalysts treated with $NaNO_3$, the highest activity was obtained on a catalyst prepared from an aqueous solution of chloroauric acid. The results in general do not reflect the periodic table trend of alkali metals.

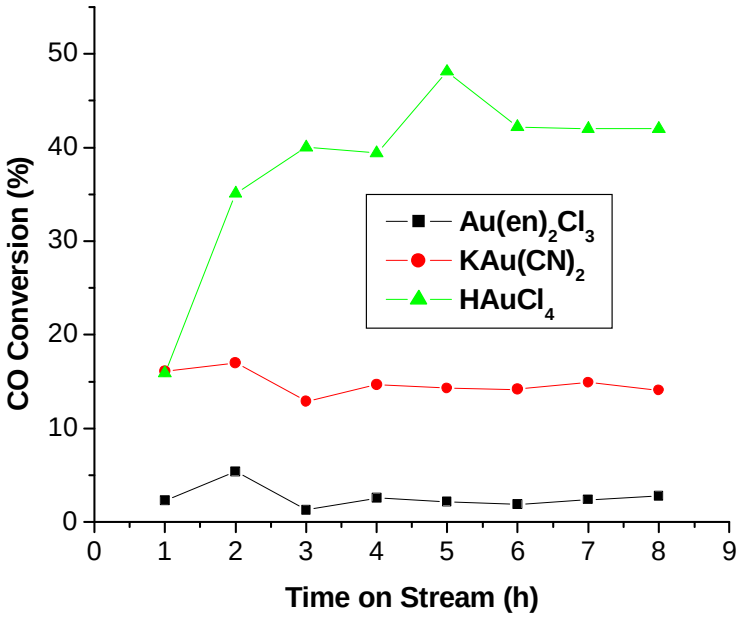

Figure 6.10: Comparison of different source of Au for CO oxidation over gold supported on potassium-modified zeolite-Y (2wt%Au).

6.4 CONCLUSIONS

We have successfully prepared Au catalysts supported on zeolite-Y which have been treated with aqueous solutions of $LiNO_3$, $NaNO_3$ or KNO_3. When the surface of the zeolite-Y is modified with different alkali metals and then doped with different sources of gold, the stability of Au particles was found to depend on the source of gold. Gold particles formed by deposition of Au from an aqueous solution of chloroauric acid were more stable than that prepared from $KAu(CN)_2$, and $Au(en)_2Cl_3$. Metallic gold formation does not depend on the type of alkali nitrate used, but is more dependent on the temperature at which CO oxidation took place.

The activity of the Au catalysts was found to depend on the source of gold used and the activity varied according the order: **$HAuCl_4$ >> $KAu(CN)_2$ > $Au(en)_2Cl_3$**

By focusing on chloroauric acid as a source of gold, it was noted that the unmodified zeolite-Y, showed low catalytic activity and the use of lithium-modified zeolite-Y did not have any positive effect on the catalytic activity of the catalyst. However, when sodium-modified zeolite-Y is used the activity of the catalyst was found to have markedly improved. X-ray fluorescence spectroscopy (XRF) has confirmed that an increase in CO oxidation activity of Au catalysts treated with $NaNO_3$ have been associated with an increase in gold content

deposited on the support. The X-ray diffractions (XRD) profiles show that the zeolite-Y crystallinity has been maintained.

The use of potassium-modified zeolite-Y, surprisingly gave low catalytic activity relative to that of sodium-modified zeolite-Y. This suggests that either an increase in Na-content on the surface of zeolites-Y or an increase in Au deposited on Na-modified zeolite-Y might be the underlying mechanism/explanation associated with the behaviour of such a catalyst. Thus, the order of the catalytic activity is as follows: Na > K > Li

6.5 REFERENCES

[1] J. N. Lin, J. H. Chen, C. Y. Hsiao, Y. M. Kang and B. Z. Wan, Appl. Cat. B: Env., **36** (2002) 19.

[2 B. Solsona, M. Conte, Y. Cong, A. Carley and G. Hutchings, Chem. Commun., (2005) 2351.

[3] T. Baba, G. J. Kim, and Y. Ono, J. Chem. Soc. Faraday Trans., **88** (1992) 891.

[4] Y. Okamoto, M. Ogawa, A. Maezawa, T. Imanaka, J. Catal. **112** (1988) 427.

[5] M. Huang, A. Adnot, S. J. Kaliaguine, J. Catal. **137** (1992) 322.

[6] V. A. Bondzie, C. Parker, and C. T. Campbell, Catalysis Letters, **63** (1999) 143.

CHAPTER 7

Catalytic activity of zeolite supported gold for ethylene hydrogenation

7.1 INTRODUCTION

Recently, the use of supported Au catalysts in other reactions producing chemical intermediates has shown that ethylene hydrogenation reaction can be catalyzed by supported gold catalysts [1]. In chapter 4, 5, and 6 several studies on CO oxidation were reported on gold/zeolite systems that comprised [(Au/HY (3.77wt%Au); Au/NaY (0.772wt%Au, treated with $NaNO_3$); and Au/M-Y (M represents Ni^{2+}, Fe^{3+}, or Cr^{3+})] and it was found that gold/zeolite systems are active catalysts for CO oxidation, with an activity depending on the source of gold and the support used.

Herein, the studies have been aimed at examining the possible catalytic activity or behaviour of gold/zeolite systems [(Au/HY (3.77wt%Au); Au/NaY (0.772wt%Au, treated with $NaNO_3$); and Au/M-Y (M represent Ni^{2+}, Fe^{3+}, and Cr^{3+})] for ethylene hydrogenation. The data will be compared with the CO oxidation activity discussed in chapter 4, 5, and 6.

7.2 EXPERIMENTAL

7.2.1 Catalyst preparation

We have investigated the catalytic activity of zeolite supported gold catalysts for ethylene hydrogenation from room temperature to 500 ^{0}C and also as a function of time on stream at either 150 ^{0}C or 260 ^{0}C. Catalysts used for this reaction are the same catalysts tested in the CO oxidation reaction and such catalysts were prepared as described in chapter 3. Catalysts used in this study were prepared from chloroauric acid, $HAuCl_4$ and potassium gold cyanide, $KAu(CN)_2$, supplied by Next Chemica (Pty) Limited, and trichlorobisethylenediamine gold (III), $Au(en)_2Cl_3$, prepared in our laboratory.

7.2.2 Catalyst pre-treatments

Catalysts were pre-treated at either 260 ^{0}C or 150 ^{0}C for 1.5 h under hydrogen gas (flow rate = 160 ml/min) unless otherwise stated. Pre-treatment started at room temperature, using a heating rate of about 10^{0}C/min, and the times indicated were counted from the moment the desired temperature was reached.

7.2.3 Temperature-programmed reduction (TPR)

Temperature-programmed reduction (TPR) profiles were obtained by means of a TPR apparatus built in our laboratory. TPR was used to monitor the different

oxidation states of Au and that of transition metals present in the catalysts. About 100 mg of sample was firstly degassed under N_2, by raising the temperature linearly (10 ^{0}C/min) from room temperature to 150 ^{0}C. The catalyst were then allowed to remain at this temperature for 30 minutes, after which they were reduced under a gaseous current consisting of 5 vol% H_2 in He, by heating at 7 ^{0}C/min from room temperature to 800 ^{0}C.

7.2.4 Catalytic activity

The reaction of ethylene under hydrogen atmosphere was followed by means of a continuous flow system operating at nearly atmospheric pressure. Analysis of the reactant mixture was carried out with an on-line gas chromatograph (FID detection), employing a Carbosieve packed column at 120 ^{0}C. Standards of up to C_{10} hydrocarbons were employed to calibrate the GC. However, only methane, ethane and ethylene were detected in the gaseous stream from the reactor.

The amount of non-volatile product (coke) was calculated by mass balance measurements. The concentration of ethylene in the gas phase entering the reactor and those of methane, ethane and ethylene were measured in the effluent. Except where noted, the reaction conditions employed was: 200 mg of catalyst sample; 160 ml/min H_2 and 40 ml/min ethylene (100 vol.%). A reaction temperature of either 260 ^{0}C or 150 ^{0}C was used.

7.3 RESULTS AND DISCUSSIONS

Historically, Au has been considered to be ineffective as a catalyst, however recent studies have shown that highly dispersed Au particles, with an average particle size < 5 nm can catalyze a variety of reactions [2]. In fact, supported nano-Au particles are now considered to be the most active catalysts for the low-temperature CO oxidation reaction. In this study the ethylene hydrogenation reaction has been investigated in a continuous flow reactor over gold/zeolite systems [(Au/HY (3.77wt%Au); Au/NaY (0.772wt%Au, treated with $NaNO_3$); and Au/M-Y (M represent Ni^{2+}, Fe^{3+}, and Cr^{3+})].

7.3.1 Reducibility of catalysts

7.3.1.1 Reducibility of gold and transition metals on Au/M-Y (M represent Ni^{2+}, Fe^{3+}, and Cr^{3+})

The TPR profile discussed in chapter 4, figure 4.3 suggested that there is an overlap of gold and transition metal peaks. Large amounts of gold were reduced at lower temperature (peak maxima at 264 ^{0}C); in the presence of Ni^{2+} when compared to samples containing Fe^{3+} and Cr^{3+} (peak maxima at 270 ^{0}C and 279 ^{0}C respectively). The reduction behaviour of stabilizing metal has a significant role on the performance of gold on zeolites, since the faster the reduction (of Ni^{2+}) to its metallic state the higher the probability that gold particles might sinter or coalesce with time on stream. However, a high ethylene hydrogenation activity

was observed in the case of nickel (reduction observed from 200 ^{0}C) as stabilizing metal. Since the catalysts were pre-treated at 260 ^{0}C for 2 h, it is possible that the activity of gold containing nickel will drop as a result of faster reduction of nickel to its metallic. This behaviour is observed in CO oxidation (activity decreases as the stabilizing metal is reduced faster) and in ethylene hydrogenation the reduction of gold to metallic gold do not seem to be the only underlying factor of the drop in activity. The activity falls above 260 ^{0}C, suggesting that reduction of nickel is influencing the ethylene hydrogenation activity as well [3].

7.3.1.2 Reducibility of gold from different sources supported on HY and Y

7.3.1.2.1 TPR profiles of Au/Y (3.67wt% Au)

The sample of Au/Y (3.67wt%Au) catalyst, discussed in chapter 4, figure 4.1 was prepared by incipient wetness of $KAu(CN)_2$ on Y zeolite. The profile suggests that gold on Y zeolite has been reduced starting from 225 ^{0}C and the peak maxima was observed at 258 ^{0}C. These results give an idea on the temperature range at which gold supported on Y is reduced.

7.3.1.2.2 TPR profile of $NaBH_4$ treated Au/HY (3.73wt%Au)

TPR profile of $NaBH_4$ treated Au/HY (3.73wt%Au) with peak maxima at 143 ^{0}C, prepared from $[Au(en)_2]Cl_3$ was discussed in chapter 5, figure 5.5. The catalyst is reduced at a lower temperature to that of gold catalysts prepared from $KAu(CN)_2$

above. However, the ethylene hydrogenation activities of these catalysts are closely related as discussed within this chapter. The gold catalysts prepared from $HAuCl_4$ on Y zeolite has been shown to be reduced at a lower temperature ~100 ^0C, [4] compared to catalysts prepared from $[Au(en)_2]Cl_3$ and $KAu(CN)_2$ as discussed above.

7.3.2 Effect of flow rate on the activity of Au/Fe-Y (5.45wt%Au:1.88wt%Fe)

The flow rate of the gases was found to show a significant influence on the catalytic activity of the catalyst in the ethylene hydrogenation reaction. The ratio of (H_2: C_2H_4) at 160 ml/min: 40 ml/min or 80 ml/min: 20 ml/min (4:1 ratio) respectively showed stable activity, with relatively high % ethylene conversion. The activity was found to increase rapidly and reached a steady state, with considerable amounts of ethane being formed. At a 3:1 ratio slower formation of ethane recorded. From these results, it was found quite convenient to use 160:40ml/min or 4:1 (H_2:C_2H_4) ratio in this work.

7.3.3 Activities of ethylene hydrogenation over gold/zeolites systems

7.3.3.1 Effect of temperature on the catalytic activity of Au/Fe-Y (1.67wt%Au:1.88wt%Fe)

The catalytic activity of Au/Fe-Y (1.67wt%Au:1.88wt%Fe) on ethylene hydrogenation seems to depend greatly on temperature (99.99% C_2H_4; H_2/C_2H_4 = 4), as shown in figure 7.1. At low temperature (25 ^{0}C to 70 ^{0}C) the catalyst remains inactive for ethylene hydrogenation. However, as the temperature is increased reaction was observed just above 100 ^{0}C, and at approximately 260 ^{0}C, the activity suddenly drops, suggesting that the catalyst is active for this reaction between 100 and 260 ^{0}C [5].

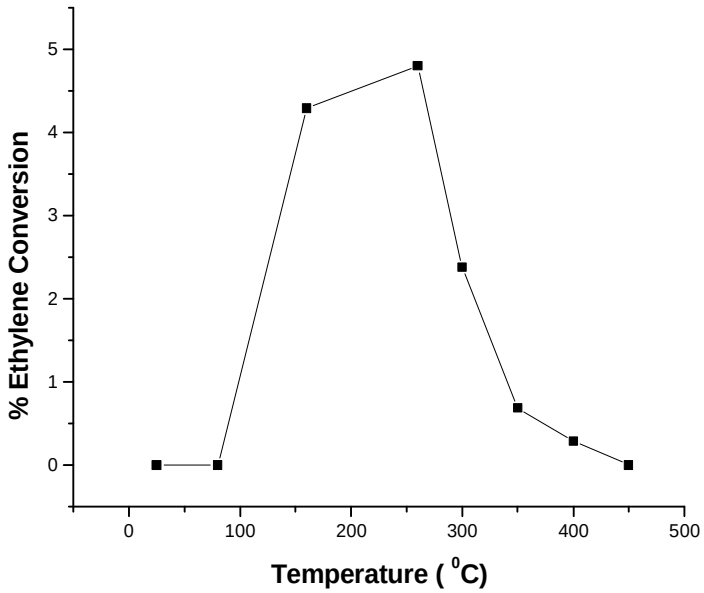

Figure 7.1: Effect of temperature on the catalytic activity of Au/Fe-Y (1.67wt%Au:1.88wt%Fe)

Above 260 ^{0}C, the catalyst rapidly deactivates, which could be due to the transition metal/stabilizing metal (Fe^{3+}) being reduced to its metallic state [see TPR profile of Au/Fe-Y (3.29wt%Au:1.88wt%Fe) in chapter 4, figure 4.3], which eventually leads to ionic gold being converted to a metallic state. Au(0) is usually associated with catalyst deactivation in the CO oxidation reaction [6]. Other reasons for deactivation of this catalyst might be due to the formation of carbonaceous species, also known as coke, on the surface of the catalyst. This will eventually block the active sites to reactants (i.e. ethylene and hydrogen gas in the ethylene hydrogenation). The activity decreases gradually to zero, above 260 ^{0}C unlike in the CO oxidation reaction wherein the activity increases with increasing temperature [7].

The ethylene hydrogenation was studied at 260 ^{0}C for most of the Au catalyst and promoted Au catalyst unless otherwise mentioned. Calcinations of Au/Fe-Y (1.67wt%Au:1.88wt%Fe) catalyst at higher temperature such as 300 ^{0}C, 400 ^{0}C and 500 ^{0}C, was found to lower the C_2H_4 conversion at 260 ^{0}C. The lowered activity might be due to sintering of Au particles and/or due to formation of carbon deposits; the mode of formation of carbonaceous deposits over acid and bifunctional catalysts depends strongly on the reaction temperature [8].

7.3.4 Effect of Au loading on the activity of Au/Fe-Y (1.88wt%Fe, containing 1.67, 3.29, 5.45, and 7.48 wt%Au, $KAu(CN)_2$ as source of gold)

The effect of Au on the ethylene hydrogenation activity of Au/Fe-Y at 260 ^{0}C (99.99% C_2H_4; $H_2/C_2H_4 = 4$) is shown in figure 7.2. Each of the catalysts is active under the reaction conditions employed. Au/Fe-Y (1.67wt%Au:1.88wt%Fe) catalysts have shown C_2H_4 conversion of 5%. However, on increasing the gold content to 3.29wt%Au, the C_2H_4 conversion increased to approximately 32%. Further increase in gold content reduced the activity of both catalysts containing 5.45wt%Au and 7.48wt%Au. This might be due to agglomeration of Au particles, when the surface area is reduced. Choudhary and co-workers [9] have demonstrated that the Au catalyst needs to be in a highly dispersed form to be active for both acetylene hydrogenation and CO oxidation reactions. This suggest that the Au particles on Au/Fe-Y (1.67wt%Au:1.88wt%Fe) catalyst might be in highly dispersed form compared to those containing 5.45wt%Au and 7.48wt%Au. Coking was more pronounced as the Au loading is increased [10]. The results are in excellent agreement with the CO oxidation activity trend observed for the four Fe promoted Au catalysts with different Au loading [7].

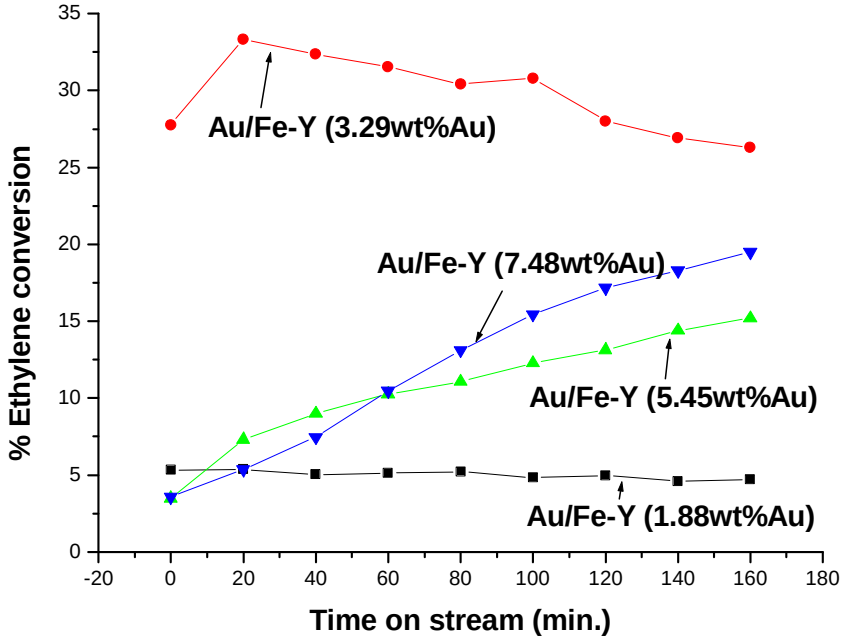

Figure 7.2: Effect of Au loading on the ethylene hydrogenation of Au/Fe-Y at 260 ^{0}C.

7.3.5 Effect of Ni^{2+}, Fe^{3+}, and Cr^{3+} on the activity of Au/Y

7.3.5.1 Catalytic activity of Au/M-Y (M represent Ni^{2+}, Fe^{3+}, and Cr^{3+}) at 260 ^{0}C

Results in figure 7.3 show the time on stream C_2H_4 hydrogenation activity for the Au/M-Y (M represent Ni^{2+}, Fe^{3+}, and Cr^{3+}) system at 260 ^{0}C (99.99% C_2H_4; H_2/C_2H_4 = 4). The Au/Ni-Y (3.35wt%Au:1.79wt%Ni) catalyst showed a high initial activity with 67% C_2H_4 conversion. However, the time on stream study indicated that Au on Ni-Y catalyst is not stable and continuously deactivated with time. Over a period of two hours the ethylene conversion decreased from 67 to 27%. Interestingly time on stream CO oxidation studies on the same catalyst at

200 ^{0}C showed stable activity for eight hours (see chapter 4). The deactivation in the case of the ethylene hydrogenation reaction may be attributed to poisoning by carbon or sintering of the Au particles [10]. The catalyst was found to regain activity following regeneration using oxidation (260 ^{0}C) treatment, suggesting that the deactivation mechanism involved carbon poisoning (see figure 7.11).

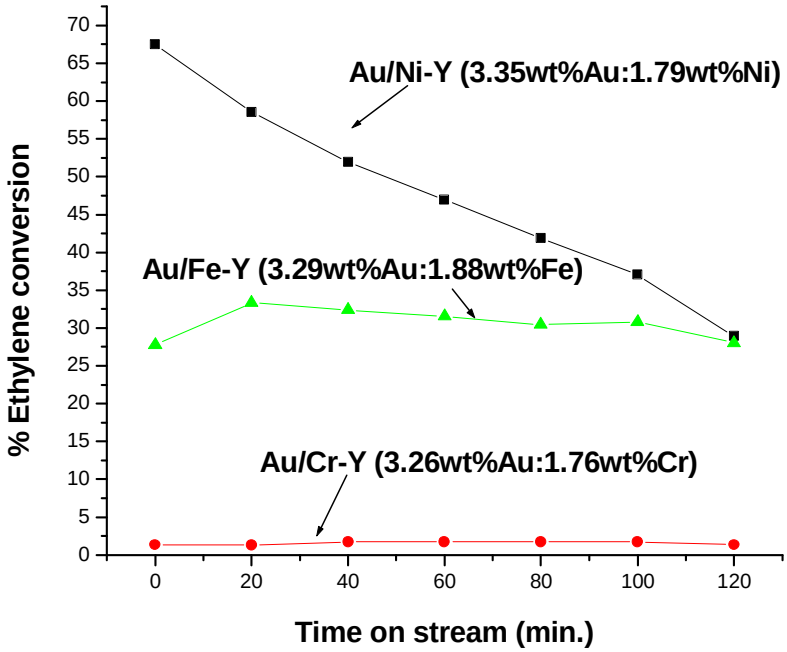

Figure 7.3: Comparison of ethylene conversion of Au/M-Y (M represent Ni^{2+}, Fe^{3+}, and Cr^{3+}) system at 260 ^{0}C.

Au/Cr-Y (3.26wt%Au:1.76wt%Cr) catalyst showed extremely poor activity for ethylene hydrogenation at 260 ^{0}C; the C_2H_4 conversion was less than 5%. The activity of Au/M-Y (M represent Ni^{2+}, Fe^{3+}, and Cr^{3+}) system for ethylene hydrogenation at 260 ^{0}C, follows a series $Ni^{2+} > Fe^{3+} > Cr^{3+}$. These results differ from the CO oxidation activity trends observed for the three catalysts containing different transition metal. This clearly suggests that, in contrast to CO oxidation

reaction, the lower the reduction potential of transition metal the higher the ethylene hydrogenation activity.

It was suggested that the observed decrease in activity of Au/M-Y (M represent Ni^{2+}, Fe^{3+}, and Cr^{3+}) systems might be influenced by the reduction potential of the transition metal (Ni^{2+}, - 0.23 << Fe^{3+}, - 0.41 < Cr^{3+}, - 0.56), because the reduction of Ni^{2+} starts occurring at approximately 250 ^{0}C as shown on the TPR profile (in chapter 4, figure 4.3). It was decided that the same reaction be undertaken at lower temperature (150 ^{0}C) where it will be certain that the reduction of transition metals might not influence the activity of ethylene hydrogenation.

Figure 7.4 shows the activity of Au/M-Y (M represent Ni^{2+}, Fe^{3+}, and Cr^{3+}) systems at 150 ^{0}C. Again the result show Au/Ni-Y (3.35wt%Au:1.79wt%Ni) catalyst having high initial activity with 60% C_2H_4 conversion at steady state. The activity at this temperature is more stable, unlike at 260 ^{0}C where the catalyst deactivated rapidly with time. However, the activity of both Au/Fe-Y (3.29wt%Au:1.88wt%Fe) and Au/Cr-Y (3.26wt%Au:1.76wt%Cr) deactivates with time on stream and the activity trend has been reversed between these two catalysts such that: Ni^{2+} >> Cr^{3+} > Fe^{3+}. This suggests that the temperature has a significant influence on the ethylene hydrogenation reaction.

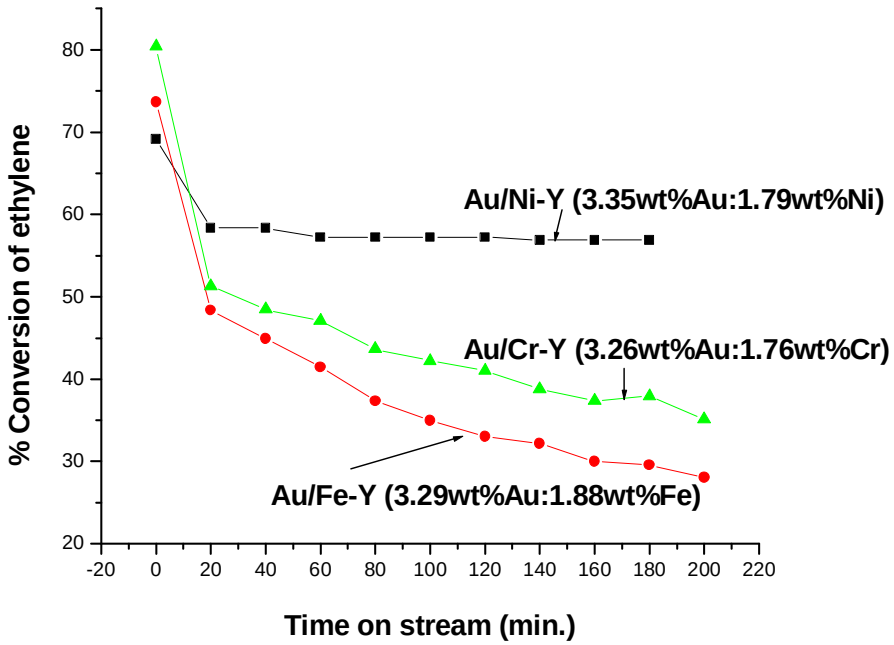

Figure 7.4: Comparison of ethylene conversion of Au/M-Y (M represent Ni^{2+}, Fe^{3+}, and Cr^{3+}) system at 150 ^{0}C.

7.3.6 Effect of preparation by using different source of Au supported on Y

Figure 7.5 shows the results of ethylene hydrogenation activity of three different source of Au used during the preparation of supported Au catalysts. The Au/Y (3.67wt%Au) catalysts prepared by impregnation of Y with an aqueous solution of potassium dicyanoaurate and by ion-exchange of Y with an aqueous solution of trichlorobisethylenediammine gold showed poor C_2H_4 conversion of 1.0% and 0.5% respectively. However, Au/Y (0.277wt%Au) prepared by anionic-exchange of Y with an aqueous solution of chloroauric acid has shown a C_2H_4 conversion of 4.3%. A ~5.1% CO conversion was observed for the Au/NaY (0.277wt%Au, treated without $NaNO_3$) at 150 ^{0}C, prepared by anionic-exchange of chloroauric

acid. The CO conversion was less than 3% at 250 ^{0}C, for both catalysts prepared by impregnation of potassium dicyanoaurate and by ion-exchange of trichlorobis-ethylenediammine. This is in excellent agreement with the CO oxidation activity trend observed for the three Au catalysts with different gold sources. This clearly suggests that similar to CO oxidation reaction, the C_2H_4 hydrogenation activity trend is as follows: $HAuCl_4$ >> $KAu(CN)_2$ > $Au(en)_2Cl_3$. Clearly, the source of Au influences the catalytic activity of supported gold catalysts.

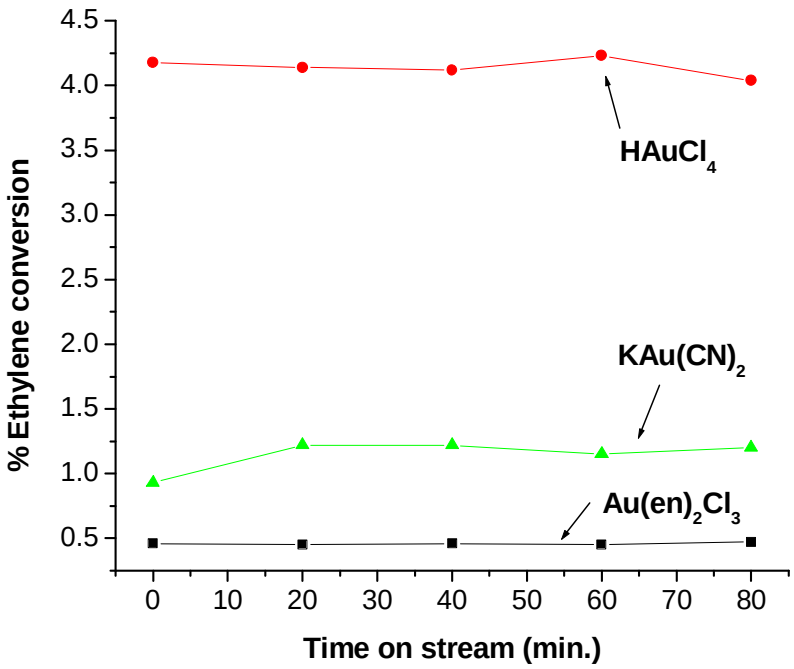

Figure 7.5: Time on stream ethylene hydrogenation activity for the Au/Y catalysts at 260 ^{0}C, prepared using different source of gold.

7.3.7 The effect of $NaNO_3$ on the activity of Au/NaY (0.772wt%Au, treated with $NaNO_3$, $HAuCl_4$ as the source of gold)

Figure 7.6 shows the time on stream C_2H_4 hydrogenation activity for the Au/NaY (0.772wt%Au, treated with $NaNO_3$) catalyst. The catalyst showed a high initial activity with 22% C_2H_4 conversion. However, the time on stream study indicated that the Au catalyst was not stable and continuously deactivated with time. As seen below, the ethylene hydrogenation conversion decreased from 22 to 6% over a period of 80 minutes. Gates et al. [1], observed similar or less than 5% C_2H_4 conversion on Au supported on MgO after 12 h. Interestingly time on stream CO oxidation studies on the same catalyst at 150 ^{0}C showed high and stable activity for 8 hours. The cause of deactivation in the case of ethylene hydrogenation reaction is thought to be due to poisoning by carbon. The decrease in activity was observed by Yide et al. [11] and Trimm et al. [12]. Yide et al. [11] reported that some carbonaceous deposits are inert and tend to cause the deactivation of the catalyst by covering the active metal species.

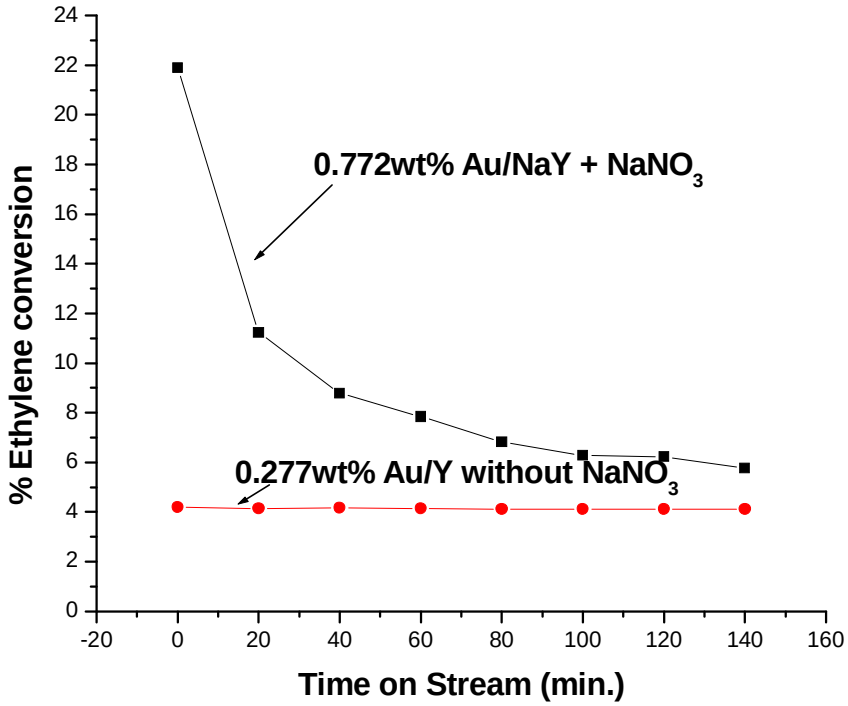

Figure 7.6: Effect of sodium nitrate on the ethylene hydrogenation activity of Au/NaY (0.772wt%Au, treated with $NaNO_3$) at 260 ^{0}C.

The untreated Au/Y (0.277wt%Au) catalyst showed less C_2H_4 conversion of 4%. This is in excellent agreement with the CO oxidation activity trend observed for the two Au catalysts. This suggests that, similar to the CO oxidation reaction, the Y-zeolite needs to be treated with $NaNO_3$ prior to Au loading for the catalyst to be more active for the ethylene hydrogenation, as demonstrated by Wan et al. [4]. They reported that prior to gold loading, the $NaNO_3$ treated Y-zeolite gave higher sodium content. An increase in sodium content resulted in higher gold loading, as is the case in this study (see Table 3.7 in chapter 3).

7.3.8 Treatment effect of $NaBH_4$ on the activity of Au/Y (3.46wt%Au) and Au/HY (3.73wt%Au)

7.3.8.1 $KAu(CN)_2$ as source of gold

Results in figure 7.7 shows the treatment effect of $NaBH_4$ on Au/Y (3.46wt%Au) at 260 ^{0}C. The untreated Au catalyst shows a stable activity with 1.7% C_2H_4 conversion while the $NaBH_4$ treated Au catalyst showed a poor C_2H_4 conversion of 0.9%. The lower activity of the $NaBH_4$ treated Au catalyst can be attributed to the possibility that since gold was reduced most of the gold particles existed in the metallic state, Au^0 and very few existed as Au^+, which is thought to be an active species for ethylene hydrogenation reaction [13]. Similar results have been observed by Gates et al. [14]. They reported that the XANES data analysis of the gold complex on MgO during ethylene hydrogenation, show that the oxidation state of gold remained as Au^{3+}. These results are to be contradicted with the CO oxidation activity trend observed for the two Au catalysts. This suggests that, opposite to the CO oxidation reaction, Au^+ species are necessary for ethylene hydrogenation reaction (as suggested by Gates et al. [1, 14]).

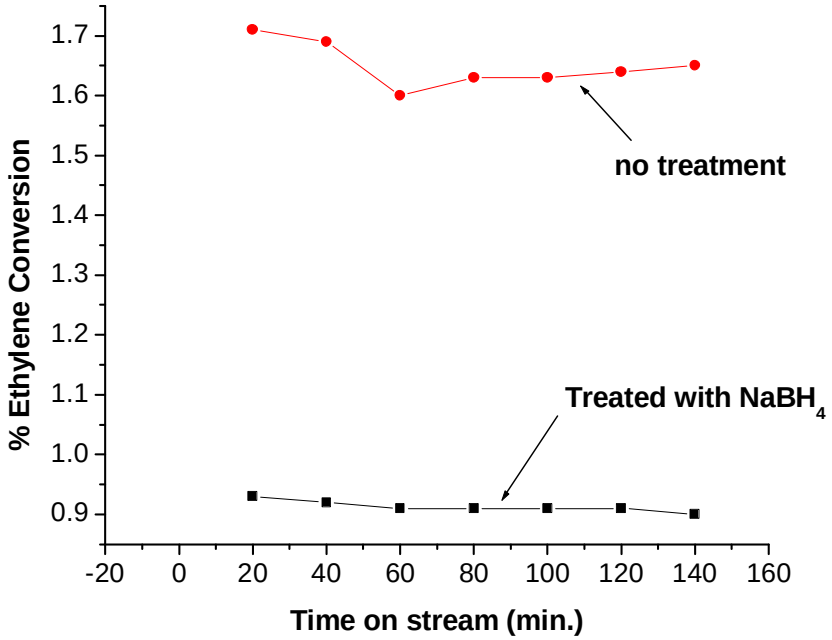

Figure 7.7: Comparison of the ethylene hydrogenation activity for the untreated Au/Y (3.67wt%Au) and Au/Y (3.46wt%Au) treated with $NaBH_4$ (Au:$NaBH_4$ = 1:1).

7.3.8.2 $Au(en)_2Cl_3$ as source of gold

Results in figure 7.8 show similar treatment effect of $NaBH_4$ on Au/HY (3.73wt%Au) at 260 ^{0}C as that discussed above for a catalyst prepared from $KAu(CN)_2$. The untreated Au catalyst shows a stable and higher activity with 0.5% C_2H_4 conversion and the $NaBH_4$ treated Au catalyst showed no activity for C_2H_4 hydrogenation. These results again contrast with that of CO oxidation reaction (chapter 6), suggesting that the treatment of Au catalyst with $NaBH_4$ is independent of the source of gold. This suggests that ionic gold species should be in excess for the Au catalyst to effectively catalyze the ethylene hydrogenation

reaction. It is noteworthy that $KAu(CN)_2$ is the better source of Au, compared to $Au(en)_2Cl_3$, since the activity is greater by 0.5% for both ethylene hydrogenation and CO oxidation reaction.

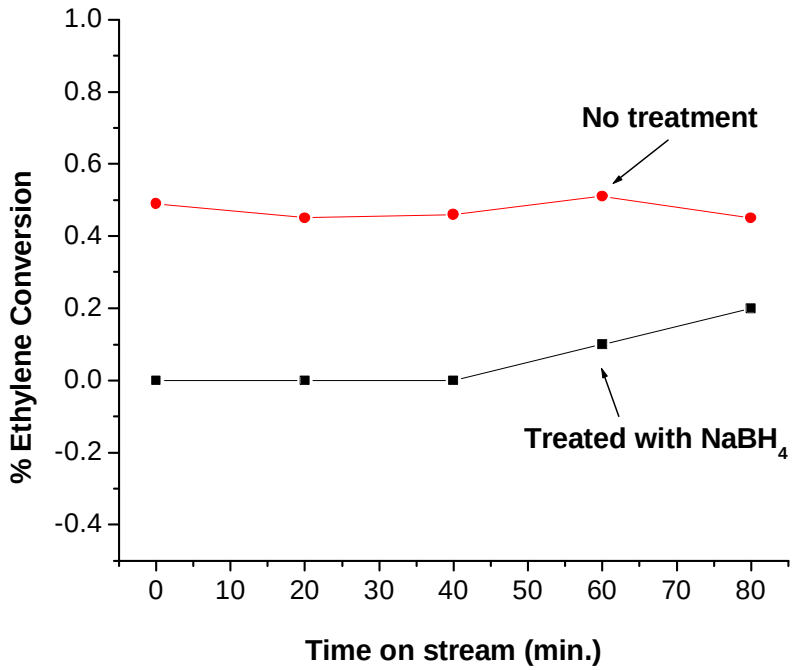

Figure 7.8: Comparison of the ethylene hydrogenation activity for the untreated Au/HY (3.77wt%Au) and Au/HY (3.73wt%Au) treated with $NaBH_4$ (Au:$NaBH_4$ = 1:1).

7.3.9 The activity of Au/Ni-Y (3.35wt%Au:1.79wt%Ni) catalyst submitted to different pre-treatments and running conditions

Since it was found that the pre-treatment of the catalyst at temperature above 260 ^{0}C causes very rapid deactivation of the catalysts and affects the final percent conversion attained by the catalyst, it was found necessary to investigate reaction temperatures below 260 ^{0}C. Au/Ni-Y (3.35wt%Au:1.79wt%Ni) catalyst was chosen for this study, since the catalyst activity has shown to be quite stable with time when the catalyst was used for the ethylene hydrogenation at 150 ^{0}C.

Figure 7.9 show activity measurements on the Au/Ni-Y sample submitted to five types of pre-treatments as indicated. It can be seen that samples pre-treated at 80 and 120 ^{0}C, and catalyze ethylene hydrogenation at 80 and 120 ^{0}C, respectively with H_2 show similar activity behaviour for the first 80 minutes.

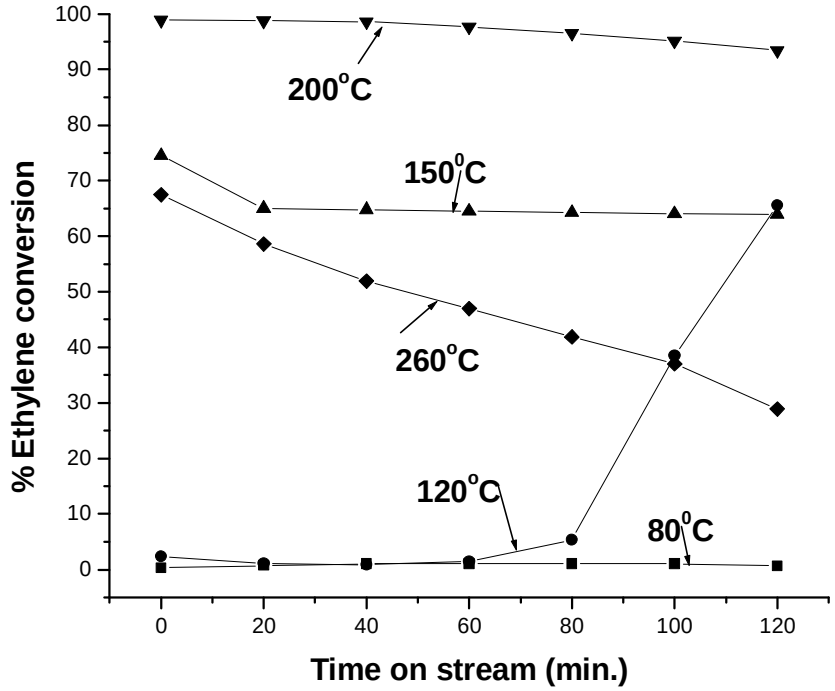

Figure 7.9: Ethylene hydrogenation over Au-Ni/Y (3.35wt%Au:1.79wt%Ni) showing the effect of pre-treatment and working conditions on C_2H_4 conversion. The catalyst pre-treatment and working conditions were performed at the indicated temperatures for each run.

The highest ethylene hydrogenation activity of close to 100 % C_2H_4 conversion was achieved at 200 ^{0}C and the activity decreases slowly. Such an increase in activity of this catalyst can be attributed to the effect of temperature on nickel. Previously, the lower ethylene hydrogenation activity above 260 ^{0}C, on this catalyst was observed. This clearly suggests that the reduction of Ni^{2+} (during pre-treatment at 260 ^{0}C) from 200 ^{0}C and above as shown by TPR profile (chapter 4, figure 4.3) is the cause of such lower initial activity. The results further, suggests that nickel plays significant role in catalyzing the ethylene hydrogenation

reaction. Gold alone has shown less ethylene hydrogenation activity and the improvement in activity is contributed by the presence of transition metals.

The high ethylene hydrogenation activity observed in this study below 260 ^{0}C is probably due to the formation of π-bonded ethylene species (at lower temperature) as demonstrated by Shen et al. [15, 16]. Their investigation near ambient pressure and temperature, show that ethylene primarily hydrogenates through a π-bonded intermediate rather than the more strongly adsorbed di-σ bonded ethylene species. They further mentioned that the π-bonded intermediate occupies only a few percent of surface sites during reaction and is in fast equilibrium with gas phase ethylene. This clearly suggests that the high production of ethane at lower temperature is closely correlated with the presence of weakly adsorbed ethylene, possibly a π-bonded state [16].

7.3.10 Regeneration of Au/Ni-Y (3.35wt%Au:1.79wt%Ni) catalyst under an O_2 atmosphere

When the Au/Ni-Y (3.35wt%Au:1.79wt%Ni) catalyst surface is examined after carrying out ethylene hydrogenation reactions, it was covered with a black layer of carbonaceous deposit. The spent Au/Ni-Y catalyst at 260 ^{0}C, which turned black after reaction suggested the removal of coke deposits by reaction with oxygen (40ml/min for 1.5 h at 260 ^{0}C). The ethylene hydrogenation reaction was undertaken on the regenerated Au/Ni-Y catalyst at 260 ^{0}C.

The results in figure 7.10 show that the regenerated Au/Ni-Y catalyst has regained some activity. However, the regeneration is incomplete presumably due to secondary effects under the severe conditions of coke removal such as high temperature, presence of water, etc [6]. The carbon deposits combines with oxygen to form carbon dioxide which escapes as a gas. The carbonaceous deposits blocking the active sites on the catalyst were removed, and the catalyst regains activity. Unlike the ethylene hydrogenation reaction the CO oxidation activity is quite stable with time and temperatures as high as 500 ^{0}C can be used without a severe deactivation of the catalyst (and independent of the source of gold).

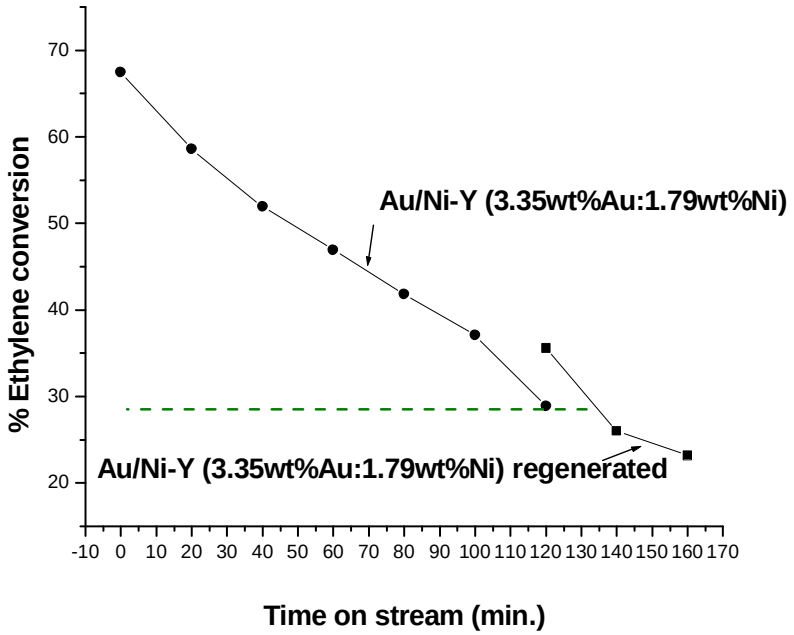

Figure 7.10: The effect of oxygen on the regeneration of Au/Ni-Y (3.35wt%Au:1.79wt%Ni) catalyst.

7.3.11 Comparison between ethylene hydrogenation and CO oxidation reactions

7.3.11.1 Activity of Au/HY, independent of the source of gold)

CO oxidation has been reported to give high activities at 450 ^{0}C with ~16% CO conversion. Upon addition of sodium borohydride to the light pink catalyst in water, the solution turned dark purple, suggesting the reduction of Au. CO oxidation activity of the $NaBH_4$ treated Au/HY (3.73wt%Au) catalyst were measured and was found to have doubled (chapter 6). However, with ethylene hydrogenation, the activity of the catalyst (~0.5%) was extremely poor. C_2H_4 conversion of $NaBH_4$ treated Au/HY (3.73wt%Au) catalyst gave zero activity, which is opposite to the activity trend observed for CO oxidation. The results suggest that the higher oxidation state of Au is necessary to catalyze ethylene hydrogenation reaction. This result is consistent with data reported by Gates et al. [1], for Au supported on MgO. Similar behaviour on ethylene hydrogenation was observed on Au supported on NaY, irrespective of the source of gold used.

7.3.11.2 Activity of Au/M-Y (M represent Ni^{2+}, Fe^{3+}, and Cr^{3+}, $KAu(CN)_2$ as source of gold).

The activity of this system for ethylene hydrogenation, similar to CO oxidation has been found to depend on the type of transition metal used. In the case of CO oxidation the chromium promoted Au catalyst was more active at 200 ^{0}C.

Chromium promoted Au catalysts for ethylene hydrogenation were found to be extremely poor catalyst and Ni containing catalyst were more active at both 150 ^{0}C and 260 ^{0}C.

7.3.11.3 Effect of preparation by using different source of gold

Different sources of Au were investigated for ethylene hydrogenation and results were in excellent agreement with the CO oxidation activity trend (chapter 6), observed for the three Au catalysts. This clearly suggests that similar to CO oxidation reaction, the Au catalyst needs to be in a highly dispersed form to be active for ethylene hydrogenation reaction. The following activity trends were observed on both reactions: $HAuCl_4$ >> $KAu(CN)_2$ > $Au(en)_2Cl_3$. Detailed information for the two test reactions investigated is summarized in table 7.1.

Table 7.1: Comparison of ethylene hydrogenation and CO oxidation reactions over gold supported catalysts, with or without promoters.

Property	**Ethylene hydrogenation**	**CO oxidation**
Feed	100% C_2H_4; H_2/C_2H_4 = 4	10%CO/He:10%O_2/He
Au/HY[a] Au-Cr/Y[b]	0.5% C_2H_4 conv. (at 260 ^{0}C) < 5.0% (at 260 ^{0}C)	29% CO conv. (at 450 ^{0}C) 52% (at 200 ^{0}C)
Reaction conditions	150 ^{0}C or 260 ^{0}C	150 ^{0}C, 200 ^{0}C, 250 ^{0}C or 450 ^{0}C
Effect of promoters on Au/Y[b]	$Ni^{2+} > Fe^{3+} > Cr^{3+}$ (at 260 ^{0}C)	$Cr^{3+} > Fe^{2+} > Ni^{2+}$ (at 200 ^{0}C)
Suggested state of Au during catalysis	Au^{3+} [14] and Au^+	Au^+ and Au^0
Treatment effect of $NaBH_4$ on Au/HY[a]	Decreases activity 0.5 to 0.0% (at 260 ^{0}C)	Increases activity 17.0 to 29.0% (at 450 ^{0}C)
$NaNO_3$ treated Au/NaY[c] (0.772wt%Au)	Increases activity 4.0 to 8.0% (at 260 ^{0}C)	Increases activity 5.0 to 60.0% (at 150 ^{0}C)
Different sources of Au	$HAuCl_4$ >> $KAu(CN)_2$ > $Au(en)_2Cl_3$ (at 260 ^{0}C)	$HAuCl_4$ >> $KAu(CN)_2$ > $Au(en)_2Cl_3$ (at 150 ^{0}C and 250 ^{0}C)
Reaction product	ethane	carbon dioxide

[a] Source of gold is $Au(en)_2Cl_3$; [b] Source of gold is $KAu(CN)_2$; [c] Source of gold is $HAuCl_4$

7.4 CONCLUSIONS

Pre-treatment at 260 ^{0}C and above had little detrimental effect on the Au/M-Y (M represent Ni^{2+}, Fe^{3+}, and Cr^{3+}) samples but they affected the Au/HY (3.77wt%Au) and Au/NaY (0.772wt%Au, treated with $NaNO_3$) catalysts. Pre-treatment and run conditions at 150 ^{0}C and 200 ^{0}C gave high and stable C_2H_4 conversion.

Monometallic gold/zeolite systems of Au/HY (3.77wt%Au) and Au/NaY (0.772wt%Au, treated with $NaNO_3$) was found to be active in the ethylene hydrogenation with ~5% C_2H_4 conversion. The $NaBH_4$ reduced Au catalysts gave lower C_2H_4 conversion, unlike in CO oxidation where the activity increased on the reduced Au catalysts. This suggests that cationic gold is responsible for the activity of the catalyst. Bimetallic catalysts Au/M-Y (M represent Ni^{2+}, Fe^{3+}, and Cr^{3+}) were found to be more active (~21% C_2H_4 conversion, for M = Fe) compared to monometallic catalysts.

The activity of monometallic systems was found to depend on the source of Au and the order of reactivity similar to that of CO oxidation was observed as follows: $HAuCl_4$ >> $KAu(CN)_2$ > $Au(en)_2Cl_3$. It was also noted that the activity of Au/M-Y (M represent Ni^{2+}, Fe^{3+}, and Cr^{3+}) system for ethylene hydrogenation at 260 ^{0}C, follows the series Ni^{2+} > Fe^{3+} > Cr^{3+}. At 150 ^{0}C, the order of activity was as follows: Ni^{2+} > Cr^{3+} > Fe^{3+}. These results have been found to contradict the CO oxidation activity trends which follow the trend: Ni^{2+} < Fe^{3+} < Cr^{3+}. This clearly

suggests that, in contrast to CO oxidation reaction, the lower the reduction potential of transition metal the higher the ethylene hydrogenation activity.

Similar to the CO oxidation reaction, treatment of zeolite-Y with $NaNO_3$ and an increase in gold content resulted in higher C_2H_4 conversion.

The deactivation of the Au catalysts was found to be accompanied by the formation of carbonaceous deposits on the surface of the catalyst especially at high temperature (260 ^{0}C and above) and at the high temperatures consumption of ethylene was considerable higher, with less ethane formation. Calcination of Au catalyst in an O_2 atmosphere slightly regenerated the ethylene hydrogenation activity.

7.5 REFERENCES

[1] J. Guzman and B. C. Gates, Comm. Angew. Chem. Inter. edition, **42** (2003) 690.

[2] G. C. Bond and D. T. Thompson, Catal. Rev. Sci. Eng. **41** (1999) 319.

[3] M. S. Tzou, B. K. Teo, and W. M. H. Sachtler, J. Catal., (1988) 220.

[4] (a) J. N. Lin, J. H. Chen, C. Y. Hsiao, Y. M. Kang and B. Z. Wan, Appl. Cat. B: Env., **36** (2002) 19. (b) Lin, Y. N. and Wan, B. Z., Appl. Catal. B: Env. **41** (2003) 83.

[5] J. M. Thomas and W. J. Thomas, Principle and Practice of Heterogeneous Catalysis, Weinheim, New York, (1997).

[6] D. L. Trimm, Applied catalysis A: General, **212** (2001) 153.

[7] T. Magadzu, and M. S. Scurrell, University of the Witwatersrand, Unpublished results.

[8] J. Matos, J. L. Brito and J. Laine, Applied Catalysis A: General, **152** (1997) 27.

[9] T. V. Choudhary, C. Sivadinarayana, A. K. Datye, D. Kumar and D. W. Goodman, Catal. Letters, **86** (2003) 1.

[10] C. H. Bartholomew, Applied Catalysis A: General, **212** (2001) 17.

[11] H. Liu, L. Su, H. Wang, W Shen, X. Bao and B. X. Yide, Appl. Catal. A: General, **236** (2002) 263.

[12] D. L. Trimm, Applied catalysis A: General, **212** (2001) 153.

[13] P. S. Cremer, X. Su, G. A. Somorjai and Y. Ron Shen, Journal of Molecular Catalysis A: Chemical, **131** (1998) 225.

[14] J. Guzman, and B.C. Gates, J. Catal. **226** (2004) 111.

[15] P. S. Cremer, X. Su, G. A. Somorjai and Y. Ron Shen, J. Mol. Cat. A: Chemical, **131** (1998), 225.

[16] T. V. W. Janssens, D. Stone, J. C. Hemminger F. Zaera, J. Catal., **177**, (1988) 284.

CHAPTER 8

Low-temperature, Water-gas shift reactions over Au supported on TiO_2, in the presence of modifier: EXAFS/XANES analysis of gold-copper ion mixtures on TiO_2 (anatase)

8.1 INTRODUCTION

To modify existing catalysts or develop new ones, it helps to understand how the existing catalysts work. Various in situ characterization methods that allow studies of heterogeneous catalysts under realistic reaction conditions have substantially improved the possibility for obtaining relevant structural information on catalysts [1-3]. In many industrial catalyst systems, the presence of a so called catalyst promoter is essential to achieve the required activity or selectivity necessary in a reaction. Usually, a promoter is defined as a substance that causes a more than proportional increase in activity or selectivity when added to the catalyst [4]. In many cases, the promoter alone is completely inactive in the catalytic process, where it is used to boost productivity. It is common practice to distinguish between structural promoters that cause an increase in the number of active sites and electronic promoters that produce active sites with a higher intrinsic activity, i.e., higher turn over frequencies. In earlier studies, Hansen et al. [5] have beautifully demonstrated that structural characterization of a catalyst's

surface in the presence of reactive gases can help to clarify how a catalyst modifier promotes a catalyst's activity (barium promoters for ammonia synthesis). An example is the work by Mittasch et al. [6], who performed systematic studies of the influence of various catalyst promoters with an ammonia synthesis catalyst. The aim of the present work is to demonstrate that structural characterization of a catalyst's surface in the presence of reactive gases can help to clarify how a catalyst modifier – in this case, a copper promoter for the water-gas shift reaction – promotes the catalyst's activity and also to elucidate the location and state of the copper promoter. The studies were conducted on a copper promoted gold catalyst on a TiO_2 support (Au-Cu/TiO_2) that has been shown to exhibit high activity and stability in the catalytic water-gas shift reaction and also on un-promoted Au/TiO_2.

8.2 EXPERIMENTAL

8.2.1 Catalyst preparation

Catalyst preparation and materials for the nitrate containing catalysts have been described in chapter 3. Catalysts were also prepared from a solution of copper acetate monohydrate supplied by Aldrich. This was introduced to the same support (TiO_2, anatase) as used for the nitrate-containing catalysts, using the incipient wetness method. Five catalysts were studied in-situ X-ray Absorption Near Edge Structure (XANES) and Extended X-ray Absorption Fine Structure

(EXAFS), two of which were made using copper nitrate as the precursor and the three using copper acetate.

8.2.2 Characterization techniques

The Au and Cu content were determined by X-ray Fluorescence Spectroscopy (XRF) at Northwestern University. EXAFS and XANES measurements were performed on beam line DND-CAT at the Argonne photon source, using an in-situ cell that has been described in chapter 3, figure 3.4. Samples were studied in the form of a 13 mm diameter pressed disc.

8.2.3 Catalyst testing

8.2.3.1 In-situ catalyst testing

Before exposure to carbon monoxide and moisture, samples were purged with flowing helium (20 ml/min) at room temperature and then examined by X-ray absorption. The helium flow was halted and the catalysts were then exposed to static carbon monoxide containing moisture at atmospheric pressure. The sample holder allowed one catalyst to be treated at a time and then studied sequentially by X-ray absorption. The spectra presented have been subjected to Fourier filtering to improve the quality of the background subtractions. The XANES data were extracted after pre-edge subtraction and normalization using the WINXAS version 3.1 programs.

8.2.3.2 Ex-situ catalyst testing

Catalytic data were measured using a laboratory microreactor equipped with mass flow controllers and with GC analysis of products. The catalyst charge was 0.1g and the reactor internal diameter was 6 mm.

Samples studied for low-temperature water-gas shift, preferential oxidation of CO in the presence of excess hydrogen and CO oxidation are shown in chapter 3, Table 3.8. The table gives detailed information on the catalyst parameters and some catalytic data under forward water-gas shift conditions.

8.3 RESULTS AND DISCUSSION

8.3.1 Catalyst characterization

8.3.1.1 X-ray fluorescence (XRF) and temperature-programmed reduction (TPR)

The TPR profile in figure 8.1 shows the Au and Cu content determined by taking the area under the H_2 consumption peak. The content was found to be 2.6wt%Au and 0.27wt%Cu. The content of both metals was verified by running XRF of a cylindrical shaped pellet, which gave 2.84wt%Au and 0.32wt%Cu.

A TPR profile shows the reduction of gold at room temperature with the peak maxima at 18 ^{0}C and Cu being reduced at higher temperature with the peak

maxima at 467 ^{0}C. Au has been completely reduced at 18 ^{0}C. The size of TPR peak was found to depend on the amount of surface oxygen anions attached to Au^{3+} and Cu^{2+} ions [7].

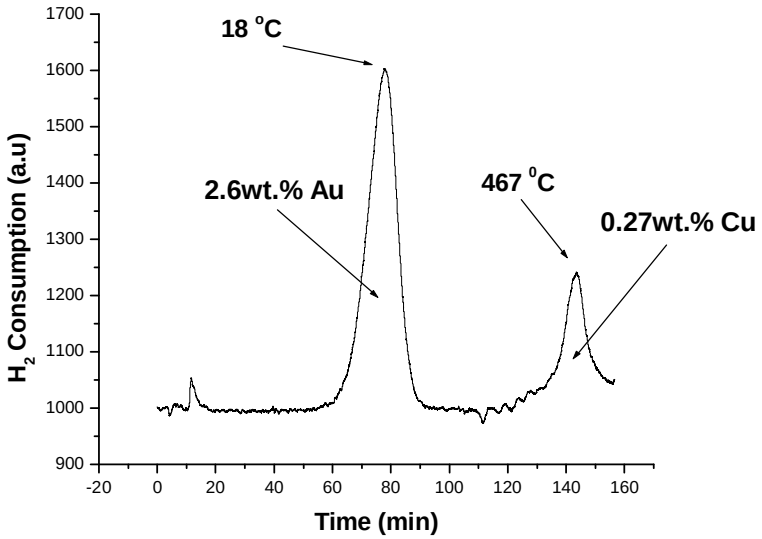

Figure 8.1: TPR profile of Au-Cu/TiO_2 showing the metal content and the temperature at which Au and Cu have been reduced.

8.3.1.2 X-ray absorption near-edge structure (XANES)

The Au K-edge XANES spectra of uncalcined as-prepared and that of a sample used for water-gas shift Au-Cu^{c}/TiO_2 (2.84wt%Au:0.32wt%Cu) are shown in figure 8.2. The XANES spectrum of uncalcined as-prepared catalysts shows a pre-edge feature (due to the 1s to 3d transition) characteristic of Au in a tetrahedral environment. The sample used for water-gas shift showed a reduction in the intensity of the pre-edge feature or white line region indicating a change in Au environment. It is interesting to note that the edge position of the water-gas shift

treated catalyst shifted to higher energy by 0.05 eV compared to the as-prepared catalyst, indicating a partial reduction of Au^{3+} to either Au^{+}/Au^{0}. Similar results were reported by Gates et al. [8] on Au supported on MgO. They reported that an exposure of the sample to H_2 at 100 ^{0}C led to a complete disappearance of the peak at position "A" and an appearance of intense peak at 25 eV above the edge. The peak at high photon energy (similar to peak position "B" in figure 8.2) above the edge became narrower. Such changes in peak position were indicative of reduction and formation of metallic gold [8].

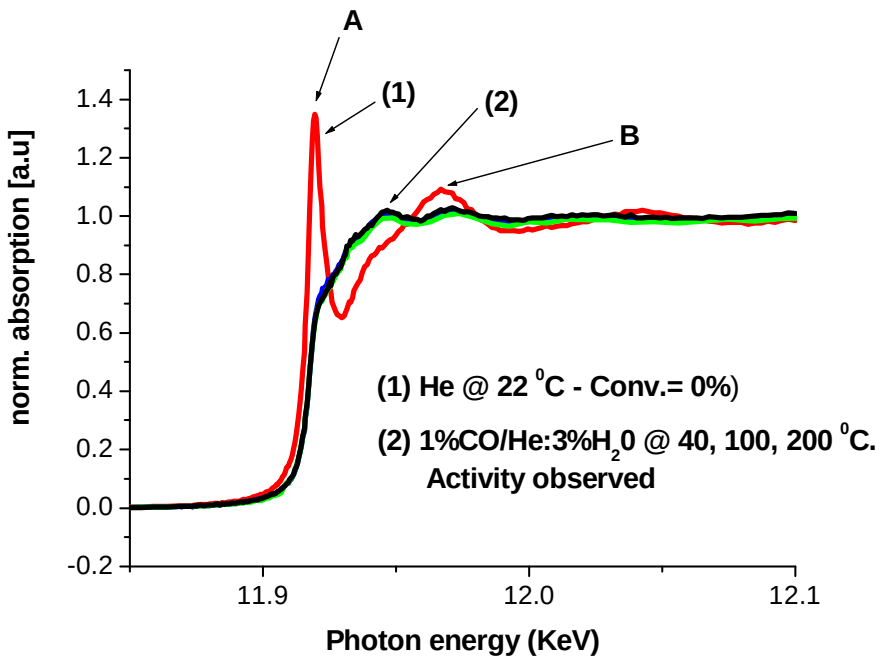

Figure 8.2: Au K-edge XANES spectra of Au-Cu^{c}/TiO_2 (2.84wt%Au:0.32wt%Cu) taken before (1) and during (2) water-gas shift reaction

Figure 8.3 shows the Cu K-edge XANES spectra of as-prepared Au-Cu^{c}/TiO_2 (2.84wt%Au:0.32wt%Cu) taken in helium at 25 ^{0}C and that of calcined Cu^{d}-Au/TiO_2 (3.74wt%Au:0.44wt%Cu) taken during water-gas shift reaction at 200

^{0}C and after regeneration in O_2/He atmosphere at 300 ^{0}C. The as-prepared Au-Cu^c/TiO_2 (2.84wt%Au:0.32wt%Cu) catalysts have shown a pre-edge feature or white line region characteristic of Cu in a tetrahedral environment. The white line region characteristic of Cu is indicative that the copper ions exist as Cu^{2+}. The intensity of the white line region of calcined Cu^d-Au/TiO_2 (3.74wt%Au:0.44wt%Cu) taken during the water-gas shift reaction at 200 ^{0}C has became smaller, suggesting a partial reduction of Cu^{2+} to Cu^+ [9]. This change in the white line region of copper can be associated with lower final activity. However, on regenerating the catalyst in O_2/He atmosphere at 300 ^{0}C, the white line region character of Cu changes to similar characteristics showing Cu on as-prepared Au-Cu^c/TiO_2 (2.84wt.%Au:0.32wt.%Cu) catalysts. This confirms that copper has been oxidized. The catalyst was found to regain its original activity following regeneration using oxidation (300 ^{0}C) treatment (see figure 8.3). However, the time on stream study has indicated that the Au catalyst was not stable and continuously deactivated with time and the white line region has shown a decrease in peak intensity.

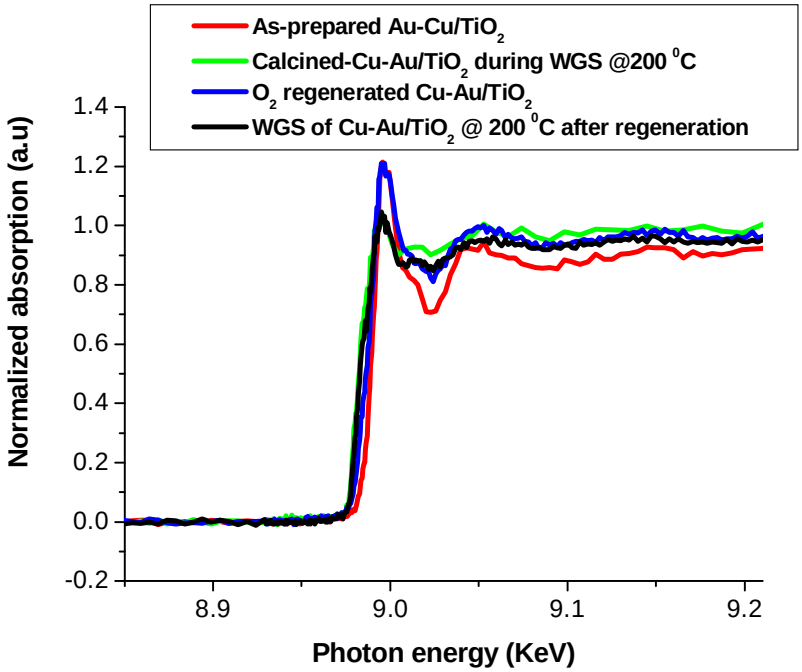

Figure 8.3: Cu K-edge XANES spectra of as-prepared Au-Cu^{c}/TiO_2 (2.84wt%Au:0.32wt%Cu) and calcined Cu^{d}-Au/TiO_2 (3.74wt%Au:0.44wt%Cu) taken during water-gas shift reaction at 200 ^{0}C and after regeneration in O_2/He atmosphere at 300 ^{0}C

In summary, an increase in gold activity on Cu^{2+} modified TiO_2 has been achieved because at least 90% of the gold has been reduced to the zero-valent state while at least 80% of the stabilizing metals (Cu^{2+}) remains in the ionic state. This indicates that during the preparation of Au-Cu^{c}/TiO_2 system, the addition of a stabilizing metal in ionic form has a marked effect on improving the initial dispersion of the reduced gold catalyst and also in maintaining a highly-dispersed state of reduced gold particles during use. The atomic ratio of stabilizing metal ions to that of gold metal plays a crucial role for maximizing the dispersion/stabilizing effects. On the

other hand, the transition metals used, instead of functioning as stabilizers can also act as promoters of catalytic activity of gold supported on TiO_2.

8.3.1.3 Extended X-ray absorption fine structure (EXAFS)

Figure 8.4 shows the absolute parts of the Fourier-Transformed K^2 Au K-edge EXAFS function in the range of 3.0 A^{-1} < k < 15.2 A^{-1} of the Au catalysts supported on TiO_2. The Au/TiO_2 catalysts showed a very distinct trend with formation of oxidic gold species (presence of Au-O shell, 1.64 Å) and weak Au-Au interactions. However on exposure to water-gas shift reaction conditions at 200 ^{0}C the Au-Au interactions peak (at 2.61 Å) increases in intensity which indicates the presence of larger number of Au atoms in the metallic phase and/or formation of large metal particles.

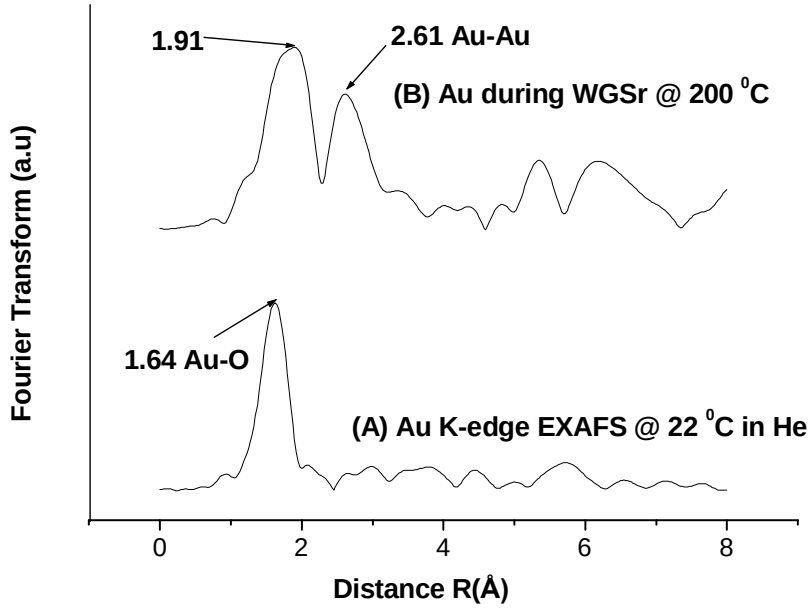

Figure 8.4: Au K-edge k^2 weighted Fourier Transform of Au/TiO_2 catalyst under: (A) helium @ 22 ^{0}C and (B) during water-gas shift reaction @ 200 ^{0}C.

Analysis of the Au K-edge EXAFS data of the as-prepared $Au\text{-}Cu^c/TiO_2$ (2.84wt%Au:0.32wt%Cu) indicates that Au is surrounded by four oxygen atoms at a distance of 1.64 Å (figure 8.5). The coordination number observed confirms the XANES observation that Au is in a tetrahedral environment. The EXAFS of the as-prepared catalyst is different from that observed for WGS treated catalyst and analysis indicates the presence of oxygens at both a short distance of 1.23 Å and a longer distance of 2.05 Å. The total coordination number of 5.5 oxygens at two distances reflects the presence of both tetrahedral and octahedral environments.

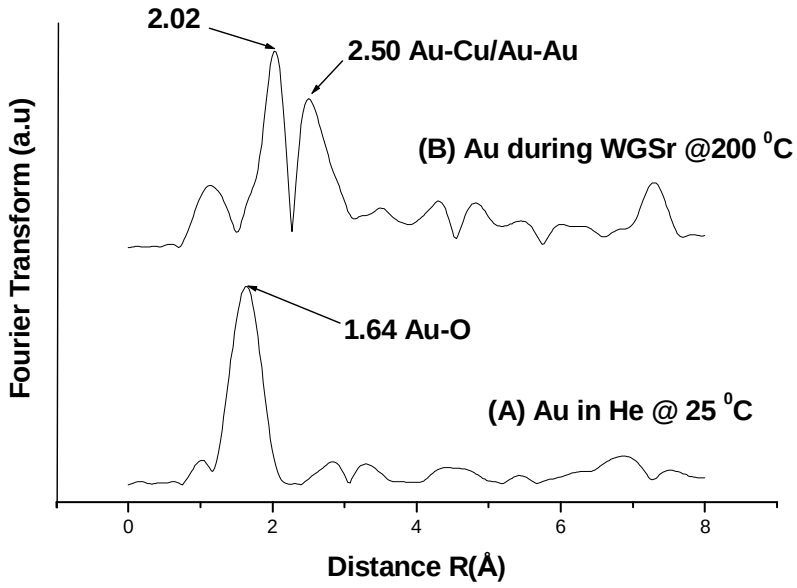

Figure 8.5: Au K-edge k^2 weighted Fourier Transform of Au-Cu^c/TiO_2 (2.84wt%Au:0.32wt%Cu) catalyst under: (A) helium @ 22 ^{0}C and (B) during water-gas shift reaction @ 200 ^{0}C.

From the Cu K-edge EXAFS (figure 8.6), it appears that there is a significant change in the Fourier transform of Cu in CO at 200 ^{0}C (the appearance of an intense peak at 2.34 Å). It is hypothesized that this is due to the presence of heavier scatterers [10]. However, the distance of 2.34 Å is very short for a direct covalent Cu – Cu or Au – Cu bond. It is therefore suggested that the peak is caused by an unusual interference pattern between the two copper contributions (i.e. Cu – O and Cu – Cu or Au – Cu). Interestingly during the WGS reaction the peak at 1.49 Å remains, suggesting that the copper environment is unchanged. The copper environment before and during the WGS reaction can be based on a simple oxygen model (4 oxygens at 1.49 Å), suggesting that the copper is found

as copper ions (Cu^{2+}) with negligible sign of clustering or particle formation; in agreement with the Cu K-edge XANES analysis (see figure 8.3).

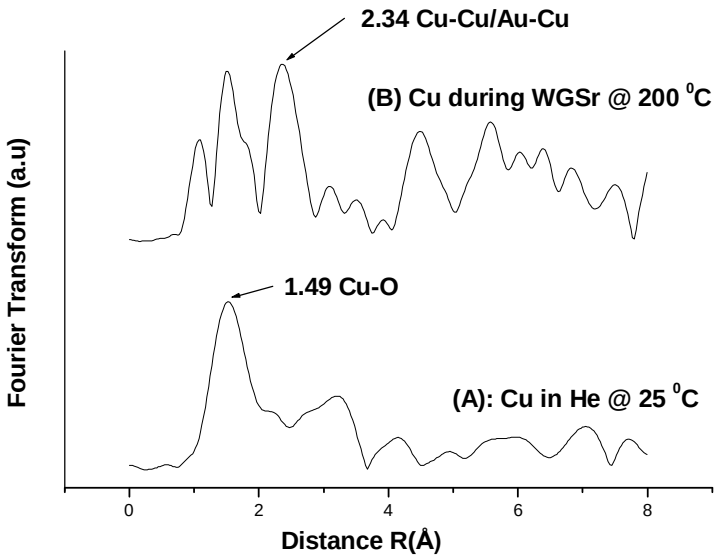

Figure 8.6: Cu K-edge k^2 weighted Fourier Transform of Au-Cu^c/TiO_2 (2.84wt%Au:0.32wt%Cu) catalyst under: (A) helium @ 22 ^{0}C and (B) during water-gas shift reaction @ 200 ^{0}C.

8.3.2 Ex-situ catalytic activities

8.3.2.1. Quantification of the amount of H_2 produced, during the WGS reaction

Figure 8.7 shows the catalytic activity for the water-gas shift reaction, and the quantification of the percentage H_2 produced at 200 ^{0}C, with respect to the amount of CO converted. This was undertaken to get an idea of the amount of oxygen from surrounding reacting with CO during the water-gas shift reaction. Based on the results in figure 8.7 and the hydrogen calibration curve in figure 8.8, it was

found that a small amount of oxygen is being consumed from the surrounding, since in the case of Au/TiO_2 (3.95wt%Au) about 60% CO conversion was obtained at steady state, which was equivalent to 0.48 % H_2 produced (GC area ~ 4395, figure 8.8). On Au/TiO_2 (World Gold Council, reference catalyst, 1.5wt%Au), approximately 30% CO conversion was obtained, which account to 0.24% H_2 produced (GC area ~ 2152). This suggests that during the WGS reaction, the 12% CO conversion (approximately 720 ppm CO at 60% conversion) was due to the reaction with surrounding oxygen. Assuming that all oxygen has reacted according to the mole ratio, this suggests that 360 ppm O_2 were being consumed from surrounding during the WGS reaction at 200 ^{0}C. However, the Au/TiO_2 alone has shown high and stable activity, when compared to Au/Fe_2O_3 catalyst [11]. The Au/TiO_2 has shown that the water-gas shift activity depends on the amount of gold loaded, similar to the results reported by Andreeva et al. [12].

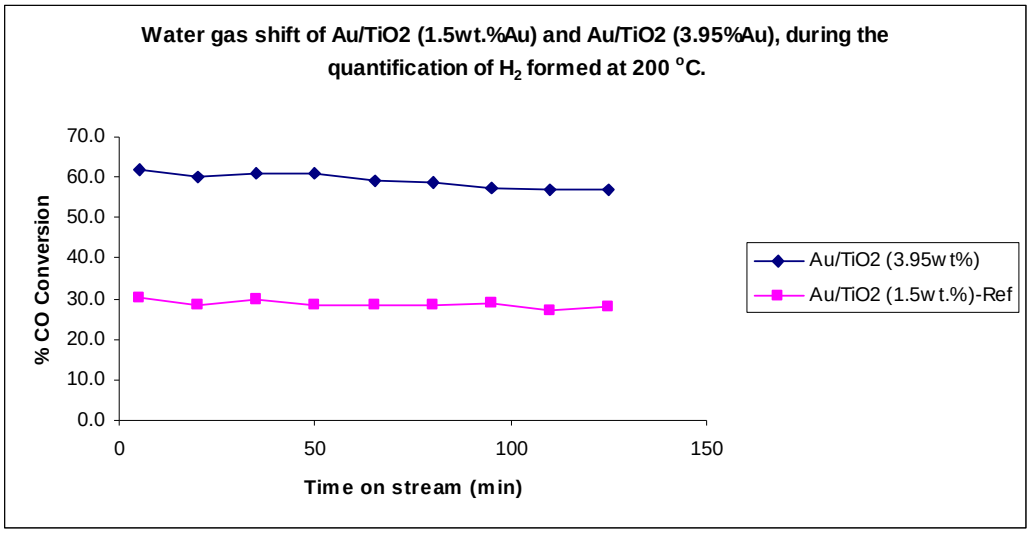

Figure 8.7: Water-gas shift of Au/TiO_2 (reference catalyst, 1.5wt%Au) and Au/TiO_2 (3.95wt%Au), during the quantification of percentage H_2 formed at 200 ^0C.

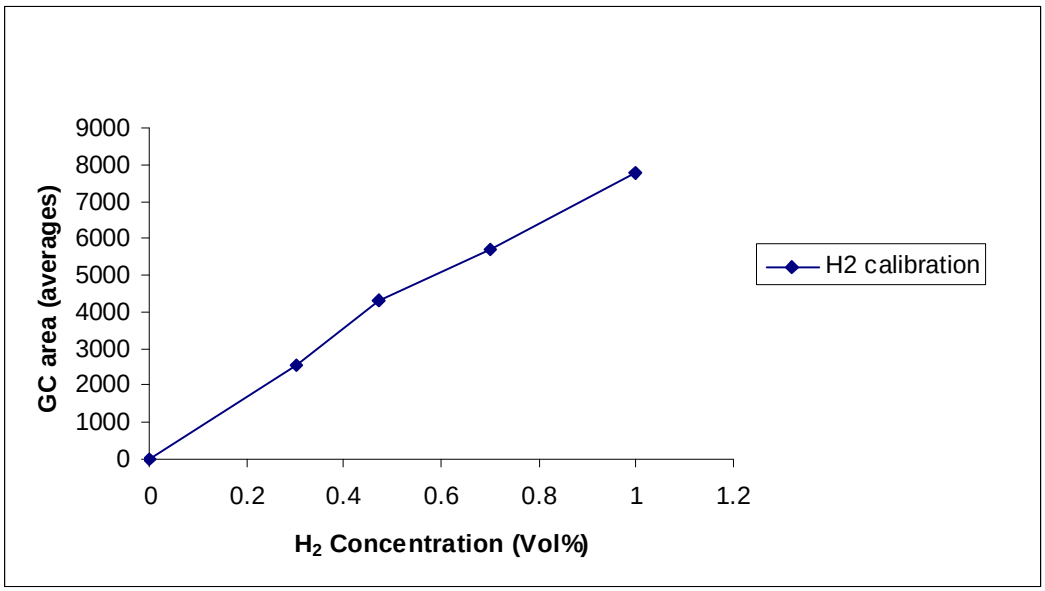

Figure 8.8: Calibration curve of H_2 concentration as a function of GC area

8.3.3 Effect of modifier on the activity and stability of Au on TiO_2 (anatase).

In all the catalysts which have been discussed below, Cu was introduced from $Cu(NO_3)_2*2.5H_2O$ (99.99% purity, Aldrich), by an incipient-wetness method, unless otherwise mentioned. The catalysts were studied for WGS reaction at 200 ^{0}C, under 1%CO/He or 1%CO/N_2 and 3% H_2O.

8.3.3.1 Au-Cu^c/TiO_2 (2.84wt%Au:0.32wt%Cu)

As shown in figure 8.9, the activity of Au in the presence of modifier has increased tremendously relative to that of Au/TiO_2 (3.74%Au). This clearly suggests the existence of a synergetic interaction between gold and copper; with Cu acting as the promoter since, the monometallic form of Cu on TiO_2 was found to be inactive for the reaction studied under the reaction conditions mentioned in figure 8.10. As seen in figure 8.9, the results suggests that the 2.84wt%Au containing TiO_2, promoted by 0.32wt%Cu is more active compared to TiO_2 (anatase) containing 3.74wt%Au (or any of the supported gold on TiO_2).

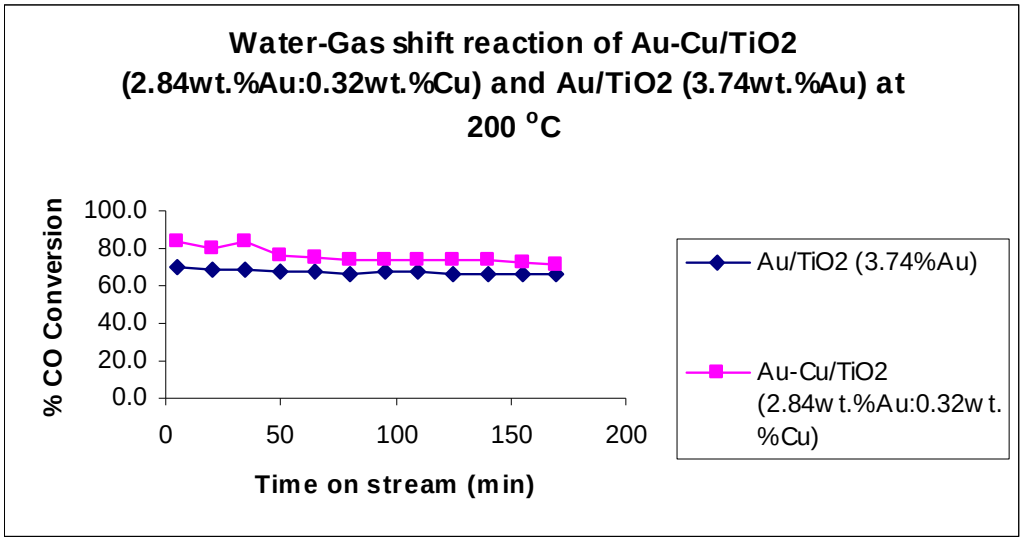

Figure 8.9: WGS on Au-Cu^{c}/TiO_2 (2.84wt%Au:0.32wt%Cu) and Au/TiO_2 (3.74wt%Au) at 200 ^{0}C, showing the effect of modifiers on activity and stability of Au.

As seen in figure 8.10, the activity of the promoter on water-gas shift reaction at 200 ^{0}C is zero. This confirm that the activity of Au-Cu^{c}/TiO_2 (2.84wt%:0.32wt%Cu) observed in figure 8.9, is mainly due to the synergetic interaction between the two metals rather than the participation of Cu in catalyzing the water-gas shift reaction. The activity and stability of Au/TiO_2 alone is related to that reported by Andreeva et al. [12]. However, the observed activity of Au-Cu^{c}/TiO_2 (2.84wt%:0.32wt%Cu) is higher than that reported on Au/CeO_2 catalysts [12].

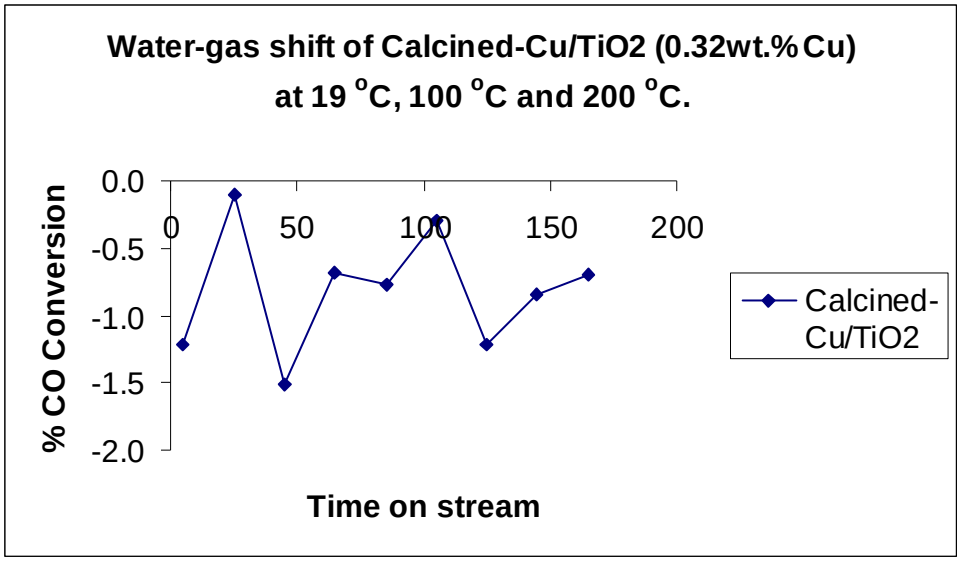

Figure 8.10: Water-gas shift reaction of calcined Cu/TiO_2 (0.32wt%Cu) at 19 ^{0}C, 100 ^{0}C and 200 ^{0}C. The first three points of percentage CO conversions were taken at 19 ^{0}C, second three points at 100 ^{0}C and last three points at 200 ^{0}C.

8.3.3.2 Calcined-[Au-Cu^c/TiO_2 (2.84wt%Au:0.32wt%Cu)] and calcined-Au/TiO_2 (3.95wt%Au)

The results in figure 8.11 show that the calcinations of both catalysts is detrimental to the activities for water-gas shift reaction, compared to as-prepared uncalcined samples. Surprisingly, opposite to the results obtained on as-prepared uncalcined samples; the activity of the calcined-[Au-Cu^c/TiO_2 (2.84wt%Au:0.32wt%Cu)] was found to be less than that of calcined-Au/TiO_2 (3.95wt%Au) as seen in figure 8.11. Furthermore the bimetallic catalyst was not stable and deactivated with time on stream, which then suggests that Cu might have enhanced the agglomeration of gold when calcined simultaneously.

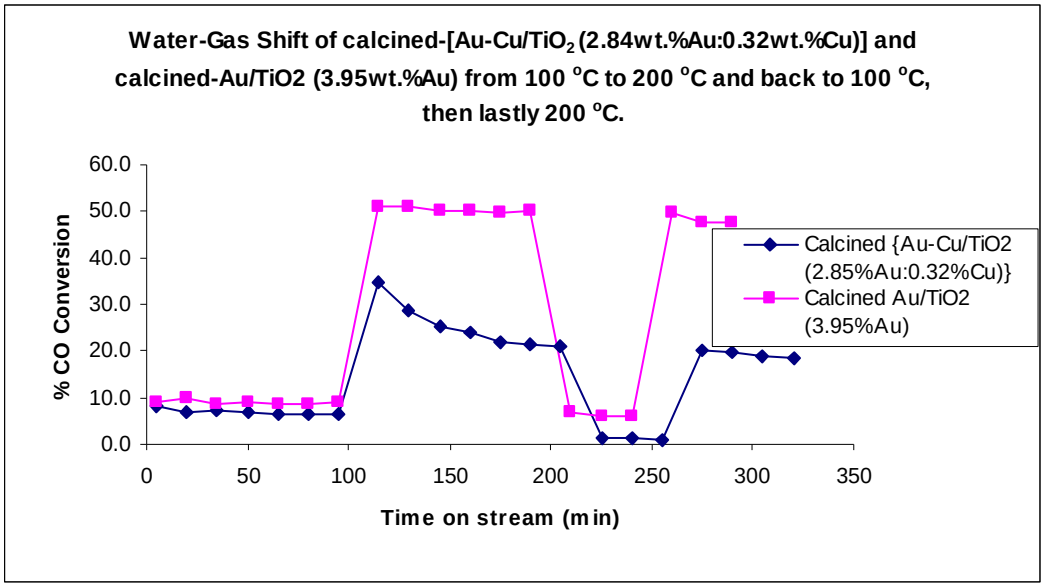

Figure 8.11: WGS reaction on calcined-[Au-Cu^{c}/TiO_2 (2.84wt%Au:0.32wt%Cu)] and calcined-Au/TiO_2 (3.95wt%Au) from 100 ^{0}C to 200 ^{0}C and back to 100 ^{0}C and lastly at 200 ^{0}C.

This suggests that metallic Au is not stable and cannot be stabilized by copper ions, and that a certain percentage of ionic species of Au is needed to catalyze the reaction. Scurrell et al. [11] has reported that the metallic and ionic gold are both required for the water-gas shift reaction. This suggests that during the reaction, there exist redox reactions between the two metals. However, if Cu is reduced during the course of the reaction, then no electrons will be available for donation to Au active species. This resulted in the observed deactivation of the bimetallic catalyst with time on stream. In-situ XANES analysis of Cu K-edge has shown the existence of ionic Cu during the WGS reaction.

8.3.3.3 Cu^{c}-Au/TiO_2 (0.44wt%Cu:3.95wt%Au)

8.3.3.3.1 Effects of nitrates on as-prepared Cu^{c}-Au/TiO_2 (0.44wt%Cu:3.95wt%Au)

Results in figure 8.12 shows the effect of nitrates on the catalyst which was prepared by incipient-wetness of $Cu(NO_3)_2$*$2.5H_2O$ (99.99% purity, Aldrich) on Au/TiO_2 (3.95wt%Au). The introduction of 0.44wt%Cu on Au/TiO_2 (3.95wt%Au), suppressed the activity of the Au catalyst, since the catalyst was used as-prepared without calcinations. The decrease in activity is attributed to the presence of nitrates, which are often converted to NO_2^- at 200 ^{0}C, and which interact with Au actives sites under working conditions. Coville et al. [13] has observed the interaction of NO_2^- with Au active sites and Kung et al. [14] has observed the enhancement of the Au agglomeration during working conditions using NO_2^-.

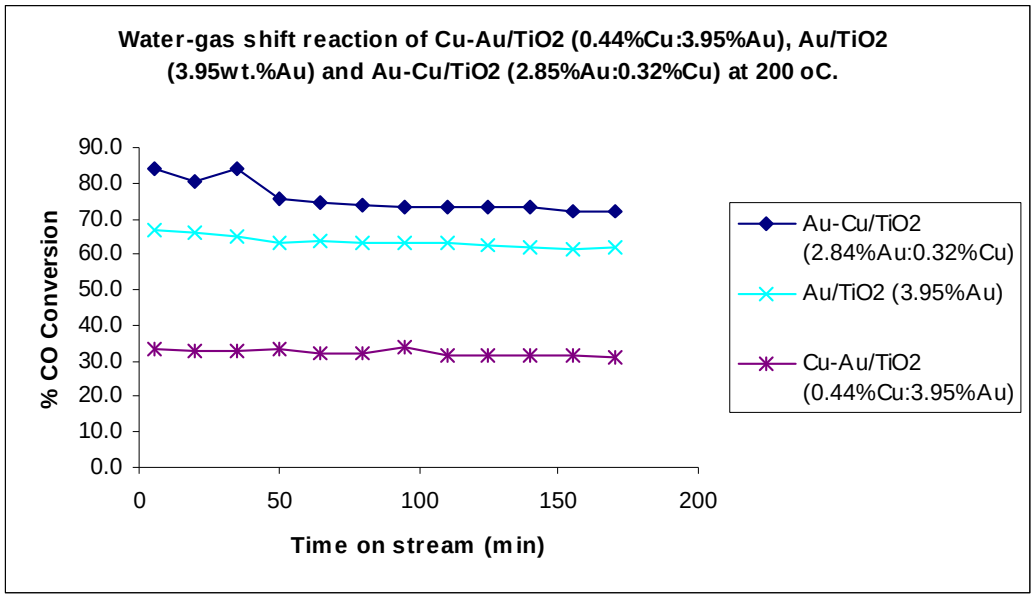

Figure 8.12: WGS of Cu^{c}-Au/TiO_2 (0.44wt%Cu:3.95wt%Au), Au-Cu^{c}/TiO_2 (2.84wt%Au:0.32wt%Cu) and Au/TiO_2 (3.95wt%Au) at 200 ^{0}C, showing the effect of modifier containing nitrates on activity of gold.

8.3.3.3.2 Effects of nitrates on as-prepared Cu-[Calcined-Au/TiO_2 (0.44wt%Cu:3.95wt%Au)]

The effect of nitrates was further noted by intentionally loading copper nitrates on calcined Au/TiO_2 (figure 8.13). The results again show that the nitrate affect suppress the activity of Au i.e. to approximately 50% CO conversion (3.95wt%Au/TiO_2). This suggests that the synergetic interaction between Au and Cu, which has been observed in the Au-Cu^{c}/TiO_2 (2.84wt%Au:0.32wt%Cu) catalyst does not exist, because of the poisoning of Au active sites by NO_2^-.

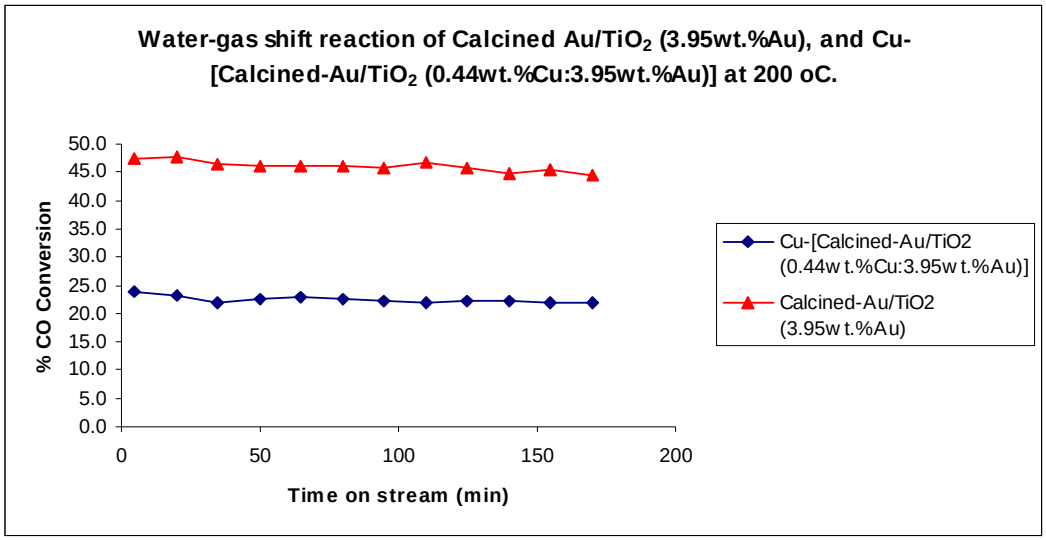

Figure 8.13: WGS of as-prepared Cu-[Calcined-Au/TiO_2 (0.44wt%Cu:3.95wt%Au)] and calcined-Au/TiO_2 (3.95wt%Au) at 200 ^{0}C, showing the effect of modifier containing nitrates on activity of gold.

8.3.3.3.3 Effect of pre-treatment on Cu-[Calcined-Au/TiO_2 (0.44wt%Cu:3.95wt%Au)] at 350 ^{0}C.

The Cu-[Calcined-Au/TiO_2 (0.44wt%Cu:3.95wt%Au)] was further treated in nitrogen (flow rate = 100 ml/min) at 350 ^{0}C for 1 h and cooled down to 200 ^{0}C in N_2. After treatment the catalyst was tested for water-gas shift reaction and it was noted that the activity kept on decreasing as shown in figure 8.14, which suggests that gold might have already agglomerated and the attempts to decompose nitrates had no influence on the already agglomerated gold particles.

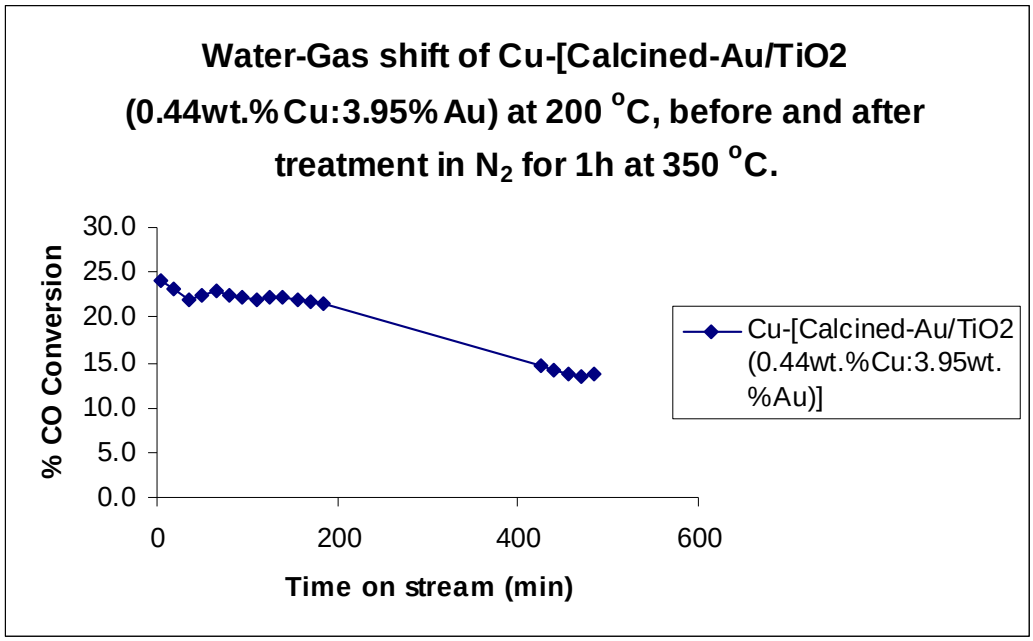

Figure 8.14: WGS of Cu-[Calcined-Au/TiO_2 (0.44wt%Cu:3.95wt%Au)] at 200 ^{0}C, before and after treatment in N_2 for 1h at 350 ^{0}C.

8.3.3.3.4 Effect of Cu introduced by ion-exchange/deposition-precipitation method on a calcined-Au/TiO_2 (4.09wt%Au)

Noting the performance of both Cu-[Calcined-Au/TiO_2 (0.44wt%Cu:3.95wt%Au)] and Cu^c-Au/TiO_2 (0.44wt%Cu:3.95wt%Au), in the presence of nitrates above, Cu was introduced by ion-exchange/deposition-precipitation onto a calcined-Au/TiO_2 (4.09wt%Au). The results in figure 8.15 show that there is an increase in activity, since less than 10% of CO conversion has been lost when compared to calcined-Au/TiO_2 (4.09wt%Au). The activity has increased, compared to the un-washed Cu-[Calcined-Au/TiO_2 (0.44wt%Cu:3.95wt%Au)] because the catalyst was washed with water after preparation, minimizing the presence of NO_3 on the support interface. The results

show that there is a necessity to get rid of nitrates in order to maintain the stability of supported gold and its interaction with the stabilizing/promoting metal.

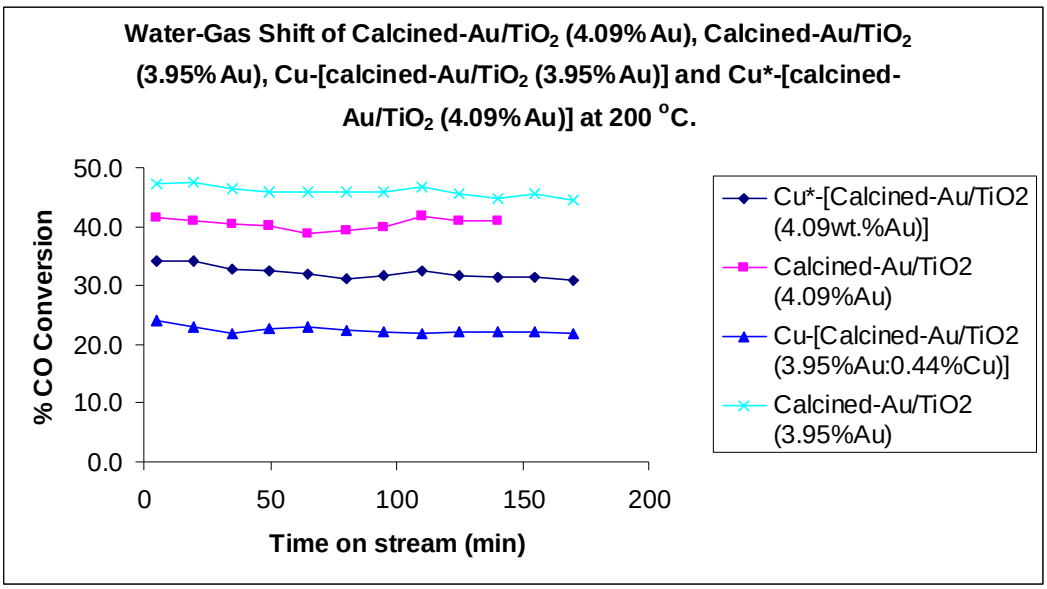

Figure 8.15: WGS of Cu*-[Calcined-Au/TiO_2 (0.44wt%Cu:4.09wt%Au)] at 200 ^{0}C. * Cu was introduced by ion-exchange/deposition-precipitation method of $Cu(NO_3)_2$*2.5H_2O (99.99% purity, Aldrich,) solution, of which the pH has been adjusted to 5.0 at 70 ^{0}C for 1.5 h, prior to addition on suspended calcined-Au/TiO_2 (4.09wt%Au), on a doubly distilled water at 40 ^{0}C for 0.5 h. The mixture was kept at 60 ^{0}C for 12 h under constant and vigorous stirring.

8.3.3.4 Catalysts prepared from Cu containing acetate, i.e. $Cu(OOCCH_3)_2*H_2O$

Since the introduction of Cu from sources containing nitrates was found to be detrimental to the activity of the modified Au/TiO_2, catalysts were then prepared from Cu containing acetate couterions by an incipient-wetness method on either calcined or uncalcined Au/TiO_2.

8.3.3.4.1 Activity of calcined-[Cu^d-Au/TiO_2 (0.44wt%Cu:3.74wt%Au)]

Cu (0.44wt%) was introduced by incipient-wetness method onto uncalcined Au/TiO_2 (3.74wt%Au) and finally, the mixture was calcined in air at 350 ^{0}C for 4 h.

The results as shown in figure 8.16, suggest that the absence of nitrate gave positive result on the activity of calcined-[Cu^d-Au/TiO_2 (0.44wt%Cu:3.74wt%Au)], when compared to calcined-Au/TiO_2 (3.74wt%Au). For the sake of comparison, it can be seen that the "Cu^c-Au/TiO_2 (0.44wt%Cu:3.95wt%Au)", of which Cu^c was introduced from a source containing nitrates its activity is much less than that of Au/TiO_2 (3.95wt%Au). However, the calcined-[Cu^d-Au/TiO_2 (0.44wt%Cu:3.74wt%Au)] was not stable and continuously deactivated with time on stream from an initial activity. Over a period of 160 minutes the activity decreased from 65 to 50%. The decrease in activity was attributed to the reduction of Cu to a lower oxidation state during use.

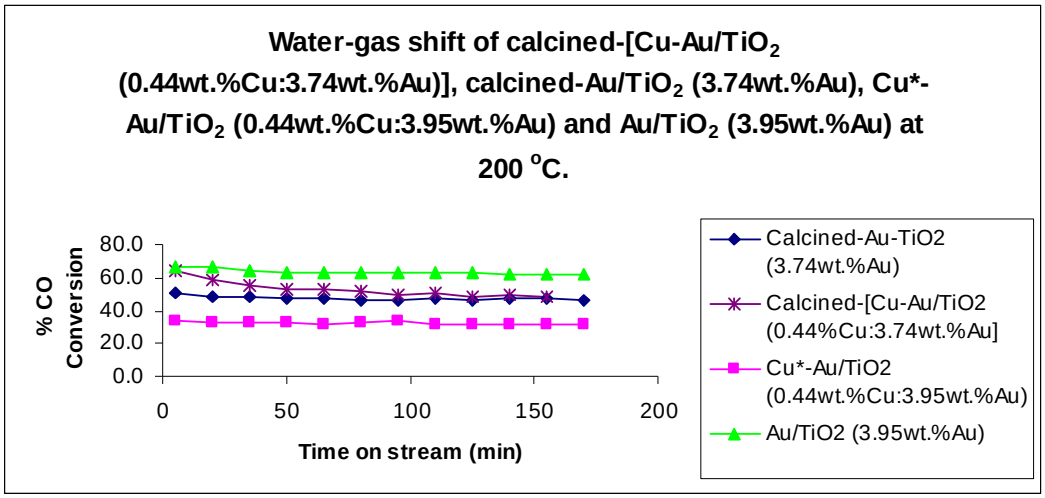

Figure 8.16: Water-Gas shift activity of calcined-[Cu-Au/TiO_2 (0.44wt%Cu:3.74wt%Au)], calcined-Au/TiO_2 (3.74wt%Au), Cu^c-Au/TiO_2 (0.44wt%Cu:3.95wt%Au) and Au/TiO_2 (3.95wt%Au) at 200 ^{0}C, showing the positive role of Cu in the absence of nitrates.

8.3.3.4.2 Catalyst regeneration of calcined-[Cu^d-Au/TiO_2 (0.44wt%Cu:3.74wt%Au)]

Figure 8.17 shows the effect of oxygen on the regeneration of calcined-[Cu^d-Au/TiO_2 (0.44wt%Cu:3.74wt%Au)]. When the 2.5%O_2/He mixture was passed through the catalyst at 300 ^{0}C for 1 h, it was found that the catalyst regained its initial activity. In-situ studies of this catalyst following the Cu K-edge XANES analysis confirms that the deactivation has been influenced by the reduction of Cu^{2+} to Cu^+ [9]. A similar result was reported by Clausen et al. [9] on Au-Ni bimetallic nanoparticles supported on silica. They reported an increase in Ni K-edge for the Au-Ni sample during oxidation at 400 ^{0}C.

This clearly suggests that for a promoter of this kind to be effective, such a promoter or stabilizer should be in the ionic form. For a catalyst of this nature which does not seem to deactivate very rapidly it will be necessary to study the effects of other metals (at a much longer periods, ~ 8 h on stream), especially those, which have higher reduction potentials. Such metal promoters (Fe, Cr, etc.,) need higher temperature for them to be reduced and if such metals are effective enough, the need for metal promoters to be in ionic form can be resolved and/or well understood.

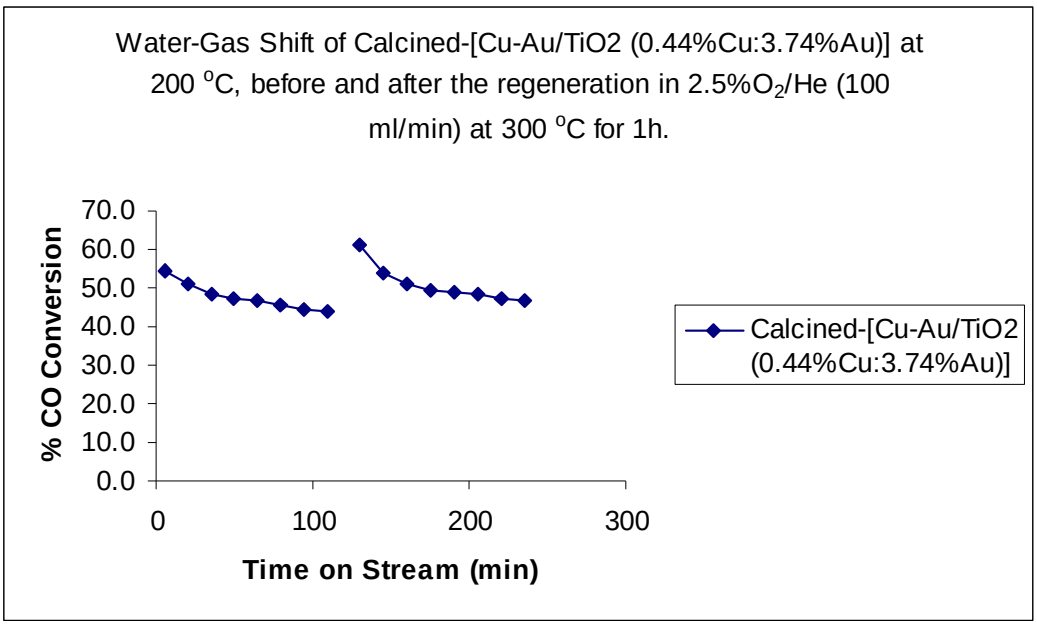

Figure 8.17: Regeneration of Calcined-[Cu^{d}-Au/TiO_2 (0.44wt%Cu:3.74%wtAu)] in 2.5%O_2/He at 300 ^{0}C for 1 h.

When the same catalyst was treated under nitrogen, under the same conditions as above the catalyst activity remained the same after treatment, which then suggests the significance of a reactive species such as oxygen.

8.3.3.5 Effect of Cu loading on the stability and activity of Au on TiO_2 (anatase, $200m^2/g$)

As shown in figure 8.18, results suggest that the activity of calcined-[Cu^d-Au/TiO_2 (0.22wt%Cu:3.74wt%Au)] and calcined-[Cu^d-Au/TiO_2 (0.44wt%Cu:3.74wt%Au)] are almost the same at steady state. However, at the start of the reaction the activity of calcined-[Cu^d-Au/TiO_2 (0.22wt%Cu:3.74wt%Au)] is slightly higher compared to that of calcined-[Cu^d-Au/TiO_2 (0.44wt%Cu:3.74wt%Au)]. This might suggest that the activity is lowered when the Cu loading is increased considering the activity of calcined-[Cu^d-Au/TiO_2 (0.88wt%Cu:3.74wt%Au)]. The interaction between the support and Au active sites that has been lost must be due to the stabilizing metal completely surrounding the Au particles.

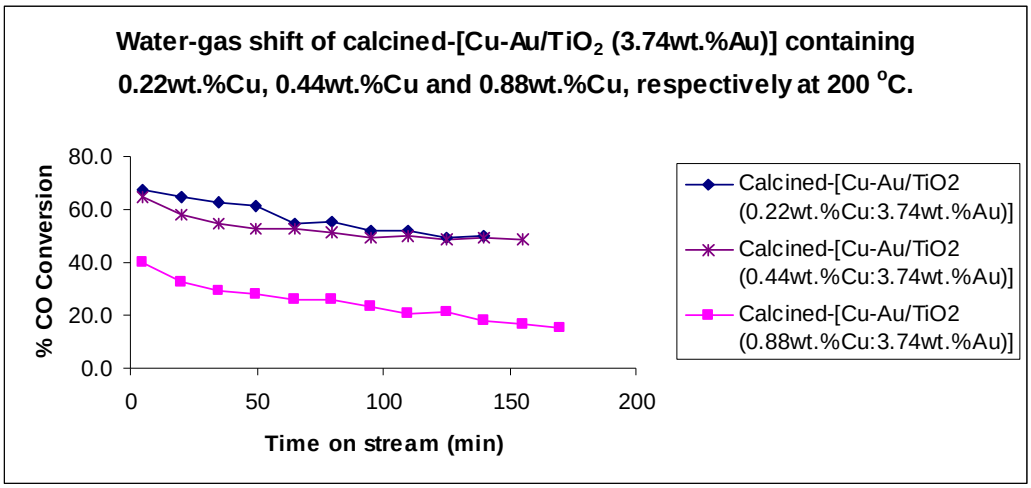

Figure 8.18: Water-gas shift activity of calcined-[Cu^d-Au/TiO_2 (0.22wt%Cu:3.74wt%Au)], calcined-[Cu^d-Au/TiO_2 (0.44wt%Cu:3.74wt%Au)], and calcined-[Cu^d-Au/TiO_2 (0.88wt%Cu:3.74wt%Au)] at 200 ^{0}C, showing the effect of Cu loading on the catalytic activity of Au on TiO_2.

8.3.4 Comparison of CO oxidation activity for Au-Cu^c/TiO_2 (2.84wt%Au:0.32wt%Cu) and Au/TiO_2 (3.95wt%Au) at -77 ^{0}C.

Results in figure 8.19 shows the time on stream CO oxidation activity for the Au-Cu^c/TiO_2 (2.84wt%Au:0.32wt%Cu) and Au/TiO_2 (3.95wt%Au) at -77 ^{0}C (5%CO/He and 2.5%O2/He, flow rate = 50 ml/min). The Au/TiO_2 (3.95wt%Au) catalyst showed a high initial activity with 95% CO conversion. However, the time on stream study indicated that Au/TiO_2 (3.95wt%Au) catalyst is not stable and continuously deactivated with time. Over a period of 30 minutes the CO conversion decreased from 95 to 40%. Au-Cu^c/TiO_2 (2.84wt%Au:0.32wt%Cu) catalyst showed a low initial activity of 92% conversion and lower steady state activity with approximately 20% CO conversion compared to that of Au/TiO_2 (3.95wt%Au) catalyst. These results suggests that for low temperature CO oxidation, the synergetic interactions between Au and Cu such as that observed on WGS reaction, does not exist.

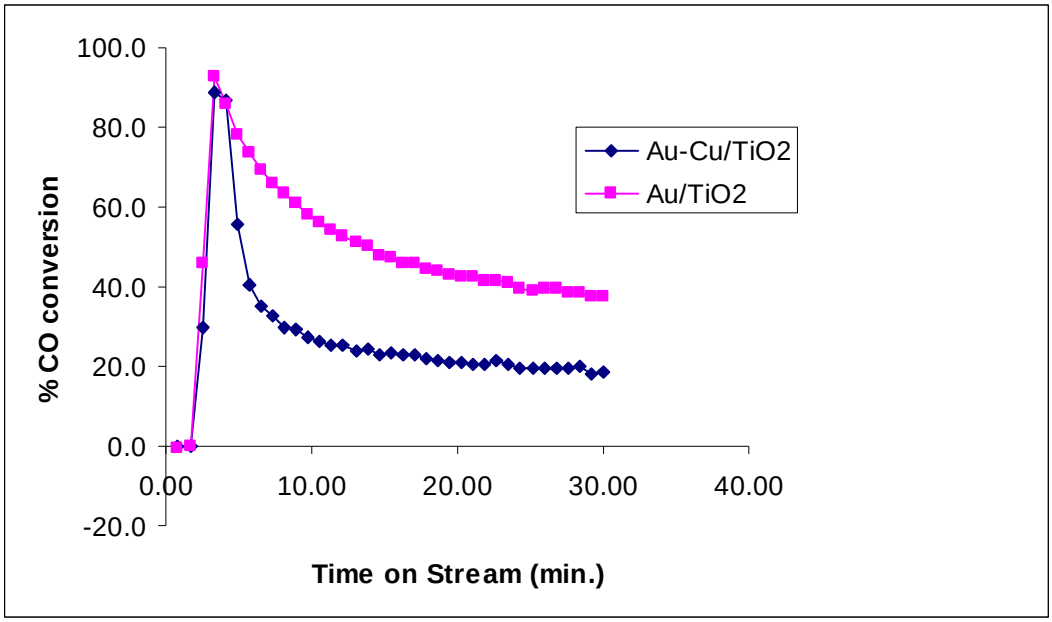

Figure 8.19: Time on stream CO oxidation of Au-Cu^{c}/TiO_2 (2.84wt%Au:0.32wt%Cu) and Au/TiO_2 (3.95wt%Au) at -77 ^{0}C.

8.3.5 Preferential oxidation of CO in the presence of excess hydrogen stream over Au-Cu^{c}/TiO_2 (2.84wt%Au:0.32wt%Cu) and Au/TiO_2 (3.95wt.%Au) at 18 ^{0}C and 100 ^{0}C.

Table 8.1 shows the preferential CO oxidation activity of Au-Cu^{c}/TiO_2 (2.84wt%Au:0.32wt%Cu), Cu^{c}-Au/TiO_2 (3.95wt.%Au:0.44wt%Cu) and Au/TiO_2 (3.95wt%Au) at 100 ^{0}C. Au/TiO_2 (3.95wt%Au) catalyst showed a selectivity to CO_2 of 86.46% at 18 ^{0}C. The Au-Cu^{c}/TiO_2 (2.84wt%Au:0.32wt%Cu) catalyst showed a low selectivity to CO_2 of 82.38% as compared to that of the Au/TiO_2 (3.95wt%Au) catalyst. These results clearly suggest that the presence of Cu on Au catalysts, does not promote the selectivity towards CO_2. Copper alone on CeO_2 was reported to give higher selectivity, up to 97 % at 145 ^{0}C [15]. Unlike the

Au/TiO_2 catalysts the Pt-group metal on alumina, [16] has been found to give higher selectivity to CO_2 at high temperatures. However, density functional theory (DFT) of both Au and Cu at lower temperature were found to be more selective PROX catalysts than Pt [17]. High selectivity to CO_2 at 100 ^{0}C was reported by Kung et al. [18, 19] on gold supported on alumina. The authors reported that the chloride facilitates the agglomeration of Au particles and inhibits the catalytic activity by poisoning the active site. This clearly suggests that alumina plays a significant role as a support of Au particles, compared to TiO_2 for selective CO oxidation. The dependence of selective CO oxidation to the support was confirmed by Behm et al. [20]. They reported that catalysts supported on reducible transition metal oxides, such as Fe_2O_3, CeO_2 or TiO_2, exhibit a CO oxidation activity of up to one magnitude higher at comparable gold particle size. They concluded that only a proper choice of the support oxide is important in order to prepare a highly active gold catalyst.

Table 8.1: Effects of Cu on Au/TiO_2 for preferential oxidation CO in the presence of excess hydrogen

Catalysts	Prep. Method	Pre-treatment	Selectivity$_{CO2}$ @ 18 ^{0}C (Average Conversion)			Selectivity$_{CO2}$ @ 100 ^{0}C (Average Conversion)		
			%CO	%O_2	%S_{CO2}	%CO	%O_2	%S_{CO2}
Au/TiO_2 3.95wt%Au	DP[a]	Au red.[d]	30.7	35.6	86.5	11.4	99.9	11.4
Au-Cu[c]/TiO_2 2.84wt%Au 0.32wt.%Cu	DP[a] of Au on calcined Cu/TiO_2	Au reduced @ 18 ^{0}C for pCO oxidation @ 18 ^{0}C	7.1	8.6	82.4	11.2	96.8	11.6
Cu[c]-Au/TiO_2 3.95wt%Au 0.44wt%Cu	IW[b] of $Cu(NO_3)_2$ on unreduced Au/TiO_2	Au reduced @ 18 ^{0}C for pCO oxidation @ 18 ^{0}C	3.9	5.0	76.9	11.6	96.7	12.0

[a] Deposition precipitation, [b] Incipient wetness, [c] X-ray Fluorescence spectroscopy and [d] Au reduced at 18 ^{0}C for ‘‘preferential’’ CO oxidation at room temperature.

8.4 CONCLUSIONS

Cu modified Au/TiO_2 (anatase, $200m^2/g$) has been prepared by an incipient-wetness method by either introducing the modifier, before or after Au has been loaded. Such catalysts were found to give higher catalytic activity for the water-gas shift reaction, when compared to unmodified Au/TiO_2 catalysts. It has been suggested that an increase in activity on modified Au/TiO_2, is mainly due to the existence of a synergetic interaction between Cu and Au, since the activity of both Cu/TiO_2 and Au/TiO_2 is lower than that of bimetallic system.

WGS activity of both as-prepared Au/TiO_2 and a $Au\text{-}Cu^c/TiO_2$ catalyst has been found to be high and stable. The presence of nitrates on $Cu^c\text{-}Au/TiO_2$ has been found to be detrimental to the activity of Au on TiO_2; due to the poisoning of Au active sites and enhancement of Au agglomeration by NO_2^- formed during the reaction. The activity of Au/TiO_2 catalysts modified with Cu containing acetate counterions has been found to decrease during the first 30 minutes on stream, reaching a constant value of 45 +/- 2 %. However, when the poisoning by NO_2^- was eliminated; the activity increased compared to Au/TiO_2 catalysts modified with Cu containing nitrate.

An increase in Cu loading was found to lower the activity of Au due to loss of interaction between Au and the support interface, since the metal catalyst, i.e., Au is completely surrounded by Cu.

The XANES spectrum of uncalcined as-prepared catalysts has shown a pre-edge feature (due to the 1s to 3d transition) characteristic of Au in a tetrahedral environment. The water-gas shift treated sample show a reduction in the intensity of the pre-edge feature or white line region indicating a change in Au environment (i.e. a partial reduction of Au^{3+} to either Au^{+}/Au^{0}).

XANES spectrum of calcined Cu^{d}-Au/TiO_2 (3.74wt%Au:0.44wt%Cu) has confirmed that Cu exists as copper ions (Cu^{+}/Cu^{2+}) before and during water-gas shift reaction. The catalyst was found to regain its original activity and the state of Cu, following regeneration using an oxidation (300 ^{0}C) treatment. However, the time on stream studies have indicated that the Au catalyst was not stable and continuously deactivated with time and the white line region has shown a decrease in peak intensity during use.

An increase in gold activity on Cu^{2+} modified TiO_2 has been achieved because at least 90% of gold has been reduced to the zero-valent state while at least 80% of the stabilizing metals (Cu^{2+}) remains in the ionic state. It is concluded that during the preparation of the Au-Cu^{c}/TiO_2 system, that the addition of a stabilizing metal in an ionic form has marked effects in improving the initial dispersion of reduced gold catalyst and also in maintaining a highly-dispersed state of reduced gold particles during use. The atomic ratio of stabilizing metal ions to that of gold metal plays a crucial role in maximizing the dispersion/stabilizing effects. On the other hand, the transition metals used, instead of functioning as stabilizer can also act as a promoter of catalytic activity of gold supported on TiO_2.

It was noted that during the water-gas shift reaction at 200 ^{0}C, a certain percentage of CO converted was due to the reaction of CO with a small amount of leaked oxygen.

Changes in the temperature range of appearance and disappearance of distinct copper and gold species and variations of their relative stability were revealed. Formation of bimetallic particles was not detected by EXAFS data analysis. The observed effects are interpreted as a mutual influence of gold and copper ions and reduced species of gold and copper due to their competing for ion exchange sites. It is unclear at present how this is achieved. However, EXAFS data analysis of both metals suggests that it is not due to a direct interaction between Au and Cu.

Copper has been found to show no promotional effect on low temperature CO oxidation and on preferential CO oxidation in excess of hydrogen.

8.5 REFERENCES

[1] J. W. Niemantsverdriet, Spectroscopy in Catalysis, Wiley-VCH, Weinheim, Germany, 1993.

[2] H. Topsøe, Stud. Surf. Sci. Catal., **1** (2000) 130.

[3] G. Ertl, H. Knozinger, J. Weitkamp, Eds., Handbook of Heterogeneous Catalysis, VCH, Weinheim, Germany, 1997.

[4] Z. Paal, G. A. Somorjai, in Handbook of Heterogeneous Catalysis, G. Ertl, H. Knozinger, J. Weitkamp, Eds., VCH, Weinheim, Germany, **3** (1997) 1084.

[5] T. W. Hansen, J. B. Wagner, P. L. Hansen, S. Dahl, H. Topsoe, and C. J. H. Jacobsen, Science **294** (2001) 1508.

[6] A. Mittasch, Adv. Catal. **2** (1950) 81.

[7] B. Harrison, A. F. Diwell, C. Hallet, Plat. Met. Rev. **32** (1988) 73.

[8] J. Guzman, and B. C. Gates, J. Phys. Chem. B: **106** (2002) 7659.

[9] A. M. Molenbroek, O. Steffensen, E. O. Tornqvist, and B. S. Clausen, Alloying in catalysts of bimetallic nano-particles, Center for Atomic-scale Materials, Technical University of Denmark, 1996.

[10] P. Rabe, G. Tolkiehn, and A. Werner., J. Phys. Chem.:Solid State Phys., **12** (1979) 899.

[11] A. Venugopal, and M. S. Scurrell, Appl. Cat. A: General, **258** (2004) 241.

[12] D. Andreeva. V. Idakiev, T. Tabakova, L. Ilieva, P. Falaras, A. Bourlinos and A. Travlos, Catal. Today, **72** (2002) 51.

[13] (a) M. A. Debeila, N. J. Coville, M. S. Scurrell and G. R. Hearne, J. Molec. Catal. A: Chemical **219** (2004) 131. (b) M. A. Debeila, N. J. Coville, M. S. Scurrell, G. R. Hearne and M. J. Witcomb, J. Phys. Chem. B: **108** (2004) 18254.

[14] H. H. Kung, and M. C. Kung, Northwestern University, Unpublished results.

[15] Y. Liu, Q. Fu, and M. F. Stephanopoulos, Catalysis Today, **93** (2004) 241.

[16] M. J. Kahlich, H. A. Gasteiger, and R. J. Behm., J. Catal. **171**, (1997) 93.

[17] S. Kandoi, A. A. Gokhale, L. C. Grabow, J. A. Dumesic, and M. Mavrikakis, Catal. Letters, **93** (2004) 1.

[18] H.-S. Oh, J. H. Yang, C. K. Costello, Y. M. Wang, S. R. Bare, H. H. Kung and M. C. Kung., J. Catal. **210**, (2002) 375.

[19] G. K. Bethke, H. H. Kung, Appl. Cat. A: General, 194 (2000) 43.

[20] M. M. Schbert, V. Plzak, J. Garche and R. J. Behm., Catal. Letters, **76** (2001) 3.

CHAPTER 9

General conclusions

Gold supported on Y and surface modified Y-zeolite (with aqueous solutions of $LiNO_3$, $NaNO_3$ or KNO_3, and NH_4NO_3) was prepared by either an incipient-wetness of $KAu(CN)_2$ or ion exchange of $Au(en)_2Cl_3$ onto the zeolites. It has been found that the activity of supported gold depends on the type of the support and alkali metal nitrate used. The activity and stability of the Au catalysts was found to depend on the source of gold used and the activity varied according the order: $HAuCl_4$ >> $KAu(CN)_2$ > $Au(en)_2Cl_3$ (for both CO oxidation and Ethylene Hydrogenation).

Gold supported on M-Y systems, have been prepared by incipient-wetness of $KAu(CN)_2$ on transition metal exchanged Y-zeolites. As the reduction potential becomes more negative, the CO oxidation activity of the gold supported on the zeolites was found to increase, following the sequence: Ni^{2+}, - 0.23 << Fe^{3+}, - 0.41 < Cr^{3+}, - 0.56. However the ethylene hydrogenation activity increased as follows: $Ni^{2+} > Cr^{3+} > Fe^{3+}$. The added nickel metal on Y zeolites seems to appear as the promoter of the gold ethylene hydrogenation activity to a greater extent than can be accounted for by the improved dispersion of gold. An increase in gold activity on Fe^{3+}, Cr^{3+} exchanged zeolite-Y and Cu^{2+} modified TiO_2 has been achieved because at least 90% of the gold has been reduced to the zero-valent

state while at least 90% of the stabilizing metals (Fe^{3+}, Cr^{3+} and Cu^{2+}) remains in the ionic state. The atomic ratio of stabilizing metal ions to that of the gold metal plays a crucial role in maximizing the dispersion/stabilizing effects. On the other hand the transition metals used, instead of functioning as stabilizer can also act as a promoter of catalytic activity of gold.

It has been noted that the presence of protons stabilizes most of the Au clusters (electron-deficient species) within the HY cages and thus results in a smaller amount of gold species migrating to the outer surface of the zeolite. The results further suggest that formation of metallic gold on Y result in higher CO oxidation activity and hence the necessity of metallic gold. The results suggest that adsorptive properties of zeolite encaged metal clusters can be 'altered' by other ions sharing the same cavities.

The induction period of supported Au is a function of how rapidly Au^{3+} can be reduced to the lower oxidation states. It was found that the choice of a reducing agent plays a significant role in the reduction of gold. The $NaBH_4$ reduced Au catalysts gave lower C_2H_4 conversion, unlike in CO oxidation where the activity increased on the reduced Au catalysts. In this work, it has been established that the reactivity and concentration of reducing agents and the redox potential of Au cations have significant effects on the formation and growth of Au nanoparticles within or on the surface of zeolites.

X-ray fluorescence spectroscopy (XRF) has confirmed that an increase in CO oxidation and Ethylene hydrogenation activity of Au catalysts treated with $NaNO_3$ have been associated with an increase in gold content deposited on the support. The activity, stability and deactivation of gold/zeolites systems for ethylene hydrogenation were found to depend on pre-treatment and activity measurements temperature.

TPR profiles, suggest that Au particles on Cr^{3+}-exchanged Y are more stable when compared to Fe^{3+}. Both of the above are highly stable when compared to Ni^{2+}. XRD profiles has shown smaller gold particles ~ 5 nm, for Cr^{3+}-exchanged Y systems, than that of Ni^{2+}-exchanged Y systems. This is related to the observed catalytic activity of Au/Cr-Y. At a higher reduction temperature, the migration of Au in the absence of an "anchor" is pronounced, resulting in Au particles as large as 20 nm presumably located at the external surface of the zeolite. However, in the presence of chromium, the migration of the Au is impeded because of the enhanced interaction with the zeolite. As a result Au particles remained smaller than 5 nm. It can be concluded that multivalent irreducible transition elements and or metal ions, such as Fe^{3+} and Cr^{3+}, can increase the interaction of Au particles with the aluminosilicate framework surface and consequently increase their thermal stability. Transition metals which are electrostatically bound to the zeolite matrix interact chemically with the Au metal particles.

Three types of gold species were observed for gold-zeolites: Au^{3+} cations, neutral charged $Au^{\sigma+}_n$ clusters suggested to be inside the zeolite channels and Au

nanoparticles with diameter varied from 2 to 20 nm located on the external surface of zeolite cages. This gold species were found to depend on zeolite type, acidity of zeolite, alkali metal, temperature of reduction and reducing agents. Gold nanoparticles were observed only as the result of reduction of the Au-exchanged forms at high temperatures due to reduction of Au^{3+} species and agglomeration of gold clusters.

Cu modified Au/TiO_2 (anatase, $200m^2/g$) has been prepared by an incipient-wetness method by either introducing the modifier, before or after Au has been loaded. Such catalysts were found to give high and stable catalytic activity for the water-gas shift reaction, when compared to unmodified Au/TiO_2 catalysts. It has been suggested that an increase in activity on modified Au/TiO_2, is mainly due to the existence of a synergetic interaction between Cu and Au, since the activity of both Cu/TiO_2 and Au/TiO_2 is lower than that of bimetallic system. The presence of nitrates on Cu^c-Au/TiO_2 has been found to be detrimental to the activity of Au on TiO_2, due to the poisoning of Au active sites and enhancement of Au agglomeration by NO_2^- formed during the reaction.

The XANES spectrum of uncalcined as-prepared catalysts has shown a pre-edge feature (due to the 1s to 3d transition) characteristic of Au in a tetrahedral environment. The water-gas shift treated sample show a reduction in the intensity of the pre-edge feature or white line region indicating a change in Au environment (i.e. a partial reduction of Au^{3+} to either Au^+/Au^0). XANES spectrum of calcined Cu^d-Au/TiO_2 (3.74wt%Au:0.44wt%Cu) has confirmed that Cu exists as copper

ions (Cu^{+}/Cu^{2+}) before and during water-gas shift reaction. The catalyst was found to regain its original activity and the state of Cu, following regeneration using an oxidation (300 ^{0}C) treatment. Formation of bimetallic particles was not detected by EXAFS data analysis. The observed effects are interpreted as a mutual influence of gold and copper ions and reduced species of gold and copper due to their competing for ion exchange sites. It is unclear at present how this is achieved. However, EXAFS data analysis of both metals suggests that it is not due to a direct interaction between Au and Cu. Copper has been found to show no promotional effect on low temperature CO oxidation and on preferential CO oxidation in excess of hydrogen.